UNIVERSIDAD COMPLUTENSE DE MADRID

FACULTAD DE CIENCIAS FÍSICAS
Departamento de Física de la Tierra, Astronomía y Astrofísica II
(Astrofísica y Ciencia de la Atmósfera)

TESIS DOCTORAL

Identificación y caracterización de estrellas poco masivas y enenas marrones con el observatorio virtual

MEMORIA PARA OPTAR AL GRADO DE DOCTOR

PRESENTADA POR

Miriam Aberasturi Vega

Directores
Enrique Solano Márquez
Eduardo Martín Guerrero de Escalante

Madrid, 2016

Identificación y caracterización de estrellas poco masivas y enanas marrones con el Observatorio Virtual

Miriam Aberasturi Vega

Universidad Complutense de Madrid
Departamento de Astrofísica y Ciencias de la Atmósfera
Centro de Astrobiología (INTA−CSIC)
Departamento de Astrofísica

Madrid 2015

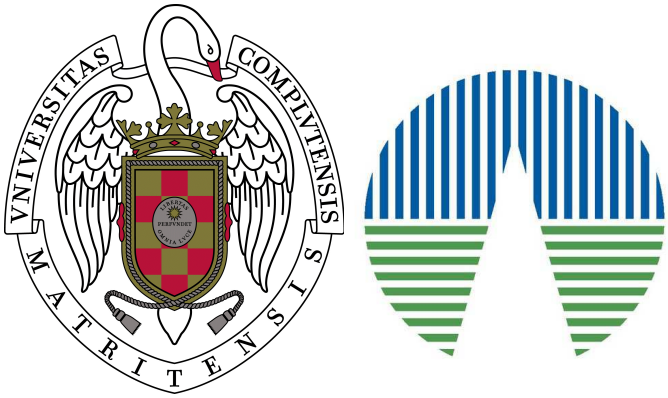

Universidad Complutense de Madrid
Departamento de Astrofísica y Ciencias de la Atmósfera
Centro de Astrobiología (INTA−CSIC)
Departamento de Astrofísica

Identification and characterization of low mass stars and brown dwarfs using Virtual Observatory tools

Memoria presentada por la Licenciada
Miriam Aberasturi Vega
para optar al título de Doctora en Ciencias Físicas.
Trabajo dirigido por los doctores,
Enrique Solano Márquez y Eduardo Martín Guerrero de Escalante

Madrid 2015

A mis abuelos,
Julián Aberasturi,
Asunción Ruiz,
Maria Jesús Crespo y
Francisco Vega

Todo lo que se necesita para que
las fuerzas del mal triunfen
es que los hombres y mujeres buenos
no hagan nada.

Edmund Burke (1729-1797). Político y escritor irlandés.

En mis momentos de duda
me he dicho a mí misma firmemente,
si no soy yo, ¿entonces quién?
si no es ahora, ¿cuándo?

Emma Watson. Septiembre del 2014, discurso en las Naciones Unidas por la igualdad entre hombres y mujeres.
http://www.heforshe.org/

Agradecimientos

Me gustaría dedicar esta tesis a todas las mujeres astronómas, empezando por las que comienzan a tener curiosidad por este campo y terminando por las que por méritos propios y con mucho sacrificio, han conseguido hacerse un hueco y ser consideradas personas referentes en el mundo de la astrofísica. ¡Bravo por ellas!

Gracias a Enrique Solano y Eduardo Martín por aceptarme para realizar esta tesis doctoral bajo su dirección. De manera especial y sincera quiero agradecer a Enrique Solano por brindarme su apoyo y confianza en mi trabajo, y por guiarme no solamente en el desarrollo de esta tesis, sino también en mi formación como investigadora. Sus ideas y su profesionalidad han sido la clave del buen trabajo que hemos realizado juntos, el cual no se puede concebir sin su siempre oportuna participación. Nunca me cansaré de repetirte que sin ti esto no habría pasado. Le agradezco a ambos el haberme facilitado siempre los medios suficientes para llevar a cabo todas las actividades propuestas durante el desarrollo de esta tesis (¡dónde incluyo todo tipo de contratos para poder terminarla!). Muchas gracias a los dos y espero que podamos seguir trabajando juntos.

Quiero expresar también mi más sincero agradecimiento a Benjamín Montesinos por su apoyo en el desarrollo de esta tesis. Debo destacar, por encima de todo, su disponibilidad y paciencia que ha hecho que aprenda muchísimo tanto a nivel científico como personal. No cabe duda que su participación a lo largo de estos años ha enriquecido el trabajo realizado y, además, ha significado el surgimiento de una sólida amistad.

Parte de mi trabajo también es gracias a Adam Burgasser. Thank you very much for you patient and you amazing spirit that you transmit not only in your team but also in your life style. Thank you very much for allowing me to live such an important experience for my training as a researcher. I will always remember my

six months in San Diego.

Quiero dar las gracias al resto de coautores de los artículos que presento en esta tesis, M. Cruz Gálvez, Jose Antonio Caballero, Alcione Mora, Dagny Looper y Neil Reid. Con ellos he tenido la oportunidad de aprender guiándome siempre de sus consejos. Todos forman parte de este trabajo.

También quiero agradecer a TODAS las personas del Centro de Astrobiología, o lo que para mi siempre será el LAEFF. En particular, a Jose Manuel Alacid, Raúl Gutierrez, Almudena Velasco, David Cabezas, María Arévalo, Julia Alfonso y Juan Ángel Vaquerizo por esos mediodías de risas distendidas en el comedor de ESAC. He de reconocer que es uno de los mejores momentos del día. A Nuria Huélamo e Ignacio Mendigutía, por ayudarme en estos últimos coletazos de la tesis. ¡Brindo por los momentos buenos vividos juntos y los que nos quedan por vivir!.

Dejo atrás una de las mejores etapas de mi vida, y aunque empiezo otra con muchísima ilusión, nunca me olvidaré de las maravillosas personas que me encontré aquel marzo del 2007 en un antiguo edificio de obra con goteras. No podría haber caído en un sitio mejor. Gracias por hacer que me sienta tan afortunada.

Y, por supuesto, el agradecimiento más profundo y sentido va para mi familia. Sin su apoyo, colaboración e inspiración habría sido imposible llevar a cabo esta tesis. A mis padres, Paco y Maribel, por su ejemplo de lucha y honestidad; a mi hermana Raquel por hacerme todas esas preguntas sobre mi trabajo con tanto entusiasmo y a Ramón, por escucharme y creer más en mí de lo que creía yo misma. Gracias por estar a mi lado durante todos estos años. A mis amigas de la infancia Ana Paula Tapia, Laura del Castillo, Nuria Jimenez y Sonia González, que aunque vivamos lejos, siempre las he sentido muy cerca de mí. A Esperanza Ibañez, que tanto me entiende y me hace ver las cosas desde otro punto de vista. ¡Gracias por ese apoyo y admiración que me habéis trasmitido siempre!

Contents

List of Figures

List of Tables

Chapter 1

Summary

Context

Two thirds of the stars in our galactic neighborhood (d $<$ 10 pc) are M-dwarfs which also constitute the most common stellar objects in the Milky Way. This property, combined with their small stellar masses and radii, increases the likelihood of detecting terrestrial planets through radial velocity and transit techniques, making them very adequate targets for the exoplanet hunting projects. Nevertheless, M dwarfs have associated different observational difficulties. They are cool objects whose emission radiation peaks at infrared wavelengths and, thus, with a low surface brightness in the optical range. Also, the photometric variability as well as the significant chromospheric activity hinder the radial velocity and transit determinations. It is necessary, therefore, to carry out a detailed characterization of M-dwarfs before building a shortlist with the best possible candidates for exoplanet searches.

Brown dwarfs (BDs) are self-gravitating objects that do not get enough mass to maintain a sufficiently high temperature in their core for stable hydrogen fusion. They represent the link between low-mass stars and giant planets. Due to their low temperatures, BDs emit significant flux at mid-infrared wavelength which makes this range very adequate to look for this type of objects.

The Virtual Observatory (VO) is an international initiative designed to help the astronomical community in the exploitation of the multi-wavelength information that resides in data archives. In the last years the Spanish Virtual Observatory is conducting a number of projects focused on the study of substellar objects taking advantage of Virtual Observatory tools for an easy data access and analysis of large

area surveys. This is the framework where this thesis has been carried out.

This dissertation addresses three problems in the framework of low-mass stars and brown dwarfs, namely, the search for brown dwarf candidates crossmatching catalogues (Chapter 4), the search for nearby bright M dwarfs and the subsequent spectroscopic characterization (Chapter 5), and a study of binarity in mid to late-T brown dwarfs (Chapter 6); the first two topics use Virtual Observatory tools.

Aims and methodology

In the first paper we carried out a search of brown dwarfs in the sky area in common to the WISE, 2MASS Point Source and SDSS catalogues. A VO-workflow with the criteria that must accomplish our candidates was built using STILTS. The workflow returned 138 sources that were visually inspected. For the six new candidates that passed the inspection, proper motions were calculated using the positions and the different observing epochs of the catalogues previously quoted. Effective temperatures were estimated using VOSA and spectral types and distances using appropriate photometric calibrations.

In the second publication we conducted an all-sky photometric search by cross-correlating the Carlsberg Meridian Catalogue (CMC14) and the 2MASS Point Source Catalogue with the aim of increasing the number of known, nearby M dwarfs that could be used as targets for exoplanet searches in general and CARMENES in particular. This VO search was combined with low-resolution spectroscopic follow-up of 27 objects using the IDS spectrograph at the Isaac Newton telescope at La Palma, as well as with an astrometric and photometric study.

In the third paper we attempted to refine the multiplicity properties of T dwarfs studying the largest sample so far observed with high angular resolution imaging. We undertook two parallel programs using the Wide Field Camera 3 (WFC3) installed on the Hubble Space Telescope (HST). We used a PSF-fitting subtraction technique to reveal the presence of any close companion to the sources in our sample. Monte Carlo simulations were carried out to estimate the capability of WFC3 to detect close binaries in terms of angular separation and magnitude difference. Simulations were also used to determine the fraction of binaries that would have been detected around each source based on assumed separations, mass ratio distributions and orientations of the systems.

Results

The main conclusion from this dissertation is that the Virtual Observatory has proved to be an excellent research methodology in the field of low mass stars and brown dwarfs. In particular, it allowed an efficient management of the queries to different catalogues and archives as well as the estimation of physical parameters through VO-tools.

In the first publication we present the identification of 31 brown dwarf (25 known and 6 strong candidates not previously reported in the literature) identified in the sky area in common to WISE, 2MASS and SDSS. This is a remarkable number considering that 2MASS has been extensively searched for ultracool dwarfs and clearly show how new surveys and the use of VO tools can help to mine older surveys. The robustness of our methodology was confirmed with the spectroscopic confirmation of our candidate targets making it an ideal technique to identify brown dwarfs and, by extension, other rare objects.

In the second paper, we show the potential of the VO and a purely photometric approach for finding new bright, nearby M dwarfs that escaped previous surveys mostly based on proper motions. We discover 24 new potential targets for exoplanet hunting (7 at less than 20 pc), 12 of which have been included in the CARMENES input catalogue of M dwarfs. We also identify three young very low-mass stars (M4-M5 spectral types) in the Taurus-Auriga region and a wide (110 AU) binary system.

In the third paper we infer an upper limit for the binary fraction of $>$T5 dwarfs of $<16 - < 25\,\%$ depending of the underlying mass ratio distribution. This binary fraction is consistent with previous estimations. From this work we also conclude that the WFC3 is more sensitive to cool companions than other HST instruments like NICMOS or WFPC2 but its lower angular resolution makes it unsuitable to detect tight brown dwarf binary systems.

Chapter 2

Resumen

Contexto

Dos tercios de las estrellas que se encuentran en nuestra vecindad solar ($d < 10\,pc$) son enanas de tipo espectral M, las cuales también constituyen los objetos más abundantes de la Vía Láctea. Esta característica, junto con el hecho de que son objetos con radios y masas pequeñas, hace que aumente la probabilidad de detectar planetas en zona de habitabilidad, haciendo de ellos objetos muy adecuados para proyectos de búsquedas de planetas extrasolares. Sin embargo, las enanas M tienen asociadas diferentes dificultades observacionales. Por un lado, son objetos fríos cuya máxima emisión electromagnética tiene lugar a longitudes de onda infrarroja y, por lo tanto, débiles en el óptico. Por otro lado, tanto la variabilidad fotométrica como la actividad cromosférica dificultan las detecciones de posibles exoplanetas por métodos de velocidad radial y de tránsito fotométrico. Por tanto, para poder construir una lista con los mejores candidatos para búsquedas de exoplanetas alrededor de enanas M, es necesario llevar a cabo previamente una caracterización detallada de las mismas.

Las enanas marrones son objetos autogravitantes que no tienen la suficiente masa para alcazar la temperatura necesaria para llevar a cabo en su núcleo reacciones de fusión del hidrógeno de forma estable. Las enanas marrones representan, por tanto, la conexión entre las estrellas poco masivas y los planetas gigantes. Debido a sus bajas temperaturas, las enanas marrones emiten mayoritariamente su flujo en el infrarrojo medio, lo que hace de este rango del espectro electromagnético el adecuado para buscar este tipo de objetos.

El Observatorio Virtual (OV) es una iniciativa internacional diseñada para

ayudar a la comunidad astronómica en la explotación de la información multi-rango que reside en los archivos de datos. Aprovechando las herramientas del OV, que permiten un análisis y un acceso fácil a gran cantidad de cartografiados de gran campo, el Observatorio Virtual Español está llevando a cabo una serie de proyectos centrados en el estudio de objetos subestelares. Éste es el marco en el que se inscribe el trabajo de tesis que aquí se presenta.

Este trabajo aborda tres problemas en el marco de las estrellas poco masivas y enanas marrones: la búsqueda de candidatos a enanas marrones utilizando catálogos de grandes cartografiados (Capítulo 2), la búsqueda de enanas M cercanas y brillantes y su caracterización espectroscópica posterior (Capítulo 3), y un estudio de la binariedad de las enanas marrones T de subtipos intermedios y tardíos (Capítulo 4); los dos primeros capítulos estan basados en la utilización de herramientas del Observatorio Virtual.

Objetivos y metodología

En el primer trabajo se realizó una búsqueda de enanas marrones con OV en la zona común del cielo de los catálogos de *W*ISE, 2MASS y SDSS. Utilizando STILTS se impusieron las condiciones fotométricas y astrométricas que debían cumplir nuestros candidatos. Obtuvimos 138 fuentes que fueron inspeccionadas visualmente. Para los seis nuevos candidatos que pasaron la inspección visual se calcularon movimientos propios utilizando las posiciones y las diferentes épocas de observación de los catálogos citados anteriormente. Las temperaturas efectivas se estimaron utilizando VOSA mientras que los tipos espectrales y las distancias se obtuvieron a partir de diferentes calibraciones fotométricas.

Con objeto de aumentar el número de enanas M que pudieran ser utilizadas para la identificación de nuevos exoplanetas, en la segunda publicación se realizó una búsqueda puramente fotométrica utilizando herramientas del OV sobre los catálogos Carlsberg Meridian Catalogue (CMC14) y 2MASS. Esta búsqueda se combinó con un seguimiento espectroscópico de baja resolución utilizando IDS en el telescopio Isaac Newton en La Palma y con un estudio fotométrico y astrométrico.

En el tercer artículo se intentó refinar las propiedades sobre la multiplicidad de enanas T estudiando la muestra más grande observada hasta ahora con imágenes de alta resolución angular. Llevamos a cabo el estudio en dos programas paralelos utilizando la Wide Field Camera 3 (WFC3) instalada en el *T*elescopio Espacial Hubble (HST). Se utilizó una técnica de sustracción PSF para revelar la posible presencia de cualquier compañero cercano a las fuentes de nuestra muestra. Se

llevaron a cabo simulaciones de Monte Carlo para estimar la capacidad de WFC3 para detectar sistemas binarios en términos de separación angular y diferencia de magnitud. Las simulaciones también se utilizaron para determinar la fracción de sistemas binarios que se habrían detectado alrededor de cada fuente en base a diferentes distribuciones de separaciones, relaciones de masa y orientaciones de los sistemas.

Resultados

La principal conclusión de esta tesis es que el Observatorio Virtual ha demostrado ser una excelente metodología de investigación en el campo de las estrellas poco masivas y enanas marrones. En particular, ha permitido una gestión eficiente de las consultas a los diferentes catálogos y archivos, así como la estimación de los parámetros físicos a través de sus herramientas.

En la primera publicación se presenta la identificación de 31 enanas marrones (25 conocidas y 6 candidatos) en el área común del cielo de *W*ISE, 2MASS y SDSS. Estos números representan una cantidad significativa de fuentes teniendo en cuenta que 2MASS ha sido ampliamente utilizado para las búsquedas de enanas ultrafrías, y muestra claramente cómo nuevos cartografiados y el uso de herramientas del Observatorio Virtual pueden ayudar a explotar de manera eficiente cartografiados más antiguos. La solidez de nuestra metodología de búsqueda se demostró con la confirmación espectroscópica de nuestros candidatos, lo que la convierte en una técnica ideal para descubrir de manera eficiente no solamente enanas marrones sino también otros objetos exóticos o difíciles de detectar.

En la segunda publicación, se muestra el potencial del Observatorio Virtual en la búsqueda puramente fotométrica de nuevas enanas cercanas y brillantes de tipo espectral M que quedaron fuera de otros trabajos anteriores basados principalmente en movimientos propios. Descubrimos 24 nuevas enanas M de potencial interés para las búsquedas de exoplanetas (7 a menos de 20 pc). 12 de esos candidatos han sido incluidos en el catálogo de entrada del proyecto CARMENES. También identificamos tres estrellas jóvenes poco masivas (tipos espectrales M4-M5) en la región de formación estelar de Taurus-Auriga y un sistema binario con amplia separación (110 UA).

En la tercera publicación se infiere un límite superior para la tasa de binariedad de tipos espectrales >T5 de $< 16 - < 25\,\%$ dependiendo de la distribución de masas y separaciones subyacente. Esta tasa de binariedad es coherente con las estimaciones anteriores. En este trabajo también se concluye que la WFC3 es más

sensible a la detección de compañeros ultrafríos que otros instrumentos del *HS*T como NICMOS o WFPC2, pero su peor resolución angular lo hace inadecuado para detectar sistemas binarios de enanas marrones con separaciones pequeñas.

Chapter 3

Introduction

Low-mass stars (LM, $<0.6\,M_{\odot}$) are the dominant stellar component of the Galaxy. They constitute $\sim$66% of all objects in the solar neighborhood (Henry et al. 2006[1]), and our knowledge of the Galaxy depends largely on the understanding of these objects. After the first proper-motion surveys in the first decades of the 20th century (van Maanen 1915; Wolf 1919; Ross 1939), the famous catalogs of Gliese (1969), Giclas et al. (1971, 1978), Luyten (1979a,b), Gliese & Jahreiss (1991) and the spectroscopic studies of Kirkpatrick et al. (1991) at the end of the millennium, LM stars were relatively forgotten in the first decade of the current century. However, LM are now again in the focus of the astrophysical community, mainly due to their importance for exoplanets studies as they have proved to be good candidates to host planets in the habitable zone, including super-Earths (Charbonneau et al. 2009; Batalha et al. 2010a; Anglada-Escudé & Tuomi 2012; Muirhead et al. 2012; Bonfils et al. 2013b; Martín et al. 2013).

Going down in the mass scale, the substellar objects appear as brown dwarfs (BDs) and gaseous giant planets. In particular, the BDs fill the gap in mass between very low mass stars (VLM$<0.1\,M_{\odot}$) and the gaseous giant planets. Assuming a solar-metallicity, when BDs are below $0.075\,M_{\odot}$[2], the core temperature and pressure are too low to burn hydrogen stably. As a consequence, BDs, unlike stars, are not dominated by thermonuclear processes becoming cooler and cooler as they age (Burrows et al. 2001).

The interiors of VLM objects are completely convective and are formed by fully ionized plasma of hydrogen, helium and electron gas completely degenerated.

[1] Updated counts provided at www.recons.org.

[2] $1\,M_{\odot} = 1047.56 \pm 0.08\,M_{\rm Jup}$

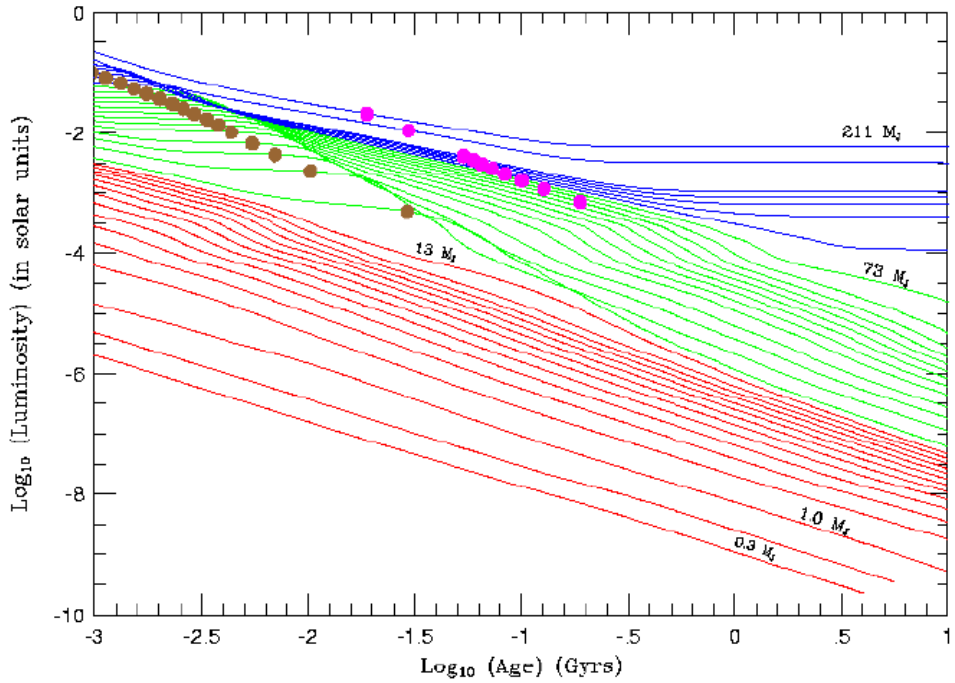

Figure 3.1: Evolution of the luminosity of isolated solar metallicity low-mass stars and substellar mass objects vs. age. Low-mass objects are shown in blue, brown dwarfs under $0.075\,M_\odot$ are shown in green and planets in red. The range of masses portrayed goes from 0.3 to $211\,M_{Jup}$ ($\sim 0.2\,M_\odot$). For a given object, the gold and magenta dots mark when 50 % of the deuterium and lithium have burned, respectively. Figure taken from Burrows et al. (2001).

As it is seen in the Figure 3.1, where the evolution of the luminosity with age for a set of masses ranging from $0.3\,M_{Jup}$ to $211\,M_{Jup}$ is shown, the separation in luminosity between LM stars (in blue) and BDs (in green) occurs at an age older than 1 Gyr. Regarding the lower mass limit, it is still open to debate. Some authors (e.g. Saumon et al. 1996; Chabrier & Baraffe 2000; Burrows et al. 2001) establish that BDs and gaseous giant planets (in red in the Figure 3.1) have different formation mechanisms. One explanation could be that the BDs form by fragmentation and collapse of cold molecular clouds while the gaseous giant planets would form in disks around stars, but the understanding of the complex formation processes for the substellar objects is still poor. A widely-accepted criterion to define the boundary between BDs and the gaseous giant planets is based on the nuclear physics which is determined by the minimum mass for a self-gravitating object to hold stable deuterium fusion inside. For solar composition, such a limit is $13\,M_{Jup}$ (Saumon et al. 1996; Chabrier & Baraffe 2000).

The BD's existence was predicted by Kumar (1962, 1963) and Hayashi & Nakano (1963), but they were not found until 30 years later when two different groups discovered the first BDs, one as companion (GJ 229B orbiting at 45 AU from the M2V star GJ229A; Nakajima et al. 1995) and two belonging to the Pleiades open cluster, Teide 1 and PPL 15 (Rebolo et al. 1995; Stauffer et al. 1994). Their distinct spectral energy distributions are governed by planetary-like molecular gas, condensate grain chemistry, and Li I in absorption for Teide 1 which was the spectroscopic criterion to confirm its substellar nature (Basri et al. 1996; Rebolo et al. 1996) (see Section 3.2). Due to their low effective temperatures ($\sim$3000 K for the youngest and most massive objects, and $\sim$ 250 K for the coolest and smallest ones), the classical spectral classification O, B, A, F, G, K, M had to be extended to include three new spectral types; L dwarfs ($T_{\rm eff}$ $\sim$ 2500 $-$ 1500 K, e.g Kirkpatrick et al. 1999, Martín et al. 1999, Basri et al. 2000 and Leggett et al. 2001), T dwarfs ($T_{\rm eff}$ $\sim$1500 K $-$500 K, e.g. Geballe et al. 2002, Burgasser et al. 2006a and Leggett et al. 2007) and the recently discovered Y dwarfs, $T_{\rm eff}\leq$ 500 K (see Table 3.1), (e.g. Kirkpatrick et al. 1999; Cushing et al. 2011a). Thousands of these low temperature sources ($\sim$1700 dwarfs[3,4]) have been identified over the past two decades in wide-field red optical and near-infrared imaging surveys such as the Two Micron All Sky Survey (2MASS, Skrutskie et al. 2006), the DEep Near Infrared Survey of the Southern Sky (DENIS, Epchtein et al. 1997), the Sloan Digital Sky Survey (SDSS, York et al. 2000), the UKIRT Infrared Deep Survey (UKIDSS, Lawrence et al. 2007), the Canada-France Brown Dwarf Survey (CFBDS, Delorme et al. 2008b) and The Wide-field Infrared Survey Explorer (*WISE*; Wright et al. 2010). Of particular interest are *W*ISE J104915.57$-$531906.1AB, at 2.0 $\pm$ 0.15 pc, being the third closest object to the Sun (Luhman 2013), and *W*ISE J085510.83$-$071442.5 at 2.2 $\pm$ 0.2 pc, being the coldest known BD with $T_{\rm eff}$ = 225-260 K (Luhman 2014; Kopytova et al. 2014; Beamín et al. 2014; Faherty et al. 2014).

The unique properties of VLM stars and BDs have stimulated theoretical advances in star and planet formation (e.g. Padoan & Nordlund 2004; Bate 2009, 2012; Tsuji 2005) , atmosphere modelling (e.g Marley et al. 2010), non-equilibrium chemistry (e.g. Saumon et al. 2006; Hubeny & Burrows 2007), molecular opacities (e.g. Freedman et al. 2008; Yurchenko & Tennyson 2014), condensate grain formation and opacity (e.g. Ackerman & Marley 2001; Helling et al. 2008), dynamics and weather in irradiated and non-irradiated atmospheres (Showman & Kaspi 2013), and magnetic field generation in fully convective objects (e.g. Dobler et al. 2006; Browning 2008), as well as philosophical discussions on the fundamental traits

[3]http://spider.ipac.caltech.edu/staff/davy/ARCHIVE/index.shtml
[4]http://jgagneastro.wordpress.com/list-of-all-known-brown-dwarfs/

that distinguish stars from giant planets (Basri & Brown 2006). VLM stars and BDs objects are now routinely uncovered as binary systems (e.g. Bouy et al. 2003), as isolated field objects (e.g. Kirkpatrick et al. 2000), as members of young open clusters (e.g. Bouvier et al. 1998), and in star-forming regions (e.g. Hillenbrand 1997).

Table 3.1: The Y dwarfs list until June 2015.

Name	SpT	Age (Gyr)	Mass (M_{Jup})	Log g (cm s^{-2})	$\mu_\alpha \cos\delta$ ($'' \, yr^{-1}$)	μ_δ ($'' \, yr^{-1}$)	π ($''$)	d (pc)	Discovery paper
Spectroscopically confirmed									
WISE J0146+4234[a]	Y0	6	31.9±0.1	5.00±0.05	−0.441±0.013	−0.026±0.016	0.094±0.014	10.6±1.5	(1); (6)
WISE J0304−2705	Y0 pec	∼10	2−3	∼4.5	−0.03±0.10	0.65±0.10	...	∼13	(9)
WISE J0350−5658	Y1	...	...	...	−0.125±0.097	−0.865±0.076	0.291±0.050	3.7±1.6	(1), (5)
WISE J0359−5401	Y0	...	...	...	−0.177±0.053	−0.930±0.062	0.145±0.039	5.9±1.3	(1), (5)
WISEPA J0410+1502[a]	Y0	6	25.3±1.8	4.87±0.10	0.974±0.079	−2.144±0.072	0.233±0.056	4.2±1.2	(2), (5)
WISE J0535−7500	≥Y1	...	...	...	−0.310±0.128	0.159±0.092	0.250±0.079	21±13	(1), (5)
WISE J0647−6232	Y1	...	...	...	...	...	0.093±0.013		(13)
WISE J0713−2917[a]	Y0	8	31.5±0.1	5.00±0.00	0.388±0.020	−0.419±0.022	0.106±0.013	9.4±1.2	(1)
WISE J0734−7157	Y0	...	...	...	...	...	...	...	(1)
WISEPC J1217+1626B	Y0	...	...	...	...	...	...	...	(3)
WISP 1305−2538	Y0	...	...	...	...	...	...	∼50	(14)
WISEPC J1405+5534[a]	Y0 pec?	...	∼30	4.5±.25	−2.297±0.096	0.212±0.137	0.133±0.081	>3.4	(2), (5)
SDWES J1433+3518	Y0	...	...	...	...	...	...	...	(14)
WISEPA J1541−2250[a]	Y0.5	<14	30.8±0.0	5.00±0.05	−0.983±0.111	−0.276±0.116	−0.021±0.094	23±1	(2), (5), (6)
WISE J1639−6847	Y0:	...	...	...	3.069±0.04	169.1±0.4	0.200±0.012	...	(4)
WISEPA J1738+2732	Y0	...	∼10–15	∼4.5	0.348±0.071	−0.354±0.055	0.066±0.050	14.6±0.1	(2), (6)
WISEPA J1828+2650[a]	≥Y2	<15	22.0±1.0	5.00±0.05	1.024±0.007	0.174±0.006	0.106±0.007	9.4±0.6	(2); (6)
WISEPC J2056+1459[a]	Y0	10	31.2±0.1	5.00±0.01	0.881±0.057	0.544±0.042	0.144±0.044	7.1±0.5	(2), (6)
WISEJ2209+2711[a]	Y0	<15	22.0±1.0	5.00±0.05	1.217±0.013	−1.372±0.015	0.147±0.011	6.8±0.5	(6)
WISE J2209+2711	Y0	...	...	...	...	...	...	...	(8)
WISE J2220−3628[a]	Y0	8	31.3±1.4	4.99±0.06	0.283±0.013	−0.097±0.017	0.136±0.017	7.4±0.9	(1); (6)
Spectroscopically not confirmed									
WD 0806-661B	Y?	∼1	∼7	...	...	...	...	19.2±0.6	(10)
CFBDSIR J1458+1013B[b]	Y?	1−5	6−15	∼4	...	...	0.433±0.045	23.1±2.4	(11)
WISE J0855-0714	Y?	1−10	3−10	...	−8.06±0.09	0.70±0.07	0.454±0.045	2.20±0.2	(12)

References: (1) Kirkpatrick et al. (2012b); (2) Cushing et al. (2011b); (3) Liu et al. (2012); (4) Tinney et al. (2012); (5) Marsh et al. (2013); (6) Beichman et al. (2014); (7) Kirkpatrick et al. (2011a); (8) Cushing et al. (2014a); (9) Pinfield et al. (2014b); (10) Luhman et al. (2011a); (11) Liu et al. (2011); (12) Luhman (2014); (13) Kirkpatrick et al. (2013); (14) Masters et al. (2012); (15) Eisenhardt et al. (2010)

[a] Ages, masses, T_{eff} and Log g from Morley et al. (2012)

[b] Ages, masses, T_{eff} and Log g from Burrows et al. (2003)

3.1 Very low-mass stars and brown dwarfs formation theories

One of the most fundamental questions about low-mass stars and BDs remains unsettled: How do they form? In the standard model (e.g., McKee & Ostriker 2007), low-mass star formation takes place in molecular clouds which remain in hydrostatic equilibrium as long as the kinetic energy of the gas pressure is in balance with the gravitational force. If the cloud is massive enough, the gas pressure is insufficient to support it and the cloud undergoes gravitational collapse. The critical mass a volume of space must contain before it will collapse under the force of its own gravity is called the Jeans mass. Although widely accepted to explain the formation of low-mass stars, this mechanism does not seem to fit well for BDs as the

lowest Jeans mass than can be achieved is typically an order of magnitude higher than the mass of a BD (Low & Lynden-Bell 1976; Zuckerman & Song 2009).

Two are the main scenarios that have been proposed to explain the formation of BDs: collapse of an interstellar cloud or evolution of a protoplanetary disk.

3.1.1 Formation from the collapse of an interstellar cloud

- **Turbulent gravitational compression.**
  Turbulent compression and fragmentation of gas in a molecular cloud produce collapsing cores over a wide range of masses, including substellar masses if the density fluctuations are large enough (Klessen et al. 2000; Klessen 2001; Padoan & Nordlund 2002, 2004; Hennebelle & Teyssier 2008; Elmegreen 2011, Boss 2001; Bonnell et al. 2008). The mass of each core determines the mass of the resulting object. Low-mass stars and BDs come from the smallest cores.

- **Ejection of protostellar embryos.**
  This scenario suggests that BDs are the result of dynamical interactions in multiple systems which produce the ejection of the least massive component. The mass accretion of the ejected object stops when they leave their parent core, so if the ejection happens early, the mass of these objects would be low (Reipurth & Clarke 2001; Bate et al. 2002; Bate 2009; Bate & Bonnell 2005; Bate et al. 2002, 2003; Umbreit et al. 2005).

- **Photo-erosion of prestellar cores.**
  This mechanism suggests that BDs may be prestellar cores whose outer layers were eroded by the ionising radiation from OB stars (Hester et al. 1996; Whitworth & Zinnecker 2004). According to simulations, this process, only possible in OB associations, requires large fluxes of ionising photons.

3.1.2 Formation from the evolution of a disk

BDs may also form within a circumstellar disk as the giant planets of the Solar System. Gravitational instabilities due to star-disk or disk-disk interactions of massive protostellar disks occurring at early stages might be responsible for the disk fragmentation, producing rocky cores that will grow by accretion to become a brown dwarf. According to simulations, part of these objects would remain bound to the central star whereas the rest of them would be ejected (e.g. Bate et al. 2002, 2003; Rice et al. 2003; Bate & Bonnell 2005; Whitworth & Stamatellos

2006; Goodwin & Whitworth 2007; Offner et al. 2008, 2009; Stamatellos et al. 2007; Stamatellos & Whitworth 2009; Attwood et al. 2009).

3.1.3 Observational constraints on the formation of brown dwarfs

To address the issue regarding the formation of BDs and constrain the above mentioned mechanisms, different lines of research have been carried out in the last years. Assessing which of these mechanisms is dominant, if any, has motivated comprehensive magnetohydrodynamic simulations (e.g., Offner et al. 2008; Bate 2009, 2012); new theoretical ideas in the initial mass function (IMF) and binary evolution (e.g., Chabrier 2002; Thies & Kroupa 2007); observational investigations aimed at measuring the full stellar, BD and free-floating planet mass function in young clusters (e.g., Caballero et al. 2007; Peña Ramírez et al. 2012) and in the field (e.g., Kirkpatrick et al. 2012b), and high angular resolution surveys to derive BD multiplicity properties (e.g., Burgasser et al. 2007b; Dupuy & Liu 2011; Kraus & Hillenbrand 2012). In what follows, I will very briefly describe some of these lines of work.

- **Binary ratio.** The incidence/tightness of binarity provides a clue on BD formation. If BDs form primarily from gas fragmentation, they should show a binary distribution similar to that of stars. This seems to be the case with a smooth transition in the binary properties from the stellar to the BD regime. Also, an important observational constraint for BD formation is the existence of wide binaries (at separations larger than 100 AU, e.g Allen 2007; Radigan et al. 2008, 2009; Luhman et al. 2009b; Burgasser et al. 2009; Duchêne & Kraus 2013; Baron et al. 2015) as the formation of these objects is rather difficult to explain in the disk fragmentation scenario and also pose some questions on the ejection mechanism (Reipurth & Clarke 2001; Bate & Bonnell 2005). Moreover, the claimed excess of wide BD-BD obtained from simulations (Kouwenhoven et al. 2010) can be explained considering that they address the very initial epoch (thousands of years) whereas observations probe present conditions (several Myr's). Interactions occurring between these two epochs will have a strong impact on the observed multiplicity properties, in particular on those of weakly bound systems, making the observed properties to differ substantially from their primordial distribution (e.g. Duchêne & Kraus 2013).

  The BD desert (the lack of companions in the mass range $10-100\,M_{Jup}$ up to a few AU around Sun-like stars) is another relevant observational input for

understanding BD formation (e.g, Dieterich et al. 2012; Grether & Lineweaver 2006 De Lee et al. 2013; Ranc et al. 2015; Evans et al. 2012). The fact that the frequency of companions increases with smaller mass below the desert and with larger mass above the desert points to different formation mechanisms between planetary and stellar companions.

- **Presence/absence of disks.**

  The presence of disks around substellar objects would imply a star-like formation scenario whereas their absence would suggest a planet-like formation mechanism followed by dynamical ejection. Different surveys have been carried out in the last decade to search for disk around young BDs in various environments. Evidences for disks around BDs has been found from the detection of near-infrared excess (e.g. Oliveira et al. 2002, Muench et al. 2002, Jayawardhana et al. 2003, 2006; Liu et al. 2015), from high resolution spectroscopy studies confirming the presence of strong Hα emission lines (Mohanty et al. 2013; Muzerolle et al. 2003, 2005) as well as other emission features such as O I (8446 Å), Ca II (8662 Å), and He I (6678 Å), characteristic of accretion on classical TTauri stars, or from spectral energy distribution model fitting (e.g. Natta et al. 2002). All these observational evidences would argue for a star-like birth process.

- **Mass function.**

  Many studies of IMF for VLM stars and BDs in the field have been carried out using wide-field surveys like 2MASS, SDSS, and UKIDSS (Reid et al. 1999; Chabrier 2002; Cruz et al. 2003; Allen et al. 2005; Metchev et al. 2008; Pinfield et al. 2008; Burningham et al. 2010b; Reylé et al. 2010). See also Kroupa et al. (1993); Kroupa (2001) and Bastian et al. (2010) for reviews on this topic.

  Recent results from the *W*ISE survey strongly support the existence of a "universal" IMF extending continuously from the stellar regime into the BDs and, thus, supporting a scenario in which BDs and stars share the same formation mechanism. Moreover this mass function greatly differs from that of planets implying that planets and BDs do not form the same way (Chabrier et al. 2014).

- **Velocity and spatial distributions.**

  Dynamical interactions can also play an important role in some of the proposed formation mechanisms for VLM stars and BDs. For example, early versions of the ejection mechanism (Kroupa & Bouvier 2003; Reipurth & Clarke

2001) predicted that young BDs should have higher velocities than stars and thus should be more widely distributed.

Nevertheless, radial velocity measurements (e.g. Kurosawa et al. 2006; Joergens & Guenther 2001; Joergens 2006b,a; Kurosawa et al. 2006; White & Basri 2003) and spatial distribution studies (Guieu et al. 2006; Luhman 2006, 2007; Parker et al. 2011 Bayo et al. 2011) seem to indicate that BDs and stars show the same dispersion in velocity. These results are consistent with most of the latest theories for the formation of brown dwarfs (e.g., Bate 2009, 2012).

3.2 The problem of the age: the lithium test

Lithium is rapidly destroyed in the stellar cores according the following P-P chain:

$$p + {}^{6}_{3}Li \longrightarrow {}^{7}_{4}Be \tag{3.1}$$

$${}^{7}_{4}Be + e^{-} \longrightarrow {}^{7}_{3}Li + \nu \tag{3.2}$$

$$p + {}^{7}_{3}Li \longrightarrow {}^{8}_{4}Be \tag{3.3}$$

$${}^{8}_{4}Be \longrightarrow 2{}^{4}_{2}He + energy \tag{3.4}$$

These reactions occur at a core temperature $T_c \sim 2x10^6$ K, below the temperature necessary to fuse hydrogen.

Whereas stars like the Sun can retain lithium in their outer atmospheres, convection in low-mass stars ensures that lithium is depleted in the whole volume of the star. According to theoretical predictions (e.g. Chabrier & Baraffe 2000), objects with $0.06-0.07\,M_{\odot}$ will destroy all their lithium after 100 Myr while less massive objects will retain the original lithium along their lifetime (Figure 3.2). This is the so-called "lithium test" (Magazzu et al. 1992, 1993; Rebolo et al. 1992, 1996) and can be used as a spectroscopic diagnostic to confirm the substellar nature of an object.

The lithium test has been successfully applied to identify substellar objects in clusters. For example, in the Pleiades ($\sim$ 125 Myr), all stars with $T_{eff} < 2500$ K have destroyed their lithium and, thus, any object showing lithium in its spectrum must be a substellar object (e.g. Stauffer et al. 1998). On the other hand, in younger clusters (e.g., Alpha Per and IC2391 (Barrado y Navascués et al. 2002); IC4665 (Manzi et al. 2008); IC2602 (Dobbie et al. 2010); NGC2547 (Jeffries et al. 2013 and Oliveira et al. 2003)), it is possible to find lithium in stars of spectral types K-M which have not had enough time to destroy it.

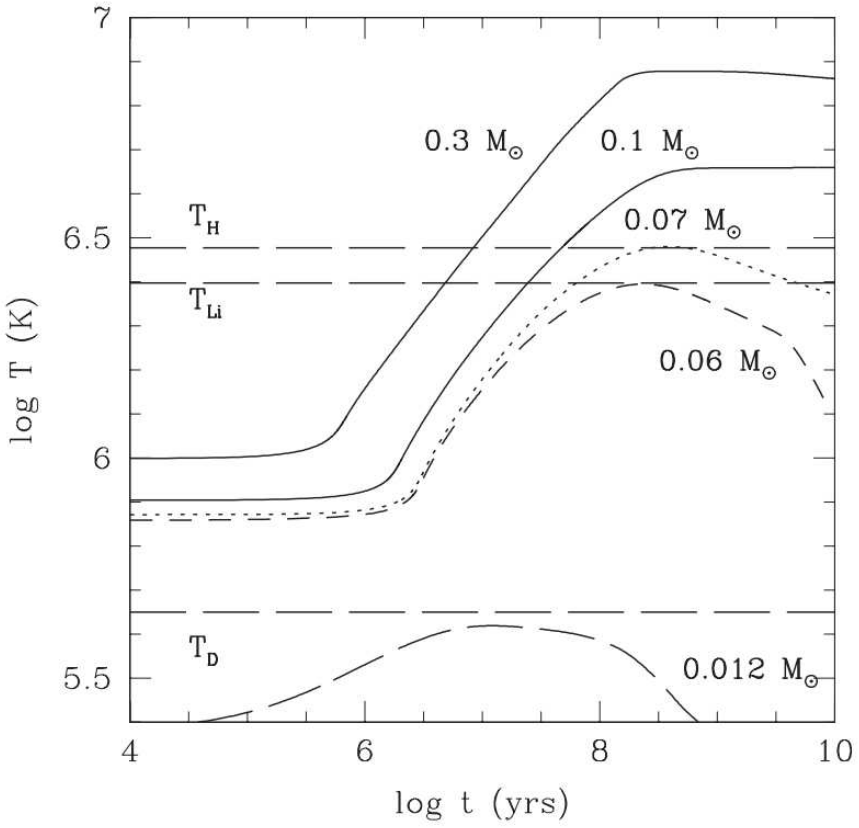

Figure 3.2: Core temperature vs. age for different masses. $T_{\rm H}$, $T_{\rm Li}$ and $T_{\rm D}$ are the burning temperatures for the hydrogen, lithium and deuterium, respectively (Chabrier & Baraffe, 2000) .

3.3 The low-mass tail of the Initial Mass Function

The stellar Initial Mass Function (IMF) is defined as the number of stars N in a volume of space V per mass interval (Miller & Scalo 1979; Scalo 1986b; Salpeter 1955). The IMF is characterized in terms of the power-law $dN/dM \propto M^{-\alpha}$ or $dN/d\log M \propto M^{\Gamma}$, where α=2.35 (Salpeter 1955) and $\alpha = \Gamma + 1$.

The IMF in the solar neighborhood and Galactic disk have been studied by numerous authors (e.g Chabrier 2001;Kroupa 2002; Bochanski et al. 2010; Luhman et al. 2012a), finding that the Salpeter's slope is valid up to $\sim 0.5\ M_{\odot}$. Then it starts to decrease towards the BDs regime (Béjar et al. 2001; Barrado y Navascués et al. 2004; Pinfield et al. 2008; Burningham et al. 2010b; Reylé et al. 2010; Bayo et al. 2011; Lodieu et al. 2011) where it exhibits a slope of $\alpha \sim 0$ (e.g., Reid et al. 1999; Chabrier 2002; Allen et al. 2005; Metchev et al. 2008; Pinfield et al. 2008; Burningham et al. 2010b; Reylé et al. 2010).

Other authors have focused the IMF studies on star forming regions (e.g., Béjar et al. 2001; Briceño et al. 2002; Barrado y Navascués et al. 2004; Moraux et al. 2004; Slesnick et al. 2008; Lodieu et al. 2011). Most of the estimated IMFs are fairly similar with $\alpha \sim 0.5$ at M$\leq$0.2 M$_\odot$. Figure 3.3 depicts the IMF for Taurus (Moraux et al. 2004), Chamaeleon I (Luhman 2007), Pleiades (Luhman et al. 2009a) and the field (Luhman 2012), whose masses were derived using evolutionary models (Baraffe et al. 1998; Chabrier et al. 2000b). Comparing these clusters, Luhman (2012) found a significant variation in the published low-mass star IMFs for the Taurus-Auriga region. This region presents a high peak mass close to K7-M1 stars ($\sim$ 0.8 M$_\odot$), showing a lack of mid-late M dwarf respect to other regions (see Figure 3.3). This means that the IMF in Taurus peaks at a higher mass than the IMF in Chamaleon I and other young clusters, which seem to be more similar among them. Some authors have tried to explain this difference assuming a higher average Jean mass in the Taurus stellar formation (Luhman 2004a, Lada et al. 2008).

The studies in the field and young clusters also indicate that the IMF extends down to, at least, 0.01 M$_\odot$. Zapatero Osorio et al. (2014a) have identified spectroscopically the least massive population in the Pleiades star cluster, allowing to derive the cluster substellar mass function across the deuterium-burning mass limit. Other authors have studied the IMF in this mass range, as for example, Peña Ramírez et al. (2012, 2015) for the σ Orionis cluster, Lodieu et al. (2013b) for Upper Scorpius and Zapatero Osorio et al. (2014a,b) for the Pleiades, but their samples are affected by large uncertainties in spectral types, ages and masses (e.g. Alves de Oliveira et al. 2013; Mužić et al. 2014).

Finally, it is noted that the overall characteristics of the IMF are well reproduced by the VLM stars and BDs different formation theories (see Section 3.1) and, thus, cannot be used as an indicator to discriminate among them. Studies along all range of masses (-2$<$ log m [M$_\odot$] $<$ 2) have been done in order to study the shape and universality of the IMF (see review of Bastian et al. 2010, Figure 3)

3.4 Spectral and photometric properties

3.4.1 Spectral characterization

Spectral characterization refers to the process of classifying an astronomical object based on its spectral characteristics. For M-spectral types and later, the traditional method of determining physical parameters from high-resolution spectra of weak

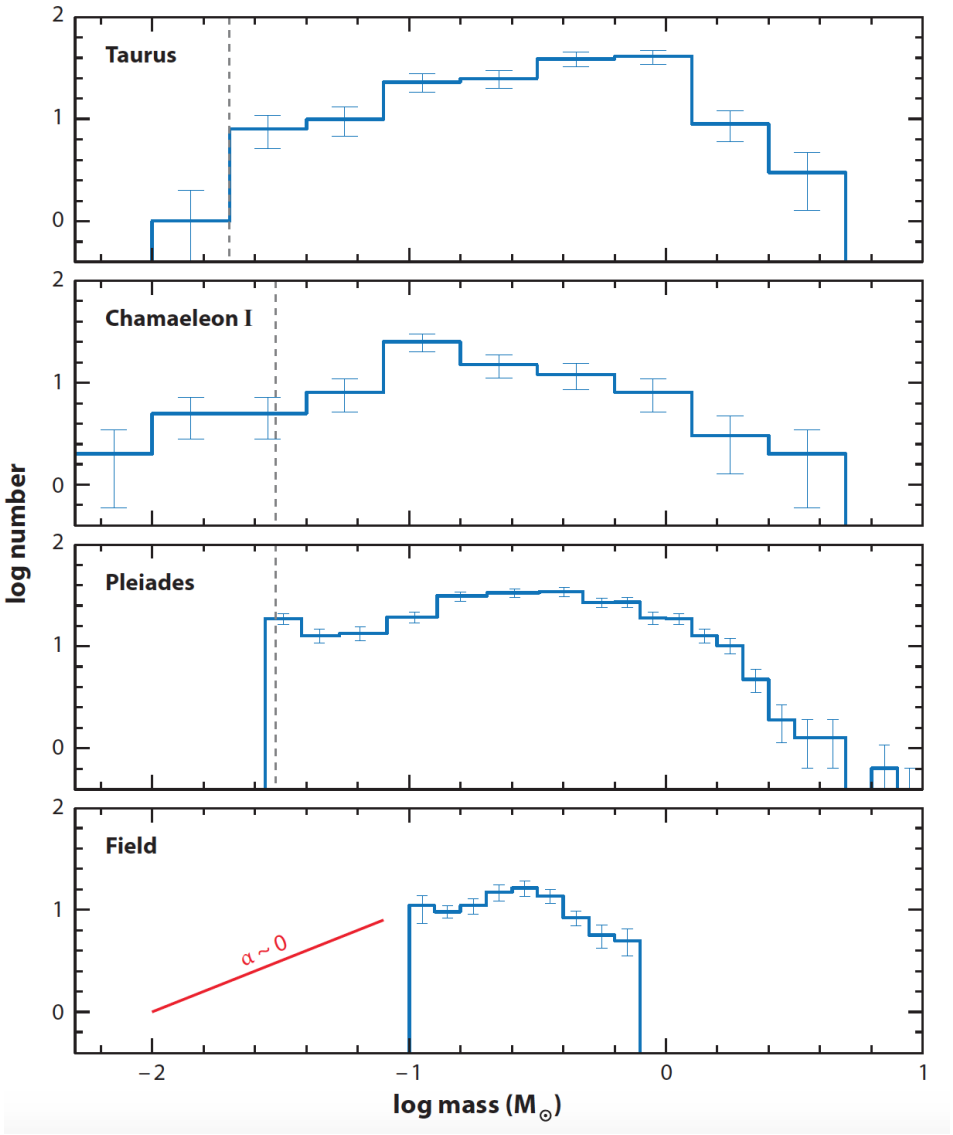

Figure 3.3: Initial Mass Function for Taurus, Chamaleon I, the Pleiades and the field (Bochanski et al. 2010; Luhman 2007; Luhman et al. 2009a; Moraux et al. 2004). Figure extracted from Luhman (2012). The completeness limits of the cluster samples are indicated by dashes lines.

atomic lines is inapplicable due to the complex absorption features of diatomic and triatomic molecules existing in the spectra of these objects. These features are typically asymmetric and very broad, leaving only a few narrow spectral bands, apparently, clear of absorption. Nevertheless, the comparison with model atmospheres (e.g. Allard 2014) indicates that even these regions are depressed from the true continuum. A solution to this problem is to define a number of flux ratios as line indices to quantify these molecular features (e.g. Reid et al. 1995). These indices are calibrated by reference to previously classified objects and offer

the advantage of providing accurate determinations without the need for a visual comparison of the spectra with others. An alternative approach is described in Martín et al. (1996) who use indices defined as ratios between the average flux at two different pseudocontinuum regions. A third, complementary, method is the comparison to standard stars with known properties or theoretical templates to infer spectral types or physical parameters as effective temperatures, luminosities and abundances (Bochanski et al. 2011; Savcheva et al. 2014).

M dwarfs

The optical spectra of M dwarfs are characterized by the presence of strong absorption bands of titanium and vanadium oxides (TiO, VO). The TiO bands increase in strength from being barely discernible at type K7 to dominating the optical spectrum at the latest M types and are, therefore, a good temperature and spectral type indicator over the range $\sim$ K7 to M6/M6.5 (Kirkpatrick et al. 1991, 1999; Martín et al. 1999). The most prominent features of titanium oxides can be found at 6600 – 6800 Å, 7050 –7250 Å, 7590 – 7680 Å, 7670 –7860 Å, 8430 – 8450 Å, and 8860 – 8940 Å (see left panel of Figure 3.4).

The Vanadium oxides begin to dominate for M5 and later types and are also a good temperature indicators (Kirkpatrick et al. 1993). The most prominent absorption bands appear at 7330 – 7530 Å, 7850 – 7970 Å, and 8520 – 8670 Å. Other interesting species is the CaH at 6400 and 6800 Å which becomes more prominent with decreasing metal abundance and is, therefore, useful in identifying halo subdwarfs and metal-poor disk dwarfs (e.g. Gizis 1997). Regarding the infrared range (Fig. 3.4, right panel), the most obvious temperature-dependent feature is the H_2O at 1.35 μm and a number of sharp absorption features at 1.169, 1.177, 1.243 and 1.252 μm due to K I. H_2O band (1.14 μm), FeH (1.2 μm) can be used as age-dependent features (Manjavacas et al. 2014). Also the triangular shape observed in the H-band and alkali lines represents a characteristic feature of young objects (e.g.,Zapatero Osorio et al. 2000; Lucas et al. 2001; McGovern et al. 2004; Meeus & McCaughrean 2005; Lodieu et al. 2008; Cruz et al. 2009).

L dwarfs

Both TiO and VO weaken rapidly beyond M-types into the L sequence (Kirkpatrick et al. 1999). As the effective temperature decreases below 2400 K (Chabrier et al. 2000b), TiO and VO lose their prominence due to dust grain condensation. Other elements

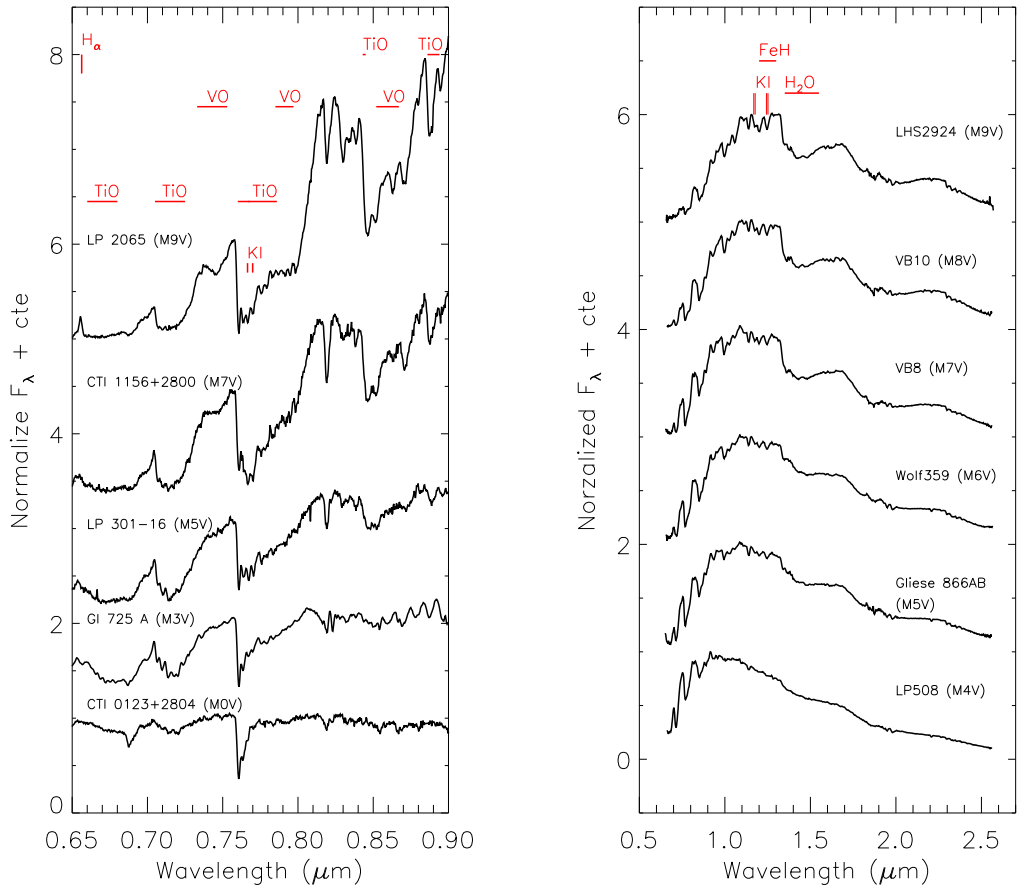

Figure 3.4: Optical (left) and near-infrared (right) spectra for M dwarf sample from the Brown Dwarfs Archive (http://spider.ipac.caltech.edu/staff/davy/ARCHIVE/index.shtml) and The SpeX Prism Spectral Libraries (http://pono.ucsd.edu/∼adam/browndwarfs/spexprism/), respectively.

with lower condensation temperatures such as the alkali metals and the hydrides FeH and CrH are relatively unaffected, favouring their detection. The most prominent features in the optical spectra of L dwarfs are: CrH (8611 and 9969 Å), FeH (8692 and 9896 Å), Na I (8183/8195 Å), K I (7665/7699 Å), Rb I (7800 /7948 Å), Cs I (8521 and 8943 Å), and Li I at 6708 Å. FeH, K I and Na I can be used as age-sensitive indices (Kirkpatrick et al. 2008; Cruz et al. 2009; Manjavacas et al. 2014).

Two schemes have been proposed for the optical classification of L dwarfs (Kirkpatrick et al. 1999 and Martín et al. 1999). The first scheme is based on several spectral indices which characterize the strength of oxides (TiO and VO) and metallic hydrides and neutral alkali, whereas the second one relies on the so-called PC3 spectral index (8230−8270/7540−7580) and a temperature scale based on the

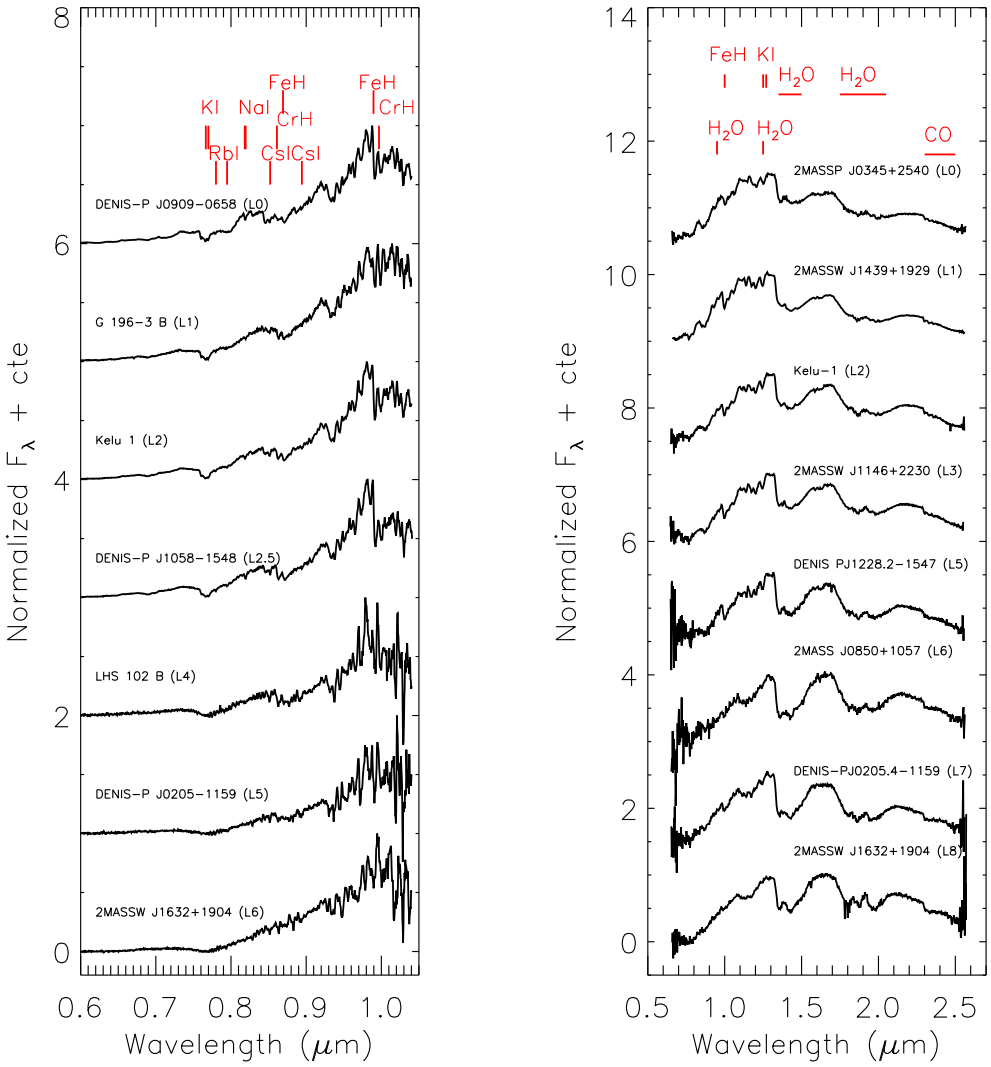

Figure 3.5: Optical (left) and near-infrared (right) spectra for L dwarfs sample provided by The SpeX Prism Spectral Libraries (http://pono.ucsd.edu/∼adam/browndwarfs/spexprism/) and libraries of stellar spectra (http://pendientedemigracion.ucm.es/info/Astrof/invest/actividad/spectra.html), respectively.

comparison with atmosphere models. Both classification systems produce similar results for early-Ls slightly diverging for late-Ls.

Near infrared spectra of L dwarfs are dominated by H_2O at $\sim$0.95 μm, $\sim$1.15 μm, 1.35−1.50 μm and 1.75−2.05 μm, as well as by the CO band head at 2.3 μm (e.g Kirkpatrick 2000, see Figure 3.5).

T dwarfs

The transformation of L dwarfs into T dwarfs is a major topic of interest due to the dramatic changes that occur in the spectra of objects lying in the L6 - T5 region over a small range of temperatures ($T_{eff} \approx 1100-1400$ K, e.g. Vrba et al. 2004; Leggett et al. 2008; Burgasser et al. 2013). These changes can be ascribed to the combination of two effects: a) the rapid removal of condensate clouds from the photosphere. As we move towards later spectral types, the dust clouds fall deeper in the atmosphere until they drop below the photosphere and the atmosphere appears cloud-free. This provoques that warm L dwarfs become redder in their $J-K$ colours; and b) the change from CO to CH_4 as the dominant carbon molecule.

In addition to the dust settling, there is another challenge for the modeling of the L6-T5 dwarfs: The non-monothonic behaviour of the $1.0-1.3\,\mu$m fluxes which appear brighter than earlier objects at T3-T5 spectral types, a phenomenon known as the J-band bump (e.g. Dahn et al. 2002; Tinney et al. 2003; Burgasser et al. 2010). This phenomenon has been attributed to dynamic atmospheric processes, such as condensate cloud fragmentation (Burgasser et al. 2002b), a sudden increase in sedimentation efficiency (Knapp et al. 2004) or a global collapse of the condensate cloud layer (Tsuji 2005). Tsuji & Nakajima (2003) have also argued that age and/or surface gravity effects could also play an important role. Nevertheless, the analysis of binary systems of similar ages and surface gravities (due to the nearly constant radii of old (>0.5 Gyr) substellar objects and the prevalence for brown dwarf binaries to have mass ration near unity), largely rules out this hypothesis (Burgasser et al. 2006b).

Although most of the T dwarfs flux is emitted in the infrared ($\sim$75 %), there is also an optical classification for these objects based on the strength of the K I red wing and the 0.9250 μm H2O band (Burgasser et al. 2003a). Regarding the near infrared, spectra of T dwarfs (see Figure 3.6) are mostly shaped by strong H_2O (1.11-1.6 μm, 1.35-1.45 μm, and 1.77-2.03 μm) and CH_4 (1.30-1.50 μm, 1.60-1.80 μm, and 2.20-2.50 μm bands), features that are stronger as the temperature decreases. Strong K I doublets at 1.17, 1.25 and 1.45 μm as well as the Na I doublet at 2.21 μm are also present. The flux suppression longwards of 2.0 μm due to H_2 collision−induced absorptions (CIA) (Saumon et al. 1994; Borysow et al. 1997) is another spectral characteristic of T-dwarfs.

Spectral indices are also used to classify T dwarfs. Burgasser et al. (2006a) provided nine T dwarf spectral standards with subtypes ranging from T0 to T8. The authors defined five spectral indices that measure the depths of the CH_4 and

H_2O bands which can be used as proxies for direct comparisons.

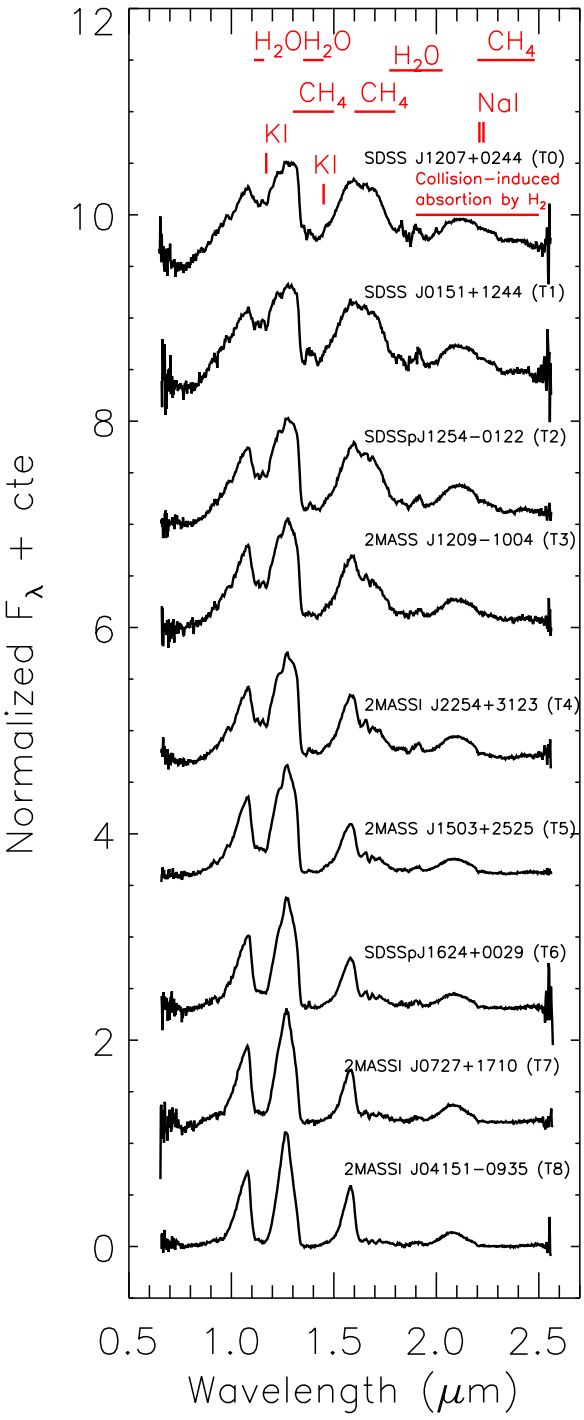

Figure 3.6: Near-infrared spectra for T dwarfs sample provided by The SpeX Prism Spectral Libraries (http://pono.ucsd.edu/∼adam/browndwarfs/spexprism/).

Y dwarfs

Theoretical models predict that as BDs cool below $T_{\rm eff}$<600 K, their atmospheres pass through a series of chemical transitions which in turn impact the appearance of their emergent spectra. At $T_{\rm eff} \sim 600$ K, we witness the appearance of NH_3 bands in the near-infrared. This is the spectral feature suggested as the trigger for the Y spectral class although their identification has proven difficult because they overlap with the strong H_2O bands and because the abundance of NH_3 can be reduced by an order of magnitude due to vertical mixing in the atmosphere (Cushing et al. 2011b). In practice, a significant decrease in the width of the J-band flux peak compared with a T9 spectral standard becomes the practical means to separate late-T and Y dwarfs. At $T_{\rm eff}$<500 K, the prominent resonance absorption lines of Na I and K I in the red optical spectra of warmer BDs weaken as Na condenses out of the gas phase into Na_2S and K condenses into KCl. Finally, H_2O and NH_3 will also condense out at $T_{\rm eff} \sim 350$ K and ~ 200 K, respectively forming clouds and depleting these species from the gas phase.

At the time of writing only 21 Y dwarfs have been spectroscopically confirmed (see Table 3.1). The spectral classification for these objects has been done both comparing the region of *J*-band and *H*-band flux peaks with late-T dwarf standards and using spectral indices (see Figure 3.7): H_2O-J, CH_4-J, H_2O-H, CH_4-H (Burgasser et al. 2006a); W_j (Warren et al. 2007b); NH_3-H (Delorme et al. 2008a) or *J*-wing (Pinfield et al. 2014c).

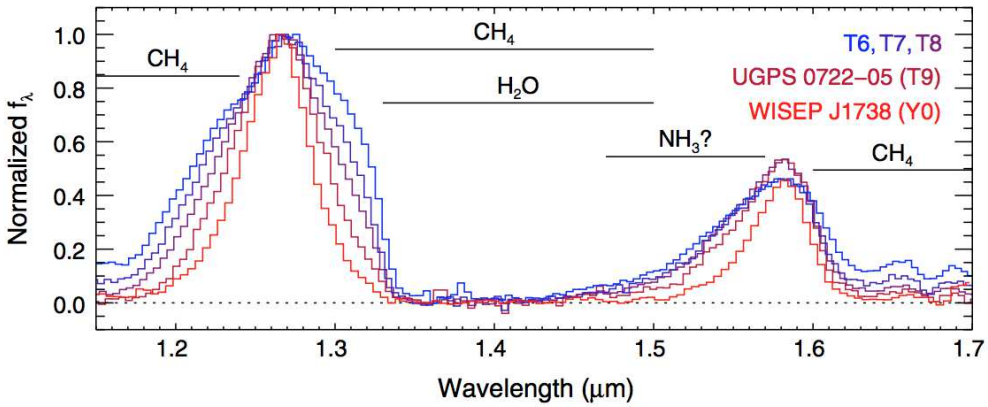

Figure 3.7: IRTF/SpeX spectrum of UGPS 0722−05 and WFC3/HST spectrum of WISEP J1738+2732 (Cushing et al. 2011b). IRTF/SpeX spectra of SDSS J162414.37+002915.6 (T6), 2MASS J07271824+1710012 (T7), and 2MASS J04151954−0935066 (T8) of Burgasser et al. (2006a). The spectra have been normalized to unity. Prominent molecular absorption bands are indicated.

3.4.2 Photometric characterization

The large-area, deep optical and infrared surveys conducted in the last decade have provided an accurate photometric characterization of VLM stars and BDs which allows to distinguish them from other astronomical sources (e.g.,Delorme et al. 2008b, Delorme et al. 2008a, Reylé et al. 2014 using CFHT data; Deacon et al. 2011a, 2014 or Aller et al. 2013 using Pan-STARRS data; and Lodieu et al. 2007a; Scholz et al. 2012; Leggett et al. 2012; Liu et al. 2011; Burningham et al. 2011; Burningham et al. 2010b; Goldman et al. (2010) using UKIDSS data). In this section, we will focus on 2MASS, SDSS, *S*pitzer/IRAC and *W*ISE photometry to characterize VLM stars and BDs. Figure 3.8 shows the filter passbands of the photometric systems utilized in some of these surveys.

Leggett et al. (2000b, 2002) and Hawley et al. (2002) studied for the first time the characterization of M, L and T dwarfs in the SDSS. Colour criteria were focused on the r', i', z' bands as the typical red colours of these objects make a significant fraction of them not be detected in the u' and g' filters. As shown in Figure 3.9, $(i' - z')$ is a useful spectral type indicator increasing from early M into the T regime although it shows some flatness at $\sim$ 1.8 between M9 an L5. Leggett et al. (2012) presented optical and near infrared colours for a sample composed majority by T dwarfs. This work concludes that $(i' - z')$, $(z' - Y)$, and $(z' - J)$ colours of T dwarfs are very red, and continue increasing through the late-type T dwarfs, with a hint of a saturation for T8/10 types. Y dwarf identification using the z' band has been done with GTC/OSIRIS (Lodieu et al. 2013a). West et al. (2005, 2008), using photometric and spectroscopic SDSS data, also provided colour vs. spectral type relations for M dwarfs. There are another works which combine SDSS and 2MASS photometry to characterize M dwarfs (Covey et al. 2007) and to characterize L and T dwafs combining SDSS, UKIDSS LAS, and WISE data (Skrzypek et al. 2015).

Kirkpatrick et al. (1999), using 2MASS data, gave the first infrared characterization of L-dwarfs. They show that $J - K_s$ increases from late M through late L before turning blue for T dwarfs. A similar behaviour is found for $J - H$, a good indicator for L-dwarfs but quite flat in the M dwarf regime (see Figure 3.10).

The *Spitzer Space Telescope*[5] opened the exploration of the mid-infrared, region where the coolest BDs emit most of their flux: At $T_{\rm eff}$ =1000 K, 30 % of the total flux is emitted at wavelengths longer than 3 μm, while at 600 K 60 % of the flux is emitted in that region (e.g Leggett et al. 2009, 2010, 2011). Patten et al. (2006) (see Figure 3.11) reported the trend of various colour indices against M, L, T spectral

[5]http://irsa.ipac.caltech.edu/data/SPITZER/docs/irac/

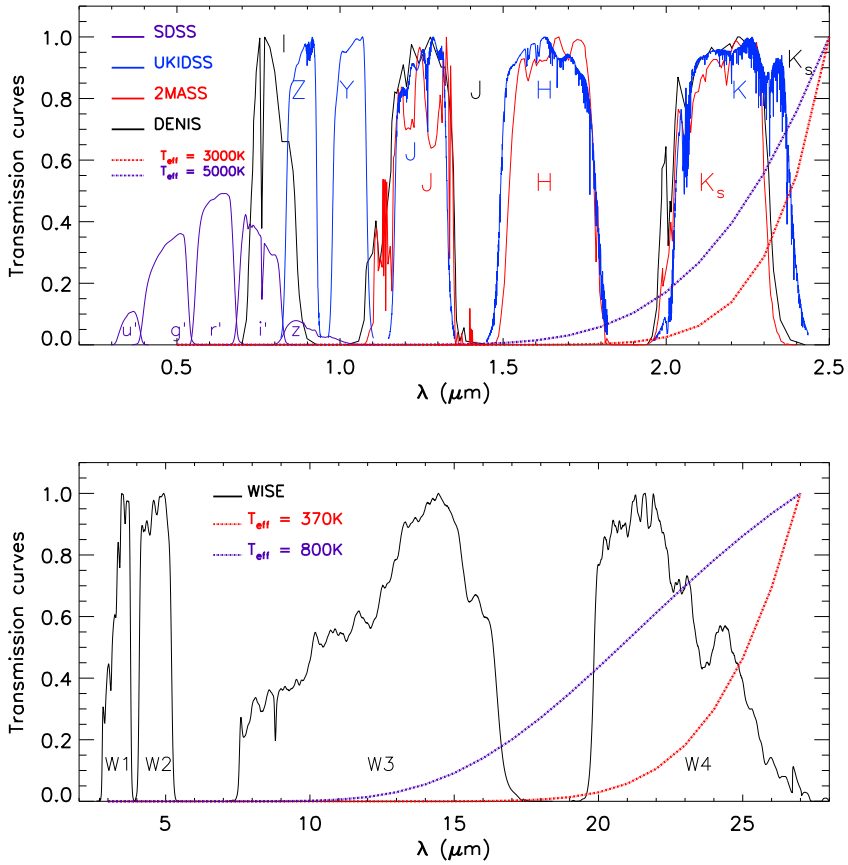

Figure 3.8: Optical and near-mid infrared filters along with black body curves for T_{eff} = 370, 800, 3000 and 5000 K.

types. Good correlation with spectral type is found for [3-6]-[4.5] and K_s-[4.5] colour indices. The first one shows a slow blueward trend through the M and early L types turning redward at mid-L due to the appearance of CH_4 absorption in the IRAC 3.6 μm bandpass). Smoother is the variation of K_s-[4.5] with the spectral type, going redward as the spectral type increases due to the onset of CH_4 absorption and CIA H_2 in the K_s band . In both cases, the redward trend is also favoured by the large amount of flux emerging in the 4.5 μm window as spectral types increases.

WISE (Wright et al. 2010) colour indices are proved to be very useful to identify cool (>T0) BDs. Kirkpatrick et al. (2011a) show the resulting trend of *WISE* $W1 - W2$ colour as a function of spectral type (Figure 3.12). Similar to what happens with [3.6]-[4.5], there is a slow increase in W1–W2 between early-M and early-L and a rapid increase at types later than T0. Although this trend makes the colour index a good indicator for cool dwarfs, red $W1 - W2$ colours are not unique for BDs. Dust-obscured galaxies (DOGs) and asymptotic giant branch stars (AGBs) are

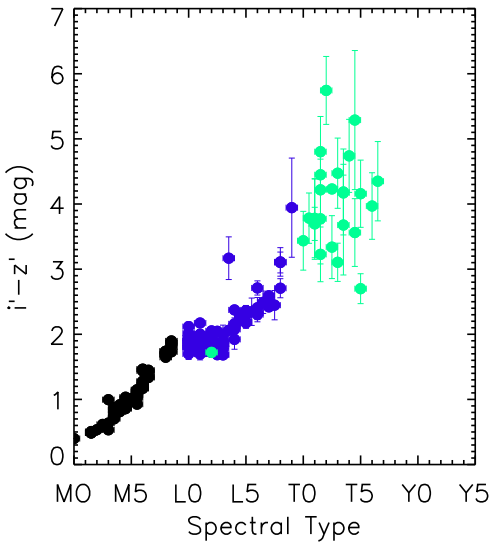

Figure 3.9: $(i' - z')$ colour vs. spectral type for the Kirkpatrick et al. (2011a) sample.

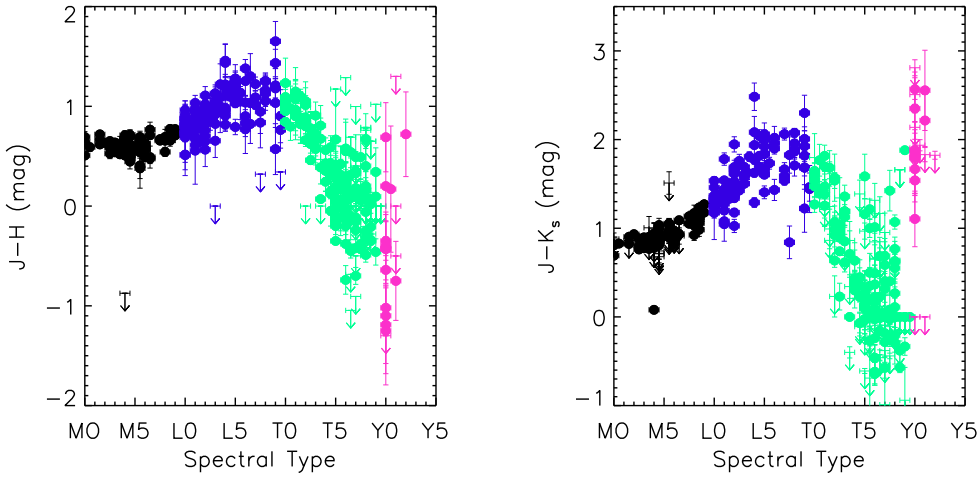

Figure 3.10: $J - H$ and $J - K_s$ colour vs. spectral type for the Kirkpatrick et al. (2011a) sample and the Y dwarfs sample given in Table 3.1.

other sources falling in the same area. As Eisenhardt et al. (2010) (see their Figure 1) showed using *Spitzer* data, it is necessary to use another colour combination to distinguish BDs from the abovementioned contaminants. In particular, T dwarfs show W2–W3 colours bluer than DOGs and AGBs being this colour index useful to separate both populations with $W1 - W2 > 0.96(W2 - W3)$ - 0.96 as the dividing line (Kirkpatrick et al. 2011a). Other colour combinations like $J - W2$ and $H - W2$ can also be useful to identify cool BDs with colours dramatically increasing beyond

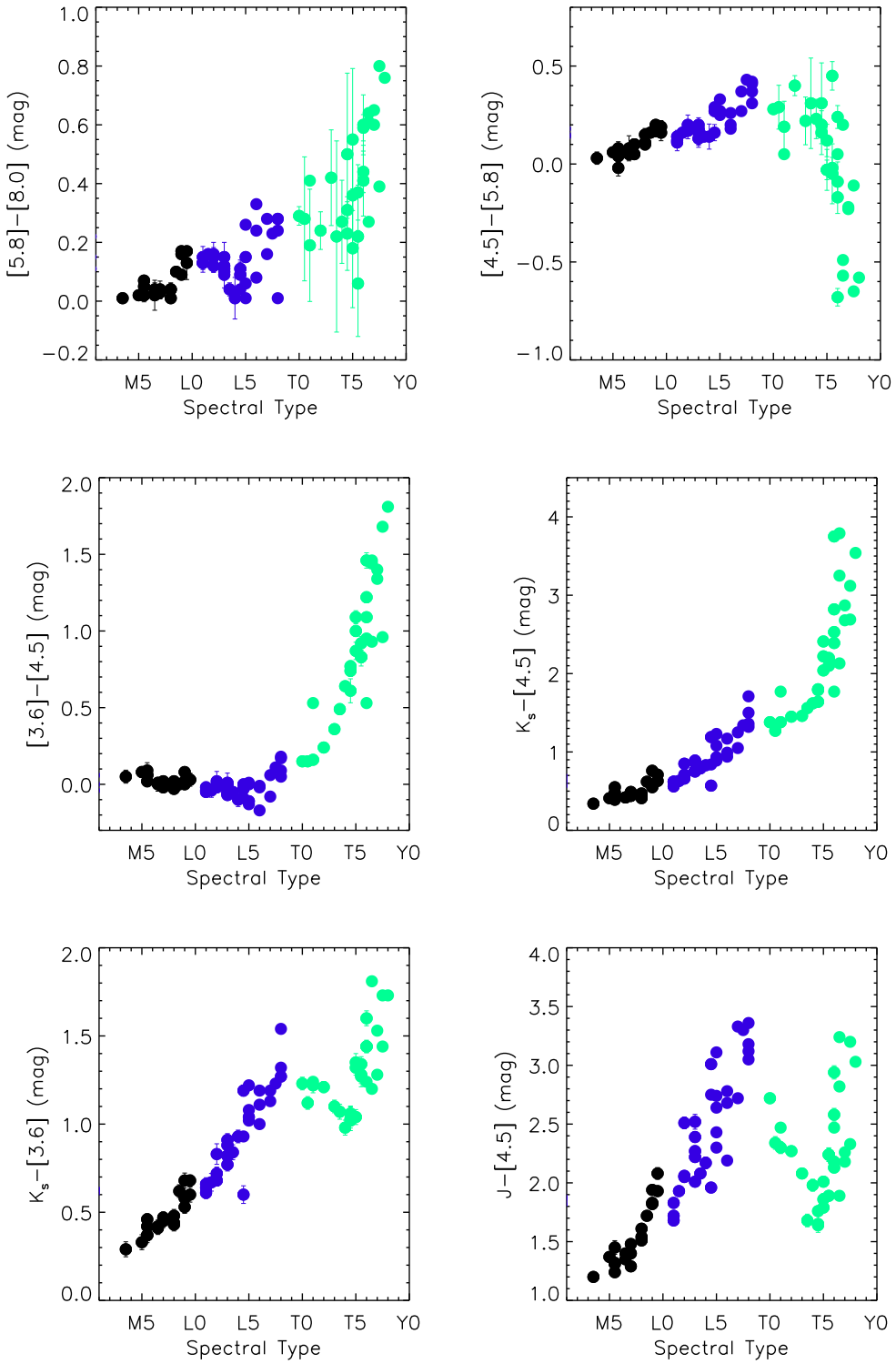

Figure 3.11: Near-mid infrared colours vs. spectral type for Patten et al. (2006) sample.

T5 (Figure 3.13).

A combination of some of these colour indices was used in this work to identify BDs using *WISE*, 2MASS and SDSS data (Chapter 4) and nearby M dwarfs using Carlsberg Meridian Catalogue 14 (CMC14[6]; Copenhagen University et al. 2006) and 2MASS (Chapter 5).

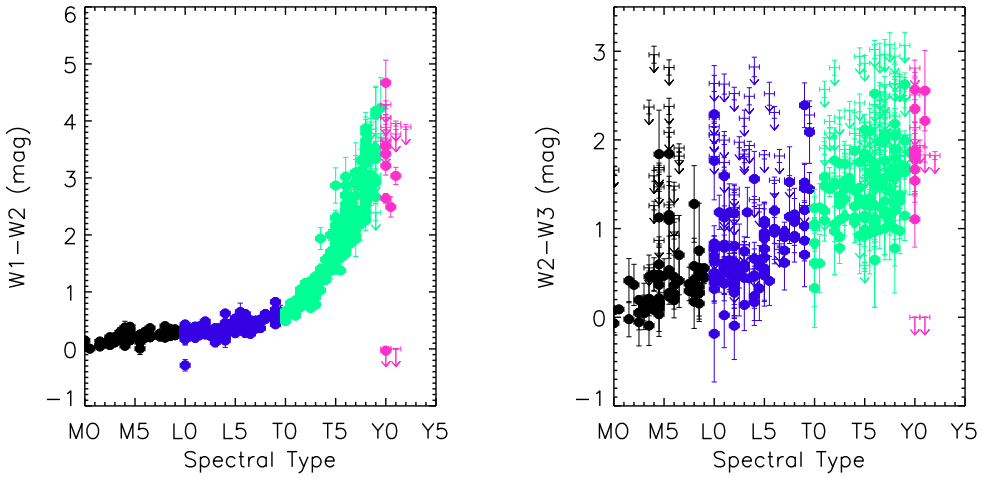

Figure 3.12: $W1 - W2$ and $W2 - W3$ colours vs. spectral types for the Kirkpatrick et al. (2011a) and the Y dwarfs sample given in Table 3.1.

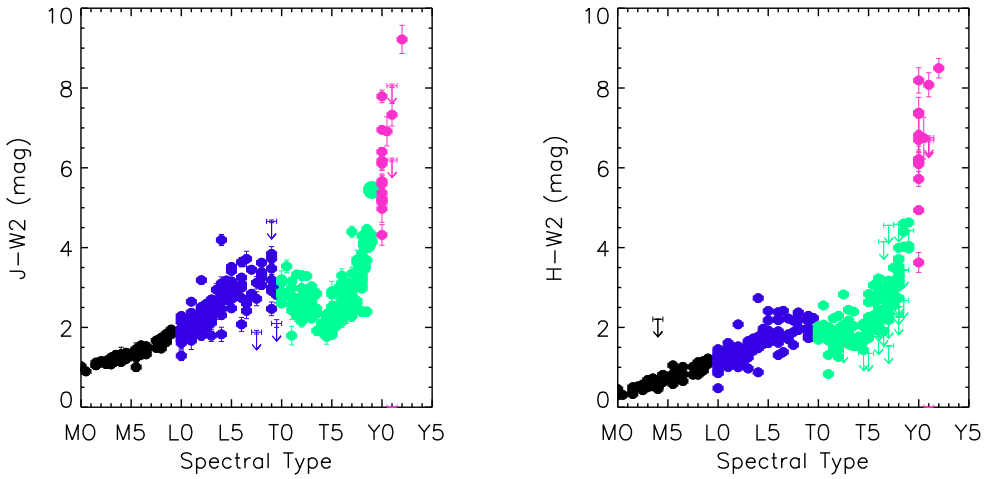

Figure 3.13: $J - W2$ and $H - W2$ colour vs. spectral types for the Kirkpatrick et al. (2011a) sample and the Y dwarfs sample given in Table 3.1.

[6] http://www.ast.cam.ac.uk/∼dwe/SRF/cmc14.html

Table 3.2: List of brown dwarfs with dynamical mass measurements.

Object	Region	Mass $M_\odot$	SpT	Radius $R_\odot$	Method	Reference
GJ 569 Ba	field	0.055−0.087	M8.5	...	Radial velocity	(1)
GJ 569 Bb	field	0.034−0.070	M9	...	Radial velocity	(1)
J05352184−0546085A	Orion	0.0541±0.0046	...	0.669±0.034	Radial velocity and transit	(2)
J05352184−0546085B	Orion	0.0340±0.0027	...	0.511±0.026	Radial velocity and transit	(2)
GJ 802B[a]	field	0.063±0.005	mid-late L	...	Radial velocity	(3)
LHS 6343C[a]	field	0.063±0.0024	...	0.833±0.021	Radial velocity and transit	(4)
HR7672B[a]	field	0.068±0.002	L4.5±1.5	...	Radial velocity	(5)
DENIS-P J0823−4912A	field	0.028±0.063	L1.5	...	Radial velocity	(6)
DENIS-P J0823−4912B	field	0.018±0.045	L5.5	...	Radial velocity	(6)
DENIS- J0630−1840A	field	0.086±0.009	M8.5	...	Radial velocity	(7)
DENIS- J0630−1840B	field	0.06 or 0.075[b]	L1.5	...	Radial velocity	(7)
PPl15 A	field	0.070±0.003	M6	...	Radial velocity	(8)
PPl15 B	field	0.060±0.003	M7	...	Radial velocity	(8)
MOA-2007-BLG-192L	field	0.062-0.120[c]	M	...	Microlensing	(9)
MOA-2007-BLG-192Lb	field	0.8-14.8[c,d]	...	...	Microlensing	(9)
2MASSW J0746+2000A	field	0.085±0.010	L0±0.5	...	Radial velocity	(10)
2MASSW J0746+2000B	field	0.066±0.006	L1.5±0.5	...	Radial velocity	(10)
Gl 417BC	field	0.099±0.003	L4.5+L6	...	Radial velocity	(11)

References: (1) Zapatero Osorio et al. (2004); (2) Stassun et al. (2006); (3) Ireland et al. (2008); (4) Johnson et al. (2011); (5) Crepp et al. (2012); (6) Sahlmann et al. (2015a); (7) Sahlmann et al. (2015b); (8) Basri & Martín (1999); (9) Kubas et al. (2012); (10) Bouy et al. (2004b); (11) Dupuy et al. (2014)

[a] I only report the mass for the substellar object in the system.

[b] The secondary mass has two allowed mode in the mass velocity curve.

[c] Range of mass values at 2σ range.

[d] Earth mass.

3.5 Multiplicity

Since the first discovery of a T dwarf as companion of an early-M dwarf (Gl229B, Nakajima et al. 1995), a large number of new VLM star and BD binary systems have been detected with different methods. Searches for systems whose mass of the primary is $M_1 < 0.1\,M_\odot$ (corresponding to spectral types $\geq$M6), have been conducted predominantly through high resolution imaging surveys (e.g., Bouy et al. 2003; Burgasser et al. 2003b; Gizis et al. 2003; Bouy et al. 2006b; Burgasser et al. 2011a; Gelino et al. 2011; Dupuy & Liu 2012a; Aberasturi et al. 2014a), and laser guide star adaptive optics observations (AO) (e.g., Close et al. 2003b; Siegler et al. 2005; Liu et al. 2012). A smaller number of high resolution spectroscopic surveys for closely separated binaries have also taken place (e.g, Basri & Martín 1999; Joergens & Guenther 2001; Reid et al. 2002; Guenther & Wuchterl 2003; Kenyon et al. 2005; Joergens 2006b; Burgasser et al. 2012). Likewise, microlensing techniques have been used in several studies (e.g, Choi et al. 2013; Shin et al. 2012; Han et al. 2013).

At time of manuscript, dynamical masses have been obtained for 9 systems (see Table 3.2).

As it is summarized in Burgasser et al. (2007b), Luhman (2012) and Duchêne & Kraus (2013), in addition to the measurement of dynamical masses, the current multiplicity studies of VLM stars and BDs include aspects about the binary fraction as function of mass in the field and open clusters, the separation and mass ratio distributions with primary mass and impact of binary systems on the IMF, to name a few.

Table 3.3: Binary fractions for very low-mass stars and brown dwarfs.

Author	Spectral/Mass Range	Region	d (pc)	Binary Fraction (%)	ρ (AU)
High angular resolution imaging surveys					
Reid & Gizis (1997b)	M5-L0	Hyades	∼47	11.3±4.6	14−825
Bouy et al. (2006b)	M5-L5	Pleiades	∼135	$13.3^{+13.7}_{-4.3}$	>7
Gizis et al. (2003)	M5-L5	field	136	15±5	1.6−16
Bouy et al. (2003)	M5-L8	field	20	∼15	1−8
Law et al. (2006)	M5-M8	field	40	$7^{+7}_{-3.0}$	1−5
Kraus et al. (2005)	M5.5-M7	Upper Sco	∼145	33±17	4−18
Bouy et al. (2006a)	M5.5-M7.5	Upper Sco	∼145	5^{+6}_{-2}	>18
Todorov et al. (2014)[a]	>M6	Taurus	∼150	4^{+3}_{-1}[a]	>10
...	...	Chamaeleon I	∼160	...	...
...	...	Upper Sco	∼145	...	...
Siegler et al. (2003)	M6-M7.5	field	∼30	5^{+4}_{-2}	3−10
Siegler et al. (2005)	M6-M7.5	field	≤30.0	9^{+4}_{-3}	≥3.0
Martín et al. (2003)	M6-M9	Pleiades	∼135	15^{+15}_{-5}	7−12
Close et al. (2003a)	M8-L0.5	field	35	19±7	>2.6
Biller et al. (2011)	<M8	Upper Sco	∼145	<9 %	10−500
Close et al. (2002)	M8-M9	field	30	14−24	>3.0
Pope et al. (2013)	M9-L8	field	19	$17.2^{+5.7}_{-3.7}$	>1.0
Reid et al. (2001)	L2-L8	field	30	20±10	1.6−7.6
Reid et al. (2008)	L8-T1	field	20	12^{+5}_{-3}	>3.0
Radigan et al. (2013)	L9-T4	field	35	13^{+7}_{-6}	0.3−3.5
Burgasser et al. (2006b)	T0-T8	field	30	12^{+7}_{-4}	1.0−5
Burgasser et al. (2003b)	T5-T8	field	20	9^{+15}_{-4}	≥1.0
Aberasturi et al. (2014a)[b]	≥T5	field	20	<16	>5.2
Aberasturi et al. (2014a)[c]	≥T5	field	20	<25	>5.2
Lodieu et al. (2012a)	0.075−0.03 $M_\odot$	Pleiades	∼135	25.6±4.5	100-200
Garcia et al. (2015)	0.025−0.04 $M_\odot$	Pleiades	∼135	$\lesssim$26[e]	$\gtrsim$4
Kraus & Hillenbrand (2012)	0.07−0.15 $M_\odot$	Taurus	∼150	21^{+7}_{-6}	∼5−10
Kraus et al. (2006)	0.015−0.12 $M_\odot$	Taurus	∼150	9^{+10}_{-3}	>4
Konopacky et al. (2007)	0.04−0.2 $M_\odot$	Taurus	∼150	18±4	4−100

Table 3.3. Continued.

Author	Spectral/Mass Range	Region	d (pc)	Binary Fraction (%)	ρ (AU)
Ahmic et al. (2007)	0.075−0.1 $M_\odot$	Chamaeleon I	∼160	11^{+9}_{-6}	$\lesssim$50
High resolution spectroscopic surveys					
Reid et al. (2002)	M7−M8.5	field	...	6.0^{+7}_{-2}	...
Guenther & Wuchterl (2003)	M5.5−L1.5	field	...	12.0^{+10}_{-4}	<3
Kenyon et al. (2005)	<0.1 $M_\odot$	σ Orionis	∼352	7-19	<1
Joergens (2006b)	<0.1 $M_\odot$	Chamaeleon I	∼160	11.0^{+18}_{-4}	<3
Maxted & Jeffries (2005)[d]	<0.1 $M_\odot$	field, σ Orionis and Cha I	...	17-30	<2.6
Maxted & Jeffries (2005)[d]	<0.1 $M_\odot$	field, σ Orionis and Cha I	...	32-45	> 2.6

[a] Combined previous high-resolution imaging surveys for Taurus, Chamaeleon I and Upper Sco regions.

[b] Assuming power law mass ratio distribution .

[c] Assuming flat mass ratio distribution.

[d] Monte-Carlo simulation with Joergens 2005, Kenyon et al. (2005) and Guenther & Wuchterl (2003) samples.

[e] At 2 σ

In Table 3.3 most of the surveys conducted with high spatial imaging and spectroscopy to look for VLM star and BD binary systems are listed. We can see how the binary fraction decreases as primary masses decrease (Duquennoy et al. 1991; Fischer & Marcy 1992; Bouy et al. 2003; Burgasser et al. 2003b; Close et al. 2003b;Basri & Reiners 2006; Bergfors et al. 2010).

The minimum separation in binary systems is typically given by the angular resolution of the imagers and AO techniques. Microlensing is, nevertheless, more sensitive at shorter separations. Recently, Choi et al. (2013) discovered two binary systems with total masses of 0.025 $M_\odot$ and 0.034 $M_\odot$, and projected separations of 0.31 AU and 0.19 AU, making them the lowest-mass and tightest field BD binaries known so far. Figure 3.14 shows the projected ρ and q for the VLM star and BD binary systems listed in Table 3.4.

In Figure 3.14, the left panel distribution seems to peak at $\sim$ 3-10 AU, where ∼50% of the sample is located. Some authors have studied the sharp decline on the right side of the histogram, estimating a binarity ratio of 2−8 % for separations ranging ρ>11−150 AU in open clusters covering different ages (Martín et al. 2003; Luhman 2005). The right panel of the Figure 3.14 indicates that BDs binaries tend to favor equal-mass systems with q>0.8 (∼68% of the Table 3.4)

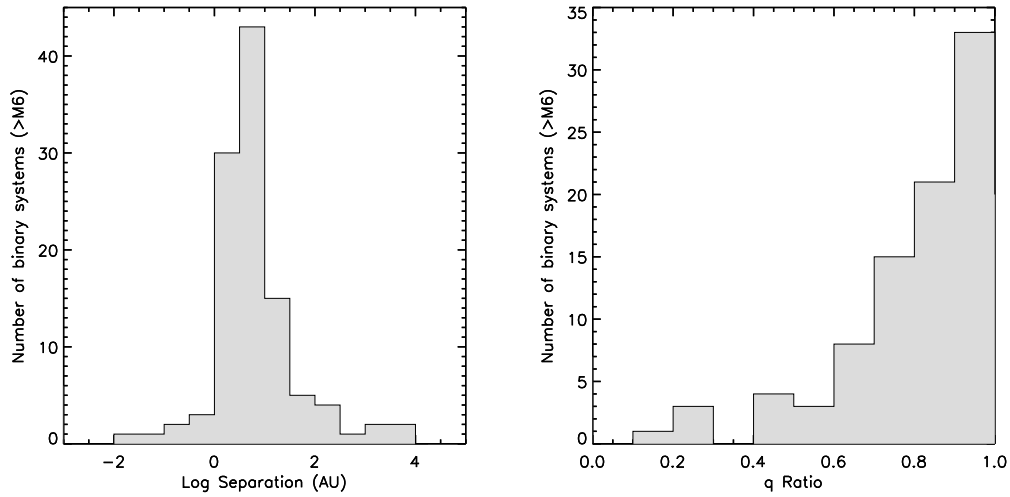

Figure 3.14: Left panel: Distribution of separations/orbital semimajor axes for known VLM star and BD binary systems (>M6). All of them are listed in the Table 3.4. Only field binary systems with known separation measurements are included in the plot. The distribution peaks at $\sim$ 3-10 AU, with steep declines at shorter and longer separations. **Right panel:** Mass ratio distribution of known VLM star and BD binary systems (>M6). Only field binary systems with mass ratio measurements are included in the plot. The distribution peaks close to the unity.

Table 3.4: List of known >M6, L and T binary systems.

Name	Separation ρ (AU)	Separation ρ ($''$)	Distance d (pc)	SpT A	SpT B	q	Location	Binary reference
WT 460	5.9±1.8	511.0±1	11.6±3.5	M6	L1	0.62	field	Montagnier et al. (2006)
2MASS J2113−1009	0.0±0.0	0.0±0.0	12.5±2.5	M6	M6	1?	field	Guenther & Wuchterl (2003)
USco CTIO-66	10.2±0.2	70.0±1	145.0±2.0	M6	M6	1.00	USco	Kraus et al. (2005)
USco CTIO-109	4.9±0.3	34.0±2	145.0±2.0	M6	M7.5	0.57	USco	Kraus et al. (2005)
MHO -Tau-8	6.2±1.1	44.0±8	142.0±3.0	M6	M6.5	0.70	Taurus	Kraus et al. (2006)
ChaHa8	1.3±0.2	0.0±0.0	168.0±10.0	M6	-	0.20	ChaI	Joergens (2006b)
2MASS J1258+4013	6700±800	63380.0±50	105.0±13.0	M6	M7	0.87	field	Radigan et al. (2009)
CFHT-Tau-18	31±1	216.0±2	142.0±3.0	M6	M9?	0.60	Taurus	Konopacky et al. (2007)
CFHT-Tau-7	32±1	224.0±2	142.0±3.0	M6	M7?	0.86	Taurus	Konopacky et al. (2007)
LHS 1901	4.0±0.3	275.0±5	11.0±1.1	M6.5	M7.5	0.96	field	Montagnier et al. (2006)
2MASS J0535−0546	0.04±0.0	0.0±0.0	435.0±55.0	M6.5	M6.5	0.63	Orion	Stassun et al. (2006)
2MASS J0126−5022	5100±400	81860.0±100	63.0±5.0	M6.5	M8	0.97	field	Artigau et al. (2007)
Koenigstuhl-1	1800±170	77760.0±70	23.0±2.0	M6:	M9.5	0.77	field	Caballero (2007b)
LSR 1610−0040	0.6±0.2	8.91±0.31	32.3±0.1	M6pec	L/T	0.60	field	Dahn et al. (2008)
PPl 15	0.03±0.0	0.0±0.0	134.0±4.0	M7	M8	0.86	Pleiades	Martín et al. (2006)
2MASS J0952−1924	0.0±0.0	0.0±0.0	0.0±0.0	M7	M7:	1?	field	Reid et al. (2002)
LP 415-20	3.6±0.6	119.0±8	30.0±5.0	M7	M9.5	0.83	Hyades	Siegler et al. (2003)
IPMBD 25	12.6±0.5	94.0±3	134.0±3.0	M7	L4	0.62	Pleiades	Martín et al. (2003)
2MASS J1101−7732	241.9±0.0	1440.0±0.0	168.0±10.0	M7	M8	0.50	ChaI	Luhman (2004b)
2MASS J1847+5522	1.9±0.3	82.0±5	23.0±4.0	M7	M7.5	0.96	field	Siegler et al. (2005)
USco-CTIO-108	670±17	4600.0±100	450.0±2.0	M7	M9.5	0.23	USco	Béjar et al. (2008)
2MASSW J1750+4424	4.9±1.0	158.0±5	31.0±6.0	M7.5	L0	0.88	field	Siegler et al. (2003)
LP 475-855	8.5±1.5	294.0±5	29.0±5.0	M7.5	M9.5	0.88	Hyades	Siegler et al. (2003)
2MASS J1311+8032	7.7±1.3	267.0±6	29.0±5.0	M7.5	M8	0.98	field	Close et al. (2003b)
2MASS J0429−3123	5.8±1.1	531.0±2	11.0±2.0	M7.5	L1	0.84	field	Siegler et al. (2005)
HD 65216B	5.9±0.4	167.0±11	35.6±0.9	M7.5	L2.5	0.88	field	Mugrauer et al. (2007)
CFHT-Pl-18	34.6±0.0	330.0±0.0	105.0±0.0	M8	M8	1.00	field	Bouy et al. (2003)
2MASS J0253+2713	0.0±0.0	0.0±0.0	0.0±0.0	M8	M8:	1?	field	Reid et al. (2002)
LHS 2397a	3.0±0.1	207.0±7	14.6±0.4	M8	L7.5	0.76	field	Freed et al. (2003)
CFHT-Pl-12	8.3±0.3	62.0±2	134.0±3.0	M8	L4	0.70	Pleiades	Caballero (2007c)
2MASS J1127+7411	8.4±1.5	246.0±8	34.0±6.0	M8	M9	0.95	field	Close et al. (2003b)
2MASS J2206−2047	4.5±0.8	168.0±7	26.7±4.5	M8	M8	0.99	field	Close et al. (2003b)
2MASS J1426+1557	4.0±0.7	152.0±6	26.1±4.5	M8	L1.5	0.86	field	Close et al. (2003b)
2MASS J1047+4026	2.8±0.5	122.0±8	23.0±4.0	M8	L0	0.91	field	Close et al. (2003b)
LP349-25	1.3±0.2	125.0±0	10.1±1.2	M8	M9	0.94	field	Forveille et al. (2005)
DENIS J2200−3038	38.2±3.0	1090.0±60	35.0±2.0	M8	L0	0.98	field	Burgasser & McElwain (2006)
2MASS J2331−0406	15.0±0.4	573.0±8	26.2±0.6	M8.5	L7	0.72	field	Bouy et al. (2003)
LHS1070B	3.4±0.2	446.0±29	7.4±0.3	M8.5	M9	0.97	field	Leinert et al. (2001)
2MASSJ1207334-393254	41.1±4.7	776.0±8	53.0±6.0	M8.5	L:	0.17	TWA	Chauvin et al. (2004)
DENISJ055146.0-443412.2	220.0±44.3	2200.0±50	100.0±20.0	M8.5	L0	0.93	field	Billères et al. (2005)
SCR 1845−6357	4.5±0.03	1170.0±3	3.85±0.02	M8.5	T6	0.44	field	Biller et al. (2006)
2MASS J0320−0446	8.3±0.0	0.33±0	25.0±3.0	M8.5	T5	0.79	field	Burgasser & Blake (2009)
2MASS J0147−4954	6.3±1.2	190.0±0.0	33.0±6.0	M8:	L2:	0.95	field	Reid et al. (2006a)
DENIS-P J0357−4417	2.2±0.0	98.0±3	22.2±0.0	M9	L1.5	0.91	field	Bouy et al. (2003)
2MASS J2140+1625	4.0±0.7	155.0±5	25.6±4.4	M9	L2	0.85	field	Close et al. (2003b)
2MASS J1707−0558	15.2±2.7	1010.0±170	15.0±1.0	M9	L3	0.93	field	Burgasser et al. (2004)
2MASS J1622−2405	243±55	1943.0±22	125.0±25.0	M9	M9.5	0.88	Oph	Jayawardhana & Ivanov (2006)
GJ 569B	0.90±0.01	103.0±1	9.8±0.2	M9.0	M9.0	0.76	Urs Maj MG	Kenworthy et al. (2001)
DENIS-P J1004−11464	6.8±0.1	146.0±3	46.8±0.0	M9.5	L0.5	0.95	field	Bouy et al. (2003)
LSPM 1735+2634	3.2±0.3	290.0±0.0	11.0±1.0	M9:	M9:	0.90	field	Law et al. (2006)
WISE J0720−0846	0.84±0.17	139±14	6.0±1.0	M9.5	T5	0.87	field	Burgasser et al. (2015)
			L/L binaries					
2MASS J1449+2355	8.5±...	134.0±3	63.7±0.0	L0	L3	0.89	field	Bouy et al. (2003)
2MASS J2147+1431	7.0±...	322.0±3	21.8±0.0	L0	L2	0.93	field	Bouy et al. (2003)
2MASSW J0746+2000	2.5±...	220.0±...	12.2±0.04	L0	L1.5	0.78	field	Reid et al. (2001)
DENIS-PJ185950.9-370632	7.7±0.0	60.0±0.0	129.0±11.0	L0	L3	0.90	R-CrA	Bouy et al. (2004a)
2MASS J1600+1708	3.5±...	57.0±3	60.6±0.0	L1	L3	0.96	field	Bouy et al. (2003)
DENIS-P J1441–0945	14.3±...	420.0±...	34.0±7.0	L1	L1	1.00	field	Bouy et al. (2003)
IPMBD 29	7.8±0.6	58.0±4	134.0±3.0	L1	L4	0.84	Pleiades	Martín et al. (2003)
2MASS J1520–4422	22±2.0	1174.0±16	19.0±0.0	L1.5	L4.5	0.94	field	Kendall et al. (2007a)
SDSS 2335–0013	3.5±...	57.0±3	62.0±0.0	L1:	L4:	0.94	field	Bouy et al. (2003)
2MASSW J1017+1308	3.4±0.5	104.0±3	33.0±5.0	L2	L2	1.00	field	Bouy et al. (2003)
2MASS J1146+2230	7.9±0.2	290.0±3	27.2±0.6	L2	L2	1.00	field	Reid et al. (2001)
Kelu-1	5.4±0.2	291.0±2	18.7±0.7	L2	L4	0.92	field	Liu & Leggett (2005)
2MASSW J1430+2915	2.6±0.1	88.0±3	29.4±0.0	L2:	L3:	0.99	field	Bouy et al. (2003)
2MASS J0700+3157	2.1±0.7	170.0±...	12.2±4.0	L3.5	L6:	0.85	field	Reid et al. (2006a)
HD 130948 B	2.4±0.1	134.0±5	17.9±0.3	L4	L4	0.86	field	Potter et al. (2002)
2MASS J0025+4759	10.2±2.0	330.0±2	31.0±6.0	L4	L4	0.98	field	Reid et al. (2006a)
2MASS J1112+3548	1.5±0.3	70.0±3	21.7±4.2	L4.5	L6	0.96	field	Bouy et al. (2003)
2MASS J0004–4044	1.0±0.3	87.0±6	15.0±3.0	L4.5	L4.5	1.00	field	Golimowski et al. (2004a)

Table 3.4. Continued.

Name	Separation (AU)	Separation ($''$)	Distance (pc)	SpT A	SpT B	q	Location	Binary reference
2MASS J1239+5515	4.5±0.1	211.0±3	21.3±0.0	L5	L5	1.00	field	Bouy et al. (2003)
DENIS-P J0205–1159	9.2±0.8	510.0±40	18.0±0.8	L5	L6	1.00	field	Koerner et al. (1999)
2MASS J2132+1341	1.8±0.3	66.0±4	28.0±4.0	L5	L7.5	0.96	field	Siegler et al. (2007)
2MASS J0856+2235	3.4±...	98.0±9	34.7±0.0	L5:	L8:	0.90	field	Bouy et al. (2003)
DENIS-PJ1228.2-1547	6.4±0.2	251.0±10	20.2±0.8	L6	L6	1.00	field	Martin et al. (1999)
;2MASS J2255–5713	1.6±0.2	138.0±41	11.6±3.1	L6	L8	0.95	field	Reid et al. (2008)
2MASS J2152+0937	6.0±1.2	250.0±2	24.2±5.0	L6:	L6:	1.00	field	Reid et al. (2006a)
2MASSW J2101+1756	7.8±0.9	234.0±3	33.2±3.8	L7	L8	0.96	field	Bouy et al. (2003)
2MASS J0915+0422	10.8±2.2	730.0±2	14.8±3.0	L7	L7	1.00	field	Reid et al. (2006a)
2MASS J0850+1057	132±5	5.0±0.8	36±6	L7	L7	...	field	Burgasser et al. (2011a)
2MASS J1728+3948	158±5	3.8±0.3	24.1±1.9	L5	L6.5	...	field	Burgasser et al. (2011a)
SIMP J1501–0135AB	30±5.0	960±	44±7	L4.5	L5.5	...	field	Artigau et al. (2011b)
2MASS 0036+1821	0.39±...	44.5±1.2	8.77±0.06	L4	L5-6	1.0	field	Pope et al. (2013)
2MASS 0045+1636	...	50.3±0.7	26.8±4.0	L0	L0	1.0	field	Pope et al. (2013)
2MASS 2028+0052	...	45.8±1.2	26.1±3.9	L3	L4	1.0	field	Pope et al. (2013)
2MASS 2351-2537	...	63.3±0.3	17.8±2.7	L0	L1	0.8	field	Pope et al. (2013)
			L/T binaries					
SDSS J0805+4812	...	...	14.6±2.5	L4.5	T5	0.88	field	Burgasser (2007b)
2MASS J0920+3517	1.5±...	70.0±...	20.8±3.0	L6.5	T:	1.00	field	Reid et al. (2001)
SDSS J0423–0414	2.5±0.07	164.0±2	15.2±0.4	L6.5	T2	0.78	field	Burgasser et al. (2005b)
2MASS J2252–1730	1.9±0.4	140.0±2	13.6±3.2	L6:	T2:	0.87	field	Reid et al. (2006b)
2MASS J0518–2828	1.8±0.5	51.0±12	34.0±6.0	L6:	T4:	0.74	field	Burgasser et al. (2006b)
Gl337 C	10.9±0.7	530.0±30	20.5±0.4	L8	T:	1.00	field	Burgasser et al. (2005a)
WISE J1049–5319	...	...	2.0±0.3	L8	T1.5	1.00	field	Luhman (2013)
2MASS 1936-5502	...	67.1±6.4	15.8±1.2	L4	T-Y	...	field	Pope et al. (2013)
			T/T binaries					
epsilonIndiB	2.6±0.01	732.0±2	3.6±0.01	T1	T6	0.60	epIndiA	McCaughrean et al. (2004a)
SDSS J1021–0304	5.0±0.7	172.0±5	24.5±6.6	T1	T5	0.84	field	Burgasser et al. (2006b)
2MASS J1404–3159	3.1±0.4	133.6±.6	23.0±3.0	T1	T5	0.75	field	Looper et al. (2008)
SDSS J1534+1615	4.0±...	110.0±5	36.0±0.0	T1.5	T5.5	0.80	field	Liu et al. (2006)
SIMP J1619+0313	15.4±2.1	691.0±2.0	22.0±3.0	T2.5	T4	...	field	Artigau et al. (2011b)
SDSS J0926+5847	2.6±0.5	70.0±6	38.0±7.0	T4:	T4:	0.87	field	Burgasser et al. (2006b)
2MASS J1534–2952	2.3±0.5	171.0±34	13.6±0.2	T5	T5	0.94	field	Burgasser et al. (2003b)
WISE J1841+7000	2.8±0.7	70.0±14.0	40.2±4.9	T5	T5	1.00	field	Gelino et al. (2011)
WISE J0612–3036	11±2	350±5	31±6	T6	T6	...	field	Huélamo et al. (2015)
2MASS J1225–2739	3.8±0.1	282.0±5	13.4±0.4	T6	T8	0.73	field	Burgasser et al. (2003b)
2MASS J1553+1532	4.2±0.7	349.0±5	12.0±2.0	T6.5	T7	0.88	field	Burgasser et al. (2006b)
WISE J1711+3500	15.0±2.0	780.0±2.0	19.0±3.0	T8	T9.5	0.46	field	Liu et al. (2012)
WISE J0458+6434	5.0±0.4	510.0±20.0	10.5±1.4	T8.5	T9	...	field	Mainzer et al. (2011)
CFBDSIR J1458+1013	2.6±0.3	110.0±0.0	23.1±2.4	T9.5	T10	0.68	field	Liu et al. (2011)
OGLE-2009-BLG–151	...	0.31±...	...	T:	T:	0.4	field	Choi et al. (2013)
OGLE-2011-BLG-0420	...	0.19±...	...	T:	T:	0.4	field	Choi et al. (2013)
			T/Y binaries.					
2MASS J1217–0311	2.1±0.8	209.0±6.0	10.0±4.0	T7.5	Y?	...	field	Saumon et al. (2007)
WISE J1217+1626	8.0±1.3	759.2±3.3	10.5±1.7	T9.0	Y0	0.58	field	Liu et al. (2012)

3.5.1 Comparison the binary fraction with theoretical models

A few sets of formation models have made specific predictions for the binary properties of VLM stars and BDs. These predictions can be compared to the observed properties, which can be summarized as follows based on the field and cluster observations: systems which primary mass is $<0.1\,M_{\odot}$ have a binary fraction of $\sim$20% (see Table 3.3), most of the binaries are tight (ρ <20 AU) and a few are

very wide (ρ>100 AU), and the mass ratios tend to approach unity (see Figure 3.14). Early models produced too few binaries and no wide systems (Bate et al. 2002; Reipurth & Clarke 2001) but newer calculations are roughly consistent with the observed data in the mass range $0.07-0.1\,M_{\odot}$ (Bate 2009, 2012). However, it remains unclear whether any of these models can make wide binary BDs in the low density conditions in which they have been primarily found. The binary FU Tau (800 AU, Luhman et al. 2009b) and the quadruple system containing 2MASS 04414489+2301513 (1700 AU, Todorov et al. 2010) would seem difficult to explain with the current formation theories. In particular, it challenges the ejection model (Reipurth & Clarke 2001; Bate & Bonnell 2005) since such fragile systems are not expected to survive the ejection process from their birth environments. They also raise some concerns on the disk fragmentation scenario (Padoan & Nordlund 2002) as such wide systems would require the existence of disks of unreasonably mass and size.

3.6 The Virtual Observatory

The digital revolution is bringing a change in paradigm in the way science is done. It is now well understood that ”data become an infrastructure that scientists can use on their way to new frontiers” and that ”they should be able to concentrate on the best ways to make use of data”. It is also understood that setting up this data infrastructure is a difficult task which has many aspects.

Astronomy has been for a long time at the forefront for widespread sharing and re-use of data. National and international ground- and space-based observatories produce terabytes of data per year which are publicly available all around the world from data centres. Theoretical models as well as results published in electronic journal are also available on line. Although this e-infrastructure should potentially lead to a more complete and less biased understanding of complex astrophysical phenomena, the reality is that the progress in the scientific exploitation is not keeping pace with the exponential growth of data. The lack of interoperability among the huge databases that populate the distributed worldwide astronomical data centres is the major limiting factor that hinders the optimum scientific and technical exploitation of the information.

The Virtual Observatory (VO) represents a step forward towards interoperability and data integration. VO, under way since the turn of the century, is an international project aiming to: a) Create a federation of astronomical archives that, with the implementation of a common set of rules ("VO standards") provides a

seamless and efficient access to astronomical data ("data grid"). b) Develop and implement analysis tools ("service grid").

The development of VO standards and tools is overseen by the International Virtual Observatory Alliance (IVOA[7], see Figure 3.15), an alliance of all Virtual Observatory initiatives (national projects or projects managed by intergovernmental agencies). IVOA was established in June 2002 and, at present, is formed by 21 members.

Nowadays, the VO is an operational research infrastructure, as demonstrated by the growing number of VO-papers published in the last years (>70 since 2009[8]).

Figure 3.15: List of IVOA member organizations.

3.6.1 The Spanish Virtual Observatory

The Spanish Virtual Observatory became an IVOA member in 2004 and, since then, is playing an active role both at technical, scientific and managerial level. The project is conducted at Centro de Astrobilogía (INTA-CSIC). The main SVO goals are outlined below:

[7]http://www.ivoa.net/
[8]http://www.euro-vo.org/?q=science/scientific-papers

Development of VO-compliant data centers

Having a scientific archive perfectly integrated in the VO framework constitutes an added value of enormous importance for an astronomical project. CAB hosts the largest astronomical data centre managed by a Spanish institution. The whole list of archives at CAB (most of them VO-compliant, including the GTC and Calar Alto Archives) can be found at http://svo.cab.inta-csic.es.

In parallel to this, SVO pursues the building of a federation of VO-compliant astronomical data centers at national level by providing technical support and VO publishing tools to the centres willing and with the necessary know-how to manage their data collections.

VO-science

The Virtual Observatory project is now mature enough to be used as a research tool for the astronomical community. The SVO fosters the collaboration with research groups having science cases that could benefit from using a VO methodology. The SVO role in these collaborations focuses on the assessment of the science case from the VO point of view, on the provision of information and support about the existing tools to tackle the scientific problem and, if necessary, on the development of new analysis tools. This thesis work is encompassed in the framework of these collaborations.

The Spanish VO is playing a leading role at international level in this line of work as demonstrated by the large number of VO-science papers published in the last years by Spanish astronomers[9].

Development of VO standards and tools

Standardization represents the first level in the bottom-up VO approach (the "interoperability layer"). The implementation of standards on the top of the data repositories allows a seamless intercomparison of data coming from different archives and services and, thus, facilitates their optimum scientific exploitation. SVO actively participates in different IVOA working groups, in particular in the definition of access protocols for theoretical models and the development of data models for time series and asteroseismology.

[9] http://www.euro-vo.org/?q=science/scientific-papers

The interaction of the VO infrastructure with end-users (the scientists) is provided by a number of applications (the VO tools). VOSA, a VO tool developed by the SVO with more than 500 active users and more than 60 refereed papers, is an excellent example of the importance of VO tools for the community. A comprehensive list of VO tools can be found at http://www.euro-vo.org/?q=science/software.

Special attention is also paid to Data Mining tools as the efficient handling of the vast amount of data that is available in the VO framework is only possible if Artificial Intelligence techniques are considered. Supervised/unsupervised classification or knowledge discovery projects using Gaia and other large photometric surveys represent the main SVO lines of work in this field.

Chapter 4

WISE/2MASS-SDSS brown dwarfs candidates using VO tools

4.1 Resumen

WISE (*Wide-field Infrared Survey Explorer*[1]) es un telescopio espacial de NASA lanzado el 14 de diciembre de 2009 con el objetivo de cartografiar el cielo en cuatro bandas del infrarrojo medio (3.4, 4.6, 12, y 22 μm). La fase criogénica en cuatro bandas terminó en agosto de 2010 aunque con posterioridad a esta fecha se han seguido realizando cartografiados en tres y dos bandas. Aberasturi et al. (2011) hizo uso del primer catálogo de fuentes *WISE* (*Preliminary Data Release*), publicado en abril de 2011. En noviembre de 2013 se publicó el catálogo final (*The AllWISE Data Release*[2]) con 747 millones de fuentes distribuidas por todo el cielo.

Las bandas fotométricas de *WISE* son excelentes para la detección de las enanas marrones más frías, las cuales emiten el 90% de su flujo en el infrarrojo medio. En particular el filtro W1, centrado en la banda de absorción de CH_4 a 3.5 μm y el filtro W2, situado en una región relativamente libre de opacidad donde emerge gran parte del flujo total, son los más utilizados para la detección de estos objetos ultrafríos (ver Figura 4.1). Los datos de *WISE* han sido utilizados para identificar $\sim$200 enanas marrones con tipos espectrales posteriores a T6 (Mainzer et al. 2011; Burgasser et al. 2011b; Scholz et al. 2011; Aberasturi et al. 2011; Kirkpatrick et al. 2011a; Cushing et al. 2011b; Kirkpatrick et al. 2012a; Tinney et al.

[1] http://irsa.ipac.caltech.edu/Missions/wise.html
[2] http://wise2.ipac.caltech.edu/docs/release/allwise

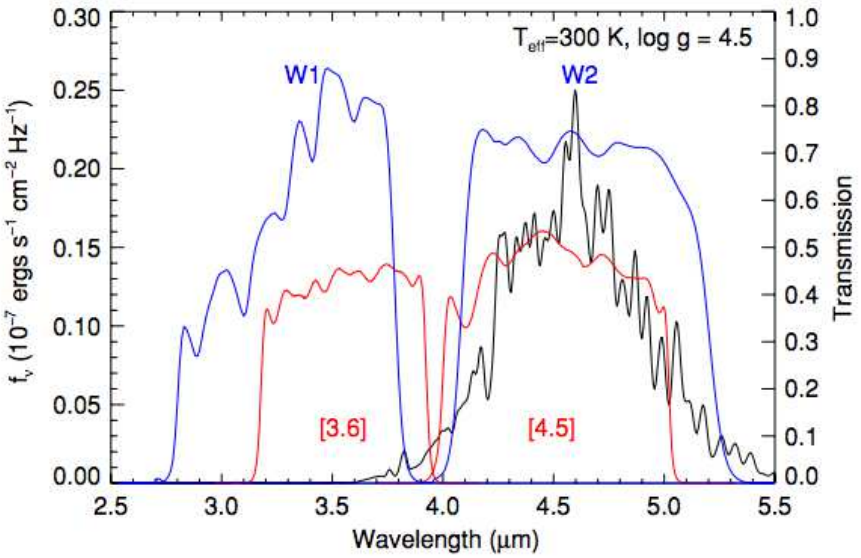

Figure 4.1: En negro se muestra la distribución espectral de energía de una enana marrón con $T_{\rm eff}$ = 300 K y log g = 4.5 cms^{-}2 (Marley et al. 2010). Asimismo se representan las funciones de respuesta de los filtros 3.6 y 4.5 μm de IRAC (en rojo) y las bandas $W1$ y $W2$ de $WISE$ (en azul). Estos dos últimos filtros fueron diseñados de manera específica para detectar la absorción en 3.5 μm debida al CH_4 y H_2O y la región relativamente libre de opacidad en 4.7 μm del espectro de las enanas marrones más frías (Figura 2 de Mainzer et al. 2011).

2012; Luhman et al. 2012b; Mace et al. 2013a; Luhman 2013; Thompson et al. 2013; Huélamo et al. 2015), incluyendo las recientemente descubiertas 21 enanas de tipo Y (Cushing et al. 2011b; Kirkpatrick et al. 2012a; Tinney et al. 2012; Liu et al. 2012; Kirkpatrick et al. 2013; Cushing et al. 2014a; Pinfield et al. 2014b)

En Aberasturi et al. (2011) presentamos uno de los primeros trabajos sobre la identificación de enanas marrones utilizando datos de *WISE*. Para ello hicimos uso de otros dos catálogos, uno en el óptico (*The Sloan Digital Sky Survey Data Release 7*, Abazajian et al. 2009), y otro en el infrarrojo cercano (*The Two Micron All Sky Survey Point Source Catalogue*, Skrutskie et al. 2006). La diferencia temporal entre los tres catálogos utilizados es de ∼10 años con una cobertura espacial en común de ∼4000 deg^2 (ver Figura 4.2).

4.1.1 Identificación y caracterización de candidatos a enanas marrones

Las herramientas de Observatorio Virtual fueron fundamentales para manejar la enorme cantidad de datos disponibles en estos catálogos. Para evitar problemas de

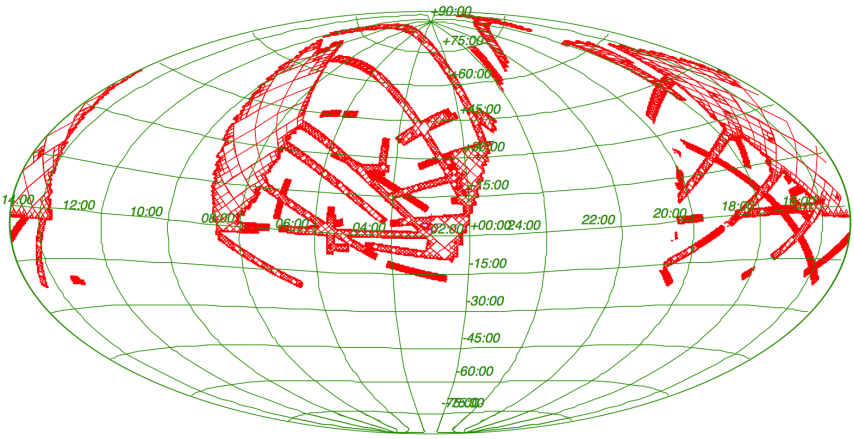

Figure 4.2: Área común rayada en rojo entre los catálogos utilizados en este estudio, *WISE*, 2MASS-PSC y SDSS–DR7.

memoria computacional, el área común entre los catálogos WISE-2MASS PSC-SDSS DR7 se dividió en regiones circulares de $30'$. La búsqueda de contrapartidas *WISE* en 2MASS y SDSS se llevó a cabo en regiones de $20''$ para no descartar objetos con alto movimiento propio. Teniendo en cuenta que la separación temporal mínima entre 2MASS y *WISE* es de $\sim$ 9 años, la adopción del criterio anterior implica la no detección de objetos con movimiento propio μ>2.2$''$/yr. Posteriormente se aplicaron una serie de filtros para seleccionar objetos que mostraran colores propios de enanas marrones (ver Figura 4.3): $(W1-W2)>0.5$, $(W2-W3)<2.5$ (Burrows et al. 2003; Golimowski et al. 2004b; Wright et al. 2010), $(J-W2)>1.8$ (Mainzer et al. 2011), $(z'-J)>2.5$ (Hawley et al. 2002) y $(i'-z')\geq 3$ mag (Hawley et al. 2002). Asimismo, para evitar un alto grado de contaminación por falsos candidatos, se impuso la condición de que la fuente *WISE* y su contrapartida 2MASS tuvieran una separación angular mayor de $1''$ lo que, teniendo en cuenta la diferencia temporal entre los dos catálogos, se traduce en la no selección de objetos con un movimiento propio μ<0.08$''$/yr.

Como resultado se obtuvieron 138 objetos entre los cuales, tras una inspección visual para eliminar falsos candidatos, fueron identificadas 31 enanas marrones, 25 de ellas previamente identificadas en la literatura, y seis nuevas candidatas (4 Ls y 2 Ts). La Figura 4.4 muestra la posición de nuestros candidatos en un diagrama $(J-H)$ vs. $(W1-W2)$.

Tras la identificación se procedió a la caracterización de los seis nuevos candidatos a enanas marrones estimando sus movimientos propios, temperaturas efectivas ($T_{\rm eff}$), tipos espectrales, magnitudes absolutas y distancias (Tabla 4.1).

Las temperaturas fueron calculadas utilizando VOSA (Bayo et al. 2008), los tipos espectrales se estimaron siguiendo la relación de Kirkpatrick (2005) y las magnitudes absolutas y las distancias a partir de las calibraciones de Cruz et al. (2003) y Burgasser et al. (2011b). Con posterioridad a la publicación del trabajo, uno de los candidatos (WISE J0821+1443) fue estudiado espectroscópicamente confirmándose su clasificación como enana marrón T tardía (Figura 4.5).

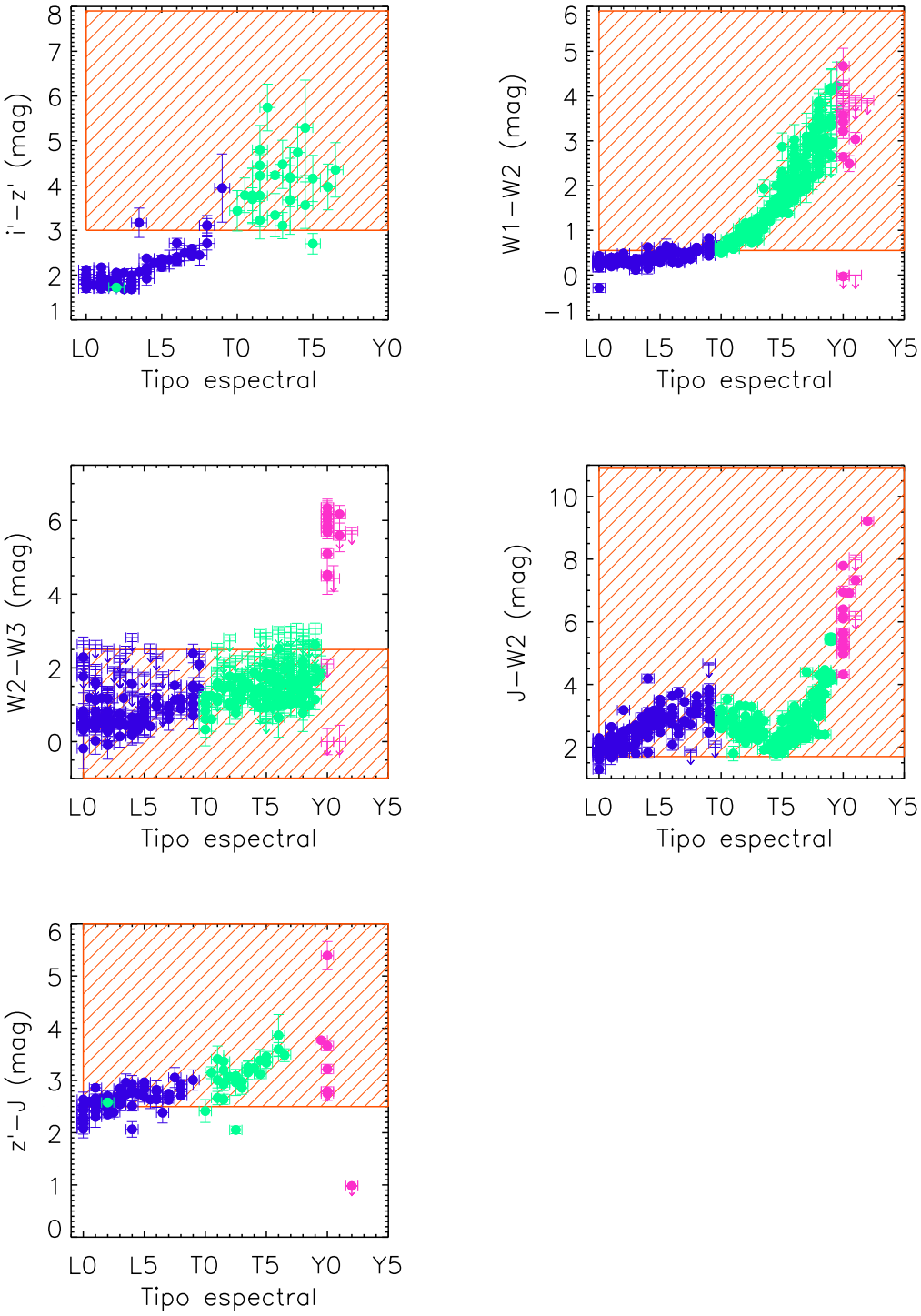

Figure 4.3: Muestra de objetos con tipo espectral L (azul), T (verde), Y (magenta) proporcionada por Kirkpatrick et al. (2011a) salvo los objetos Y del diagrama $(z' - J)$ vs. tipo espectral, los cuales han sido proporcionados por Lodieu et al. (2013a). El área rayada roja representa los cortes de color utilizados para la selección de candidatos.

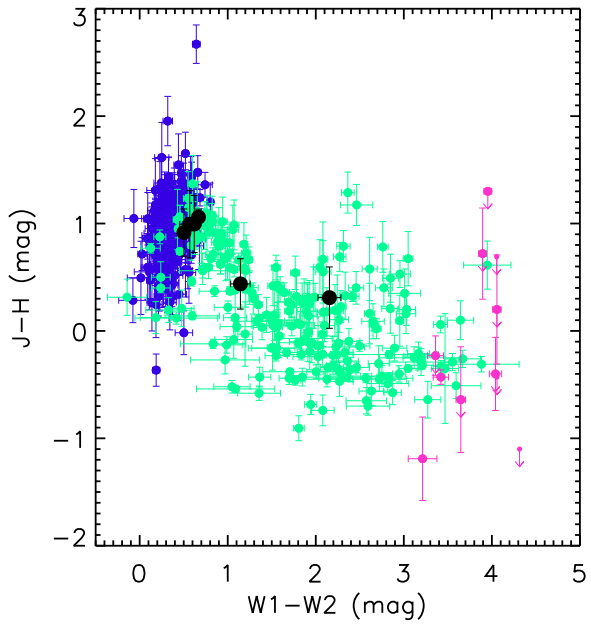

Figure 4.4: Diagramas color-color para enanas L, T e Ys incluidas en DwarfArchives con contrapartidas en 2MASS / UKIDSS, SDSS y *WISE*. El código de colores es igual al de la Figura 4.3. Los círculos negros rellenos representan nuestros seis candidatos.

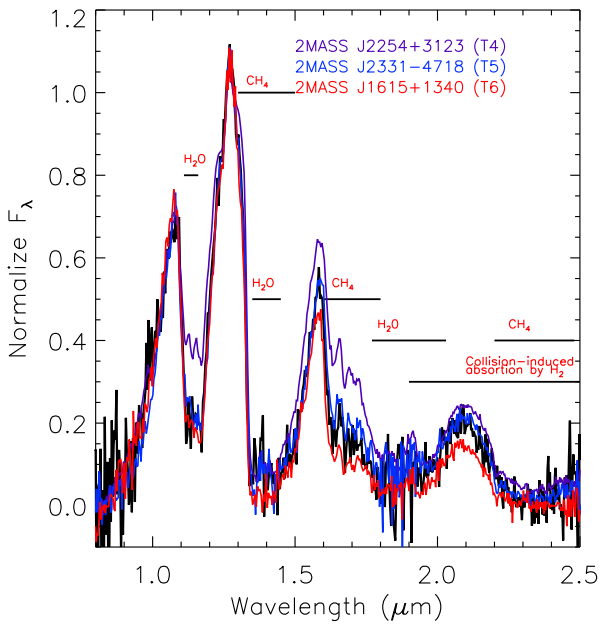

Figure 4.5: Espectro en el infrarrojo cercano de WISE J0821+1443 utilizando el espectrógrafo SpeX (R $\sim$ 1000). Se aprecian claramente las bandas de absorción de agua y metano propias de una enana T tardía.

4.1.2 Impacto de los resultados obtenidos

Entre los seis candidatos a enanas marrones hay dos de especial interés y que han sido fuente de estudio en trabajos posteriores. Estos objetos son WISE J0838+1511 y WISE J0920+4538.

Radigan et al. (2013) estudió una muestra de objetos en la transición L-T entre los que se encontraba WISE J0838+1511. Como se describió en la introducción de esta Tesis, la región de transición L-T comprende los tipos espectrales L6-T5 y se caracteriza por una rápida evolución espectral en el infrarrojo cercano ($\sim$1 μm) mientras que la temperatura efectiva permanece constante con un valor de $\sim$1200 K (Golimowski et al. 2004b; Stephens et al. 2009). Los cambios espectrales están asociados a la desaparición de las nubes en las fotosferas de estos objetos.

En particular, el trabajo de Radigan et al. (2013) se centraba en la identificación de sistemas múltiples. El descubrimiento y caracterización de este tipo de objetos es altamente interesante ya que, por un lado, permite arrojar luz a la pregunta abierta sobre el posible exceso de binarias en la región de transición sugerido por algunos autores (e.g. Burgasser 2007a) y, por otro lado, constituye un excelente banco de pruebas para los modelos teóricos al poder fijar parámetros como la metalicidad y la edad.

Mediante imágenes de alto contraste, los autores descubrieron que WISE J0838+1511 es, en realidad, un sistema triple (ver Figura 4.6), el primero descubierto en el que todas las componentes del sistema son enanas de tipo T, una de ellas separada a 0.5″ mientras que las otras dos constituyen un sistema mucho más cerrado (separación de $\sim$0.05″). Además de astrométricamente, los autores caracterizan el nuevo sistema triple mediante la estimación de sus parámetros físicos fundamentales.

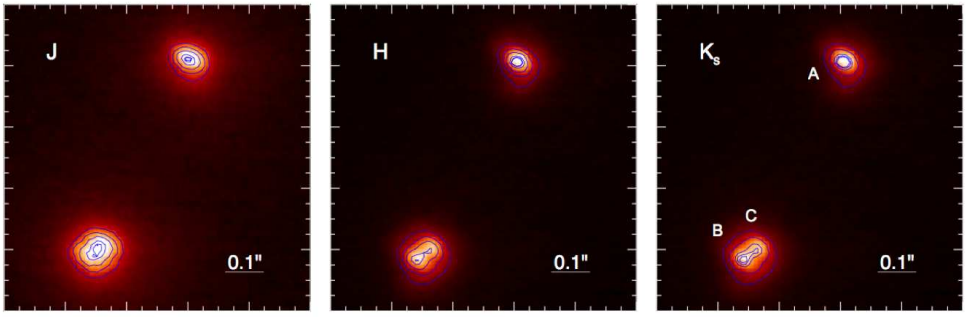

Figure 4.6: Imagen del sistema WISE J0830+1511 tomada por la cámara infrarroja de alta resolución NIRC2/*HST*

Por otro lado, Aberasturi et al. (2011) clasificaron a WISE J0920+4538 como L4-L5 en base al ajuste de la distribución espectral de energía basada en información fotométrica. El seguimiento espectroscópico de este objeto reveló un tipo espectral más tardío (L9, ver Figura 4.7), consistente con el análisis realizado por Mace et al. (2013a). Estos autores dejan abierta la posibilidad de que este objeto sea realmente un sistema binario (una primaria de tipo espectral L7.5±1.5 y una secundaria de tipo T1.5±1.5) en base a su pobre ajuste espectral. Best et al. (2013), por su parte, asignan a este objeto un tipo espectral L9.5 y apuntan la posibilidad de variabilidad en el infrarrojo cercano indicando, no obstante, que es necesario realizar más observaciones para poder confirmar esta hipótesis.

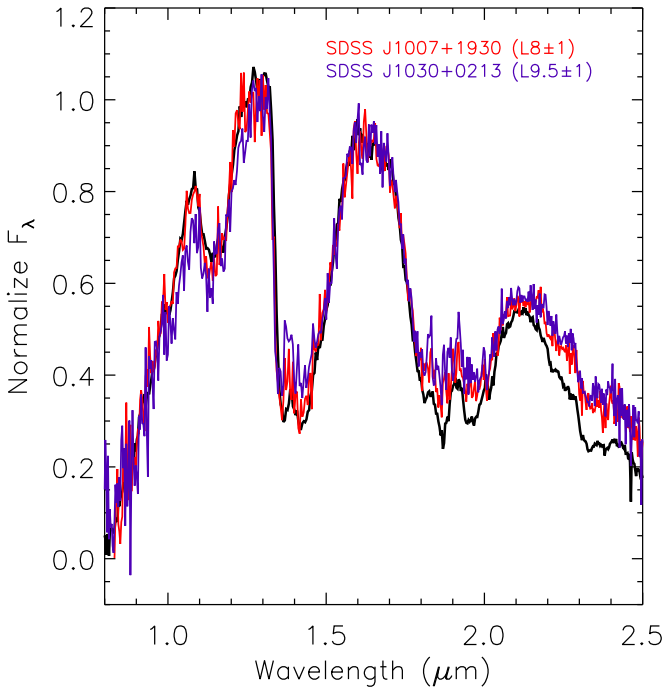

Figure 4.7: Espectro en el infrarrojo cercano del objeto WISE J0920+4538 con R $\sim$ 1000 utilizando el espectrógrafo SpeX.

WISE/2MASS-SDSS brown dwarfs candidates using Virtual Observatory tools

2011,A&A, 534L, 7A

Authors:
M. Aberasturi[1,2], E. Solano[1,2], E. L. Martín[1]
Affiliation:
[1] Centro de Astrobiología (INTA-CSIC), Departamento de Astrofísica, P.O. Box 78, E-28691 Villanueva de la Cañada, Madrid, Spain
[2] Spanish Virtual Observatory.

Abstract

Massive far-red and infrared imaging surveys in different bandpasses are the main contributors to the discovery of brown dwarfs (BDs). The Virtual Observatory (VO) represents an adequate framework to handle these vast datasets efficiently and filter them out according to specific requirements. A statistically significant number of BDs is mandatory for understanding their general properties better for identifing peculiar objects. WISE, an all-sky survey in the mid-infrared, provides an excellent opportunity to increase the number of BDs significantly, in particular those at the lower end of the temperature scale. We aim to demonstrate that VO tools are efficient in identifing and characterizing BDs by cross-correlating public catalogues released by large surveys. Using VO tools we performed a cross-match of the WISE Preliminary Release, the 2MASS Point Source and the SDSS Data Release 7 catalogues over the whole area of sky that they have in common ($\sim$ 4000 deg^2). Photometric and proper motion criteria were used to obtain a list of BD candidates. A temperature estimate is provided for each candidate based on their spectral energy distribution using VOSA, a VO tool for SED (Spectral Energy Distribution) fitting. We derive the spectral types from the effective temperatures. Distances, calculated from the absolute magnitude- spectral type relation, place our candidates at 14-80 pc from the Sun, assuming that they are single. We have identified 31 BD candidates, 25 of which have already been reported in the literature. The remaining six candidates have been classified as L- (four) and T-type (two) objects. The high rate of recovery of known BDs ($\sim$ 90% of the T dwarfs catalogued in 2MASS) demonstrates the validity of our strategy to identify them with VO tools. An application of this method for a deeper search that covers the whole sky in common to WISE and UKIDSS will be presented in a forthcoming work.

4.2 Introduction

Brown dwarfs (BDs), self-gravitating objects that form like stars but do not get enough mass to maintain a sufficiently high temperature and pressure in their cores for stable hydrogen fusion, provide a natural link between very low-mass stars and gaseous giant planets. Theoretically proposed fifty years ago (Kumar 1963), it was not until 1995 when the first BDs were discovered (Rebolo et al. 1995; Nakajima et al. 1995). Since then, hundreds of

BDs have been found mainly thanks to the advent of large-area optical and near-infrared surveys such as the Two Micron All Sky Survey (2MASS, Skrutskie et al. 2006; Looper et al. 2007), the DEep Near Infrared Survey of the Southern Sky (DENIS, Epchtein et al. 1997; Delfosse et al. 1997; Martín et al. 1999), the Sloan Digital Sky Survey (SDSS, York et al. 2000; Chiu et al. 2006), the UKIRT Infrared Deep Survey (UKIDSS, Lawrence et al. 2007; Lodieu et al. 2007b; Burningham et al. 2010b) and the Canada-France Brown Dwarf Survey (CFBDS, Delorme et al. 2008b; Albert et al. 2011)[3].

The Wide-field Infrared Survey Explorer (WISE; Wright et al. 2010) is a NASA mission that has mapped the sky at 3.4 (W1), 4.6 (W2), 12 (W3), and 22 (W4) μm in 2010 with an angular resolution of 6.1", 6.4", 6.5", and 12.0", respectively. WISE achieved 5σ point-source sensitivities better than 0.08, 0.11, 1 and 6 mJy in unconfused regions on the ecliptic in the four bands. The dataset obtained by the WISE imaging survey constitutes an excellent resource for finding new brown dwarfs, in particular the coldest members, because they emit a substantial part of the spectral flux in the mid-infrared. The recent discoveries of T dwarfs reported by different authors (Burgasser et al. 2011; Mainzer et al. 2011; Scholz et al. 2011) confirm the high expectations placed on the mission. The WISE Preliminary Release[4] is available to the astronomical community since April 14, 2011 and includes photometric information for over 257 million objects observed during the first 105 days of the survey.

The Virtual Observatory[5] (VO) is an international initiative designed to help the astronomical community in the exploration of the digital, multi-wavelength universe that is resides in the astronomical data archives. The VO is already an operational research infrastructure, as demonstrated by the growing number of VO-papers published in the last years ($>$ 50 since 2009)[6]. In this work we have made use of VO tools to benefit from an easy data access and analysis.

We present here the identification of 31 BDs (25 known and 6 strong candidates not previously reported in the literature) identified in the sky area in common to the WISE Preliminary Release and the 2MASS Point Source and SDSS Data Release 7 catalogues. In Sect. 2 we describe the methodology devised to search for T dwarfs. In Sect. 3 we derive proper motions, effective temperatures ($T_{\rm eff}$), spectral types, and distances for our candidates. Finally, we summarize conclusions in Sect. 4.

4.3 Candidate selection

We built a VO-workflow with the STILTS[7] scripting capabilities with criteria that must accomplish our preliminary list of candidates. The workflow consisted in the following steps:

[3]See http://dwarfarchives.org for an updated list of L and T dwarfs
[4]http://irsa.ipac.caltech.edu/Missions/wise.html
[5]http://www.ivoa.net
[6]http://www.euro-vo.org/pub/fc/papers.html
[7]http://www.star.bris.ac.uk/$\sim$mbt/stilts/

- Cross-match. To avoid memory overflow problems associated to the data processing of large volumes of data, we divided the common WISE-2MASS-SDSS sky into overlapping circular regions of 30′. After different tests, we adopted a matching radius of 20″ to ensure that objects with high proper motion were not left out while at the same time avoiding an unmanageable number of false positives. Only the closest 2MASS and SDSS counterparts to each WISE source were considered.

- Filters on photometry.

  - Xflg=0, Aflg=0, to avoid sources flagged in 2MASS as minor planets or contaminated by nearby extended sources.

  - $9 < J$, to exclude of too bright sources that typically have associated large uncertainties.

  - Qflg(J) ≠ "U", to discard sources with upper limits in the J band.

  - $g' > 22.2$, $r' > 22.2$ (SDSS limiting magnitudes), because T dwarfs should not be detected in these bands.

  - $i' > 21.3$ (SDSS limiting magnitude) or (i'-z') ≥ 3 (Hawley et al. 2002).

  - $z' < 20.5$ (SDSS limiting magnitude)

  - (W1-W2)>0.5 , W2<15.5, (W2-W3)< 2.5. The W1 and W2 WISE bands were specifically designed to distinguish T dwarfs from background sources. W1 includes much of the CH_4 fundamental absorption band and W2 includes the pseudo-continuum peak that is present for all objects cooler than 3000 K (Burrows et al. 2003; Golimowski et al. 2004b). Mainzer et al. (2011) suggest a (W1-W2) > 1.8 for cool T dwarfs. Because we search for T dwarfs at all spectral subtypes, we relaxed this criterion up to the stellar boundary, (W1-W2)> 0.5. A side effect of this approach was the identification of four new L-type candidates. The (W2-W3)< 2.5 criterion was selected to exclude extragalactic sources (Wright et al. 2010). W2=15.5 indicates the limiting magnitude (5σ) in the W2 band.

  - (J-W2)>1.8 and (z'-J)>2.5 as suggested by Mainzer et al. (2011) and Hawley et al. (2002), respectively.

- Filter on astrometry and proper motions (PMs).

  - The angular separation between the WISE source and the 2MASS counterpart must be greater than 1″ (WISE 2σ astrometric accuracy). Assuming a minimum difference epoch between 2MASS and WISE of nine years (Feb 2001 - Jan 2010), this criterion implies that we are loosing objects with PMs lower than 0.11″/yr. On the other hand, the 20″ matching radius will limit the detection of T dwarfs with PM higher than 1.53″/yr given the maximum difference epoch between 2MASS and WISE (Jun 1997 - Apr 2010).

  - There must not be counterparts in the source table of the Supercosmos Science Archive (Hambly et al. 2001) at less than 1″ from the WISE source.

- The differences in the PMs derived from WISE-2MASS and WISE-SDSS must be less than 50%.

This query returned 138 candidates. They were visually inspected using the scripting capabilities of Aladin[8] (Bonnarel et al. 2000). Aladin is a VO-compliant software that allows users to visualize and analyze digitised astronomical images, and superimpose entries from astronomical catalogues or databases available from VO services. Sources from DENIS, 2MASS, SDSS, Supercosmos and UKIDSS as well as images from UKIDSS, 2MASS and SDSS were used in the analysis. One hundred and seven candidates were rejected due to several reasons (artifacts, presence of a nearby bright star, etc.), the most likely being the mismatch between WISE sources and 2MASS/SDSS counterparts: due to the different depth of the surveys it may happen that a 2MASS source is wrongly associated to a SDSS source without a real counterpart in 2MASS. Thirty one candidates passed the visual inspection. Twenty three sources were identified as known BDs (7 L- and 16 T-dwarfs) in a cross-match with SIMBAD[9] and the DwarfArchives, providing an independent sanity check of our selection method. Two out of the remaining eight candidates were published during the preparation of this letter: WISE J1625+1528 (Deacon et al. 2011a) and WISE J1627+3255 (Gelino et al. 2011). Multiwavelength charts and the astrometric and photometric information of the six newly discovered BD candidates are given in Fig. 4.8 and Table 4.1, respectively. Figure 4.9 compares in a color-color diagram our six candidates with a sample of known L and T dwarfs (Mainzer et al. 2011, Scholz et al. 2011, Burgasser et al. 2011b). All our candidates have W1,W2 signal-to-noise ratios (SNR) $\geq$ 10 and can be considered as point sources (w2rchi2 $\leq$ 3). They were also searched for common PM companions within a radius of $10'$ in the WISE and 2MASS catalogues but none was found.

Finally, we assessed the efficiency of our search by estimating the false negative rate (number of known T dwarfs that were not rediscovered in the analysis). Thirty six T dwarfs catalogued in the DwarfArchives were not found with our methodology. Most of them (33) were too faint to be detected in 2MASS and the remaining three did not meet some of the photometric criteria explained above.

4.4 Physical parameters

4.4.1 Proper motions

The long baseline between WISE and 2MASS/SDSS, the excellent astrometry of these catalogues (less than $0.5''$ with respect to 2MASS in the case of WISE (Wright et al. 2010), together with the fact that brown dwarfs are nearby objects and therefore typically show high proper motions facilitates the measurement of reliable angular separations between the WISE sources and their respective counterparts in the 2MASS and SDSS catalogues.

[8] http://aladin.u-strasbg.fr/
[9] http://simbad.u-strasbg.fr/simbad/

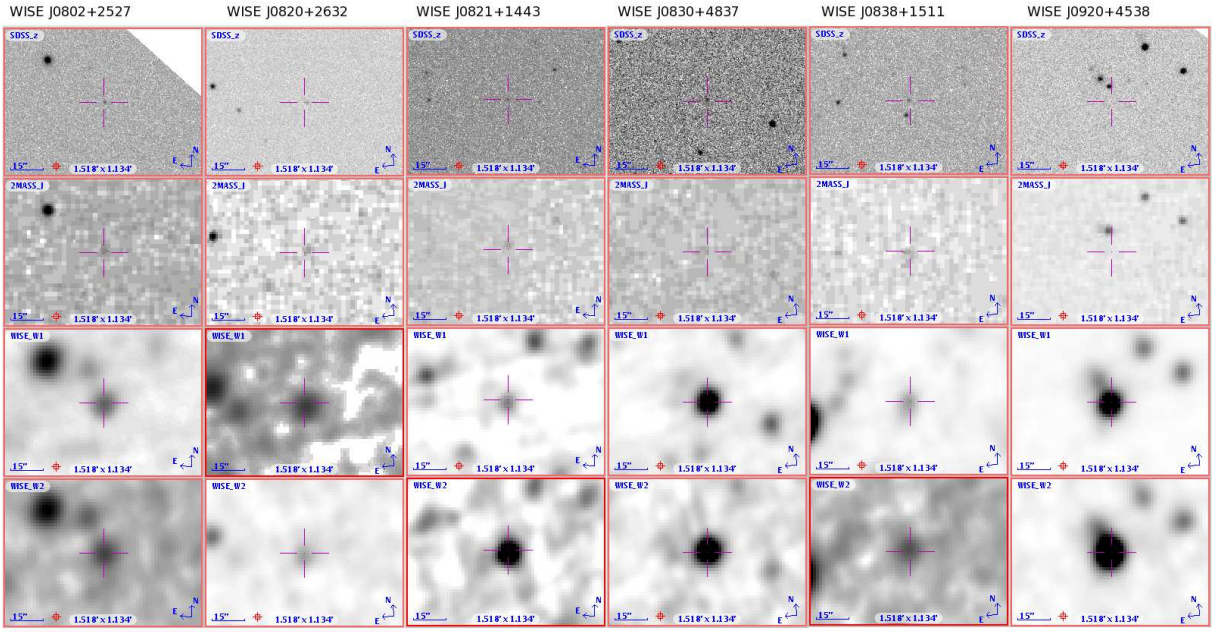

Figure 4.8: Four-band charts showing the area around the six new BD candidates. The fields are $1.5' \times 1.1'$ oriented with North up and East to the left. For each source, the SDSS(z'), 2MASS(J), WISE(W1) images are centered on the WISE(W2) coordinates. Fast motion between 2MASS and WISE epochs is clearly visible in WISE J0920+4538.

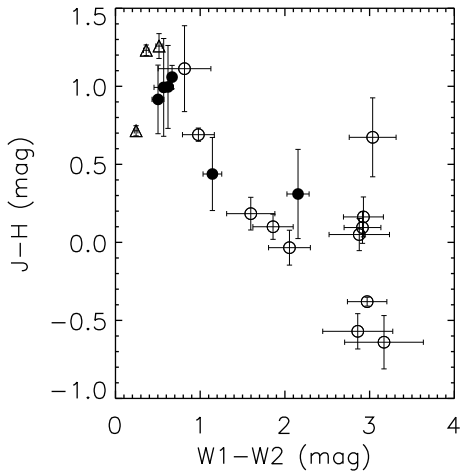

Figure 4.9: Colour-colour diagram of our six candidates (black full circles) compared with a sample of known L and T dwarfs (triangles and circles, respectively) observed with WISE (Mainzer et al. 2011; Scholz et al. 2011; Burgasser et al. 2011.)

Proper motions were computed using a linear least-squares fit to the coordinates given in the WISE, 2MASS and SDSS catalogues and weighted by their astrometric errors. No correction for parallactic motion was considered. The small separation between the

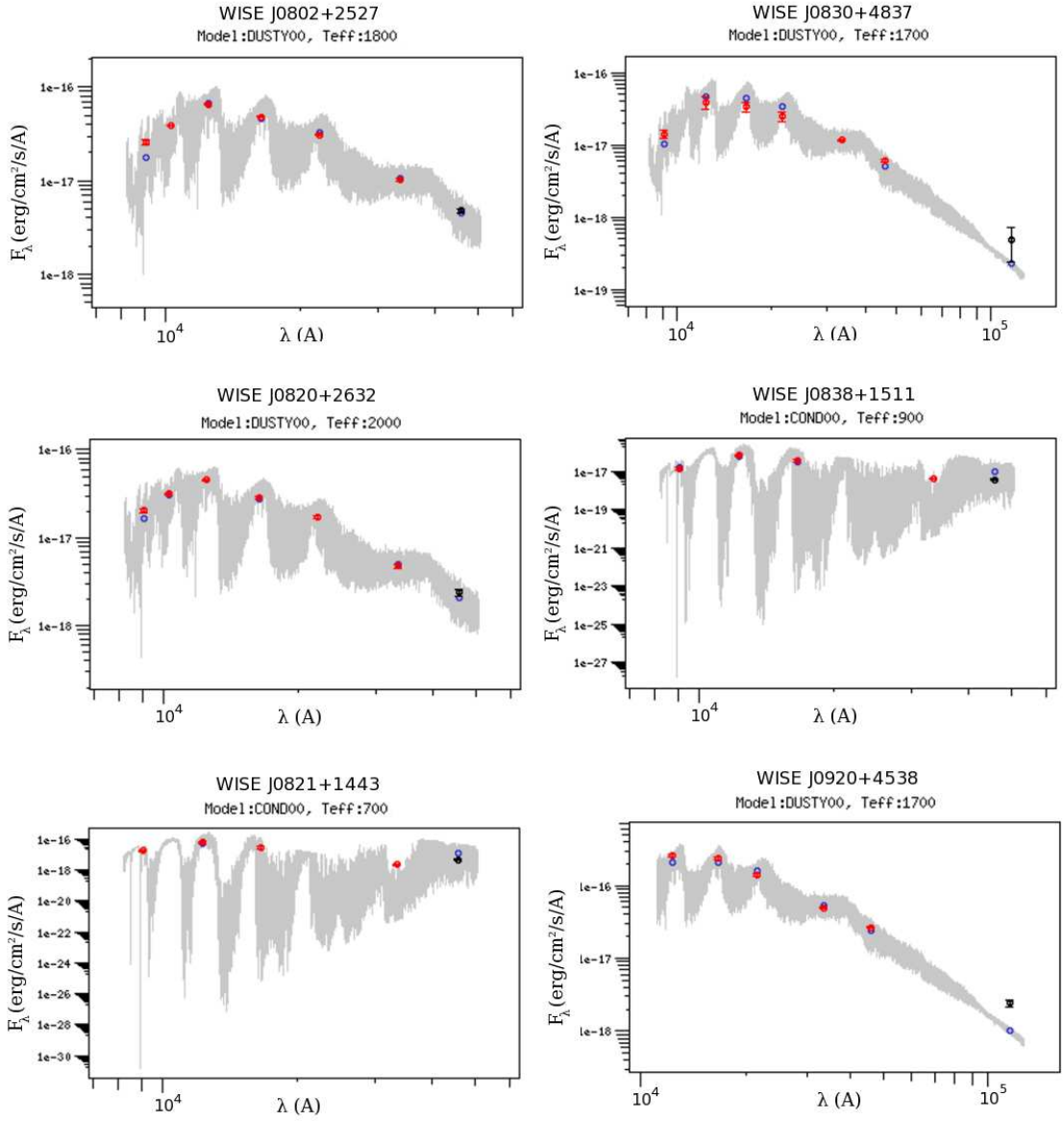

Figure 4.10: VOSA SED fitting for our six BD candidates. Catalogue and synthetic photometric points are represented in red and blue, respectively. Points not considered in the fitting are shown in black. Spectral bands are those listed in Table 1. The theoretical spectrum that best fits (and from which the synthetic photometry was computed by convolving with the corresponding filter profiles) is also plotted in grey.

Table 4.1: Astrometry, photometry and physical parameters for the six new BDs candidates. See Sect. 3 for a detailed description on how effective temperatures, spectral types, absolute magnitudes and distances were obtained. J and W2 absolute magnitudes were only computed for L and T dwarfs respectively. Also, the uncertainty in W3 is not provided for four of the candidates. According to the WISE source catalogue user's guide, this happens if the W3 profile-fit magnitude is a 95% confidence upper limit or if the source is not measurable.

Parameter	WISE J0802+2527	WISEJ0820+2632	WISE J0821+1443	WISE J0830+4837	WISE J0838+1511	WISE J0920+4538
RA(J2000)	08 02 02.86	08 20 07.35	08 21 31.63	08 30 41.67	08 38 11.45	09 20 55.41
Dec(J2000)	+25 27 18.5	+26 32 28.5	+14 43 19.4	+48 37 15.0	+15 11 15.1	+45 38 56.4
$\mu_\alpha cos\delta$ ($''$/year)	-0.011±0.026	0.087±0.042	-0.115±0.035	-0.125±0.026	-0.121±0.031	-0.075 ±0.010
μ_δ ($''$/year)	-0.125±0.055	-0.208±0.062	-0.297±0.054	-0.058±0.050	-0.032±0.051	-0.833±0.045
z'	19.238±0.069	19.514±0.067	19.732±0.118	19.905±0.153	19.907±0.142	21.002±0.658
Y (UKIDSS)	17.914±0.012	18.145±0.029	...	...	...	...
J (2MASS)	16.713±0.157	16.988±0.222	16.825±0.155	17.275±0.199	16.645±0.159	15.223±0.052
J (UKIDSS)	16.626±0.010	17.036±0.015	...	...	...	...
H (2MASS)	15.797±0.154	15.995±0.221	16.515±0.240	16.279±0.176	16.207±0.172	14.164±0.054
H (UKIDSS)	15.937±0.019	16.487±0.038	...	...	...	...
K_s (2MASS)	15.397±0.151	15.881±0.251	...	15.596±0.165	...	13.728±0.050
K_s (UKIDSS)	15.248±0.016	15.883±0.028	...	...	...	...
W1	14.758±0.037	15.578±0.057	16.438±0.114	14.620±0.034	15.712±0.068	13.059±0.025
W2	14.256±0.060	15.009±0.099	14.283±0.064	14.000±0.047	14.568±0.087	12.391±0.026
W3	11.965±...	12.658±...	12.572±...	12.828±0.539	12.285±...	11.063±0.115
W1−W2	0.502	0.569	2.155	0.62	1.144	0.668
W2−W3	2.291	2.351	1.711	1.172	2.283	1.328
$T_{\rm eff}$ (VOSA) (K)	1800	2000	700	1700	900	1700
SpT ($T_{\rm eff}$)	L3-L4	L2-L3	T8	L4-L5	T6-T7	L4-L5
M_J	13.08	12.48	...	13.31	...	13.31
M_{W2}	...	...	13.47	...	13.07	...
d (pc)	53	80	15	62	20	24

2MASS and SDSS positions (less than $1''$ for five of our candidate BDs) and the lack of 2MASS K_s photometry for two of them are the main reasons for their omission in previous 2MASS/SDSS-based PM searches.

4.4.2 Effective temperature and spectral types

Effective temperatures for our candidate BDs were obtained from the spectral energy distribution (SED) χ^2 fitting between the observed photometry and a suite of collections of theoretical models. The temperature determination was carried out using VOSA[10] (Virtual Observatory SED Analyzer, Bayo et al. 2008). VOSA is a VO-tool designed to query several photometric catalogues that are accessible through VO services as well as VO-compliant theoretical models and perform a statistical test to determine which model reproduces the observed data best. $T_{\rm eff}$ is then estimated from the best fit. Two different model collections were used in our analysis: DUSTY (Allard et al. 2001) and COND (Chabrier et al. 2000b), which have $T_{\rm eff}$ models ranging from 4000 to 100K and 3900 to 500K in 100K steps, respectively. Effective temperatures obtained with VOSA are shown in Fig. 4.10 and Table 4.1.

Spectral types were then estimated following the effective temperature–spectral type relation given in Kirkpatrick (2005). The 23 BDs found in our analysis with spectral types previously reported in the literature were used as benchmarks to calibrate the method.

[10]http://svo.cab.inta-csic.es/theory/vosa/

Typical errors of $\sim$0.5 spectral types were found. The main contribution to the error budget comes from the degeneracy in the $T_{\rm eff}-$ spectral. type relation between L4 and T4.

4.4.3 Distances

Distances for the L dwarfs were calculated using the absolute *J* magnitude (2MASS) – spectral type relation given in Cruz et al. (2003), whereas the distances to the T dwarfs were estimated using the absolute W2 magnitude (WISE) – spectral type relation derived by Burgasser et al. (2011b). The calculated values for the distances are given in Table 4.1. The uncertainties in the derived distances are dominated by the uncertainty in the spectral type because the errors in the 2MASS J photometry are typically only 0.1-0.2 mag, whereas the errors in the spectral type are 0.5 types. This leads to a 30% uncertainty on distance, assuming all our candidates are single. An unresolved multiplicity would imply an underestimate of distance.

4.5 Conclusions

Taking advantage of VO tools, we reported the discovery of six BD candidates in the region of the sky in common to 2MASS Point Source, SDSS (Data Release 7) and the WISE Preliminary Release catalogues. The six candidates are clearly visible in the WISE W1 and W2 bands with SNR $\geq$ 10 and show physical parameters typical of L and T-type objects. The number of new candidates is remarkable, considering that 2MASS has been extensively searched for ultracool dwarfs.

These results clearly show how new surveys and the use of VO tools can help to mine older surveys: all but one of our BD candidates are very close to the 2MASS limiting magnitude, which puts them beyond the limits of previous, much shallower 2MASS-based BD searches (e.g. J$<$16, Looper et al. 2007). Also remarkable is the fact that the methodology used in this paper is not limited to brown dwarfs but can be easily extrapolated to searches for other rare objects (e.g. high-z quasars).

Finally, our work clearly demonstrates the suitability of exploiting WISE data following a VO methodology and increases the expectations of building an accurate census of substellar objects in the solar vicinity.

4.5.1 Acknowledgements

This research has made use of the WISE data hosted at the NASA/ IPAC Infrared Science Archive, which is operated by the Jet Propulsion Laboratory, California Institute of Technology, under contract with the National Aeronautics and Space Administration. This publication has also made use of the SIMBAD, Vizier and Aladin services, operated at CDS,

Strasbourg, France. Our research has benefitted from the M, L, and T dwarf compendium housed at DwarfArchives.org and maintained by Chris Gelino, Davy Kirkpatrick, and Adam Burgasser. Effective temperatures were estimated using VOSA, a VO-tool developed under the Spanish Virtual Observatory project supported from the Spanish MICINN through grant AyA2008-02156.

Chapter 5

Search for bright nearby M dwarfs with VO tools

5.1 Resumen

Las enanas de tipo espectral M (3900 K $\leq T_{\rm eff} \leq$ 2500 K, Rajpurohit et al. 2013), representan el 70 % de los objetos (Reid & Cruz 2002; Covey et al. 2008; Bochanski et al. 2010), y el 40% de la masa total de la Galaxia (Chabrier 2003). En los últimos años las enanas M se han convertido en objetos de gran interés para las búsquedas de exoplanetas ya que son objetos muy adecuados para la detección de planetas tipo Tierra utilizando técnicas de efecto Doppler o tránsitos fotométricos. Además, las enanas M, en particular a partir del tipo espectral M5, son mucho menos luminosas que las estrellas de tipo solar, situando la zona de habitabilidad (ZH) más cercana a la estrella y haciendo más probable la detección de planetas con agua líquida sobre su superficie (Tarter et al. 2007; Gaidos et al. 2007). No obstante, solamente se conocen 91 planetas orbitando alrededor de enanas tipo M[1] , un número pequeño comparado con los 1912 planetas descubiertos hasta la fecha (abril 2015). 57 de estos 91 planetas han sido descubiertos mediante el método de velocidad radial, mientras que tan sólo 11 han sido descubiertos por tránsitos . El primer exoplaneta descubierto alrededor de una enana M fue Gliese 876 b mediante la técnica de velocidad radial (Delfosse et al. 1998).

El reducido número de planetas detectados alrededor de enanas M se puede explicar por la débil emisión de estos objetos en el rango visible, que es el que ha venido siendo utilizado por las principales técnicas de detección de exoplanetas. Esto ha llevado a que las búsquedas se hayan limitado a las enanas M más cercanas y brillantes. Espectrógrafos de alta resolución trabajando en el rango infrarrojo como SPIRou (Artigau et al. 2014), HPF (Hearty et al. 2014) o CARMENES (Quirrenbach et al. 2010) o misiones espaciales para la

[1] http://exoplanet.eu

detección de planetas en tránsito alrededor de estrellas de la secuencia principal brillantes y cercanas (TESS, Ricker et al. 2015) aumentarán de manera significativa en los próximos años el número de planetas conocidos alrededor de enanas M. A la dificultad de detección de este tipo de objetos debido a su baja luminosidad hay que añadir fenómenos como la variabilidad fotométrica debido a la modulación rotacional y evolución temporal de manchas y fulguraciones (Hartman et al. 2011), que dificultan sensiblemente la detección de tránsitos, o la existencia de actividad cromosférica y su influencia en las medidas de velocidad radial (Isaacson & Fischer 2010; Lépine et al. 2013). Se deduce, por tanto, que una de las claves del éxito en la detección de exoplanetas se basa en disponer de catálogos de enanas M brillantes caracterizadas de manera precisa tanto fotométrica como espectroscópicamente.

Diferentes trabajos sobre la identificación de nuevas enanas M han sido publicados en los últimos años. Lépine & Gaidos (2011) presentaron un catálogo de 8889 fuentes con J <10 mag y tipos espectrales K7 - M4. Las fuentes se obtuvieron en una búsqueda basada en movimientos propios (μ) y colores ópticos e infrarrojos. Lépine et al. (2013) presentó el análisis espectroscópico de 1564 fuentes de Lépine & Gaidos (2011) situadas en el hemisferio norte y con magnitudes J<9 mag. Frith et al. (2013) realizó una búsqueda de enanas M con $K_s < 9$ mag utilizando el catálogo PPXML (Roeser et al. 2010), identificando 1193 candidatas no incluidas en catálogos anteriores. Recientemente Gaidos et al. (2014) realizó una revisión de Lépine & Gaidos (2011) en base a nuevos criterios y catálogos (e.g. APASS). La Tabla 5.1 muestra las principales características de estos trabajos.

Table 5.1: Catálogos de enanas brillantes de tipo espectral M.

Catálogo	Criterio μ (mas/yr^{-1})	Número fuentes	Banda Infrarroja	Region cubierta
Lépine & Gaidos (2011)	>40	8889	J<10	Todo el cielo
Lépine et al. (2013)	>40	1564	J<9	Hemisferio norte
Frith et al. (2013)	...	4054	K<9	Todo el cielo
Gaidos et al. (2014)	>40	2970	J<9	Hemisferio norte
	>80			Hemisferio sur

5.1.1 Identificación de enanas M

A pesar de los esfuerzos realizados en los últimos años, el censo de enanas M cercanas y brillantes dista de ser completo. En Aberasturi et al. (2014b) se hizo uso de nuevo de herramientas de Observatorio Virtual (Aladin, STILS y VOSA) para la identificación y caracterización de nuevas enanas M. Para ello se realizó una correlación entre los catálogos 2MASS-PSC y *Carlsberg Meridian Catalogue 14* (CMC[2]; Copenhagen University et al. 2006). Para evitar problemas de memoria dividimos el área común entre los catálogos (25078 deg^2, ver Figura 5.1) en pequeñas regiones de 30′ de radio. En cada una de estas regiones aplicamos filtros de color adecuados para el tipo de objetos que pretendíamos encontrar

[2] http://www.ast.cam.ac.uk/∼dwe/SRF/cmc14.html

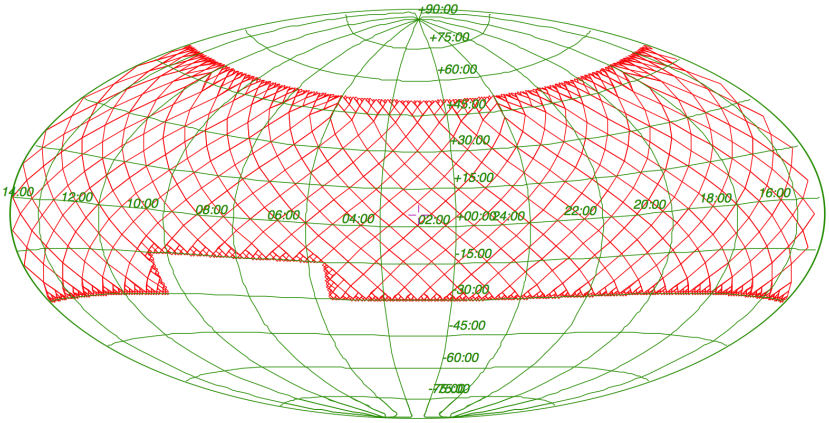

Figure 5.1: Área común rayada en rojo entre los catálogos 2MASS-PSC y CMC14.

(M4V-M8V). En particular seleccionamos objetos con $r' - J > 3.9$ mag, $0.8 < J - K_s < 1.0$ mag y $J < 10.5$ mag. A diferencia de los trabajos incluidos en la Tabla 5.1, no impusimos ninguna condición en movimiento propio (μ). Identificamos un total de 828 objetos que se muestran en la Figura 5.2. Tras una clasificación de las fuentes en enanas conocidas, gigantes, posibles gigantes u objetos jóvenes, seleccionamos 27 candidatos sin información espectroscópica para su seguimiento (ver Tabla 5.2). Los espectros fueron tomados con el espectrógrafo de dispersión intermedia (IDS) situado en el telescopio Isaac Newton de 2.5 m en el Roque de los Muchachos de La Palma (Islas Canarias) con una resolución de R = 1600 y sobre un rango espectral de 360 – 900 nm (ver Figura 5.3). Los tipos espectrales fueron determinados gracias a nuevo índice espectral $\Re = (F_{7470} - F_{7530})/(F_{7105} - F_{7165})$. Este índice posee un rango dinámico que hace posible una determinación espectral entre subtipos más precisa que otros definidos en trabajos previos.

Para estimar la temperatura efectiva y gravedad superficial usamos la herramienta del observatorio virtual VOSA (ver Figura 5.5 y Tabla 5.4). Los valores de la gravedad calculados con VOSA fueron confirmados espectroscópicamente utilizando el doblete de Na I λ 818.3 – 819.5 nm. Asimismo, buscamos sistemas de movimiento propio común entre nuestros 27 candidatos, identificando uno no descrito en trabajos previos (J0326+3929 / LSPMJ0326+3929W). La astrometría de dicho sistema fue caracterizada en detalle utilizando posiciones (RA, DEC) que cubrían una línea temporal de ~ 50 años. Por último también estimamos las distancias fotométricas de los objetos de la muestra y la actividad cromosférica mediante la emisión en Hα.

El análisis espectroscópico confirmó que los 27 objetos resultaron ser enanas M de tipos espectrales M2.5V - M5V lo que corrobora la robustez de nuestros criterios de selección. Los tipos espectrales calculados a partir de la espectroscopia'ía difieren de los estimado con VOSA en ± 0.5 subtipos. Dos de estos objetos se encuentran a menos de 10 pc y otros 4 en el rango de 10 –15 pc, todos ellos objetos relativamente brillantes, de baja

actividad y que no forman parte de sistemas binarios resueltos. Finalmente, indicar que doce de las enanas M descubiertas en este trabajo son candidatos potenciales a ser incluidos en el catálogo de final de CARMENES: J0012+3028, J0013+2733, J0024+2626, J0058+3919, J0156+3033, J0327+2212, J0507+3730, J0515+2336, J0909+2247, J1547+2241, J2211+4059 y J2248+1819.

5.1.2 Nuevos objetos pertenecientes a Taurus-Auriga

Durante el análisis de los datos identificamos en nuestra muestra tres nuevos miembros y cuatro candidatos a ser miembros de la región de formación estelar Taurus-Auriga basándonos en su movimiento propio, posición en el cielo, diagramas color-magnitud y actividad cromosférica. Éste es un resultado altamente interesante ya que apuntaría hacia una función inicial de masas estándar para Taurus-Auriga, explicando el posible déficit de objetos en el rango M2-M4 reportado por algunos autores (e.g. Luhman 2012) como una falta de completitud en las búsquedas realizadas hasta la fecha.

5.1.3 Conclusiones

En nuestro trabajo mostramos el potencial del Observatorio Virtual para encontrar nuevas enanas M cercanas ($d \leq 45$ pc) y brillantes (<10.5 mag), algunas de las cuales forman ya parte de listas de observación para búsquedas de exoplanetas. Identificamos y caracterizamos 27 objetos en el rango espectral M2.5 $-$ M5V. Dos de los objetos identificados por primera vez en este trabajo se encuentran a <10 pc (J0122+2209 y J2211+4059) y otros 4 en un rango de $10-15$ pc (J0012+3028, J0058+3919, J1518+2036 y J2259+3736), todos ellos objetos relativamente brillantes, de baja actividad y no forman parte de sistemas binarios resueltos. También encontramos tres nuevos miembros y 4 candidatos a la región de formación estelar de Taurus-Auriga, y encontramos un sistema con movimiento propio común caracterizado como una M4.5V y M5.0V.

A pesar de su brillo ($J<10.2$ mag para siete objetos y $J<9.7$ mag para un objeto), 16 enanas M no habían sido identificadas en trabajos previos. Esto es debido principalmente a que, a diferencia de otros estudios, nuestra búsqueda es puramente fotométrica y el movimiento propio no ha sido el principal criterio de selección. De este modo hemos sido capaces de encontrar enanas M con movimientos propios significativamente menores que los típicos de este tipo de objetos, explorando un espacio de parámetros no cubierto hasta la fecha.

Search for bright nearby M dwarfs with Virtual Observatory tools

2014, AJ, 148, 36A

Authors:
M. Aberasturi, J. A. Caballero, B. Montesinos, M. C. Gálvez-Ortiz, E. Solano and E. L. Martín
Affiliation:
Centro de Astrobiología (INTA-CSIC), Departamento de Astrofísica, P.O. Box 78, E-28691 Villanueva de la Cañada, Madrid, Spain

Abstract

Using Virtual Observatory tools, we cross-matched the Carlsberg Meridian 14 and the 2MASS Point Source catalogs to select candidate nearby bright M dwarfs distributed over ∼25,000 deg^2. Here, we present reconnaissance low-resolution optical spectra for 27 candidates that were observed with the Intermediate Dispersion Spectrograph at the 2.5 m Isaac Newton Telescope ($\mathcal{R} \approx 1600$). We derived spectral types from a new spectral index, $\Re$, which measures the ratio of fluxes at 7485–7015 and 7120–7150. We also used VOSA, a Virtual Observatory tool for spectral energy distribution fitting, to derive effective temperatures and surface gravities for each candidate. The resulting 27 targets were M dwarfs brighter than J = 10.5 mag, 16 of which were completely new in the Northern hemisphere and 7 of which were located at less than 15 pc. For all of them, we also measured Hα and Na I pseudo-equivalent widths, determined photometric distances, and identified the most active stars. The targets with the weakest sodium absorption, namely J0422+2439 (with X-ray and strong Hα emissions), J0435+2523, and J0439+2333, are new members in the young Taurus-Auriga star-forming region based on proper motion, spatial distribution, and location in the colour-magnitude diagram, which reopens the discussion on the deficit of M2–4 Taurus stars. Finally, based on proper motion diagrams, we report on a new wide M-dwarf binary system in the field, LSPM J0326+3929EW.

5.2 Introduction

M dwarfs are the most common stars in the universe. Not only is the closest star to the Sun an M dwarf (Proxima Centauri), but also 66 % of the nearest stars in our Galactic neighborhood ($d < 10$ pc) are M dwarfs[3]. However, after the first key proper-motion surveys in the first decades of the 20th century (van Maanen 1915; Wolf 1919; Ross 1939), the famous catalogs of Gliese (1969), Giclas et al. (1971, 1978), Luyten (1979a,b), Gliese & Jahreiss (1991), and the concluding spectroscopic studies of Kirkpatrick et al. (1991) and the RECONS Research Consortium of Nearby Stars (Reid et al. 1995; Hawley et al. 1997) at the end of the millennium, M dwarfs were relatively forgotten in the first decade of the current century. This apparent falling into oblivion, apart from a few honorable exceptions

[3] `http://www.recons.org/`

(e.g., Lépine et al. 2003b; Lépine & Shara 2005), was mostly due to many stellar astronomers focusing on the search and characterization of cooler objects with later spectral types: L, T, and, quite recently, Y (e.g., Martín et al. 1997, 1999, Kirkpatrick et al. 1999; Burgasser et al. 2002a; Cushing et al. 2011b).

Almost twenty years later, there have been a rebirth of M-dwarf studies. A few examples in the last four years are the possible existence of exoplanets in habitable zones around M dwarfs (Charbonneau et al. 2009; Anglada-Escudé et al. 2012; Bonfils et al. 2013a), a high occurrence of Earth-like-radius transiting exoplanets around cool stars in the *Kepler* field (Batalha et al. 2010b; Howard et al. 2012; Muirhead et al. 2012) and close to the Sun (Apps et al. 2010; Johnson et al. 2010; Bonfils et al. 2011), transmission spectra of super-earths around M dwarfs (Miller-Ricci & Fortney 2010; Berta et al. 2012), the luminosity and mass functions of low-mass stars in the solar neighborhood from Sloan data (Bochanski et al. 2010; West et al. 2011), low contrast ratios that favor the detection of very faint, close-in (planetary) companions (Chauvin et al. 2010), high-precision dynamical masses of very low-mass binaries (Konopacky et al. 2010), the complete new field of M-dwarf metallicity (Schlaufman & Laughlin 2010; Rojas-Ayala et al. 2010, 2012), fragile low-mass binaries (Burningham et al. 2010a; Faherty et al. 2010; Dhital et al. 2010), or even a rebith of activity studies in light of new magnetohydrodynamic models (Morin et al. 2010; Browning et al. 2010). Many exoplanet hunters turn now their eyes to M dwarfs, both with current instruments (CRIRES: Bean et al. 2010; NIRSPEC: Blake et al. 2010; MEarth: Irwin et al. 2011, Berta et al. 2013; APOGEE: Zasowski et al. 2013; *Kepler*: Martín et al. 2013) and with future ones (SPIRoU: Artigau et al. 2011a; CARMENES: Quirrenbach et al. 2012; HPF: Mahadevan et al. 2012; *TESS*: Ricker et al. 2010; *EChO*: Tinetti et al. 2012). In parallel, many research teams now focus on searching for the best M dwarfs for radial-velocity and transit exoplanet surveys (e.g., Reiners et al. 2010; Lépine & Gaidos 2011; Lépine et al. 2013; Frith et al. 2013; Caballero et al. 2013), apart from characterizing in detail such potential targets.

In this work we search for unidentified bright intermediate M dwarfs in the solar neighborhood using Virtual Observatory (VO[4]) techniques. The VO is *"an international initiative designed to provide the astronomical community with the data access and the research tools necessary to enable the exploration of the digital, multi-wavelength universe that is resident in the astronomical data archives"*. The VO is already an operational research infrastructure as demonstrated by the growing number of papers using VO tools (see, for instance, Caballero 2009; Valdivielso et al. 2009; Aberasturi et al. 2011; Lodieu et al. 2012b; Luhman 2013; López Martín et al. 2013; Malo et al. 2013, or Stelzer et al. 2013 for recent examples of VO science papers focused on low-mass stars). Besides, in this work we combine our VO search with a low-resolution spectroscopic follow-up, an astrometric and photometric study, and an activity analysis (based on our Hα measurements and X-ray emission from public databases) to successfully identify not only potential targets for exoplanet hunting at less than 20 pc, but also to serendipitously identify three young very low-mass stars in the Taurus-Auriga region.

[4] `http://www.ivoa.net`

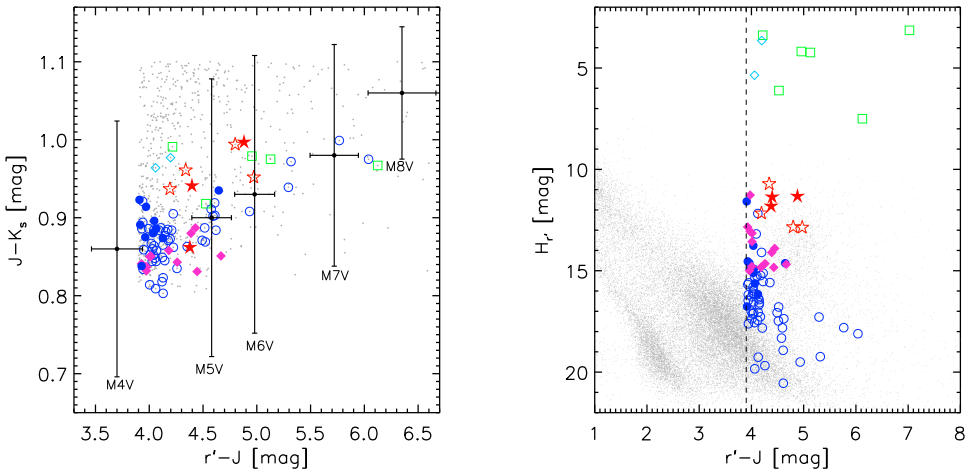

Figure 5.2: *Left panel:* $J - K_s$ vs. $r' - J$ colour-colour diagram. Small gray solid points represent the full cross-matched sources. Filled symbols are for stars spectroscopically investigated in this work, while open symbols are for the cross-matched known stars in Table 5.6.1. New field M dwarfs reported here for the first time are drawn with (magenta) rhombs, previously known field M dwarfs with (blue) circles, members in Taurus-Auriga with (red) stars, M giants with (green) squares, and reddened Cygnus OB2 massive stars with (cyan) rhombs. Black error bars represent the average colours of typical dwarfs of spectral types M4 V to M8 V (West et al. 2008). *Right panel:* same as left panel but the tiny gray points represent stars in Lépine & Shara (2005) with the CMC14 counterpart. The vertical dashed line at $r' - J = 3.9$ mag indicates our colour cut. The two Galactic disk dwarf and halo subdwarf sequences are distinguishable in the bottom left corner.

5.3 Observations and analysis

5.3.1 Candidate selection

First of all, we cross-matched the whole Carlsberg Meridian Catalogue 14 (CMC14[5]; Copenhagen University et al. 2006 – see Evans et al. 2002 for a description of a previous release) with the Two-Micron All Sky Survey (2MASS; Skrutskie et al. 2006). This correlation was performed with the help of the Aladin sky atlas (Bonnarel et al. 2000) and the Starlink Tables Infrastructure Library Tool Set (STILTS; Taylor 2006). To avoid memory overflow problems, we divided the 25 078 deg^2 of common CMC14-2MASS sky (i.e., the CMC14 area – over 60 % of the whole sphere) into overlapping circular regions of 30 arcmin radius. We used a matching radius of 5 arcsec, which ensured that objects with high proper motions of up to $\mu \sim 1700$ mas a^{-1} (given the typical baseline between 2MASS and CMC14 astrometric epochs) were not left out. Only the closest 2MASS counterpart to each CMC14 source was considered.

[5] `http://www.ast.cam.ac.uk/~dwe/SRF/cmc14.html`

Table 5.2: Basic Data of the 27 Spectroscopically Analysed M Candidates[a]

ID	Alternative Name	α (J2000)	δ (J2000)	b (deg)	$\mu_\alpha \cos\delta$ (mas a^{-1})	μ_δ (mas a^{-1})	$r'-J$ (mag)	$J-K_s$ (mag)	$H_{r'}$ (mag)
J0012+3028	...	00:12:13.43	+30:28:44.2	−31.6	+52.7±5.1	−25.9±5.1	3.97	0.83	13.06
J0013+2733	...	00:13:19.52	+27:33:30.8	−34.6	+16.3±4.4	−116.4±4.4	4.00	0.85	14.79
J0024+2626	LSPM J0024+2626	00:24:03.81	+26:26:29.7	−36.0	+7.0±6.4	−30.1±6.4	3.90	0.92	11.58
J0058+3919	PM I00580+3919	00:58:01.13	+39:19:11.2	−23.5	−102.6±9.3	+34.1±9.3	4.04	0.88	13.77
J0122+2209	G 34−23	01:22:10.32	+22:09:03.0	−40.2	+237.0±5.3	−152.7±5.3	3.96	0.87	14.63
J0156+3033	NLTT 6496 (Kö4A)	01:56:45.76	+30:33:28.8	−30.2	+219.2±4.6	−12.5±4.6	4.13	0.87	16.16
J0304+2203	...	03:04:44.10	+22:03:21.2	−31.2	+37.8±5.1	−49.3±5.1	4.44	0.83	13.90
J0326+3929	LSPM J0326+3929W	03:26:34.20	+39:29:02.5	−14.2	+61.4±5.7	–144.1±5.7	4.00	0.91	14.94
J0327+2212	...	03:27:30.87	+22:12:38.1	−27.9	−39.0±6.3	−53.0±6.3	4.01	0.85	13.15
J0341+1824	...	03:41:43.87	+18:24:06.2	−28.6	+23.9±4.7	−42.2±4.7	3.93	0.84	12.84
J0342+2326	LR Tau	03:42:53.29	+23:26:49.5	−24.6	+176.7±4.7	−61.2±4.7	4.06	0.89	15.63
J0422+2439	...	04:22:54.17	+24:39:53.6	−17.3	+5.0±4.5	−22.3±4.5	4.88	1.00	11.32
J0424+3706	...	04:24:21.51	+37:06:20.8	−8.6	+47.3±6.5	−57.6±6.5	4.01	0.85	13.56
J0435+2523	...	04:35:47.79	+25:23:43.6	−14.6	+2.9±4.5	−21.6±4.5	4.40	0.94	11.36
J0439+2333	...	04:39:04.54	+23:33:19.9	−15.3	−0.9±4.6	−24.6±4.6	4.38	0.86	11.81
J0507+3730	...	05:07:14.45	+37:30:42.1	−1.9	−105.5±5.0	−8.0±5.0	4.43	0.89	14.84
J0515+2336	...	05:15:17.54	+23:36:25.9	−8.6	+36.7±4.6	−71.5±4.6	4.39	0.88	14.10
J0630+3003	...	06:30:10.18	+30:03:39.5	+9.0	−1.6±8.2	+28.1±8.2	3.97	0.84	11.27
J0909+2247	...	09:09:07.97	+22:47:41.2	+39.8	−81.2±4.2	−71.8±4.2	4.18	0.86	14.83
J1132+1816	...	11:32:23.00	+18:16:22.4	+69.8	+136.4±5.5	+58.6±5.5	3.96	0.84	14.99
J1241+1905	G 59−34	12:41:29.00	+19:05:00.7	+81.6	+68.6±4.9	−305.4±4.9	3.92	0.89	16.76
J1459+3618	RX J1459.4+3618	14:59:25.04	+36:18:32.3	+61.4	−123.9±5.2	+76.1±5.2	4.03	0.88	15.10
J1518+2036	...	15:18:31.45	+20:36:28.3	+55.9	+10.1±4.6	+94.8±4.6	4.67	0.85	14.68
J1547+2241	LSPM J1547+2241	15:47:40.69	+22:41:16.5	+50.0	−180.9±5.0	−29.5±5.0	4.05	0.90	14.90
J2211+4059	1RXS J221124.3+410000	22:11:24.14	+40:59:58.9	−12.4	−89.6±4.9	+68.0±4.9	4.65	0.93	14.63
J2248+1819	PM I22489+1819	22:48:54.58	+18:19:58.9	−35.7	−24.7±5.1	−132.8±5.1	3.93	0.84	14.54
J2259+3736	...	22:59:14.81	+37:36:39.6	−20.1	+96.2±4.7	−28.9±4.7	4.26	0.84	14.65

[a]Identification, discovery name (blank if new), right ascension and declination from 2MASS, Galactic latitude, proper motions from PPMXL, $r'-J$ and $J-K_s$ colours, and reduced proper motion $H_{r'} = r' + 5\log\mu + 5$.

Constraints based on the colours expected for M dwarfs with spectral types M4 V and later were imposed. In particular, we selected objects with colours $r'-J > 3.9$ mag and 0.8 mag $< J-K_\mathrm{s} < 1.1$ mag (e.g., West et al. 2008) and high quality 2MASS flags (AAA).

Since we were interested in *bright* M dwarfs, our last restriction was $J < 10.5$ mag. We did not expect to identify any dwarfs later than M8 V ($r'-J \gtrsim 6.5$ mag) because the CMC14 completeness magnitude is $r' \approx 17.0$ mag in the Sloan passband (slightly variable by 0.1–0.2 mag from one sky region to another). After these colour and magnitude cuts, we expect to find M4 V (M8 V) stars within 45 pc (7.5 pc) the Sun using the M_J-SpT relation in Caballero et al. (2008, Table 3). The selection of the resulting 828 sources with $r'JHK_\mathrm{s}$ photometry is illustrated in the left panel of Figure. 5.2.

We prepared a list of high-priority targets for a spectroscopic run planned for the Canarian winter (see Section 5.3.2). Of the 828 stars, we selected objects visible during the season (i.e., with right ascensions 22 h $< \alpha <$ 16 h) and with minimum zenith distances

during culmination (i.e., with declinations +18 deg $< \delta <$ +41 deg). We imposed an extra cut at colours $J - K_s < 1.0$ mag, thus making the near-infrared colour constraint actually 0.8 mag$< J - K_s < 1.0$ mag. The 125 sources passing these filters were inspected visually with Aladin and classified into five groups: (1) known dwarfs, (2) known giants, (3) known young stars (T Tauri and reddened massive stars), 4) probable giants, and (5) probable dwarfs. There was only one artifact from an incorrect CMC14-2MASS cross-match of a visual binary, which resulted in a final list of 124 stars. For the classification, we used additional information gathered from the SIMBAD[6] and ADS[7] services, and the PPMXL catalog of positions and proper motions on the ICRS (PPMXL; Roeser et al. 2010) and *IRAS* point source (Helou & Walker 1988). Field giants in the investigated magnitude range have in general very low proper motions, lower than 5 mas a^{-1}, near-infrared colours close to the upper limit ($J - K_s \approx 1.0$ mag), flux excess in the *IRAS* passbands, and, in some cases, photometric variability due to pulsations (see, e.g., the recent VO-based survey for bright Tycho-2 stars with red colours by Jiménez-Esteban et al. 2012).

The 97 cross-matched known dwarfs, giants and young stars with spectral-type determination and probable dwarfs and giants without spectral typing are shown in Table 5.6.1. All the known dwarfs (55) except one have spectral types M4.0 V or later (the exception is G 98–52 A, which has an M3.5 V spectral type). Table 5.6.1 includes four pre-main sequence T Tauri stars in Taurus-Auriga (XEST 16–045, FW Tau AB, V927 Tau AB, and Haro 6–36; see Section 5.4.4) and a couple of reddened massive stars in Cygnus OB2 ([CPR2002] A20 and [CPR2002] A25; Comerón et al. 2002). Field M giants, T Tauri stars, and reddened Cygnus OB2 massive stars fall in well-defined locations in a reduced-proper-motions diagram, as the one shown in the right panel of Figure. 5.2.

The remaining 27 high-priority dwarf candidates, shown in Table 5.2, were selected for spectroscopic follow-up. They all had proper motions greater than 20 mas a^{-1}, no *IRAS* detection, and magnitudes and colours consistent with intermediate or late M spectral type and luminosity class V. Of them, only 11 were previously identified and classified as M dwarf candidates based only on photometry by Giclas et al. (1959, 1961), McCarthy & Treanor (1964), Luyten (1979b), Fleming (1998), Lépine & Shara (2005), and Lépine & Gaidos (2011).

5.3.2 Spectroscopy

On 2012 January 11–13, we used the Intermediate Dispersion Spectrograph (IDS) at the 2.5 m Isaac Newton Telescope (INT) in the Observatorio del Roque de Los Muchachos (La Palma, Spain). We used the configuration with the Red+2 detector, the R300V grating centered on 550 nm, and the 1.0 arcsec wide slit, which provided a resolution $\mathcal{R} \approx 1600$ over a wide wavelength interval from 360 to 900 nm. The actual useful wavelength interval was, however, a bit narrower, from 425 to 825 nm.

[6] `http://simbad.u-strasbg.fr/simbad/sim-fid`
[7] `http://adswww.harvard.edu/`

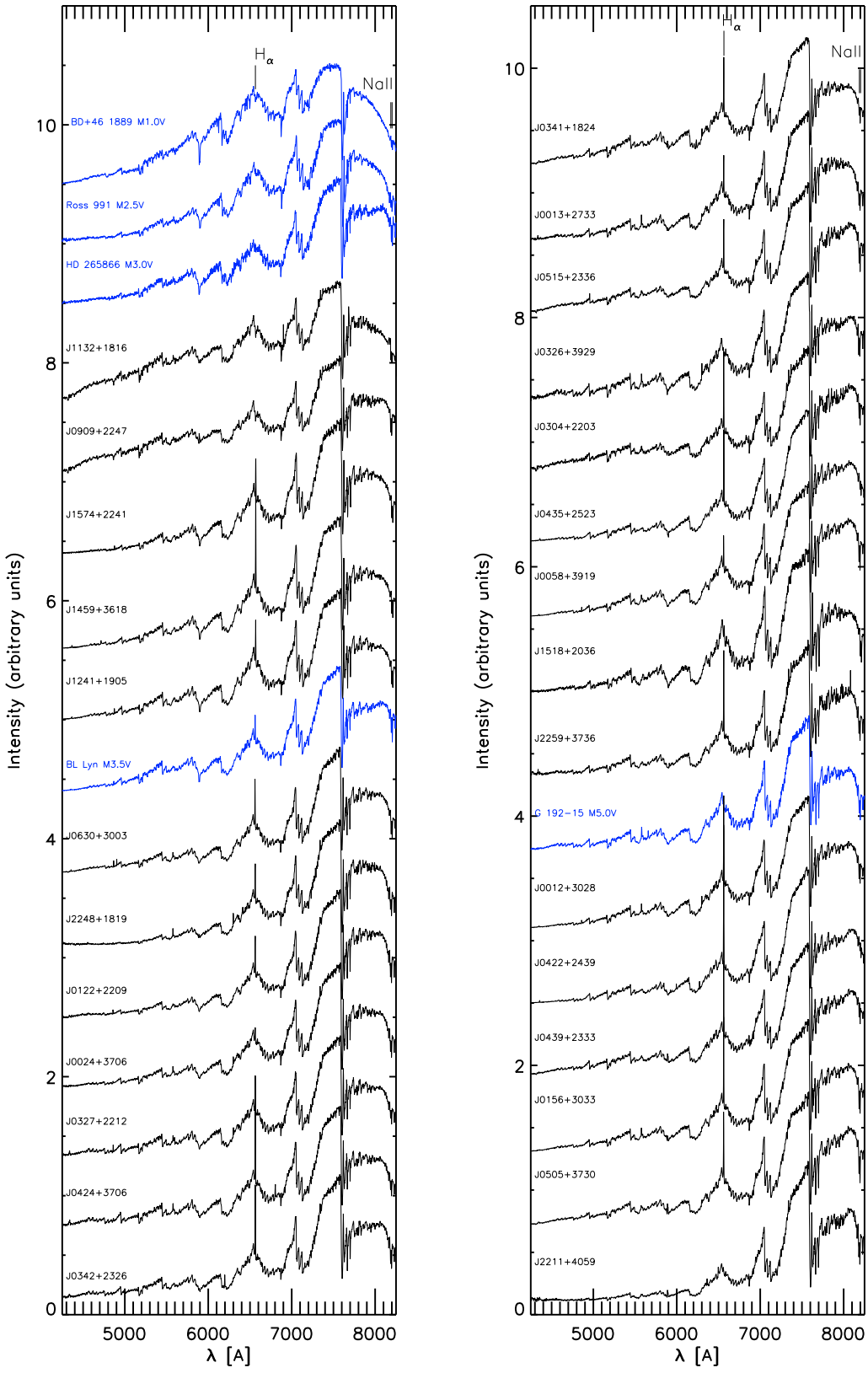

Figure 5.3: IDS/INT spectra of our 27 M dwarf candidates (in black) and five reference stars (in blue), normalized at 7400 Å.

Table 5.3: Spectral-type reference stars

Name	GJ	α (J2000)	δ (J2000)	SpT PMSU[a]	SpT Simbad
G 192–15	3380	06:02:29.18	+49:51:56.2	M5.0 V	M5.0 V
HD 265866	251	06:54:48.96	+33:16:05.4	M3.0 V	M4.0 V
BL Lyn	277 B	07:31:57.33	+36:13:47.4	M3.5 V	M4.5 V
Ross 991	3748	12:47:00.99	+46:37:33.4	M2.5 V	M2.0 V
BD+46 1889	521	13:39:24.10	+46:11:11.4	M1.0 V	M2.0 V

[a] The Palomar/Michigan State University survey (Reid et al. 1995; Hawley et al. 1996

We collected low-resolution spectra of the 27 high-priority dwarf candidates and 5 reference stars for spectral-type determination, which are shown in Table 5.3. Exposure times ranged between 700 and 2400 s, depending on target brightness. Raw data were next reduced following standard procedures within the IRAF environment (bias and flat-field correction, cosmic-ray rejection, and optimal extraction). Wavelength calibration was carried out with spectra of Cu-Ne arc lamps taken during the run. Figure. 5.3 shows the 32 final spectra of bright M dwarf candidates and reference stars sorted by spectral type.

5.4 Results

5.4.1 Spectral types

As explained above, 11 of the 27 high-priority M-dwarf candidates observed spectroscopically were previously known. Of them, seven had spectral-type estimations from colours (from digitization of blue and red photographic plates –Giclas et al. 1961; Lépine & Gaidos 2011– or from optical and near-infrared multi-band photometry –Fleming 1998), and two from real spectra (J0122+2209 from Lépine et al. 2013 and J1241+1905 from Reid et al. 2003).

For the 27 stars, we derived our own spectral types with a custom-made spectral index. Spectral indices have been extensively used in the classification of M dwarf spectra (Kirkpatrick et al. 1991; Reid et al. 1995; Martín et al. 1996, 1999; Hawley et al. 2002; Lépine et al. 2003a; Slesnick et al. 2006a,b; Shkolnik et al. 2011; Seeliger et al. 2011).

We took advantage of this knowledge for defining the $\Re$ index, which better fits the useful wavelength interval, resolution, and maximum efficiency of our IDS/INT spectra. The numerator and denominator of the $\Re$ index are the fluxes contained in the 30 Å bands centered on 7500 and 7135 Å, which correspond to the pseudo-continuum at the red side and to the minimum of the strong ∼7000–7350 Å TiO band, respectively. Basically, $\Re$ is similar to the Martín et al. (1996) PC2 index (7560±20 Å / 7040±10 Å), which accounts mostly for the TiO and VO contributions, but with the numerator wavelength interval at the bottom of a deep water vapor band head. The $\Re$ index is not sensitive to luminosity, log g or

Table 5.4: Miscellaneous Data of the 27 Investigated Stars[a]

ID	SpT (biblio.)	ℜ	SpT (IDS)	pEW(Hα)[b] []	pEW(Na I) []	$T_{\rm eff}$ [K]	$\log g$	d[c] [pc]	1RXS	ρ [arsec]	X-CR [s^{-1}]	$HR1$
J0012+3028	...	2.87	M5.0 V	−10.3±0.2	+4.5±0.2	3100	5.5	14±4	J001213.6+302906	21.9	0.02	−0.08
J0013+2733	...	2.56	M4.5 V	−4.4±0.2	+6.1±0.2	3100	5.5	20±5	...	...	...	...
J0024+2626	...	2.43	M4.0 V	−2.0±0.2	+6.3±0.2	3100	5.5	18±5	...	...	...	...
J0058+3919	m5: V	2.76	M4.5 V	−3.4±0.3	+5.0±0.3	3100	5.5	14±3	J005802.4+391912	14.8	0.02	−0.25
J0122+2209	M4.5 V	2.43	M4.0 V	−4.8±0.2	+6.7±0.3	3100	5.5	8±2	J012210.9+220909	10.4	0.19	−0.22
J0156+3033	m4.5: V	3.00	M5.0 V	−9.3±0.3	+5.4±0.3	3100	6.0	15±4	J015645.8+303332	3.25	0.04	−0.54
J0304+2203	...	2.62	M4.5 V	−8.5±0.3	+3.7±0.3	3000	5.5	21±5	J0304441.3+220320	30.0	0.02	+0.10
J0326+3929	k7: V	2.61	M4.5 V	> −1.0	+5.7±0.3	3100	4.5	17±4	...	...	...	...
J0327+2212	...	2.46	M4.0 V	−3.7±0.1	+4.4±0.2	3100	5.5	17±4	...	...	...	...
J0341+1824	...	2.53	M4.0 V	−6.0±0.2	+3.2±0.3	3100	5.5	21±5	...	...	...	...
J0342+2326	m: V	2.52	M4.0 V	−7.7±0.2	+6.4±0.3	3100	6.0	18±5	...	...	...	...
J0422+2439	...	2.93	M5.0e	−20.9±0.5	+2.1±0.5	2900	3.0	∼140	J042254.9+243950	10.4	0.03	+1.0
J0424+3706	...	2.49	M4.0 V	−8.8±0.2	+4.7±0.3	3100	6.0	18±5	J042421.4+370609	11.4	0.03	−0.66
J0435+2523	...	2.65	M4.5	−9.0±0.2	+2.7±0.5	3000	3.5	∼140	...	...	...	...
J0439+2333	...	3.00	M5.0	−8.2±0.3	+2.2±0.5	3000	4.0	∼140	...	...	...	...
J0507+3730	...	3.02	M5.0 V	−7.4±0.4	+5.6±0.3	3000	5.5	15±4	J050714.8+373103	21.8	0.04	−0.34
J0515+2336	...	2.59	M4.5 V	−5.3±0.2	+5.5±0.3	3000	5.5	18±5	...	...	...	...
J0630+3003	...	2.30	M4.0 V	−4.4±0.2	+5.7±0.2	3100	5.5	22±5	...	...	...	...
J0909+2247	...	1.98	M3.0 V	> −1.0	+4.6±0.2	3000	5.0	44±11	...	...	...	...
J1132+1816	...	1.84	M2.5 V	> −1.0	+2.2±0.3	3200	5.5	39±10	...	...	...	...
J1241+1905	M4.5 V	2.23	M3.5 V	−3.7±0.2	+5.6±0.3	3100	5.5	33±8	...	...	...	...
J1459+3618	...	2.19	M3.5 V	−8.4±0.2	+5.7±0.3	3100	6.0	31±8	J145924.6+361826	8.24	0.02	+0.04
J1518+2036	...	2.78	M4.5 V	−1.1±0.1	+7.4±0.3	2900	5.0	14±3	...	...	...	...
J1547+2241	m5: V	2.16	M3.5 V	−3.9±0.1	+6.0±0.3	3100	6.0	22±5	J154741.3+224108	11.7	0.03	−0.56
J2211+4059	m7: V	3.30	M5.5 V	−5.4±0.2	+7.1±0.3	2900	5.0	9±2	J221124.3+410000	2.04	0.06	+0.11
J2248+1819	m5: V	2.42	M4.0 V	−4.2±0.2	+7.1±0.3	3100	5.5	16±4	...	...	...	...
J2259+3736	...	2.81	M4.5 V	−9.8±0.2	+5.9±0.3	3000	4.5	12±3	...	...	...	...

[a]Spectral types from the bibliography and our IDS/INT spectra (photometric spectral types are listed with 'm' and 'k'), ℜ index, pseudo-equivalent widths of Hα λ656.3 nm and Na I $\lambda\lambda$818.3,819.5 nm from our spectra, $T_{\rm eff}$ (±100 K) and $\log g$ (±0.5) from our VOSA fits, derived heliocentric distance, and key data from the *ROSAT* All-Sky Bright and Faint Survey Catalogues (1RXS name, angular separation between the X-ray and 2MASS coordinates, count rate, and hardness ratio).
[b]Two stars had previous pEW(Hα) determinations: J0122+2209 of –4.1±0.7 Å and J1459+3618 of –6.9±0.6 Å (Mochnacki et al. 2002).
[c]Three stars had previous distance determinations: J0122+2209 at 10.5 pc and J1459+3618 at 22.0 pc (Fleming 1998), J0156+3033 at 19^{+6}_{-4} pc (Caballero, 2012).

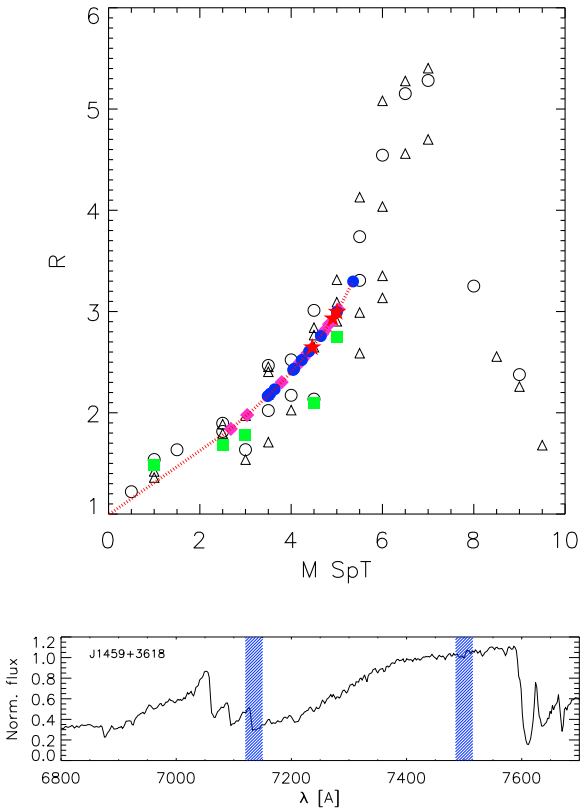

Figure 5.4: *Top panel*: our spectral index $\Re$ measured for M1–9 V spectral type templates observed by Leggett et al. (2000a) and Cruz & Reid (2002) (black empty circles and triangles, respectively) compared with our 24 field M dwarfs (blue filled circles), 3 T∼Tauri M-type objects (red filled stars), and 5 reference field dwarfs (green filled squares). *Bottom panel*: wavelength intervals used to define the Re index on an example spectrum.

metallicity. To minimize the dependence of our index on flux calibration calibration issues, we normalized our spectra to a pseudo-continuum traced by joining the highest points of the observed spectra (skipping Hα). The ratios were measured on the "normalized" spectra. As templates for determining the $\Re$-spectral type relation, we used the spectra of 58 M1–9 V stars of Leggett et al. (2000a) and Cruz & Reid (2002), together with our 5 reference stars, normalized in the same way as the target spectra. As illustrated by Figure. 5.4, the $\Re$ index has the advantage of having a fairly large dynamic range, covering values from about 1.0 to 5.5. We fit the $\Re$-SpT pairs to a parabola (i.e., SpT$(\Re) = a + b\Re + c\Re^2$), and derived spectral types for our 27 targets with an estimated uncertainty of $\pm$0.5 spectral subtypes. The relation to estimate the spectral type, valid between M0.0 V and M5.5 V, was:

$$SpT = -0.58\Re^2 + 4.8\Re - 4.2 \tag{5.1}$$

The results are listed in the third column of Table 5.4. We calculate 18 new spectral

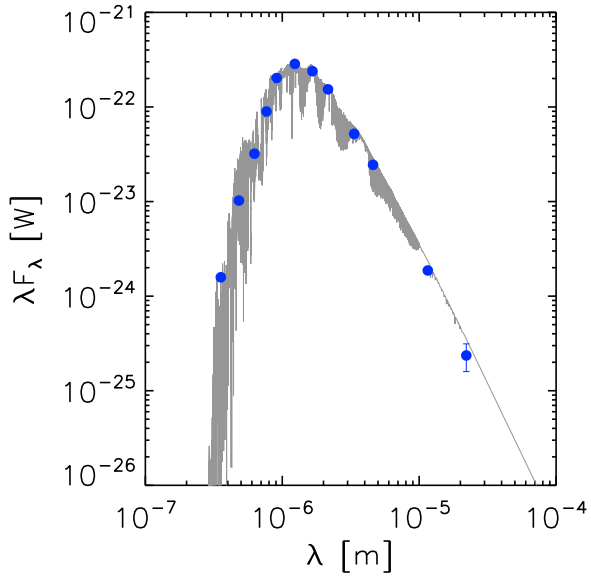

Figure 5.5: Spectral energy distribution of J1459+3618 from 350 nm (u') to 22,100 nm ($W4$), in blue filled circles, and the corresponding best-fit NextGen model provided by VOSA.

types for the first time and improve previous determinations for other 7 dwarfs. Derived spectral types vary from M2.5 V in the case of J1132+1816 to M5.5 V in the case of J2211+4059 (PM I22489+1819), with the majority of them in the narrow interval from M3.5 V to M4.5 V, which fully backs our initial colour criteria for selecting intermediate M dwarfs (the original cut in $r' - J$ was for selecting >M4 V stars). Some of the stars M4 V and later are bright enough to be potential targets for exoplanet surveys, such as CARMENES (Quirrenbach et al., 2012; Caballero et al., 2013). Interestingly, the latest M dwarf in our sample had a spectral-type estimation from $V_{\rm phot} - J$ photometry at M7: V. We agree with Lépine et al. (2013) and Mundt et al. (2013) that spectral types from this colour are systematically later than those actually measured on real spectra (at least for spectral types later than M2–3 V).

5.4.2 Effective temperatures and surface gravities

We used another VO tool, the VO Spectral energy distribution Analyzer (VOSA[8]; Bayo et al. 2008), to derive effective temperatures ($T_{\rm eff}$) and surface gravities ($\log g$) of our 27 targets from fits of observed spectral energy distributions to theoretical models. Apart from the CMC14 (r') and 2MASS (JHK_s) photometric data, we also used those of the *Wide-field Infrared Survey Explorer* ($W1$–4; *WISE*, Cutri & et al. 2012) and, when available, the Fourth U. S. Naval Observatory CCD Astrograph Catalogue ($Bg'Vi'$; UCAC4, Zacharias et al. 2012), and Sloan Digital Sky Survey ($u'g'$; SDSS DR9, Aihara et al. 2011). We did not use the Hartman et al.

[8] `http://svo2.cab.inta-csic.es/theory/vosa/`

(2011) V-band photometry of J1459+3618/RX J1459.4+3618 because of an incorrect absolute calibration (besides, they found a period of photometric variability of 4.17 d, but with a V-band amplitude of only 49 mmag). Key photometry of the 27 targets is provided in Table 5.7.

In VOSA, we used the BT-Settl theoretical models (Allard, 2014) between 1 600 and 4 000 K in $T_{\rm eff}$ and between 3.5 and 6.0 in $\log g$ for solar metallicity. The uncertainty in the best fit was the size of the grid, which was of 100 K in $T_{\rm eff}$ and 0.5 in $\log g$. Anayway, the VOSA $\log g$ values have to be taken with caution and refined using other indicators. Figure. 5.5 illustrates one of our VOSA fits as an example.

Derived values ranged between 2800 and 3400 K in $T_{\rm eff}$, and 3.5 and 6.0 in $\log g$, which roughly match our spectral types and the surface gravity expected values for normal mid-M dwarfs in the field (e.g., Rajpurohit et al. 2013). As a matter of fact, the star with the latest spectral type in our sample (J2211+4059, M5.5 V) also had the lowest effective temperature ($T_{\rm eff}$ = 2900$\pm$100 K).

We double-checked the VOSA values of $\log g$ with an atomic gravity-sensitive feature present in our spectra, the Na I doublet at 818.3–819.5 nm (Steele & Jameson 1995; Guieu et al. 2006; Slesnick et al. 2006a; Martín et al. 2010; Schlieder et al. 2012). At a given spectral type in low-mass stars (and brown dwarfs), the weaker the alkali doublet, the lower the gravity. In its turn, low gravity is an indicator of youth (Béjar et al. 1999; McGovern et al. 2004; Burningham et al. 2005; Soderblom et al. 2013 and references therein). We measured the pseudo-equivalent widths of the alkali doublet in our IDS/INT spectra with the IRAF task `splot`. The results, given in Table 5.4, showed that there are three M4.0–5.0 stars with significantly weak sodium absorption, of pEW(Na I) $<$ 3 Å; two of them also had the lowest surface gravities ($\log g$ = 3.5$\pm$0.5) in the VOSA fits. The other 24 stars had sodium absorptions typical of field dwarfs of the same spectral types (see Table 4 in Schlieder et al. 2012).

The compiled photometry also allowed us to search for infrared excesses, which may be ascribed to circumstellar disks. In particular, two stars, J0515+2336 and J0507+3730, had a significantly bright $W4$ magnitude (at 22.1 μm) with respect to the other *WISE* and 2MASS magnitudes (Table 5.7). However, their apparent $W4$-band excess came instead from an incorrect background subtraction at very low Galactic latitudes (column b in Table 5.2). All in all, no star in our sample displayed a clear mid-infrared flux excess attributable to a disks.

5.4.3 Activity

We tried to quantify the magnetic activity of the stars in our sample. First, we measured pseudo-equivalent widths of the Hα λ656.3 nm line, pEW(Hα)s, in our IDS/INT spectra. Error bars for each target were assigned by manual repetition of measurements making educated visual inspections of the continuum levels and the line limits. As expected for intermediate- and late-type M dwarfs (Hawley et al. 1996; Gizis et al. 2000; West et al. 2004), most of our stars showed Hα in emission. Indeed, two of the three non-Hα emitters are the earliest stars in our sample (M2.5–3.0 V). However, one of the stars displayed an Hα pseudo-

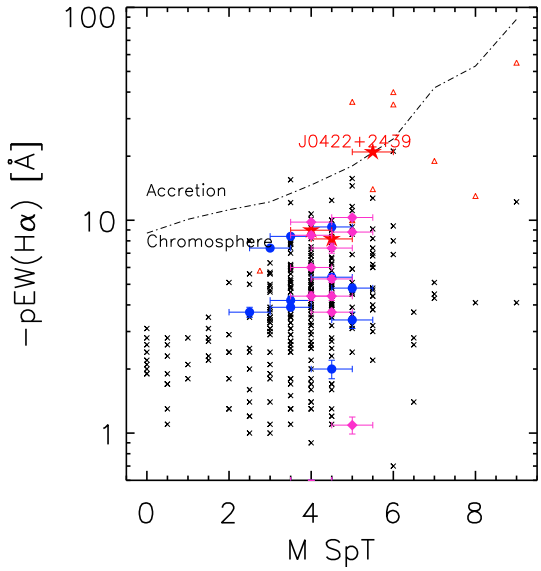

Figure 5.6: Pseudo-equivalent widths of Hα as a function of spectral type with the Barrado y Navascués & Martín (2003) accretion-chromosphere boundary. Small (black) crosses are field M dwarfs from Gershberg et al. (1999), (red) triangles are confirmed Taurus-Auriga members from Martín et al. (2001), Luhman et al. (2003), and Muzerolle et al. (2003), (magenta and blue) filled circles are the 24 (new and known) field stars investigated here, and (red) filled stars are our three new Taurus-Auriga member candidates, including J0422+2439.

equivalent width that stood out among the other measurements: J0422+2439, with pEW(Hα) = –20.9$\pm$0.5 Å. We used the Barrado y Navascués & Martín (2003) empirical criterion for ascertaining the origin of the Hα emission. As illustrated by Figure. 5.6, the emission of all stars in our sample except J0422+2439 is consistent with chromospheric activity. J0422+2439, one of the three low-gravity stars described in Section 5.4.2, showed Hα emission very close to the criterion boundary separating accretion and chromospheric emission.

There were two stars, J0122+2209/G 34–53 and J1459+3618/RX J1459.4+3618, for which Hα emission had been investigated previously by Mochnacki et al. (2002) (Table 5.4). Their and our measurements of pEW(Hα) match each other within the uncertainties.

Second, we searched for counterparts in the *ROSAT* All-Sky Bright and Faint Survey Catalogues (Voges et al., 1999). We applied a search radius of 30 arcsec due to the low *ROSAT* astrometric precision. Of the 27 stars in our sample, 11 stars (∼40 %) had appreciable emission in the 0.2–2.0 keV energy band at the time of the *ROSAT* observations.

The brightest star in our sample in the visible and near-infrared, J0122+2209/G 34–53, also has the highest X-ray count rate by far. Perhaps because of that reason, it has been the subject of a few all-sky X-ray surveys for low-mass stars (Fleming 1998; Zickgraf et al. 2003; Fuhrmeister & Schmitt 2003; Haakonsen & Rutledge 2009). Another

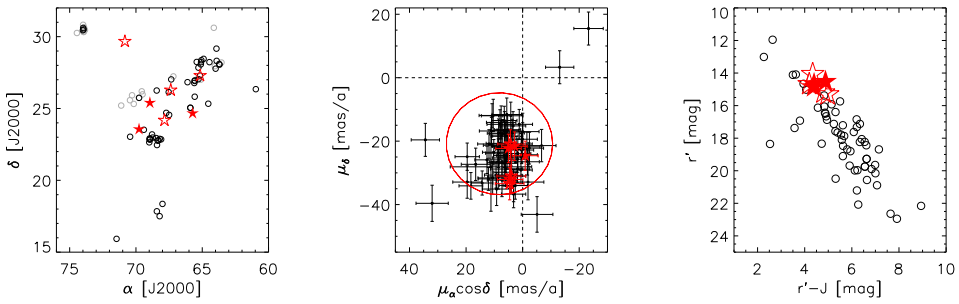

Figure 5.7: *Left panel:* spatial distribution of candidate members in the Taurus-Auriga star-forming region. (Red) filled stars are our three new candidates with IDS/INT spectroscopy, (red) open stars are the four known Taurus-Auriga T Tauri stars identified in the 2MASS-CMC14 cross-match and listed in Table 5.6.1, and (black) open circles are Taurus-Auriga members from Luhman (2004a), Luhman et al. (2006, 2009a), and Guieu et al. (2006). *Middle panel:* same as the left panel, but for the proper-motion diagram. The ellipse indicates the average values and standard deviations of proper motions in Taurus-Auriga from Bertout & Genova (2006), *Right panel:* same as the left panel, but for the r' vs. $r' - J$ colour-magnitude diagram.

three known dwarfs had also been cataloged as X-ray emitters: J0156+3033/NLTT 6896 (Caballero, 2012), J1459+3618/RX J1459.4+3618 (Fleming 1998), and J2211+4059/1RXS J221124.3+410000 (Haakonsen & Rutledge 2009). In this work, we report for the first time the X-ray emission of one known M dwarf, J0058+3919/PM I00580+3919, and six new M dwarfs.

For the 11 X-ray stars, we calculated the distance-independent parameter F_X/F_J ($\equiv L_X/L_J$), which is a proxy of $L_X/L_{\rm bol}$ (Caballero et al. 2010). We computed F_X from the X-ray count rates and hardness ratios as in Schmitt et al. (1995). Six stars had F_X/F_J ratios above 0.7×10^{-3}, with only one of them having a ratio of $\sim 1.1 \times 10^{-3}$. This relatively strong X-ray emitter is just J2211+4059/1RXS J221124.3+410000, the primary of an ultra fragile binary system. The other five intense emitters are J0122+2209/G 34–53 (the brightest star of our list), J0156+3033/NLTT 6896 (the primary of the Koenigstuhl 4 wide binary system), J0422+2439 (the accreting star with strong Hα emission and low surface gravity), and J0304+2203 and J0507+3730 (two new, M4.5-5.0 V stars identified in this work). The latter three intense X-ray emitters are shown here for the first time. The other six stars with *ROSAT* data are relatively faint X-ray emitters.

5.4.4 Three new member candidates in Taurus

The strong Hα emission, low surface gravity, and relatively intense X-ray emission of the possibly accreting star J0422+2439 led us to investigate it in detail. Its coordinates, as well as those of the other two stars with weak Na I absorption, resembled those of the four known young T Tauri stars in Table 5.6.1, so we considered their membership in the young star-

forming region of Taurus-Auriga ($\tau \sim 1$–2 Ma, $d \sim 140$ pc; Kenyon et al. 2008).

First of all, we compiled an exhaustive list of Taurus-Auriga members and member candidates from Luhman (2004a), Luhman et al. (2006, 2009a), and Guieu et al. (2006) and cross-matched that list with 2MASS, CMC14, and PPMXL. Figure. 5.7 illustrates our analyses. From left to right, our three new Taurus-Auriga member candidates with spectroscopy (and the four T Tauri stars in Table 5.6.1) (1) are spatially located towards the densest filaments of Taurus-Auriga (see also Figure 1 in Luhman et al. 2009a), (2) have proper motions consistent with membership in Taurus-Auriga (Bertout & Genova 2006; Mooley et al. 2013), and (3) follow the Taurus-Auriga sequence in optical-near-infrared colour-magnitude diagrams[9]. Taking into account these facts, the low surface gravity of the three new member candidates, and the intense Hα and X-ray emission of the accreting star, we concluded that J0422+2439, J0435+2523, and J0439+2333 do belong to Taurus-Auriga.

We further characterized the three identified T Tauri stars. At $d \sim 140$ pc, the Taurus-Auriga distance modulus is $m - M \sim 5.7$ mag. With the J-band apparent magnitudes, the maximum Êabsolute magnitudes range between 3.9 and 4.7 mag. Actual absolute magnitudes must be brighter than that interval because of variable extinction toward Taurus-Auriga. The detection of J0422+2439 by *ROSAT* implies that it is located in the closer side of the cloud, with subsequent low extinction (X-rays are absorbed by interstellar dust and gas). Something similar happens to J0435+2523 and J0439+2333, whose SEDs and colours do not deviate significantly from the other M dwarfs in the field. By assuming conservatively that the J-band extinction is lower than 0.5 mag and using the NextGen models (Baraffe et al. 1998) at 1–2 Ma, we derived theoretical masses in the interval 0.17–0.57 $M_\odot$ for the three new T Tauri low-mass stars, well above the hydrogen burning mass limit. The three young stars could be at distances slightly closer than 140 pc because they are on the near sides of the clouds, which are rather large. We will know their distances with the advent of the ESA/*Gaia*/ space mission.

Some authors have argued against the universality of the initial mass function based on the hypothetical deficit of low-mass stellar objects ($<0.5\,M_\odot$, M2–4) in Taurus-Auriga (Briceño et al. 1998, 2002; Luhman et al. 2003, 2009a; Guieu et al. 2006; Güdel et al. 2007; Scelsi et al. 2007; Perger et al. 2013). The detection of three stars just in the deficit range may point out that the initial mass function in Taurus-Auriga is actually standard, and that previous surveys had not been successful enough for detecting intermediate M dwarfs. Simple VO surveys such as the one presented here may cover that gap.

5.4.5 Distances

The three young stars in Taurus-Auriga are consequently located at $d \sim 140$ pc (Kenyon et al. 2008 and references therein). However, some of our targets were expected to be located very

[9]Note the previously known Taurus-Auriga candidates with discordant proper motions or blue $r' - J$ colours for their r' magnitudes (CFHT-BD-Tau 19, KPNO-Tau 6, 2MASS J04201611+2821325, 2MASS J04202144+2813491, ITG 34 and FS 115.

Table 5.5: Relative Astrometry of the LSPM J0326+3929EW (Koenigstuhl 7 AB) Common Proper Motion Pair

ρ [arcsec]	θ [deg]	Date	Origin
6.5±0.5	236±6	1955 Feb 13	POSS-I Red
5.7±0.5	229±6	1989 Sep 29	POSS-II Red
6.2±0.5	229±6	1994 Nov 28	POSS-II Blue
5.9±0.5	228±6	1995 Nov 14	POSS-II IR
6.37±0.06	227.7±1.0	1998 Nov 1	2MASS
6.38±0.10	227.3±1.0	2001 Dec 26	CMC14
6.45±0.09	227.4±1.0	2003 Jan 7	SDSS-DR9
6.70±0.11	229.4±1.0	2010 Jul 1	*WISE*

close to the Sun because of their late spectral types and relative brightness. We used the absolute magnitude M_J-spectral type relation in Caballero et al. (2008) for deriving spectrophotometric distances for the 24 investigated field M dwarfs, which are given in Table 5.4. We assumed generous uncertainties in the M_J-SpT relation, apart from those in our SpT determination and the 2MASS J magnitudes, which translated into typical error bars of about 20 %. There have been previous determinations of the distances to three known dwarfs based solely on VI-band (Fleming 1998) and optical and near-infrared photometry (Caballero, 2012). Those determinations are consistent with ours within conservative error bars.

All of our field M dwarfs except four (which are M2.5–3.5 V stars) are located at less 25 pc. Of them, seven are at 15 pc or less, of which only three were previously known (J0122+2209/G 34–53 at 8±2 pc, J0156+3033/NLTT 6496 at 15±4 pc, and J2211+4059/1RXS J221124.3+410000 at 9±2 pc). The other four were identified in this work for the first time (J0012+3028, J0507+3730, J1518+2036, and J2259+3738 at 12–15 pc).

5.4.6 Common proper motion pairs

We took advantage of the Aladin sky atlas and the VOTable Plotting tool VOplot to look for proper-motion companions to our 27 stars. We loaded PPMXL data in a circular area of 30 arcmin radius centered on our targets and plotted proper-motion diagrams (μ_δ versus $\mu_\alpha \cos\delta$). We recovered one known binary system (Königstuhl 4 AB; Caballero 2012) and reported and characterized for the first time another one.

The new binary, not tabulated in the Washington Double Star Catalog (Mason et al. 2001), consists of J0326+3929/LSPM J0326+3929E and its close companion LSPM J0326+3929W. The two stars were reported first by Lépine & Shara (2005), who did not provide any clues of their possible binarity (the Lépine & Shara 2005 catalog is a very useful source of new proper motion pairs identified by amateur astronomers – e.g., López et al. 2012; Rica 2012). However, because of its angular separation that is shorter than 55 arcsec and identical proper motions, the pair probably is one of the 19,836 highly probable wide binaries reported by

Lépine (2011).

We applied the method of (Caballero, 2007a) of confirming membership in a common proper motion pair by comparing multi-band photometry (in this case, $u'g'r'i'JHK_sW1W2W3$) of the two components and measuring constant angular separation ρ and position angle θ on a long time baseline. Table 5.5 summarizes our astrometric analysis of SuperCOSMOS digitizations of the First and Second Palomar Observatory Sky Survey (Hambly et al. 2001) and other public databases. With a significant proper motion of $\mu \sim 160\,\mathrm{mas\,a^{-1}}$, the two stars would be separated by up to 15 arcsec in the 1955 POSS-I images if the secondary star were in the background. However, ρ and θ kept constant at 6.3 ± 0.3 arcsec and 229 ± 3 deg in a 55.4 a long interval, from which we concluded that the two stars travel together. Both LSPM J0326+3929E and W were saturated in all POSS photographic plates and, because of their proximity, there were large uncertainties in the determination of the photocentroids. We determined more precise mean angular separation and position angle at $\rho = 6.48\pm0.16$ arcsec and $\theta = 227.9\pm1.0$ deg by averaging only the last four astrometric epochs ($\Delta t = 11.7$ a). With the distance computed in Section 5.4.5 ($d = 17\pm4$ pc), we derived a projected physical separation of $s = 110\pm30$ au. From the spectral type of the primary, M4.5 V, and the magnitude differences between the two components, of $\Delta r' = 0.357\pm0.004$ mag and $\Delta J = 0.28\pm0.04$ mag, we estimated a spectral type M5.0: V for the secondary.

5.5 Discussion and conclusions

We showed the potential of the Virtual Observatory for finding new bright nearby M dwarfs, some of which can be targeted by current or forthcoming exoplanet surveys. In this pilot program, we cross-matched the photometric CMC14 (r') and 2MASS (JHK_s) catalogs in the whole overlapping area of 25 078 deg^2, imposed colour restrictions in $r'-J$ and $J-K_s$, and selected 828 sources brighter than $J = 10.5$ mag for follow-up. Some of them turned out to be background M giants or even reddened, massive early-type stars in distant open clusters. Proper motions were used in a second step in giving priorities in the spectroscopic follow-up.

We used the Intermediate Dispersion Spectrograph at the 2.5 m Isaac Newton Telescope for obtaining low-resolution optical spectroscopy of 27 targets, 25 of which had not been spectroscopically analyzed before. We determined spectral types with a custom-made spectral index, $\Re$, which accounts mostly for the absorption of a TiO band at 7100–7500 Å. Derived spectral types of all the stars ranged between M2.5 V and M5.5 V, with the bulk of them in the narrower M3.5–5.0 V interval, which demonstrated the success of our search.

In spite of their relative brightness, $J < 10.2$ mag in seven cases (and $J < 9.7$ mag in one case), 16 (60 %) M dwarfs had escaped previous surveys and are, therefore, discovered and characterized here for the first time. This fact may be due to that our survey, contrary to most searches for M dwarfs, was purely photometric and that most of our stars fell above

the main-sequence locus in a reduced-proper-motion diagram. That is, proper motions of our targets are lower than average for typical dwarfs of the same $r' - J$ colours. Without an appropriate radial-velocity study, one cannot deduce low total Galactic velocity from low tangential velocity (M dwarfs can move fast in the visual direction instead), but one can at least conclude that proper-motion surveys are inefficient in the identification of slow M dwarfs, even if they are bright and nearby.

Indeed, among our 27 M dwarfs, there are two stars at less than 10 pc, to which we recommend measuring the parallax: J0122+2209/G 34–53 (M4.0 V, $d = 8\pm2$ pc) and J2211+4059/1RXS J221124.3+410000 (M5.5 V, $d = 9\pm2$ pc). There are another five stars at 10–15 pc, four of which are presented here for the first time. The identification of new relatively bright, low-active, single stars much closer to Earth than the median distance to M-dwarf exoplanet-survey targets ($\gg$13 pc) is still a matter of interest. In summary, this kind of VO colour-based search may shed light on the complete identification and characterization of all M dwarfs in the 10 pc radius sphere centered on the Sun, until the ESA space mission Gaia delivers its final catalog by 2022.

We were genuinely surprised by the discovery of three slow M dwarfs with low surface gravities from weak Na I absorption in our IDS/INT spectra and from VOSA fits to observed multi-wavelength spectral energy distributions. Besides, one of them, J0422+2439, had a strong Hα emission indicative of accretion (the pEW(Hα)s of the other 26 stars were consistent with the chromospheric activity). This fact led us to study the X-ray emission of the sample stars in the *ROSAT* Bright Source Catalogue. Of the 11 (40 %) positive cross-matches with *ROSAT*, 7 were new detections, which suggests that previous all-sky X-ray surveys for low-mass stars have been incomplete. The coolest star in our sample, J2211+4059 (M5.5 V), had also the highest L_X/L_J ratio, slightly above those of four other stars, including J0422+2439.

We assigned membership of J0422+2439 to the Taurus-Auriga star-forming region based not only on low surface gravity and Hα and X-ray emissions, but also on coincidence of spatial location, proper motions, and colour-magnitude combinations with a large sample of known Taurus-Auriga members. We also assigned membership of J0435+2523 and J0439+2333, the other two low-gravity stars, in the star-forming region. The identification of three new intermediate M dwarfs in Taurus-Auriga may help alleviate the reported lack of them, which has made many authors to claim the uniqueness of the initial mass function in Taurus-Auriga.

We also looked for proper-motion companions to our 27 stars. We recovered a fragile, wide, already known pair and reported and characterized a new pair, an M4.5 V star and an M5.0: V companion separated by 6.5 arcsec ($\sim$110 AU).

We will continue to search with VO tools for slow bright nearby M dwarfs, in particular for potential targets for exoplanet hunting. For that, we will not only plan to conclude the analysis of our CMC14+2MASS data with a new spectroscopic follow-up, but also start a new study with the latest release of the Carlsberg Meridian Catalogue

(CMC15[10]), which will be more extensive than the CMC14 one. Extra VO works for the identification of slow bright nearby M dwarfs unnoticed by previous surveys will include massive cross-matches between existing databases relevant for this topic: 2MASS, PPMXL, UCAC4, *WISE*, *GALEX*, *ROSAT*, VISTA, and VST. These works will pave the way for further 'super-massive' correlations when the first *Gaia* and *EUCLID* data releases are available.

5.5.1 Acknowledgements

We gratefully thank F. J. Alonso-Floriano, P. Cruz-Gamba, A. Klutsch, and B. Stelzer for their helpful feedback and data provision. This publication is based on observations made with the Isaac Newton Telescope operated on the island of La Palma by the Isaac Newton Group in the Spanish Observatorio del Roque de los Muchachos of the Instituto de Astrofísica de Canarias. This publication has made use of the SIMBAD, VizieR and Aladin, operated at center de Données astronomiques de Strasbourg, France, the Washington Double Star Catalog maintained at the U.S. Naval Observatory, and VOSA, a Virtual Observatory tool developed under the Spanish Virtual Observatory project supported from the Spanish MICINN through grant AyA2008-02156. MCGO acknowledges the support of a JAE-Doc CSIC fellowship cofunded with the European Social Fund under the program Junta para la Ampliación de Estudios. Financial support was provided by the Spanish Ministerio de Ciencia e Innovación under grants AyA2011-24052 and AYA2011-30147-C03-03.

5.6 Appendix Material

5.6.1 Appendix A1

Table 5.6: The 97 cross-matched objects that passed the final filters and were not spectroscopically analyzed

Name	α (J2000)	δ (J2000)	SpT	Class
	hh mm ss	dd mm ss		
LP 404–33	00 08 53.92	+20 50 25.2	M4.5	Dwarf
TYC 2268-648-1	00 13 22.97	+33:47:02.2	...	Giant?
GJ 1011	00 23 28.03	+24 18 24.4	M4.0	Dwarf
G 130–68	00 24 34.78	+30 02 29.5	M4.5	Dwarf
G 132–25 AB	00 45 56.63	+33 47 11.0	M4.5+	Dwarf
G 69–32	00 54 48.03	+27 31 03.6	M4.5	Dwarf
IX And	01 01 40.56	+37 53 46.5	M4.0:	Giant
LSR J0155+3758	01 55 02.30	+37 58 02.8	M5.0	Dwarf
2MASS J02132062+3648506	02 13 20.63	+36 48 50.7	M4.5	Dwarf

[10] `http://svo2.cab.inta-csic.es/vocats/cmc15/`

Table 5.6. Continued.

Name	α (J2000)	δ (J2000)	SpT	Class
LP 245–10	02 17 09.93	+35 26 33.0	M5.0	Dwarf
FBS L 14-14	02 35 41.64	+26 03 03.2	M6.5:	Giant
G 36–26	02 36 44.13	+22 40 26.5	M5.0	Dwarf
TYC 1779-1379-1	02 36 31.24	+29 35 55.7	....	Giant?
LSPM J0256+2359	02 56 13.96	+23 59 10.5	M5.5	Dwarf
LP 355–27	03 07 46.82	+24 57 55.6	M4.5	Dwarf
G 6–7	03 26 44.96	+19 14 40.3	M4.5	Dwarf
RX J0332.6+2843	03 32 35.79	+28 43 55.5	M4.0	Dwarf
XEST 16–045	04 20 39.18	+27 17 31.7	M4.0:	Young
GJ 1070	04 22 33.49	+39 00 43.7	M5.0	Dwarf
G 8–31	04 22 59.26	+25 59 14.8	M4.0	Dwarf
FW Tau AB	04 29 29.71	+26 16 53.2	M5.5e+	Young
V546 Per	04 30 25.27	+39 51 00.0	M4.5	Dwarf
V927 Tau AB	04 31 23.82	+24 10 52.9	M4.5e+	Young
G 8–41	04 33 33.93	+20 44 46.2	M4.0	Dwarf
LP 415-1644	04 37 21.91	+19 21 17.4	...	Dwarf?
Haro 6–36	04 43 20.23	+29 40 06.0	M5.0e	Young
RX J0447.2+2038	04 47 12.25	+20 38 10.9	M4.5	Dwarf
GJ 1072	04 50 50.83	+22 07 22.5	M5.0	Dwarf
LSPM J0501+2237	05 01 18.03	+22 37 01.6	M4.5	Dwarf
HD 285190 BC	05 03 05.63	+21 22 36.2	M4.5+	Dwarf
IRAS 05090+2027	05 12 03.98	+20 30 53.7	....	Giant?
[LH98] 190	05 24 25.72	+19 22 07.0	...	Dwarf?
V780 Tau A	05 40 25.71	+24 48 09.0	M5.5	Dwarf
LHS 6097	05 58 53.33	+21 21 01.1	M4.5	Dwarf
G 98–52 A	06 11 55.99	+33 25 50.6	M3.5	Dwarf
0628+2052	06 28 35.97	+20 52 37.6	....	Giant?
IRAS 06386+2330	06 41 41.14	+23 27 41.4	...	Giant?
IRAS 06562+2229	06 59 18.80	+22 24 53.4	...	Giant?
GJ 1093	06 59 28.69	+19 20 57.7	M5.0	Dwarf
GJ 1096	07 16 18.02	+33 09 10.4	M4.0	Dwarf
BD+20 2091	08 28 24.90	+19 35 44.5	M6.0:	Giant
DX Cnc	08 29 49.34	+26 46 33.7	M6.0	Dwarf
CV Cnc BC	08 31 37.44	+19 23 49.5	M4.0+	Dwarf
ρ Cnc B	08 52 40.85	+28 18 58.9	M4.0	Dwarf
EI Cnc AB	08 58 15.19	+19 45 47.1	M5.5+	Dwarf
LP 368–128	09 00 23.59	+21 50 05.4	M6.5	Dwarf
2MASS J09165078+2448559	09 16 50.78	+24 48 56.0	M4.5	Dwarf
DX Leo B	09 32 48.27	+26 59 44.3	M5.5	Dwarf
Ross 92	09 41 02.00	+22 01 29.2	M4.5	Dwarf

Table 5.6. Continued.

Name	α (J2000)	δ (J2000)	SpT	Class
LHS 2206	09 53 55.23	+20 56 46.0	M4.5	Dwarf
BD+25 2207	10 09 27.78	+24 57 31.8	M5.0:	Giant
TYC 1968-490-1	10 13 52.77	+22 56 48.5	....	Giant?
G 54–19	10 14 53.16	+21 23 46.4	M4.5	Dwarf
LP 374–39	11 23 08.00	+25 53 37.0	M5.0	Dwarf
G 121–28	11 52 57.91	+24 28 45.4	M4.5	Dwarf
G 148-47 B	12 21 26.69	+30 38 37.0	...	Dwarf?
Sand 58 A	12 21 27.05	+30 38 35.7	M5.0	Dwarf
HD 108421 C	12 26 57.37	+27 00 53.7	M4.5	Dwarf
G 123–45	12 36 28.70	+35 12 00.8	M3.5	Dwarf
LP 377–36	12 39 43.54	+25 30 45.7	M4.5	Dwarf
Sand 214	13 06 50.25	+30 50 54.9	M5.0	Dwarf
GJ 1167 A	13 09 34.95	+28 59 06.6	M4.0	Dwarf
EK CVn	13 14 32.49	+34 20 55.9	M6.0:	Giant
GJ 1171	13 30 31.06	+19 09 34.0	M4.5	Dwarf
LP 323–169	13 32 39.09	+30 59 06.6	M4.5	Dwarf
GJ 1179 A	13 48 13.41	+23 36 48.6	M5.5	Dwarf
G 166–33	14 29 59.56	+29 34 02.9	M4.0	Dwarf
NLTT 39916	15 19 21.23	+34 03 42.8	...	Dwarf?
G 167–47	15 31 54.27	+28 51 09.6	M4.5	Dwarf
G 180–11 AB	15 55 31.78	+35 12 02.9	M4.5+	Dwarf
HD 190360 B	20 03 26.52	+29 52 00.0	M4.5	Dwarf
J2006+3651	20 06 54.00	+36 51 48.3	...	Giant?
J2011+3423	20 11 56.42	+34 23 58.1	...	Giant?
J2014+3943	20 14 55.51	+39 43 26.7	...	Dwarf?
HD 346301A	20 19 02.83	+22 05 21.4	...	Giant?
J2022+4030	20 22 14.67	+40 30 02.7	...	Giant?
J2023+2451	20 23 34.27	+24 51 20.1	...	Giant?
J2024+3930	20 24 38.71	+39 30 30.1	...	Giant?
J2026+3733	20 26 16.44	+37 33 01.2	...	Giant?
G 210-20	20 28 22.08	+34 12 08.7	...	Dwarf?
[CPR2002] A25	20 32 38.44	+40 40 44.5	O8 III	Young
J2032+4042	20 32 43.88	+40 42 17.1	...	Giant?
[CPR2002] A20	20 33 02.92	+40 47 25.4	O8 II((f))	Young
[CPR2002] A22	20 33 11.29	+40 42 33.7	...	Giant?
G 210-26	20 33 15.77	+28 23 44.0	...	Dwarf?
J2038+4021	20 38 17.13	+40 21 06.0	...	Giant?
LSPM J2045+3508	20 45 22.16	+35 08 15.1	...	Dwarf?
G 211–9	21 02 46.06	+34 54 36.0	M4.5	Dwarf
IRAS 21044+2818	21 06 35.76	+28 31 06.1	...	Giant?

Table 5.6. Continued.

Name	α (J2000)	δ (J2000)	SpT	Class
V445 Vul	21 08 01.33	+23 43 44.6	M7.0:	Giant
TYC 2710-1557-1	21 09 13.22	+34 08 48.0	...	Giant?
LSR J2124+4003	21 24 32.34	+40 04 00.0	M6.5	Dwarf
BD+29 4448	21 33 57.94	+29 49 11.4	...	Giant?
J2154+1914	21 54 51.21	+19 14 10.7	...	Giant?
G 130-31	23 59 19.80	+32 41 23.7	...	Dwarf?
G 127–50	22 43 23.13	+22 08 17.9	M4.5	Dwarf
GJ 1288	23 42 52.74	+30 49 21.9	M4.5	Dwarf

[a] Dwarf: known dwarf; Giant: known giants; Young: known young stars (T Tauri and reddened massive stars); Dwarf?: probable dwarf; Giant?: probable giants

5.6.2 Appendix A2

Table 5.7: Photometry of the 27 investigated stars

ID	u' [mag]	B [mag]	g' [mag]	V [mag]	r' [mag]	J [mag]	H [mag]	K_s [mag]	$W1$ [mag]	$W2$ [mag]	$W3$ [mag]	$W4$ [mag]
J0012+3028	17.884±0.013	16.361±0.180	15.801±0.004	14.864±0.060	14.216	10.242±0.023	9.683±0.022	9.410±0.021	9.233±0.022	9.039±0.020	8.929±0.026	8.784±0.386
J0013+2733	19.224± 0.039	16.753±0.080	16.012±0.003	15.115±0.060	14.437	10.431±0.020	9.837±0.020	9.581±0.018	9.376±0.024	9.210±0.022	9.077±0.027	8.592±0.317
J0024+2626	18.122±0.018	16.343±0.130	15.550±0.003	14.735±0.040	14.131	10.222±0.020	9.592±0.019	9.299±0.017	9.188±0.023	8.959±0.020	8.819±0.025	8.543±0.298
J0058+3919	17.552±0.01	15.837±0.050	15.078±0.003	14.168±0.030	13.598	9.561±0.026	8.947±0.029	8.680±0.018	8.489±0.023	8.303±0.020	8.150±0.017	8.009±0.133
J0122+2209	...	14.722±0.030	13.763±0.04	12.996±0.030	12.375	8.412±0.021	7.820±0.016	7.537±0.017	7.341±0.027	7.167±0.020	7.055±0.016	6.856±0.060
J0156+3033	...	16.532±0.050	15.786±0.08	15.105±0.050	14.449	10.323±0.023	9.718±0.031	9.449±0.021	9.267±0.023	9.074±0.019	8.925±0.028	9.075±0.540
J0304+2203	...	17.164±0.030	16.199±0.05	15.564±0.030	14.931	10.486±0.022	9.933±0.021	9.655±0.018	9.427±0.023	9.226±0.022	9.098±0.032	8.476: [a]
J0326+3929[b]	17.991±0.013	...	15.546±0.003	...	13.968	9.998±0.025	9.412±0.026	9.084±0.017	8.884±0.028	8.701±0.026	8.616±0.030	8.017±0.274
J0327+2212	...	16.252±0.120	15.314±0.04	14.654±0.090	14.055	10.044±0.022	9.477±0.020	9.194±0.017	9.077±0.022	8.872±0.020	8.730±0.029	8.812±0.434
J0341+1824	...	16.577±0.030	15.669±0.03	14.958±0.100	14.412	10.484±0.021	9.858±0.023	9.643±0.023	9.435±0.023	9.245±0.021	9.175±0.036	8.866:[a]
J0342+2326	...	16.609±0.060	15.667±0.05	14.984±0.060	14.267	10.202±0.022	9.545±0.023	9.316±0.023	9.158±0.025	8.979±0.022	8.817±0.028	8.076±0.354
J0422+2439[b]	18.426±0.014	...	16.092±0.003	...	14.529	9.648±0.021	8.947±0.022	8.651±0.020	8.467±0.032	8.185±0.030	8.162±0.028	8.014±0.269
J0424+3706	17.711±0.012	16.337±0.020	15.718±0.005	14.668±0.030	14.203	10.191±0.026	9.553±0.030	9.340±0.020	9.184±0.023	9.009±0.019	8.830±0.030	8.193:[a]
J0435+2523[b]	18.303±0.014	...	16.189±0.004	...	14.669	10.272±0.022	9.618±0.030	9.331±0.021	9.216±0.023	8.997±0.020	8.821±0.027	8.249±0.262
J0439+2333	18.433±0.015	17.028±0.120	16.240± 0.004	15.392±0.010	14.856	10.479±0.023	9.893±0.021	9.617±0.017	9.471±0.024	9.258±0.020	9.131±0.033	8.530±0.381
J0507+3730	...	16.986±0.230	16.018±0.03	15.349±0.060	14.713	10.284±0.020	9.703±0.021	9.397±0.018	9.223±0.022	9.008±0.019	8.686±0.024	7.656±0.133
J0515+2336	...	16.977±0.010	16.031±0.05	15.245±0.040	14.574	10.186±0.030	9.602±0.035	9.306±0.024	9.067±0.024	8.897±0.020	8.672±0.026	7.397±0.175
J0630+3003	...	...	...	...	14.020	10.045±0.018	9.484±0.018	9.208±0.018	9.025±0.023	8.847±0.018	8.700±0.029	8.090±0.256
J0909+2247	18.856±0.018	17.172±0.010	16.230±0.004	15.266±0.010	14.656	10.474±0.023	9.915±0.032	9.616±0.018	9.367±0.021	9.206±0.020	8.996±0.030	8.470:[a]
J1132+1816	18.223±0.016	16.354±0.070	15.625±0.004	14.751±0.050	14.137	10.175±0.023	9.599±0.030	9.338±0.022	9.138±0.024	8.961±0.021	8.821±0.024	9.182±0.534
J1241+1905[b]	18.369±0.017	16.750±0.080	15.882±0.004	15.048±0.030	14.284	10.368±0.022	9.792±0.026	9.477±0.018	9.314±0.023	9.136±0.019	8.978±0.025	8.336±0.225
J1459+3618	18.183±0.012	16.566 ±0.040	15.784±0.004	14.845±0.080	14.292	10.257±0.018	9.647±0.016	9.377±0.016	9.230±0.022	9.070±0.020	8.939±0.021	9.123±0.353
J1518+2036	...	...	...	15.455±0.010	14.786	10.119±0.021	9.606±0.022	9.268±0.019	9.039±0.022	8.839±0.020	8.641±0.019	8.515±0.194
J1574+2241	17.438±0.013	15.955±0.040	15.139±0.004	14.197±0.010	13.589	9.543±0.022	8.932±0.030	8.647±0.022	8.475±0.023	8.305±0.020	8.145±0.017	8.007±0.157
J2211+4059	18.465±0.015	16.963±0.090	16.081±0.003	15.139±0.010	14.371	9.725±0.020	9.097±0.017	8.790±0.016	8.565±0.021	8.404±0.020	8.213±0.019	8.661±0.304
J2248+1819	17.838±0.011	16.115±0.080	15.461±0.005	14.535±0.040	13.886	9.957±0.021	9.388±0.020	9.119±0.017	8.945±0.022	8.760±0.020	8.604±0.023	8.523:[a]
J2259+3736	...	16.942±0.020	16.043±0.05	15.357±0.120	14.638	10.378±0.029	9.890±0.037	9.535±0.024	0.257±0.023	9.062±0.020	8.925±0.025	8.509±0.264

[a] Poor quality flags.
[b] The SDSS i' band was not use to estimated the $T_{\rm eff}$

Chapter 6

Binary properties of mid to late-T dwarfs from HST/WFC3

6.1 Resumen

Los sistemas múltiples son fundamentales para entender los procesos de formación estelar ya que cualquier modelo teórico debe ser capaz de crear sistemas binarios y de reproducir la frecuencia y las principales características físicas de los mismos.

Desde el descubrimiento de la primera binaria compuesta por dos enanas marrones (Basri & Martín 1999) se han identificado un total de >100 sistemas compuestos por objetos con tipos espectrales posterior a M6. La mayoría de los sistemas han sido detectados a través de imágenes de alta resolución espacial obtenidas por el *Hubble Space Telescope* (*HST*) o aplicando técnicas de óptica adaptativa desde tierra (e.g., Martin et al. 1999; Reid et al. 2001, 2006a; Bouy et al. 2003, 2004b, 2006b; Burgasser et al. 2007b; Burgasser et al. 2003b, 2006b; Close et al. 2003b,c; Siegler et al. 2005; Liu et al. 2006; Scholz et al. 2004, 2010; Radigan et al. 2013; Dupuy et al. 2009b,a; Dupuy & Liu 2012a; Dupuy et al. 2015; McCaughrean et al. 2004b, King et al. 2010; Stassun et al. 2004). Otros sistemas han sido identificados como eventos de microlente gravitacional o través de observaciones espectroscópicas de alta resolución. Estadísticamente estos sistemas se caracterizan por tener una tasa de binariedad del $\sim$20 %, unas separaciones entre sus componentes de $\rho\sim$20 A.U y un cociente de masas q=$M_2/M_1>0.8$ (Burgasser et al. 2007b).

Si bien los valores anteriores parecen estar de acuerdo con las predicciones teóricas asociadas a los modelos de eyección, fragmentación de un disco masivo y fragmentación turbulenta (e.g Stamatellos & Whitworth 2009; Jumper & Fisher 2013; Bate et al. 2002) así como las de las simulaciones magnetohidrodinámicas (Bate 2012), una de las principales interrogantes asociadas a los valores observaciones (frecuencia, ρ, q) es saber si éstos representan la distribución real de los sistemas binarios de baja masa o son simplemente

producto de los efectos de selección de las muestras observadas.

6.1.1 Descripción de la muestra y metodología

En este trabajo usamos la cámara WFC3 instalada en el *HST* para observar 37 enanas marrones cercanas (d $\leq$ 30 pc) de tipo espectral L-T identificadas previamente por 2MASS, DENIS, SDSS y UKIDSS (ver Tabla 6.1). La muestra se dividió en dos programas:

- El programa 11631 incluía 11 enanas de tipos espectrales L y T tempranas y tenía como objetivo estudiar la multiplicidad en la región de transición L/T y obtener nuevas relaciones magnitud-color y magnitud-tipo espectral (infrarrojo). La muestra incluye el sistema binario previamente conocido 2MASS J1520-4422AB (Burgasser et al. 2007a) formado por una enana L1.5 y otra L4.5.
- El programa 11666 incluía 26 enanas cercanas (d$\leq$20 pc), de tipos espectrales en el rango T5-T8.5 y tenía como objetivo la identificación de compañeras enanas de tipo Y. Esta muestra representa el 29 % de todas las enanas conocidas con tipos espectrales posteriores a T5 y situadas a menos de 20 pc, por lo que consideramos que es estadísticamente significativa para estimar la tasa de binariedad en dicho rango espectral.

Debido a las características espectrales de las enanas marrones de tipo T, en las observaciones se utilizaron los filtros F110W (λ_c= 1.1191μm), F127M (λ_c= 1.274 μm), F139M (λ_c= 1.3838 μm) y F164N (λ_c= 1.6460μm). Se realizó fotometría de apertura utilizando Sextractor y se obtuvieron nuevas calibraciones color$-$tipo espectral (ver sección 6.4 y figura 6.3).

Para la búsqueda de compañeras se utilizó nuestra propia rutina iterativa en los cuatro filtros utilizados para la observación. La rutina se basa en un ajuste de PSF similar al descrito en Burgasser et al. (2003b). En primer lugar se calcularon las posiciones iniciales y flujos para las dos componentes haciendo uso del pico de detección para la primaria y de la imagen residual una vez sustraída la PSF, para la secundaria. La rutina nos proporcionaba la posible separación entre las componentes, ángulo paraláctico y diferencia de magnitudes (ver Tabla 6.5). Un ejemplo de los resultados obtenidos con nuestro algoritmo se muestra en la Figura 6.4. Para evaluar la significancia estadística del modelo de PSF binario aplicamos un test de tipo F[1]. El único sistema binario identificado por nuestra rutina fue el ya conocido 2MASS J1520$-$4422AB (L1.5 + L5.4) cuya separación (ρ = 22$\pm$2 AU) coincide, dentro de los errores, con determinaciones ya publicadas (Burgasser et al 2007a). La diferencia de magnitud entre las componentes para este sistema fue de 0.7 mag para el filtro F127M. La identificación de un sistema binario ya conocido nos confirma la idoneidad de nuestra metodología para realizar este tipo de búsquedas. El hecho de que no hayamos encontrado ningún sistema binario nuevo nos indica que las fuentes estudiadas son bien objetos

[1] ver más detalles en https://people.richland.edu/james/lecture/m170/ch13-f.html

individuales o bien sistemas binarios no resueltos en el rango de resolución y sensibilidad proporcionado por WFC3.

Con objeto de estudiar los límites de detección de WFC3 en términos de separación angular y diferencia de magnitudes, se llevó a cabo una simulación de Montecarlo sobre los cuatro filtros utilizados en este trabajo, F110W, F127M, F139M y F160N. Ésta consistió en la generación de 10^5 estrellas artificiales con diferentes magnitudes (Δm entre 0 y 5 mag) y a diferentes orientaciones y distancias (de 1 a 6 píxeles) de cada uno de los objetos de nuestra muestra. Los resultados de la simulación nos indicaron que la WFC3 es capaz de detectar compañeras a separaciones mayores de 0.325 ”y con diferencia de magnitudes entre 2.25 y 3.0 mag según el filtro utilizado. Teniendo en cuenta los límites de sensibilidad de nuestro instrumento y el número de sistemas binarios T5+$\geq$T5 conocidos, llegamos a la conclusión de que la probabilidad de encontrar sistemas binarios en nuestra muestra es del 4.4 %, resultado compatible con la ”no-detección” anteriormente descrita.

Finalmente realizamos una nueva simulación de Montecarlo para estimar el número de fuentes detectadas suponiendo que todas fueran binarias. Para ello generamos una muestra de 5 x10^6 primarias con masas dadas según la siguiente distribución: $dN/dM \alpha M^{-5}$ (Burgasser 2004b; Burningham et al. 2013). Las masas de las secundarias se obtuvieron utilizando bien una distribución plana o una ley de potencias ($P(q) \propto q^{1.8}$; Allen 2007). Se adoptó una distribución uniforme en edades entre 0.1 y 10 Gyr . A partir del flujo bolométrico obtenido utilizando modelos, estimamos las correspondientes magnitudes en el filtro F127M. Para las órbitas se utilizó la distribución que se describe en Allen (2007).

Los resultados de la simulación se muestran en la Tabla 6.7. Según estos resultados, si todos nuestros objetos fueran sistemas binarios, deberíamos haber detectado entre 13 y 21 sistemas, dependiendo de la distribución adoptada. El hecho de que no detectemos ninguno implica un límite superior de la tasa de binariedad $<16 - <25$ %. El posterior trabajo realizado en las Pléyades por Garcia et al. (2015), utilizando el catálogo de Lodieu et al. (2012a) avala nuestro resultado de no deteción de sistemas binarios compuestos por enanas marrones con WFC3/*HST*. Siguiendo una metodología similar a la nuestra, este trabajo concluye con una tasa de binariedad <26 % a 2σ para objetos de las Pleiades con masas comprendidas entre $25-40\,M_{Jup}$ y a separaciones >4 AU.

Estos valores son consistentes con estimaciones previas (Burgasser et al. 2003b, 2006b; Allen 2007) y apoyan la hipótesis de que, en el régimen subestelar, la tasa de binariedad disminuye con la masa de la primaria. Simulaciones hidrodinámicas llevadas a cabo por Bate (2009, 2012) también son consistentes con la tasa de binariedad obtenida en este trabajo.

En base a los resultados obtenidos en este artículo podemos concluir que, si bien la WFC3 tiene una mayor sensibilidad que NICMOS y la WFPC2, su menor resolución angular la hace menos adecuada para la identificación de sistemas de binarios de enanas marrones.

Binary properties of mid to late-T dwarfs from HST/WFC3

2014, AJ, 148, 129A

Authors:
M. Aberasturi[1,5], A.J. Burgasser[2], A. Mora[3], E. Solano[1,5], E. L. Martín[4], I. N. Reid[6] and D. Looper[7]
Affiliation:
[1] Centro de Astrobiología (INTA-CSIC), Departamento de Astrofísica, P.O. Box 78, E-28691 Villanueva de a Cañada, Madrid, Spain
[2] Center for Astrophysics and Space Science, University of California San Diego, La Jolla, CA, 92093, USA
[3] ESA−ESAC, Gaia SOC. P. O. Box 78 E-28691 Villanueva de la Cañada, Madrid, Spain
[4] Centro de Astrobiología (INTA-CSIC), Departamento de Astrofísica. Carretera de Aljalvir km 4, E-28550 Torrejón de Ardoz, Madrid, Spain
[5] Spanish Virtual Observatory, Spain
[6] Space Telescope Science Institute, 3700 San Martin Drive, Baltimore, MD 21218, USA
[7] Institute for Astronomy, University of Hawaii, 2680 Woodlawn Drive, Honolulu, HI 96822

Abstract

We used HST/WFC3 observations of a sample of 26 nearby ($\leq$20 pc) mid to late T dwarfs to search for cooler companions and measure the multiplicity statistics of brown dwarfs. Tightly-separated companions were searched for using a double-PSF fitting algorithm. We also compared our detection limits based on simulations to other prior T5+ brown dwarf binary programs. No new wide or tight companions were identified, which is consistent with the number of known T5+ binary systems and the resolution limits of WFC3. We use our results to add new constraints to the binary fraction of T−type brown dwarfs. Modeling selection effects and adopting previously derived separation and mass ratio distributions, we find an upper limit total binary fraction of <16% and <25% assuming power law and flat mass ratio distributions respectively, which are consistent with previous results. We also characterize a handful of targets around the L/T transition.

6.2 Introduction

Since their first theoretical prediction (Kumar 1963; Hayashi & Nakano 1963), brown dwarfs (BDs), objects with insufficient mass to sustain stable hydrogen fusion, have bridged the gap in temperature and mass between cold, very low mass stars (VLM; $M_{\odot} \geq 0.075 M_{\odot}$) and the hottest, most massive giant planets ($M_{\odot} \leq 0.013\ M_{\odot}$; Chabrier et al. 2000a; Burrows et al. 2003). Since the first discoveries of brown dwarfs as companions to low

luminosity sources, GD165B (Becklin & Zuckerman, 1988) and Gl229B (Nakajima et al. 1995; Golimowski et al. 1995; Oppenheimer et al. 1995) and free-floating systems (Rebolo et al. 1995; Ruiz et al. 1997; Martín et al. 1997), three new spectral classes have been introduced to characterize these low mass objects: L dwarfs ($T_{eff} \sim$ 2500 K $-$ 1500K, Kirkpatrick et al. 1999, Martín et al. 1999), T dwarfs (T_{eff} ∼1500 K $-$500K, Burgasser et al. 2006a) and Y dwarfs ($T_{eff} \leq$ 500 K; Cushing et al. 2011a). With photospheres dominated by condensate clouds in L dwarfs and molecular gas species in T and Y dwarfs, BDs allow us to study planetary-like atmospheres without having to eliminate the glare of a host star. Thanks to wide-field infrared and optical imaging surveys such as the Two Micron All Sky Survey (2MASS, Skrutskie et al. 2006) and the DEep Near Infrared Survey of the southern sky (DENIS, Epchtein et al. 1997) and spectroscopic surveys as Sloan Digital Sky Survey (SDSS, York et al. 2000), we now know ∼1000 L and T type BDs belonging to the field and young stellar clusters[2]. More recently, deeper near and mid$-$infrared surveys like the UKIRT Infrared Deep Sky Survey (UKIDSS, Lawrence et al. 2007), the Canada-France Brown Dwarf Survey (CFBDS, Delorme et al. 2008b) and the Wide-field Infrared Survey Explorer (WISE; Wright et al. 2010), have allowed us to explore the regime of late T and Y dwarfs. Most Y dwarfs have been identified as isolated field objects in WISE (e.g., Kirkpatrick et al. 2011b; Tinney et al. 2012), but discoveries such as WD 0806-661B (Luhman et al., 2011b) and CFBDSIR J1458+1013B (Liu et al., 2011), demonstrate the continued utility of companion searches.

Beyond their discovery, searches for companions allow us to measure the statistics of multiple BDs systems, which are particularly useful for testing formation scenarios for VLM stars and BDs. While the binary fraction (BF) of solar$-$type stellar systems is ∼ 65% (Duquennoy & Mayor, 1991) and early$-$type M stars ∼30%$-$40% (Reid & Gizis 1997b; Delfosse et al. 2004), measurement of multiplicity statistics for BDs have inferred fractions of 15%$-$30% (Allen 2007; Burgasser 2007a), indicating a mass dependence either in multiple formation or in the subsequent evolution of multiple systems.

The majority of the ∼ 100 VLM binary systems known up to now have been discovered in high angular resolution Hubble Space Telescope (*HST*) and/or ground$-$based adaptive optics (AO) imaging programs (Liu et al. 2006; Siegler et al. 2007). Those studies found that BD systems peak in mass ratio at $M_2/M_1 \approx 0.8$ with separations typically closer than ρ<20 AU (Allen, 2007). The statistics of VLM binaries have motivated new theories of BD formation, via turbulent fragmentation (Bate, 2009) or gravitational instability in circumstellar disks (Stamatellos & Whitworth, 2009). Other techniques such as astrometry and analysis of microlensing events are reaching the sensitivity required to detect BD binaries with low mass ratios, and even giant planets at small separations (Burgasser et al. 2010, Rodler et al. 2011; Sahlmann et al. 2013; Choi et al. 2013).

These studies can be advanced by increasing the population of known brown dwarf binary systems. To do this, we undertook two parallel programs using the Wide Field Camara 3 (WFC3) installed on the Hubble Space Telescope. Observations, sample selection and data reduction are described in Section 6.3. In Section 6.4 we present the photometric

[2]See http://dwarfarchives.org for an up-to-date list of L, T and Y dwarfs.

results and define new colour/spectral type relations. In Section 6.5 we describe the results of point−spread function (PSF) fits to our sample and results. We also derive the WFC3 detection limits which prove to be the limitation on our study. In section 6.6, we infer a bias corrected BD binary fraction through simulation, and compare these results with previous surveys. Finally, in Section 6.7 we summarize the main results of our project.

6.3 Observations

6.3.1 Sample

Our original sample consists of 37 nearby sources (d$\leq$ 30 pc) identified as L or T dwarfs based on prior searches of 2MASS, DENIS, SDSS or UKIDSS. Measurements of the infrared photometry (2MASS and MKO systems), proper motions (PMs) and distances for the whole sample are listed in Table 6.1. We have used the Dupuy & Liu (2012b) absolute magnitude−SpT relation to estimate the photometric distances for six objects without parallax measurement. The sources were observed as part of two HST(WFC3) programs (11631 and 11666) with slightly different goals:

- Program 11631 targeted 11 L and early T dwarfs, including one known resolved binary 2MASS J1520−4422AB (Burgasser et al., 2007a) and one previously unreported L3 source, DENIS J1013−7842 (Looper et al in prep). We present additional information of these sources in Appendix 6.8.1 and 6.9, respectively. The 11631 program aimed to explore multiplicity across the L/T transition and was used here to estimate magnitude-colour and colour-near infrared spectral type (NIR SpT) relations. The observations were obtained between January 2010 and June 2011.
- Program 11666 targeted 26 mid and late-T dwarfs (from T5 to T8.5) to search for T and Y dwarf companions, with measured or estimated distances $\leq$ 20 pc not previously observed by HST or ground-based AO programs, with the exception of two sources with insufficient data (SDSS J1346−0031 and 2MASS J0727+1710). The observations were obtained between November 2009 and October 2010. The sample includes two of the coolest objects known at that time: ULAS J0034-0052 (Warren et al., 2007b) and ULAS J1238+0953 (Burningham et al., 2008). We included one previously unreported T6 dwarf, 2MASS J2237+7228 (see more details in Appendix 6.10). In Fig.6.1 we compare our sample against the number of known T5+ dwarfs within 20 parsecs; our sample includes $\sim$29% of such systems. We consider this sample statistically representative to estimate the binary fraction (BF) for the mid-late T dwarfs.

The programs were originally planned for the Near Infrared Camera and Multi-Object Spectrometer (NICMOS/NIC1), given this instrument had demonstrated its ability to identify cold BD companions (Burgasser et al. 2006b, Stumpf et al. 2011). However, but an instrument failure forced the change to the WFC3.

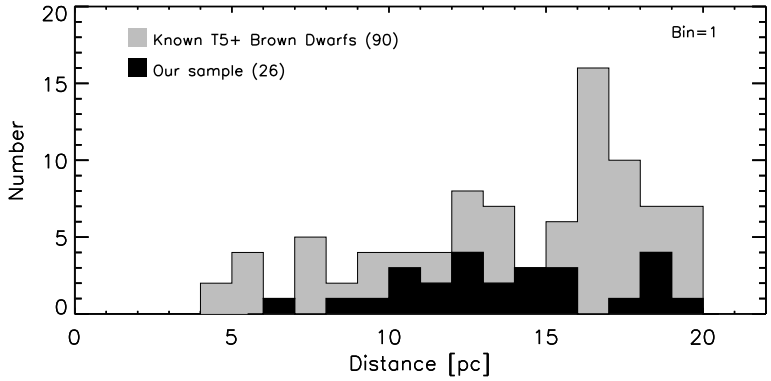

Figure 6.1: Number of known brown dwarfs with SpT $\geq$ T5 from Brown Dwarf Archive, Gelino et al. 2011, Mužić et al. 2012, Bihain et al. 2013, Beichman et al. 2013 and Cushing et al. 2014b. The photometric distances were determined using the Dupuy & Liu (2012b) absolute magnitude−SpT relation.

Table 6.1: L and T dwarfs sample.

Name	NIR−SpT Literature	α (J2000) hh:mm:ss	δ (J2000) hh:mm:ss	J (mag)	H (mag)	K_s (mag)	$\mu_\alpha cos_\delta$ (mas yr^1)	μ_δ (mas yr^1)	Distance (pc)	π (mas)	References
(1)	(2)	(3)	(4)	(5)	(6)	(7)	(8)	(9)	(10)	(11)	(12)
Program 11631											
2MASSI J0340-6724	L7::[a]	03:40:09.42	-67:24:05.1	14.74 ±0.03	13.59±0.03	12.93± 0.03	−318.0±7.0	508.0±18.0	11.0±3.0	...	(1);(15)
SDSS J0739+6615	T1.5+/-1	07:39:22.26	+66:15:03.9	16.82 ±0.13	16.00±0.10	15.83± 0.18	180.0±10. 0	−77.0±26.0	34.0±4.0	...	(2);(15)
DENIS J1013-7842	L3[a]	10:13:25.88	-78:42:55.3	13.84±0.03	12.74±0.03	12.03±0.03	...	...	14.2±1.3[c]	...	(21)
2MASS J1122-3512	T2	11:22:08.26	-35:12:36.3	15.02±0.04	14.36±0.05	14.38± 0.07	−150.0±40.0	−250.0±30.0	15.0±1.0	...	(3);(15)
SDSS J1439+3042	T2.5	14:39:45.95	+30:42:21.0	17.22±0.23	>16.28	>15.88	...	...	29.9±7.5[c]	...	(2)
SDSS J1511+0607	T2	15:11:14.66	+06:07:43.1	15.88±0.02	15.14±0.02	14.52± 0.10	−255.6±7.1	−238.0±7. 0	18.0±3.0	36.7±6.4	(23);(16)
2MASS J1520-4422A	L1.5	15:20:02.30	-44:22:41.9	13.22±0.03	12.36±0.03	11.89± 0.03	−630.0±30.0	−370.0±20.0	19.0±1.0	...	(4);(15);(20)
2MASS J1520-4422B	L4.5	15:20:02.30	-44:22:41.9	14.70±0.07	13.70±0.05	13.70± 0.05	−630.0±30.0	−370.0±20.0	19.0±1.0	...	(4);(15);(20)
Program 11666											
ULAS J0034-0052[b]	T8.5	00:34:02.76	-00:52:08.0	18.15±0.08	18.49±0.04	18.48±0.05	...	...	12.6±0.6	79.60±3.80	(5);(16)
HD3651B[b]	T7.5	00:39:18.61	+21:15:12.7	16.16±0.03	16.68±0.04	16.87±0.	−461.1±0.7	−370.9±0.7	11.0±0.1	90.03±0.72	(6);(17);(15)
2MASS J0050-3322	T7	00:50:19.92	-33:22:41.4	15.93±0.07	15.84±0.19	15.24 ±0.19	1200.0±110.0	900.0±120.0	8.0±1.0	94.6±2.4	(3);(15);(22)
SDSS J0325+0425	T5.5	03:25:53.11	+04:25:40.0	16.25±0.14	>16.08	16.37± 0.06	−163.7±5.8	−59.6±5.7	19.0±2.0	55.6±10.9	(2);(16)
2MASS J0407+1514	T5	04:07:08.94	+15:14:55.4	16.06 ±0.09	16.02±0.21	15.92±0.26	106.0±16.0	−110.0±17.0	17.0±2.0	...	(7);(15)
2MASS J0510-4208	T5	05:10:35.32	-42:08:08.2	16.22 ±0.09	16.24±0.16	16.0± 0.28	104.0±15.0	580.0±21.0	18.0±2.0	...	(8);(15)
2MASSI J0727+1710	T7	07:27:19.07	+17:09:52.2	15.60 ±0.06	15.76±0.17	15.55±0.19	1046.0±4.0	−767.0±3.0	9.1±0.2	110.14±2.34	(9);(18)
2MASS J0729-3954	T8pec	07:28:59.47	-39:53:46.3	15.92 ±0.08	15.98±0.18	>15.29	−566.6±5.3	1643.4±5.5	6.0±1.0	126.3±8.3	(8);(16)
2MASS J0741+2351	T5	07:41:48.96	+23:51:25.9	16.15±0.10	15.84±0.18	>15.85	−243.0±13.0	−143.0±14.0	18.0±2.0	—	(10);(15)
2MASS J0939-2448	T8	09:39:35.87	-24:48:38.0	15.98 ±0.11	15.80±0.15	>16.56	558.1±5.8	−1030.5±5.6	10.0±2.0	196.0±10.4	(3);(16)
2MASS J1007-4555	T5	10:07:32.99	-45:55:13.3	15.65 ±0.07	15.68±0.12	15.56 ±0.23	−723.5±3.4	148.7±3.6	15.0±2.0	71.0±5.2	(8);(16)
2MASS J1114-2618	T7.5	11:14:48.90	-26:18:27.2	15.86±0.08	15.73±0.12	>16.11	−2927.2±7.0	−374.2±7.2	10.0±2.0	176.8±7.0	(3);(16)
2MASS J1231+0847	T5.5	12:31:46.74	+08:47:22.3	15.57±0.07	15.31±0.11	15.22±0.19	−1176.0±21.0	−1043.0±21.0	12.0±1.0	...	(7);(15)
ULAS J1238+0953[b]	T8.5	12:38:28.57	+09:53:51.3	18.95±0.02	19.20±0.02	...	...	...	18.5±4.3[c]	...	(11)
SDSS J1250+3925	T4	12:50:11.67	+39:25:47.9	16.54±0.11	16.18±0.18	15.05± 0.24	−15.0±80	−828.0±11.0	23.0±2.0	...	(2);(15)
SDSSP J13464-0031	T6.5	13:46:46.04	-00:31:51.3	16.00 ±0.10	15.46±0.12	15.77± 0.27	−503.0±3.0	−114.0±2.0	14.6±0.5	68.3±2.3	(12);(19)
SDSS J1504+1027	T7	15:04:11.74	+10:27:16.8	17.03±0.23	>16.90	>17.02	373.8± 7.9	−322.5±7.7	15.9±2.5[c]	52.5±7.1	(2);(16)
SDSS J1628+2308	T7	16:28:38.99	+23:08:18.4	16.45±0.10	16.11±o.15	15.87± 0.24	497.0±20.0	−461.0±21.0	14.0±4.0	75.1±0.9	(2);(15);(22)
2MASS J1754+1649	T5	17:54:54.56	+16:49:18.1	15.81±0.07	15.65±0.13	15.55±0.16	113.5±9.1	−141.4±9.2	14.3±1.3[c]	87.6±10.2	(13)
SDSS J1758+4633	T6.5	17:58:05.49	+46:33:17.1	16.15 ±0.08	16.25±0.21	15.46± 0.19	26.0± 15.0	594.0±16.0	12.0±2.0	71.0±1.9	(10);(15);(22)
2MASS J1828-4849	T5.5	18:28:36.01	-48:49:02.6	15.18 ±0.06	14.91±0.07	15.18 ± 0.14	231.4±10.5	52.4±10.9	11.0±1.0	83.7±7.7	(7);(16)
2MASS J1901+4718	T5	19:01:05.89	+47:18:09.9	15.86 ±0.07	15.47±0.09	15.64 ± 0.29	−110.0±20.0	−360.0±20.0	15.0±2.0	...	(7);(15)
SDSSJ 2124+0100	T5	21:24:14.02	+01:00:02.7	16.03 ±0.07	16.18±0.20	>16.14	202.0±14.0	287.0±14.0	18.0±2.0	...	(10);(15)
2MASS J2154+5942	T5	21:54:32.98	+59:42:14.4	15.66±0.07	15.76±0.17	>15.34	−182.0±9.0	−445.0±17.0	10.0±1.0	...	(8);(15)
2MASS J2237+7228	T6[a]	22:37:20.47	+72:28:35.3	15.76±0.07	15.94±0.21	>15.99	−73.0±2.0	−116.0±2.0	13.0±2.0	...	(8)
2MASS J2331-4718	T5	23:31:23.84	-47:18:28.2	15.66±0.07	15.51±0.15	15.39± 0.2	104.0±13.0	−49.0±19.0	13.0 ±2.0	...	(7);(15)
2MASS J2359-7335	T6.5	23:59:41.09	-73:35:04.9	16.17±0.04	16.06±0.07	16.05±0.13	...	...	12.3±1.9[c]	...	(14)

(1) Cruz et al. (2007); (2) Chiu et al. (2006); (3) Tinney et al. (2005); (4) Burgasser et al. (2007a); (5) Warren et al. (2007b); (6) Mugrauer et al. (2006); (7) Burgasser et al. (2004); (8) Looper et al. (2007); (9) Burgasser et al. (2002a); (10) Knapp et al. (2004); (11) Burningham et al. (2008); (12) Tsvetanov et al. (2000); (13) Faherty et al. (2012) ; (14) Kirkpatrick et al. (2011b); (15) Faherty et al. (2009); (16) Warren et al. (2007b); (17) Luhman et al. (2007); (18) Vrba et al. (2004); (19) Tinney et al. (2003); (20) Kendall et al. (2007b); (21) Looper et al., in prep. (22) Dupuy & Liu (2012b); (23) Albert et al. (2011)

[a] Optical spectral type.

[b] *MKO* photometry.

[c] Distance estimated from the Dupuy & Liu (2012b) absolute magnitude−SpT relation.

6.3.2 Imaging and data reduction

The IR channel of WFC3 was used in both programs. The detector (HgCdTe) is a 1024x1024 pixel array with an angular resolution of 0.13″/pixel and a field of view of 123″x136″ . The camera has 16 filters covering wide (W), medium (M) and narrow (N) bands from 800 to 1700nm. The observations analysed here use the F110W, F127M, F139M and F164N filters (see Fig. 6.2). F110W ($\lambda_c \equiv 1.1191$ μm) is the widest filter covering Y and J bands, encompassing the peak emission of flux from L and T dwarfs in the near infrared. F127M ($\lambda_c \equiv 1.274\mu$m) covers the 1.27$\mu$m peak in late-T dwarfs. Finally F139M ($\lambda_c \equiv 1.3838\mu$m) and F164N ($\lambda_c \equiv 1.6460$ μm) cover H_2O and CH_4 absorption bands in L and T dwarfs, respectively. Program 11631 (L and early T dwarfs) utilised the F127M, F139M and F164N filters; Program 11666 (mid-late T dwarfs) data were taken using the F110W, F127M and F164N filters.

Images were taken in MULTIACCUM mode following a standard dither pattern (4 dithers). Exposure times ranged from 111.0s for the widest filter to 1197.7s for the narrowest one (Table 6.2). Due to read time limits the images in F110W, F127M and F139M filter (in program 11631) cover an area of 35.88″x 31.98″(276 x 246 pixels), while the images in F164N filter and F127M (in program 11666) cover 141.70″ x 125.32″ (1090 x 964 pixels). We used the pipeline processed images, which include the analog−to−digital correction, subtraction of bias and dark current, linearity correction for readout artifacts, flat−field image and photometric calibration. The corrected images were used as input in MultiDrizzle (Fruchter & Hook, 2002) to perform the geometric distortion correction on all individual images , cosmic-ray rejection, and the final combination of the dithered images into a single output final image.

Upon visual inspection of the images, we rejected three objects from our original sample: 2MASS J094908.6−154548.5 (Tinney et al., 2005) was rejected due to poor image quality. Due to its high proper motion, 2MASS J11263991-5003550 (Folkes et al., 2007) was located outside the field of view at the time at observations. Finally, SIMP J132407.76+190627.1 (Deacon et al., 2011b) was missed due to erroneous telescope pointing. Therefore, our final sample consists of 34 sources.

6.4 WFC3 photometry

6.4.1 Measurements

We used SExtractor (Bertin & Arnouts, 1996) to perform aperture photometry for our final calibrated images. We used different aperture diameters, from 2 to 19 pixels (0.26″- 2.6″) around each source, and a common background annulus of 25 pixels (3.25″). The integrated counts were transformed to Vega magnitudes with the corresponding conversion factors provided in the WFC3 instruments manual.

Table 6.2: Log of observations. Magnitude limits for ρ=0.6″

Name	F110W			F127M			F139M			F164N			Observation
	t[a]	Δm_{lim}[b]	m_{lim}[c]	t	Δm_{lim}	m_{lim}	t	Δm_{lim}	m_{lim}	t	Δm_{lim}	m_{lim}	UT Date
	(s)	(mag)	(mag)	(s)	(mag)	(mag)	(s)	(mag)	(mag)	(s)	(mag)	(mag)	
(1)	(2)	(3)	(4)	(5)	(6)	(7)	(8)	(9)	(10)	(11)	(12)	(13)	(14)
Program 11631													
2MASS J0340−6724	...	...	...	413	2.5	17.25	413	2.0	17.45	413	2.0	15.60	2011-08-06
SDSS J0739+6615	...	...	...	413	2.0	18.61	413	1.5	19.82	413	2.0	18.03	2011-06-03
2MASS J1013−7842	...	...	...	413	2.0	16.19	413	2.25	16.53	413	1.75	14.49	2011-07-23
2MASS J1122−3512	...	...	...	413	1.75	16.45	413	1.75	18.30	413	1.75	16.01	2011-08-13
SDSS J1439+3042	...	...	...	413	2.0	18.78	413	1.75	20.25	413	2.0	18.50	2011-07-16
SDSS J1511+0607	...	...	...	413	2.0	17.60	413	2.0	18.68	413	2.0	17.11	2011-05-08
2MASS J1520−4422A	...	...	...	413	2.25	16.14	413	2.0	16.10	413	1.5	14.23	2011-07-01
Program 11666													
ULAS J0034−0052	111.0	2.0	21.46	997	2.0	19.71	...	...	...	1198	1.75	21.36	2010-12-27
HD3651B	133.0	2.5	19.94	997	1.75	17.60	...	...	...	1198	2.5	21.21	2010-12-30
2MASS J0050−3322	155.1	2.25	19.17	997	2.25	17.87	...	...	...	1198	2.25	18.89	2011-06-08
SDSS J03255+0425	111.0	2.75	19.92	997	2.0	17.78	...	...	...	1198	2.25	18.75	2010-12-02
2MASS J04070+1514	111.0	1.75	18.45	997	3.0	18.72	...	...	...	1198	2.25	18.41	2011-03-24
2MASS J0510−4208	67	2.0	19.12	997	2.25	18.00	...	...	...	1348	2.5	18.74	2011-04-03
2MASSI J0727+1710	133	1.75	18.13	997	2.75	17.93	...	...	...	1198	2.5	18.87	2010-11-11
2MASS J0729−3954	177	2.0	19.00	997	3.0	18.46	...	...	...	1198	2.0	18.64	2011-05-29
2MASS J07414+2351	133	2.0	18.92	997	2.25	18.23	...	...	...	1198	1.75	18.29	2010-11-09
2MASS J0939−2448	133	2.25	19.17	997	2.0	17.64	...	...	...	1198	2.0	18.92	2010-12-12
2MASS J1007−4555	111	2.25	18.64	997	2.25	17.85	...	...	...	1198	1.5	17.57	2011-05-14
2MASS J1114−2618	133.	2.0	18.62	997	2.25	17.87	...	...	...	1198	1.5	18.19	2010-12-08
2MASS J1231+0847	111	2.25	18.72	997	2.0	17.22	...	...	...	1198	3.0	18.72	2011-07-15
ULAS J1238+0953	111	2.25	21.88	997	1.75	19.98	...	...	...	1198	1.25	21.56	2011-02-23
SDSS J1250+3925	177	2.5	19.91	997	2.25	18.38	...	...	...	1198	2.25	18.41	2011-06-08
SDSSP J1346−0031	111	1.75	18.91	997	3.0	18.48	...	...	...	1198	2.0	18.46	2011-07-17
SDSS J1504+1027	111	1.5	18.87	997	2.0	18.12	...	...	...	1198	1.5	18.88	2011-06-24
SDSS J1628+2308	133	2.0	19.29	997	2.5	18.44	...	...	...	1198	1.25	18.49	2011-02-10
2MASS J1754+1649	133	2.5	18.91	997	2.0	17.53	...	...	...	1198	1.75	17.55	2011-07-19
SDSS J1758+4633	111	1.75	18.65	997	2.0	17.70	...	...	...	1348	1.75	18.35	2010-12-09
2MASS J1828−4849	111	1.75	17.95	997	1.75	16.79	...	...	...	1348	1.75	17.00	2011-10-23
2MASS J1901+4718	111	2.0	18.45	997	2.25	17.67	...	...	...	1348	1.5	17.20	2010-12-14
SDSS J21241+0100	111	2.5	19.41	997	2.25	17.97	...	...	...	1198	2.0	18.19	2010-11-21
2MASS J2154+5942	177	2.0	18.38	997	2.75	18.24	...	...	...	1198	1.75	17.873	2010-12-01
2MASS J2237+7228	177	1.5	17.90	1197	2.5	18.10	...	...	...	1348	1.5	17.41	2011-05-18
2MASS J2331−4718	111	2.25	18.50	997	2.25	17.58	...	...	...	1348	2.0	17.53	2011-04-13
2MASS J2359−7335	177	2.5	19.62	1197	2.25	18.24	...	...	...	1348	1.75	18.77	2010-11-02

[a]Exposure time.

[b]Limit Δm measured from Monte Carlo simulations for each object (see Section 6.5.3).

[c]Limiting magnitude calculated from Monte Carlo simulations and their respective magnitudes for each object.

In order to estimate the aperture correction for our sample we chose three isolated sources common in F110W, F127M and F164N, namely SDSSJ0325+0425, 2MASSJ1231+0847 and SDSSJ1346-0031. We used 2MASS J0340−6724, SDSS J0739+6615 and SDSS J1511+0607 for the F139M filter. Comparison of integrated flux profiles as a function of aperture size normalized to a 20-pixel aperture demonstrates excellent agreement between the sources, with deviations of less than 0.009 mag for apertures wider than 10 pixels (see Table 6.3). We adopted a 6 pixel aperture diameter (0.78″) to extract the photometry. To calculate the total uncertainties in the magnitude corrections, we combined count uncertainties, a 1% error due to instrumental photometric stability, and 1% due to flux calibration uncertainty (see WFC3 manual[3]). The final values are listed in Table 6.4.

[3]http://www.stsci.edu/hst/wfc3

Table 6.3: WFC3 aperture corrections.

Radius (pixels)	F110W (mag)	F127M (mag)	F39M (mag)	F164N (mag)
2	−1.38±0.08	−1.26±0.1	−1.08±0.05	−1.30 ±0.07
3	−0.77±0.06	−0.62±0.06	−0.59±0.05	−0.72±0.04
4	−0.42±0.05	−0.36±0 .04	−0.32±0.02	−0.43±0.03
5	−0.27±0.03	−0.23±0.03	−0.21±0.01	−0.28±0.01
6	−0.20±0.03	−0.17±0.02	−0.16±0.007	−0.20±0.01
7	−0.17 ±0.02	−0.15±0.02	−0.13±0.005	−0.15±0.007
8	−0.14±0.02	−0.12±0.01	−0.12±0.004	−0.13±0.006
9	−0.11 ±0.01	−0.10±0.01	−0.10±0.003	−0.11±0.004
10	−0.09±0.01	−0.08±0.009	−0.08±0.003	−0.09±0.003
11	−0.08 ±0.01	−0.07±0.008	−0.06±0.002	−0.08±0.0002
12	−0.07±0.009	−0.06±0.007	−0.05±0.002	−0.06±0.001
13	−0.06±0.007	−0.05±0.006	−0.04±0.003	−0.05±0.001
14	−0.05±0.006	−0.04±0.004	−0.04±0.003	−0.04±0.001
15	−0.04±0.005	−0.03±0.003	−0.03±0.003	−0.03±0.001
16	−0.03±0.003	−0.02±0.002	−0.02±0.001	−0.03±0.001
17	−0.02±0.002	−0.02±0.002	−0.01±0.001	−0.02±0.0007
18	−0.012±0.001	−0.01±0.001	−0.01±0.002	−0.01±0.0009
19	−0.006±0.0006	−0.005±0.0006	−0.006±0.001	−0.006±0.0004

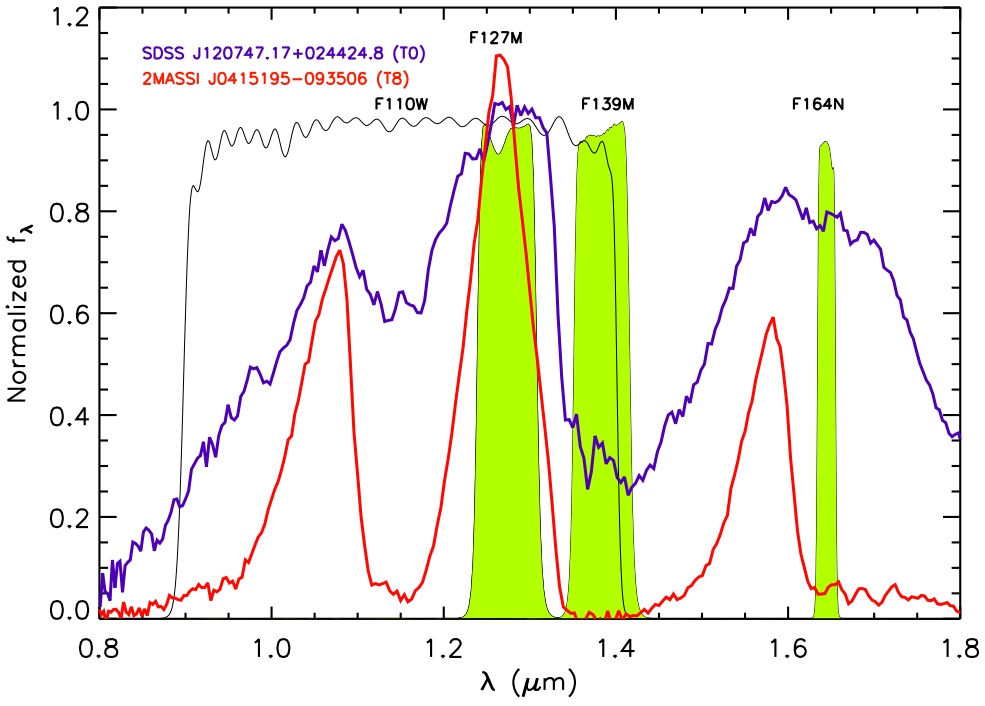

Figure 6.2: Filter transmission profiles of F110W (black line), F127M, F139M and F164N (green areas), compared to the near infrared spectra of the T8 2MASS J0415-0935 (Burgasser et al., 2004) and the T0 SDSS J1207+0244 (Looper et al., 2007)

Table 6.4: WF3 Photometry for 11631 and 11666 programs.

Name	NIR−SpT	F110W	F127M	F139M	F164N	F127M - F164N
	Literature	(mag)	(mag)	(mag)	(mag)	(mag)
(1)	(2)	(3)	(4)	(5)	(6)	(7)
			Program 11631			
2MASS J0340-6724	L7::	...	14.76±0.02	15.45±0.01	13.60±0.01	1.16±0.02
SDSS J0739+6615	T1.5+/-1	...	16.61±0.02	18.32±0.01	16.03±0.01	0.58±0.02
2MASS J1013-7842	L3	...	14.19±0.02	14.28±0.01	12.74±0.01	1.45±0.02
2MASS J1122-3512	T2	...	14.70±0.02	16.55±0.01	14.26±0.01	0.44±0.02
SDSS J1439+3042.	T2.5	...	16.78±0.02	18.50±0.01	16.50±0.01	0.28±0.02
SDSS J1511+0607.	T2	...	15.60±0.02	16.68±0.01	15.11±0.01	0.49±0.02
2MASS J1520-4422A	L1.5	...	13.89±0.02	14.10±0.01	12.73±0.01	1.16±0.02
2MASS J1520-4422B	L4.5	...	14.57±0.02	15.06±0.01	13.60±0.01	0.97±0.02
			Program 11666			
ULAS J0034-0052	T8.5	19.46±0.03	17.71±0.02	...	19.61±0.02	-1.90±0.03
HD 3651B	T7.5	16.92±0.03	15.98±0.02	...	16.54±0.01	-1.85±0.02
2MASS J0050-3322	T7	16.92±0.03	15.62±0.02	...	16.64±0.01	-1.03±0.02
SDSS J0325+0425	T5.5	17.17±0.03	15.78±0.02	...	16.50±0.01	-0.72±0.02
2MASS J0407+1514	T5	16.70±0.03	15.72±0.02	...	16.16±0.01	-0.44±0.02
2MASS J0510-4208	T5	17.12±0.03	15.75±0.02	...	16.24±0.01	-0.49±0.02
2MASSI J0727+171	T7	16.38±0.03	15.18 ±0.02	...	16.37±0.01	-1.18±0.02
2MASS J0729-3954	T8pec	17.00±0.03	15.46±0.02	...	16.64±0.01	-1.18±0.02
2MASS J0741+2351	T5	16.92±0.03	15.98±0.02	...	16.54±0.01	-0.56±0.02
2MASS J0939-2448	T8	16.92±0.03	15.64±0.02	...	16.93±0.01	-1.28±0.02
2MASS J1007-4555	T5	16.39±0.03	15.60±0.02	...	16.07±0.01	-0.47±0.02
2MASS J1114-2618	T7.5	16.62± 0.03	15.62±0.02	...	16.69±0.01	-1.07±0.02
2MASS J1231+0847	T5.5	16.47± 0.03	15.22±0.02	...	15.73±0.01	-0.50±0.02
ULAS J1238+0953	T8.5	19.63±0.03	18.23±0.02	...	20.31±0.01	-2.08±0.04
SDSS J1250+3925	T4	17.42±0.03	16.13±0.02	...	16.16±0.01	-0.03±0.02
SDSSP J1346-0031	T6.5	17.16±0.03	15.48±0.02	...	16.46±0.01	-0.99±0.02
SDSS J1504+1027	T7	17.37± 0.03	16.13±0.02	...	17.38±0.01	-1.25±0.02
SDSS J1628+2308	T7	17.29±0.03	15.94±0.02	...	17.24±0.01	-1.29 ±0.02
2MASS J1754+1649	T5	16.41±0.03	15.53±0.02	...	15.80±0.01	-0.27±0.02
SDSS J1758+4633	T6.5	16.90±0.03	15.70±0.02	...	16.60±0.01	-0.89±0.02
2MASS J1828-4849	T5.5	16.20±0.03	15.04±0.02	...	15.24±0.01	-0.20±0.02
2MASS J1901+4718	T5	16.45 ±0.03	15.43±0.02	...	16.70±0.01	-0.27±0.02
SDSS J2124+0100	T5	16.91±0.03	15.72±0.02	...	16.19±0.01	-0.47±0.02
2MASS J2154+5942	T5	16.39 ±0.03	15.50±0.02	...	16.12±0.01	-0.63±0.02
2MASS J2237+7228	T6	16.40±0.03	15.60±0.02	...	15.91±0.01	-0.31±0.02
2MASS J2331-4718	T5	16.25±0.03	15.33±0.02	...	15.53±0.01	-0.19±0.02
2MASS J2359-7335	T6.5	17.12 ±0.03	16.00±0.02	...	17.02±0.01	-1.03±0.02

6.4.2 L and T dwarf colours

To provide adequate colour discrimination of L and T-dwarfs from background sources, we examined all possible colour combinations. While the majority of background sources have neutral NIR colours, our targets show very red colours (see Table 6.4) due to molecular absorption. Figure 6.3 displays the magnitude vs. colour and colour vs. NIR-SpT[4] of our targets. The (F110W−F164N) shows considerable scatter vs. spectral type, so we did not

[4]Except for 2MASSI J0340−6724, 2MASS J1013−7842 and 2MASS J2237+7228 where only the optical spectral type was available.

calculate a spectral type relation for this colour. This is likely due to the width of the F110W filter. The (F127M - F139M) colour displays a strong trend with spectral type in the late−L and early−T dwarfs. A linear fit to (F127M−F139M) colour yields,

$$SpT = 1.56 - 6.25 * (F127M - F139M) \tag{6.1}$$

where SpT(L0) = 0, SpT(T5) = 15 and, SpT(Y0) = 20. The scatter is 1.2 subtypes.

Similarly, a quadratic fit of (F127M−F164N) colour to SpT yields,

$$SpT = 13.22 - 5.37 * (F127M - F164N) - 1.56 * (F127M - F164N)^2 \tag{6.2}$$

The scatter in this relation is 0.6 subtypes and hence this colour is a more accurate proxy for spectral type than F127M-F139M colour.

Both trends reflect the strengthened H_2O and CH_4 absorption bands along the L and T sequence. Because these bands saturate, continuum fluxes also decline in the Y dwarf regime (Cushing et al. 2011a; Kirkpatrick et al. 2011b), so the trends may not persist to arbitrarily low temperatures.

6.5 WFC3/HST PSF fitting analysis

The main goal of this study is to identify binary systems in the sample. There are no well-resolved pairs other than the previously identified 2MASS J1520−4422AB (Burgasser et al. 2007a; Kendall et al. 2007a). To identify more closely-separated pairs with blended PSFs, we used a PSF-fitting algorithm similar to that described in Burgasser et al. (2003b).

6.5.1 Method

In previous studies (Burgasser et al. 2006b; Dupuy & Liu 2012b), the Tiny Tim[5] program (Krist, 1995) has been used to generate a super−sampled PSF model that takes into account the source SED and instrument response. This tool does not currently implement oversampling for WFC3, so we decided to generate PSF models of each filter from the data. The WFC3 diffraction limit goes from 0.096″ for the bluest filter, F110W, to 0.142″ for the reddest one F164N. Therefore, we extracted subimages of 20x20 pixels (2.6″x 2.6″) centered on point sources, which were then resampled at ten times the original pixel size and recentered by subpixel offsets. We median-combined 83 background sources in F110W, 399 sources in F127M, 12 sources in F139M and 515 sources in F164N images to create the PSF

[5]http://tinytim.stsci.edu/cgi-bin/tinytimweb.cgi

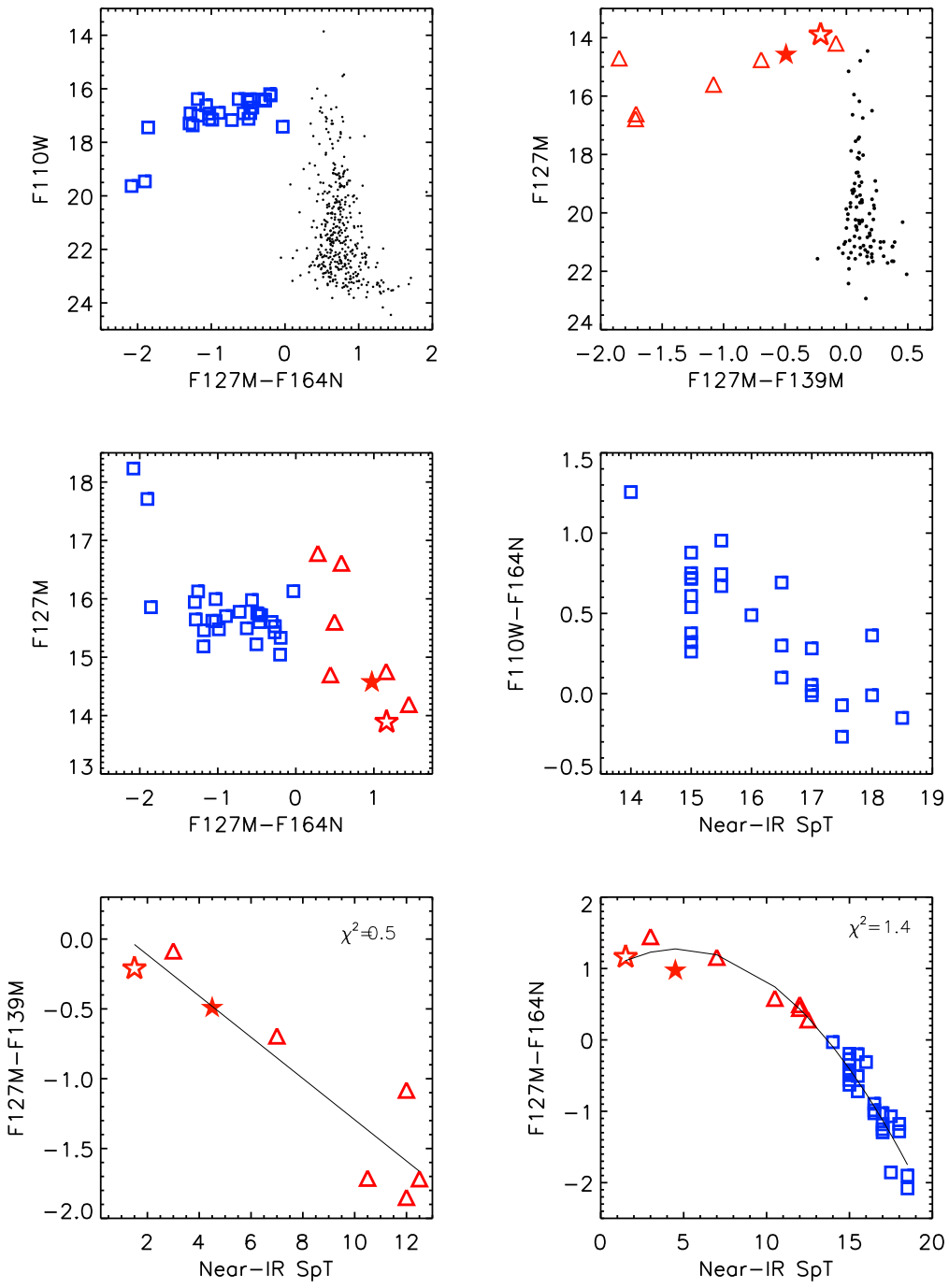

Figure 6.3: Segregation of L and T dwarfs with WFC3 photometry. Magnitude vs. colour and colour vs. NIR SpT for 11666 (full blue circles) and 11631 (red triangles) programs, including the known binary system 2MASS J1520−4422AB (red stars), respectively. Background sources are represented by black points. Linear (for F127M-F139M) and quadratic (for F127M-F164N) fits to the photometric data are indicated by the solid lines. Spectral types are encoded as SpT(L0) = 0, SpT(T5) = 15 and, SpT(Y0) = 20. The uncertainties are smaller than the symbol size.

models. We found these models provide superior fits to the target than the WFC3 TinyTim model.

To search for faint companions, we used an iterative routine focused on the same 2.6″x 2.6″subimages centered on each target. First, initial guesses for the positions and fluxes for two components were made using a simple peak detection on the original image (for the primary) and on the residual image after PSF subtraction (for the secondary). The routine then finds the optimal primary and secondary position by shifting in steps of 0.1 pixels and flux scaling in steps of 1% (0.01mag). The quality of fit was assessed using the χ^2 statistic:

$$\chi^2 = \sum_{ij} \frac{(D_{ij} - \alpha M_{ij})^2}{\sigma_{ij}^2} \tag{6.3}$$

Here D_{ij} is the data, M_{ij} is the model, α is the scaling value between the data and model and σ_{ij}^2 is the data variance. An illustration of this algorithm is shown in Figure 6.4. Fits were done with both single and binary PSF models, and to assess the statistical significance of the latter we use the one-side F-test.

$$F = \frac{min(\chi^2_{single})/\nu_s}{min(\chi^2_{binary})/\nu_b} \tag{6.4}$$

where ν_s and ν_b are the degrees of freedom for the singles and binary fits, respectively, because some parts of the image do not contribute to the fit (i.e. regions with no source flux). So, the degrees of freedom were calculated taking into account the effective pixels involved in the fitting,

$$Pixels_{eff} = \frac{\sum_{ij} M_{ij}}{max(M_{ij})} \tag{6.5}$$

$$\nu_{s,b} = Pixels_{eff} - N_{parameters} \tag{6.6}$$

where $N_{parameters}$ is 3 for the single model, and 6 for the binary (Burgasser et al. 2010).

6.5.2 Results

The results of these fits are summarized in Table 6.5 for F127M. The only binary system identified by our PSF−fitting routine was the previously-known wide binary, 2MASS J1520−4422AB with separation 1.20±0.01″and PA=29.°65±0.°70. These values are marginally consistent with previous determinations (Burgasser et al., 2007a). We can conclude that our routine gives us reliable results for resolved BD binary systems.

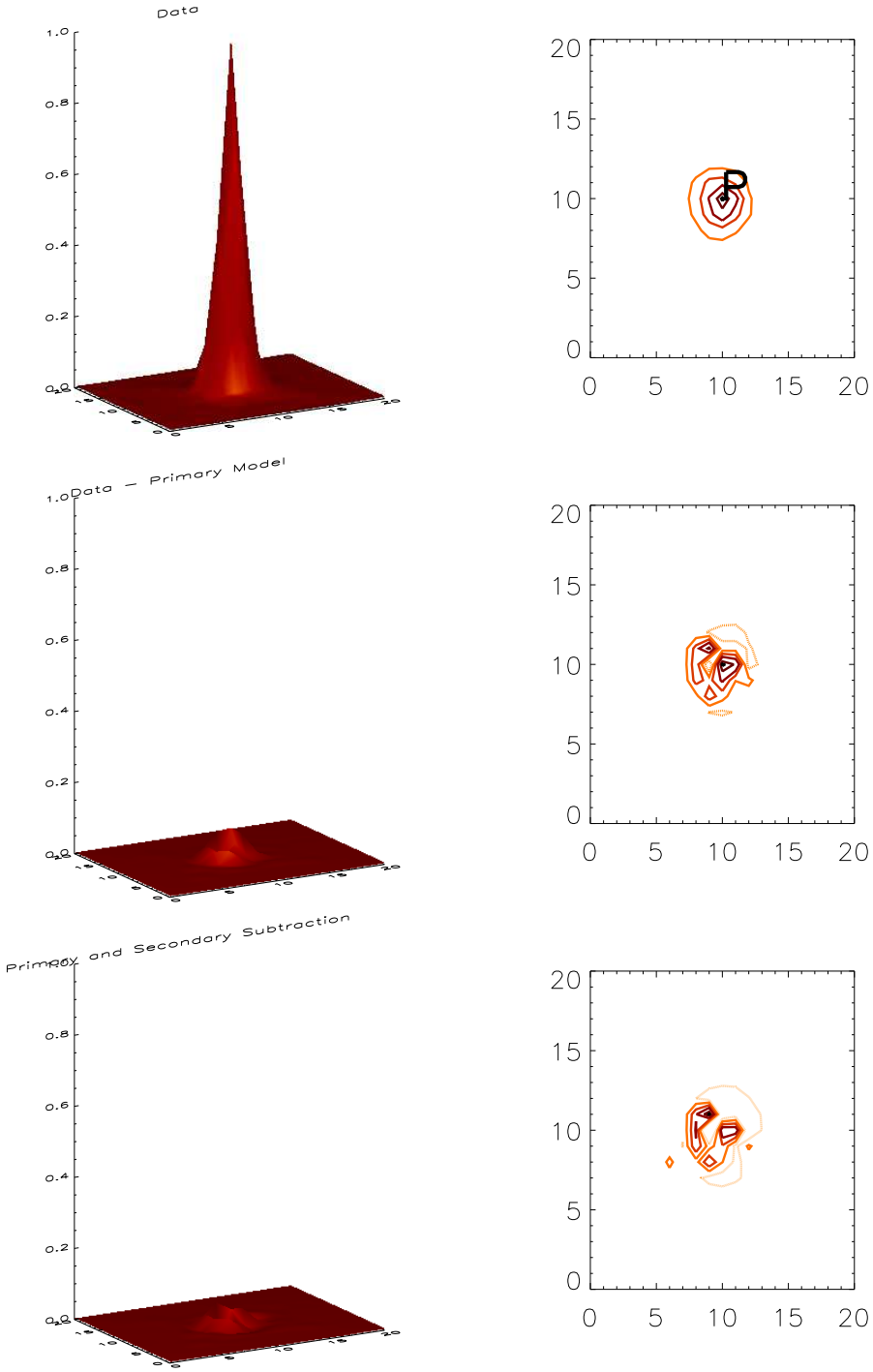

Figure 6.4: 2MASS J0727+1710 in F127M filter. In the upper part of the figure are shown the surface and contour plots previous to the PSF subtraction. The red letter 'P' represents where the primary BD's coordinates are located. In the middle and bottom part of the figure are shown the surface and contour plots for the residuals after the primary PSF-model subtraction and the residuals after primary and secondary PSF-models subtraction, respectively. The contour levels represent the –0.3, –0.2, –0.1 (dashed lines), 0.1, 0.3, 0.5, 0.8, 0.95 (solid lines) of the maximum flux from the data, and after the primary and secondary PSF-subtraction.

Table 6.5: The statistical analysis for F127M filter.

Name	χ^2_{single}	χ^2_{binary}	F-test	ρ^a	ρ^a	P.A.^{b}	Δm
			(%)	(pixel)	($''$)	$^\circ$	(mag)
(1)	(2)	(3)	(4)	(5)	(6)	(7)	(8)
Program 11666							
2MASS J0340−6724	95.9	99.4	44	0.83	0.108	69.53	2.82
SDSS J0739+6615	288.7	328.0	40	0.81	0.106	184.96	2.08
2MASS J1013−7842	70.7	52.4	60	1.51	0.197	253.44	2.18
2MASSJ1122−3512	5328.8	4908.3	43	0.06	0.008	191.42	2.11
SDSS J1439+3042	100.2	115.7	41	1.19	0.155	118.42	2.14
SDSS J1511+0607	270.7	282.3	43	0.55	0.071	233.01	2.14
2MASS J1520−4422A	0.1	0.01	100	9.23	1.200	29.65	0.04
Program 11666							
ULAS J0034−0052	42.2	42.1	45	0.61	0.080	68.11	2.31
HD 3651B	1878.6	1721.7	44	0.08	0.011	21.14	2.16
2MASS J0050−3322	400.0	369.7	44	0.12	0.015	259.21	2.43
SDSS J0325+0425	686.9	867.8	36	0.88	0.115	115.58	2.27
2MASS J0407+1514	16.3	14.8	50	0.83	0.108	27.53	3.20
2MASS J0510−4208	149.1	162.3	43	0.97	0.126	20.59	2.35
2MASSI J0727+1710	173.8	166.0	43	0.0	0.0	304.01	3.08
2MASS J0729−3954	93.3	84.7	48	1.07	0.139	98.61	3.08
2MASS J0741+2351	77.1	62.9	52	1.75	0.227	51.73	2.55
2MASS J0939−2448	68.1	49.5	59	1.84	0.239	122.55	2.39
2MASS J1007−4555	58.7	41.7	60	1.60	0.208	30.35	2.38
2MASS J1114−2618	307.7	302.6	41	0.14	0.018	136.22	2.93
2MASS J1231+0847	513.6	473.0	44	0.09	0.011	69.78	2.30
ULAS J1238+0953	56.5	79.2	33	0.74	0.096	312.23	2.02
SDSS J1250+3925	33.4	34.3	45	0.62	0.080	143.86	2.58
SDSSP J1346−0031	453.4	413.1	44	0.13	0.017	219.76	3.25
SDSS J1504+1027	1100.8	1358.7	37	0.88	0.114	82.03	2.18
SDSS J1628+2308	1139.3	1070.8	43	0.06	0.008	24.22	2.74
2MASS J1754+1649	44.2	53.7	38	1.34	0.174	87.38	2.28
SDSS J1758+4633	571.6	705.5	37	0.88	0.114	122.45	2.36
2MASS J1828−4849	99.6	58.5	68	1.21	0.157	104.86	1.89
2MASS J1901+4718	1203.8	1132.1	42	0.0	0.0	201.57	2.39
SDSS J2124+0100	247.0	234.8	42	0.06	0.008	154.92	2.65
2MASS J21547+5942	472.6	448.1	42	0.12	0.0161	63.44	2.59
2MASS J2237−7228	116.3	108.5	45	1.06	0.138	307.22	2.99
2MASS J2331−4718	106.0	54.5	69	1.59	0.206	44.28	2.39
2MASS J2359−7335	116.2	94.4	53	1.82	0.236	15.22	2.53

[a]Separation between the primary and secondary components after the PSF fitting.

[b]Position angle.

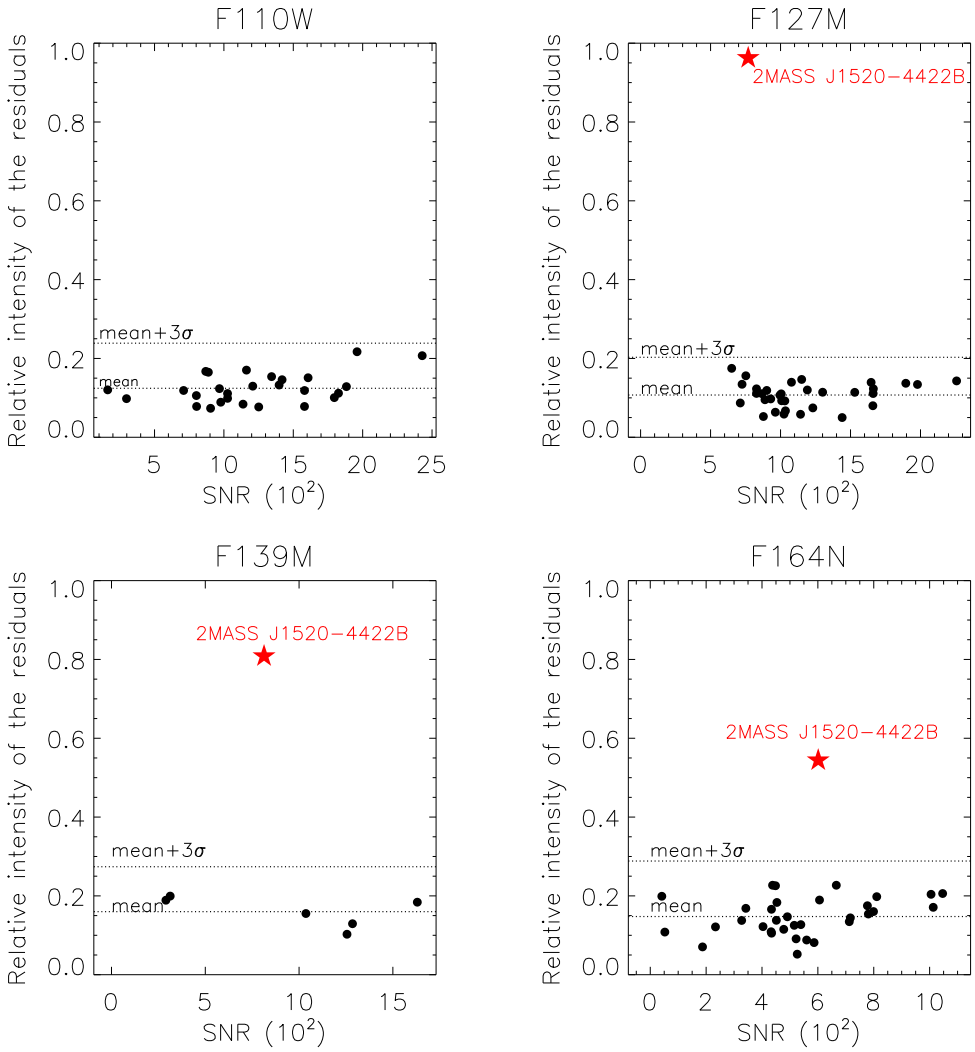

Figure 6.5: Relative intensity of the residuals after the primary PSF subtraction as a function of the Signal to Noise Ratio. The only objetct detected is 2MASS J1520−4422B, which is shown with red star above the median + 3σ value.

No other sources were found to be significally better fit by a binary PSF model, implying that they are single or unresolved with WFC3's resolution and sensitivity.

To check our results is to quantify the relative intensity of the residuals after the primary PSF subtraction. Figure 6.5 shows the result of this analysis showing images after the PSF subtraction. The 2MASS J1520−4422AB system clearly has the highest residuals compared to the rest of the sample because of its resolved secondary. None of the others targets show clear evidence of multiplicity.

Table 6.6: Summary of know mid, late-T dwarfs binary systems closer than 20 pc.

Object	Instrument	Δm_{F127M} (mag)	ρ (AU)	ρ (mas)	Distance (pc)	Spt. A	Spt. B	Binary Reference
(1)	(2)	(3)	(4)	(5)	(6)	(7)	(8)	(9)
2MASS J1534−2952[a]	*HST* WFPC2	0.16±0.28[b]	2.3±0.5	140.3±0.57[b]	13.6±0.2	T5	T5	Burgasser et al. (2003b)
2MASS J1225−2739	*HST* WFPC2	1.227±0.05	3.8±0.1	282±5	13.4±0.04	T6	T8	Burgasser et al. (2003b)
2MASS J1553−1532	*HST* NICMOS	0.052±0.02	4.2±0.7	349±5	12±2.0	T6.5	T7	Burgasser et al. (2006b)
WISE J0458+6634	Keck NIRC2	0.944±0.09	5±0.4	510±20	10.5±1.4	T8.5	T9	Gelino et al. (2011)
CFBDSIR J1458+1013	Keck NIRC2	1.721±0.07	2.6±0.3	110±5	23.1±2.4	T9.5	>T10	Liu et al. (2011)
WISE J1217+1626	Keck NIRC2	2.021±0.03	8.0±1.3	759.2±3.3	10.5±1.7	T9	Y0	Liu et al. (2012)
WISE J1711+3500	Keck NIRC2	2.722±0.03	15.0±2.0	780.0±2.0	19.0±3.0	T8	T9.5	Liu et al. (2012)

[a] This source was not resolved with WFPC2.

[b] Δm and ρ measured by Keck LGS AO observations on K_s filter (Liu et al. 2008).

6.5.3 Searching limits

To assess our detection limits for mid-late T companions we performed a multi-step Monte Carlo simulation to calculate the detection and false positive rates as a function of separation and relative magnitude for each source in three WFC3 filters (F110W, F127M and F164N). Our simulation used 10^5 fake stars (generated from the PSF model) implanted around each target with different orientations, distances (from 1 to 6 pixels) and Δm (from 0 to 5 mag). Our PSF-fitting routine was then used to recover the implants with steps in distance and magnitude of 0.5 pixels and 0.2 magnitudes to find the limit beyond which the fake stars are not correctly recovered. To quantify the effect of false positives, we performed another Monte Carlo simulation adding 10^3 variations of Gaussian noise to each image and seeing where a (false) secondary is found.

These procedures were done for each source in our sample; an example is shown in Figure 6.6. Sensitivity maps in Δm and separation were determined based on the fraction of implants recovered, and nulling regions with high false positive rates. We find WFC3 is able to detect companions at separations greater than 0.325″ and with $\Delta m_{F110W} \leq 2.75$ mag, $\Delta m_{F127M} \leq 3.0$, $\Delta m_{F139M} \leq 2.25$ and $\Delta m_{F164N} \leq 2.5$. Thus, F127M is the most sensitive filter to detect faint companions both due to better image quality (sharper PSF), and since cool (T, Y) companions tend to have a flux distribution that peaks in F127M.

6.6 Analysis

6.6.1 Comparison with known mid and late-T dwarfs binary systems

High resolution searches with *HST*/NICMOS-WFPC2 and Keck/NIRC2 instruments have resulted in the detection of seven mid to late T dwarf binary systems at distances closer than 20 pc (see Table 6.6). With a total of 90 such sources within that distance limit, the corresponding visual BF is $7.8^{+7.5}_{-3.9}$%. However, a proper comparison requires a quantification of selection effects.

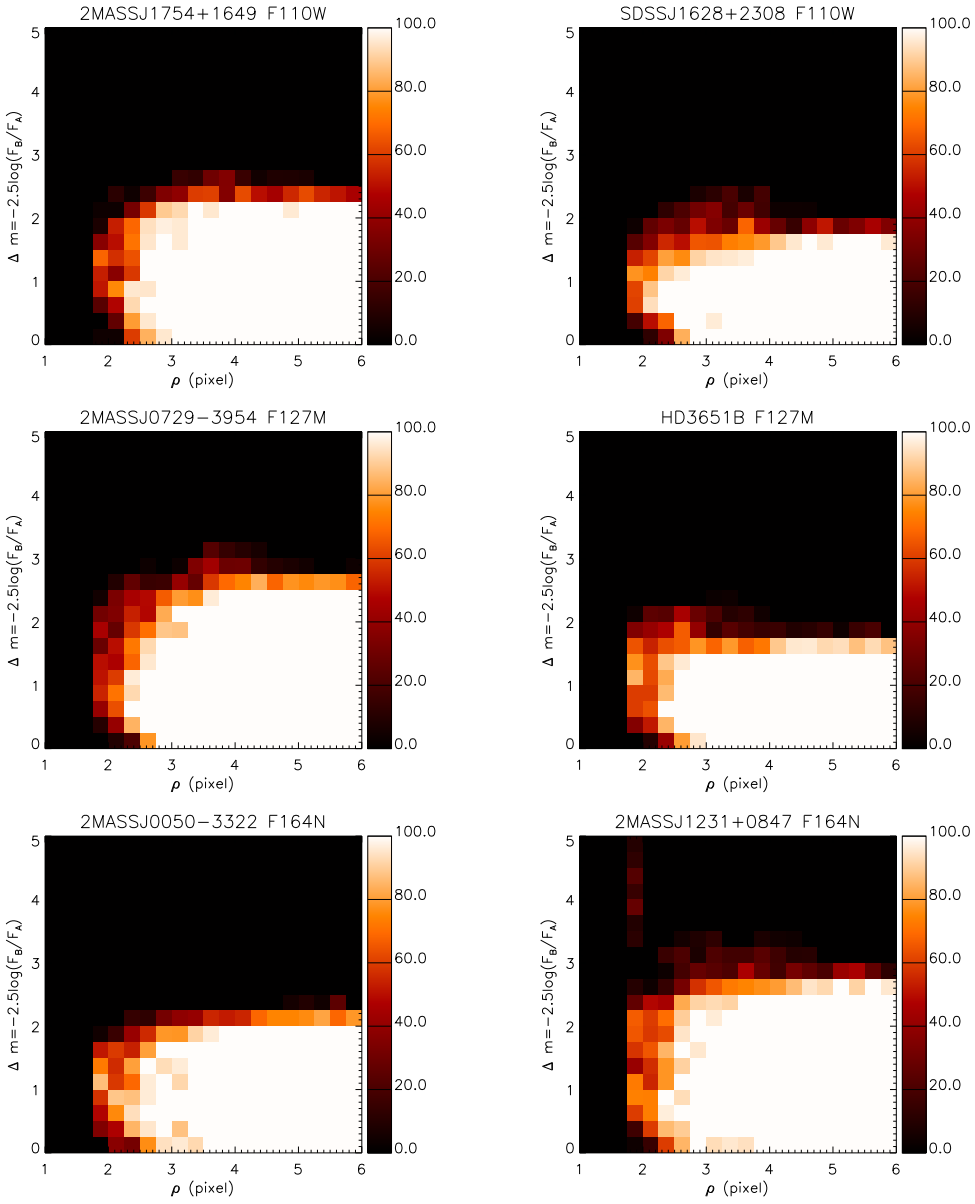

Figure 6.6: Samples of selection probabilities based on Monte Carlo simulations described in the text, showing 2MASSJ1754+1649 and SDSS J1628+2308 in F110W filter, 2MASS J0729−3954 and HD3651B in F127M filter, and finally 2MASS J0050−3322 and 2MASS J1231+0847 in F164N filter. Detection probabilities are indicated by colour scale.

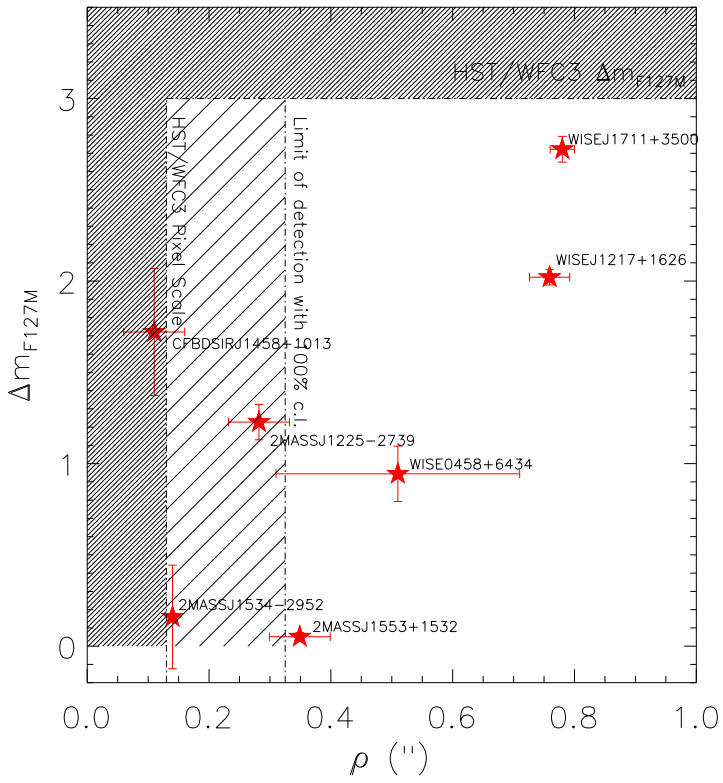

Figure 6.7: Mid, late-T dwarf binary systems discovered with Keck II LGS-AO and *HST*/NICMOS-WFPC2. Sources are plotted in Δm_{F127M} vs. separation and detection limits for the WFC3 program are overlaid.

We first calculated the probability of resolving the known mid, late T dwarf binaries in our sample with WFC3. We transformed resolved J magnitudes to F127M using synthetic colours computed from low- resolution near-infrared spectra of L0-T9 dwarfs from the SpeX Prism Spectral Libraries[6]. Figure 6.7 compares separations and relative magnitudes for these systems to our WFC3 sensitivity limits. Only 2MASS J1553+1532, WISE J0458+6434, WISE J1217+1626 and WISE J1711+3500 are within the WFC3 limits. Multiplying the visual BF with the probabilities $P(\rho \geq 0.325'')$ and $P(\Delta m_{F127M} \leq 3$ mag), the probability of finding T5+$\geq$T5 dwarf binaries in our sample is 4.4%, which is in agreement with the null binary detection in the studied sample.

[6]We generated a 6^{th} order polynomial to fit synthetic colours for 543 L0-T9 dwarfs, F127M-J = $\sum_{i=0}^{6} a_i \mathrm{SpT}^i$, where SpT(L0) = 20, SpT(T0) = 30, etc. The fit coefficients $\vec{a}$ = [-9.94976e1, 2.11571e1, -1.84264e0, 8.40307e-2, -2.11748e-3, 2.79814e-5, -1.51800e-7] have a standard deviation of 0.016 mag.

6.6.2 Inferring the binary fraction of brown dwarfs for T5+

Given the WFC3 pixel scale, the absence of any new discoveries in this sample is not wholly unexpected. Nevertheless, our sample, is the largest containing T5+ sources, so it allows us to more tightly constrain the underlying binary fraction. To do this, we applied the detection and false positive rate maps computed for each source in the F127M filter to another Monte Carlo simulation that determines the probability that each source, if it were a binary, would have been uncovered.

We generated a large sample (5×10^6) of binaries by first drawing primary masses from a power-law mass distribution quantified as $\mathrm{d}N/\mathrm{dM} \propto \mathrm{M}^{-0.5}$ (Burgasser, 2004b; Burningham et al., 2013). Secondary masses were then computed assuming either a flat mass ratio distribution ($P(q \equiv \mathrm{M}_2/\mathrm{M}_1) \propto$ constant) or a power-law distribution ($P(q) \propto q^{1.8}$; Allen 2007), imposing a minimum mass of 0.005 $\mathrm{M}_\odot$. Adopting a uniform age distribution between 0.1 Gyr and 10 Gyr for the simulated systems, the component masses were converted to bolometric luminosities using the evolutionary models of Burrows et al. (2001), and these transformed into spectral types and absolute J magnitudes using the relations given in Dupuy & Liu (2012a). J magnitudes were then transformed to F127M using synthetic colours computed as above. We then computed relative F127M magnitudes for each of the simulated binaries. For the orbits, we assigned semimajor axes assuming either a flat ($P(a) \propto$ constant) or lognormal distribution:

$$P(\log a) \propto e^{-\left(\frac{\log a - 0.86}{0.28}\right)^2} \tag{6.7}$$

(Allen, 2007) where a is in AU and constrained to be <25 AU, a limit which encompasses known T dwarf field binaries. We assumed uniform distributions of mean anomaly, longitude of ascending node, and argument of periapsis, a sin i distribution for inclination, and a uniform distribution of eccentricities over $0 < e < 0.6$ based on the analysis of Dupuy & Liu (2011). These orbital elements were projected onto the sky and transformed into angular separations at the distance of each system. We selected only those systems whose primary spectral type was within 1 subtype of the target, and determined the fraction of these that could have been resolved with WFC3 based on our detection and false positive rate maps. We further assumed that companions wider than 0.″6 could be detected to the sensitivity limit of each image (Table 6.2). We computed fractions for the four possible combinations of mass ratio and separation distributions as described above (see Table 6.7).

Table 6.7 lists the resulting probabilities of detection, while Figure 6.8 illustrates how WFC3 selection effects impact observed distributions of binary separation and mass ratio in the case of 2MASS J1828−4849. Not surprisingly, both the closest systems (<1 AU) and lowest-q systems ($q < 0.6$) are preferentially lost, the latter having the more significant impact on overall recovery rate. The most distant targets in our sample have the lowest detection probabilities and the largest differences in detectability based on the assumed separation distribution, a consequence of the peak of the lognormal distribution falling below angular resolution limits. Detection probabilities are consistently lower for flat versus power-law mass ratio distributions.

By adding up the individual source probabilities, we find that if all our targets had companions we should have detected between 13 and 21 binaries, depending on the assumed underlying distribution. The lack of detections implies a binary fraction upper limit of $<16-<25\%$ assuming a binomial distribution with 95% of confidence level[7].

These values are consistent with previous *bias-corrected* estimates of the field brown dwarf binary fraction (Burgasser et al., 2003b, 2006b; Allen, 2007) and supports the hypothesis that multiplicity rates decline with decreasing primary mass into the substellar regime (see Figure 6.9; Fischer & Marcy 1992; Reid & Gizis 1997a; Bouy et al. 2003; Close et al. 2003b; Kraus & Hillenbrand 2012; Bate 2012). However, our estimates are subject to the same limitations on probing the closely separated (<1 AU) binary population as prior imaging programs. The resolving limit of HST and AO imaging coincides with the peak of the brown dwarf binary separation distribution, suggesting that tighter binaries may be plentiful (Burgasser et al. 2006b). Alternate detection methods such as RV monitoring (e.g., Basri & Martín 1999; Blake et al. 2010) or spectral blend detection (e.g., Burgasser et al. 2010) are still needed to determine if the brown dwarf binary fraction may in fact be much higher than imaging studies indicate.

6.7 Conclusions

We have analysed data obtained in two imaging survey of 34 BDs with HST/WFC3. The sample comprises 8 L and T dwarfs that we have used to study colour-colour and colour-SpT relations, and 26 mid- to late T dwarfs employed in a search for $\geq$T5 dwarfs companions. Only one previously identified widely-separated system was recovered: 2MASS J1520-4422AB. PSF-fitting uncovered no new close companions to mid-late T sources in our sample.

Based on Monte Carlo simulation we should have been able to detect faint objects at separations $\geq 0.325''$ and with $\Delta m_{F127M} \leq 3.0$. Our failure to detect such companions implies a low binary fraction or a significant population of tight binaries. We determined the fraction of binaries that would have been detected around each source based on assumed separation and mass ratio distributions and all possible orientations of these systems. Due to the WFC3 separation limit that makes the null detection of these sources, we infer an upper limit for the binary fraction of $<16-<25\,\%$, depending of the underlying mass ratio distribution. Comparing with previous BD binary surveys made with HST, we can conclude that WFC3 is more sensitive to cool companions than NICMOS and WFPC2 but its lower resolution makes it poorly suited for typically tight brown dwarf binary systems.

[7] To calculate the confidence limits we use the Clopper-Pearson exact method based on the beta distribution (Brown et al. 2001).

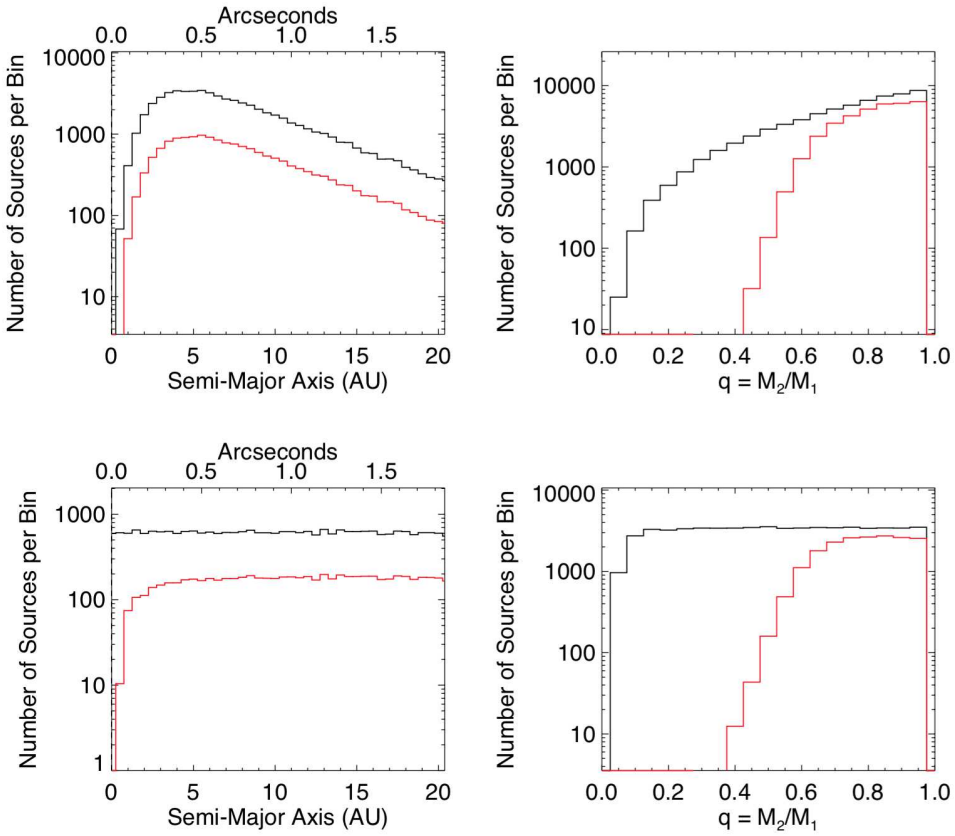

Figure 6.8: Binary detection probability distributions for the T5.5 2MASS J1828−4849 as a function of semi-major axis (left) and mass ratio (right) based on the simulations described in the text. Each panel displays the distributions of input (black lines) and recovered (red lines) systems based on WFC3 selection function for this source. The top and bottom left panels compare lognormal and constant input distributions for semi-major axis; the top and bottom right panels compare power-law and constant input distributions in mass ratio, respectively. The resulting total binary recovery rate for this and other sources in our sample are given Table 6.7.

6.7.1 Acknowledgments

Based on observations made with the NASA/ESA Hubble Space Telescope, obtained from the Data Archive at the Space Telescope Science Institute, which is operated by the Association of Universities for Research in Astronomy, Inc., under NASA contract NAS 5-26555. These observations are associated with programs GO-11631 and GO-11666. Support for these programs were provided by NASA through a grant from the Space Telescope Science Institute, which is operated by the Association of Universities for Research in Astronomy, Inc., under NASA contract NAS 5-26555. We acknowledge that this project has benefited from contributions by T. Dupuy, J. Faherty, M. Ireland and M. Liu who were co-investigators and helped develop the original HST proposals, GO 11631 and GO 11666. They provided proprietary information on target selection

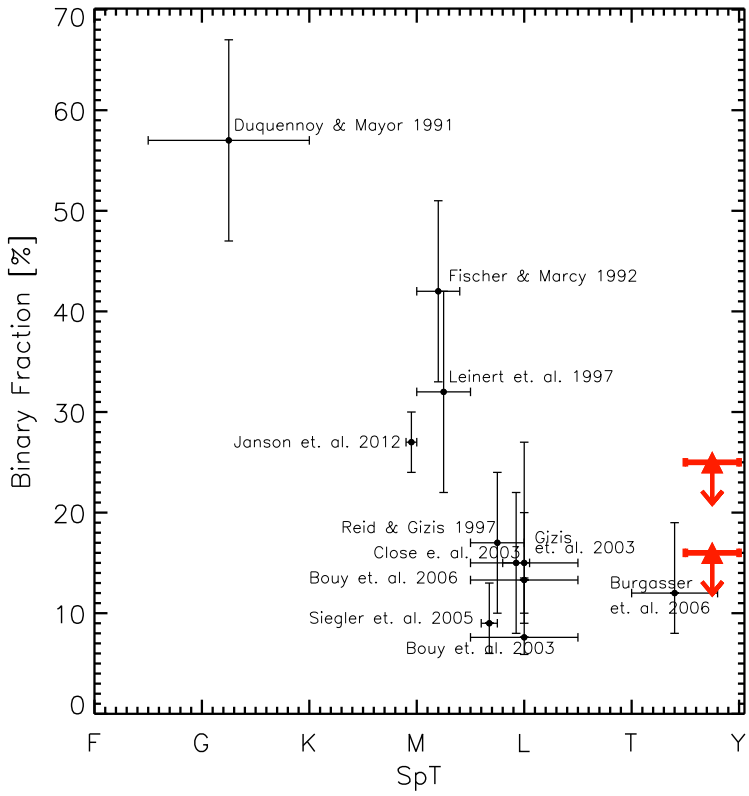

Figure 6.9: Binary frequency as a function of the spectral type in the field and in clusters. The upper limits determined in this work are shown with red triangles.

based on ongoing surveys with ground-based laser guide-star adaptive optics (Liu, Dupuy, and Ireland) and astrometry (J. Faherty). This research has made possible thanks to an international grant from the Spanish Industry Ministry. This research has been supported by the Spanish Virtual Observatory (http://svo.cab.inta-csic.es), project funded by MICINN / MINECO through grants AyA2008-02156, AyA2011-24052. This research has benefitted from the M, L, T, and Y dwarf compendium housed at DwarfArchives.org and has benefitted from the SpeX Prism Spectral Libraries, maintained by Adam Burgasser at http://pono.ucsd.edu/ adam/browndwarfs/spexprism. Special thanks to Daniella Bardalez Gagliuffi, Juan Carlos Muñoz, Julia Alfonso Garzón and Benjamin Montesinos.

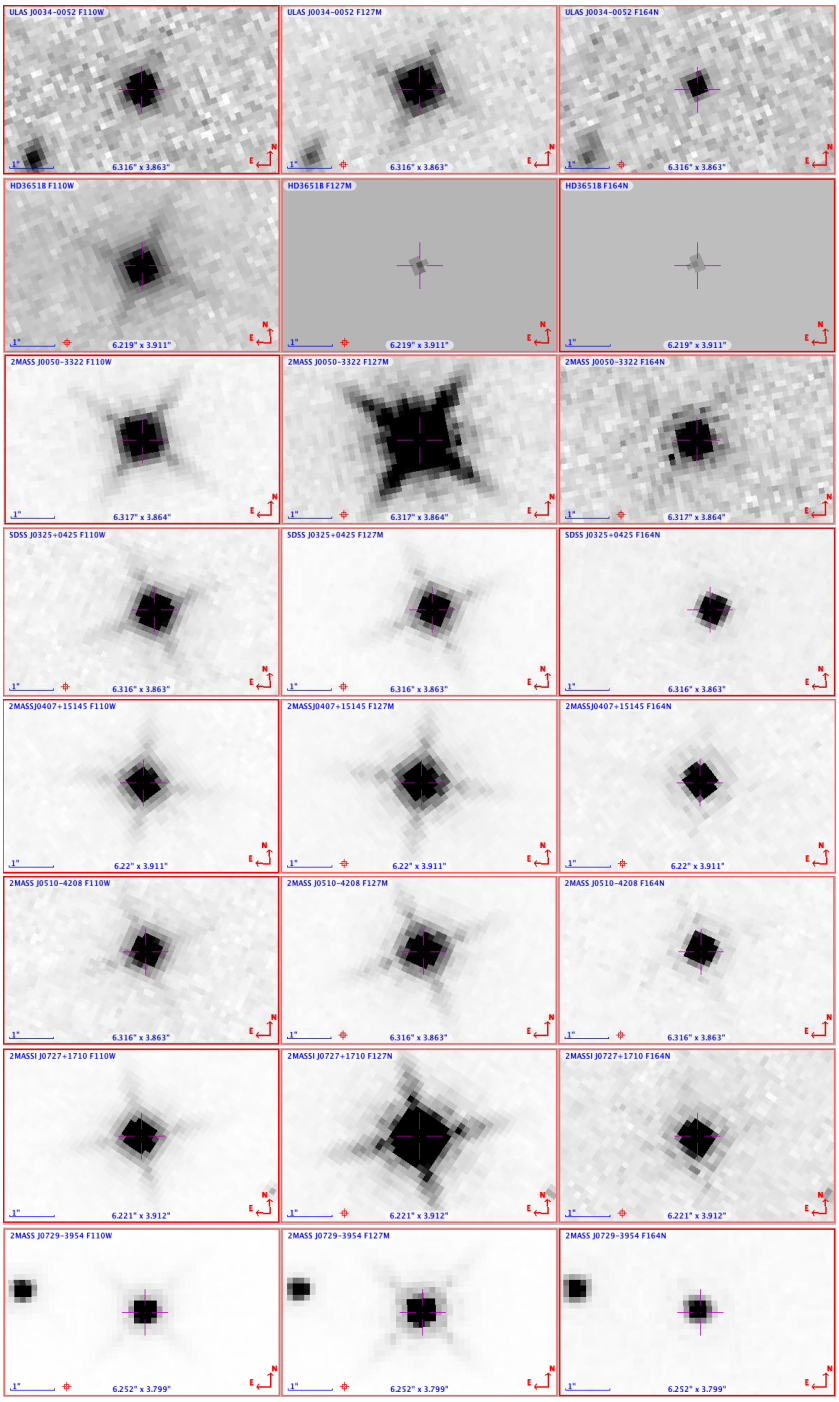

Figure 6.10: WFC3 F110W (lelf), F127M (center) and F164N (right) images of mid-late T dwarfs observed in 11666 program. All images are centered at the target with North up and East to the lelf. Image scales are indicated.

Table 6.7: Companion detectability with WFC3.

Name	SpT	Distance (pc)	Power-Law q Lognormal a	Power-law q Flat a	Flat q Lognormal a	Flat q Flat a
(1)	(2)	(3)	(4)	(5)	(6)	(7)
ULAS J0034−0052	T8.5	12.6±0.6	82%	84%	60%	61%
HD 3651B	T7.5	11.0±0.1	74%	74%	45%	45%
2MASS J0050−3322	T7.0	8.00±1.0	80%	81%	51%	52%
SDSS J0325+0425	T5.5	19.0±2.0	69%	75%	44%	47%
2MASS J0407+1514	T5.0	17.0±2.0	83%	86%	60%	63%
2MASS J0510−4208	T5.0	18.0±2.0	72%	79%	46%	51%
2MASSI J0727+1710	T7.0	9.10±0.2	88%	88%	62%	62%
2MASS J0729−3954	T8.0	6.00±1.0	94%	93%	76%	76%
2MASS J0741+2351	T5.0	18.0±2.0	75%	80%	50%	52%
2MASS J0939−2448	T8.0	10.0±2.0	82%	82%	56%	56%
2MASS J1007−4555	T5.0	15.0±2.0	77%	80%	51%	53%
2MASS J1114−2618	T7.5	10.0±2.0	83%	83%	57%	56%
2MASS J1231+0847	T5.5	12.0±1.0	76%	78%	48%	48%
ULAS J1238+0953	T8.5	18.5±4.3	70%	77%	47%	53%
SDSSP J1346−0031	T6.5	14.5±0.5	82%	87%	59%	63%
SDSS J1504+1027	T7.0	15.9±2.5	69%	75%	42%	46%
SDSS J1628+2308	T7.0	14.0±4.0	78%	82%	52%	56%
2MASS J1754+1649	T5.0	14.3±2.4	74%	77%	46%	48%
SDSS J1758+4633	T6.5	12.0±2.0	76%	77%	48%	48%
2MASS J1828−4849	T5.5	11.0±1.0	69%	73%	40%	43%
2MASS J1901+4718	T5.0	15.0±2.0	75%	80%	48%	52%
SDSS J2124+0100	T5.0	18.0±2.0	74%	79%	50%	52%
2MASS J2154+5942	T5.0	10.0±1.0	86%	86%	60%	61%
2MASS J2237+7228	T6.0	13.0±2.0	79%	82%	51%	55%
2MASS J2331−4718	T5.0	13.0±2.0	78%	81%	50%	52%
2MASS J2359−7335	T6.5	12.3±1.9	79%	80%	51%	52%
Total Expected			20.2	21.0	13.5	14.0
T5+ Dwarf Binary fraction[a]			<17%	<16%	<25%	<23%

[a] with 95% of confidence level.

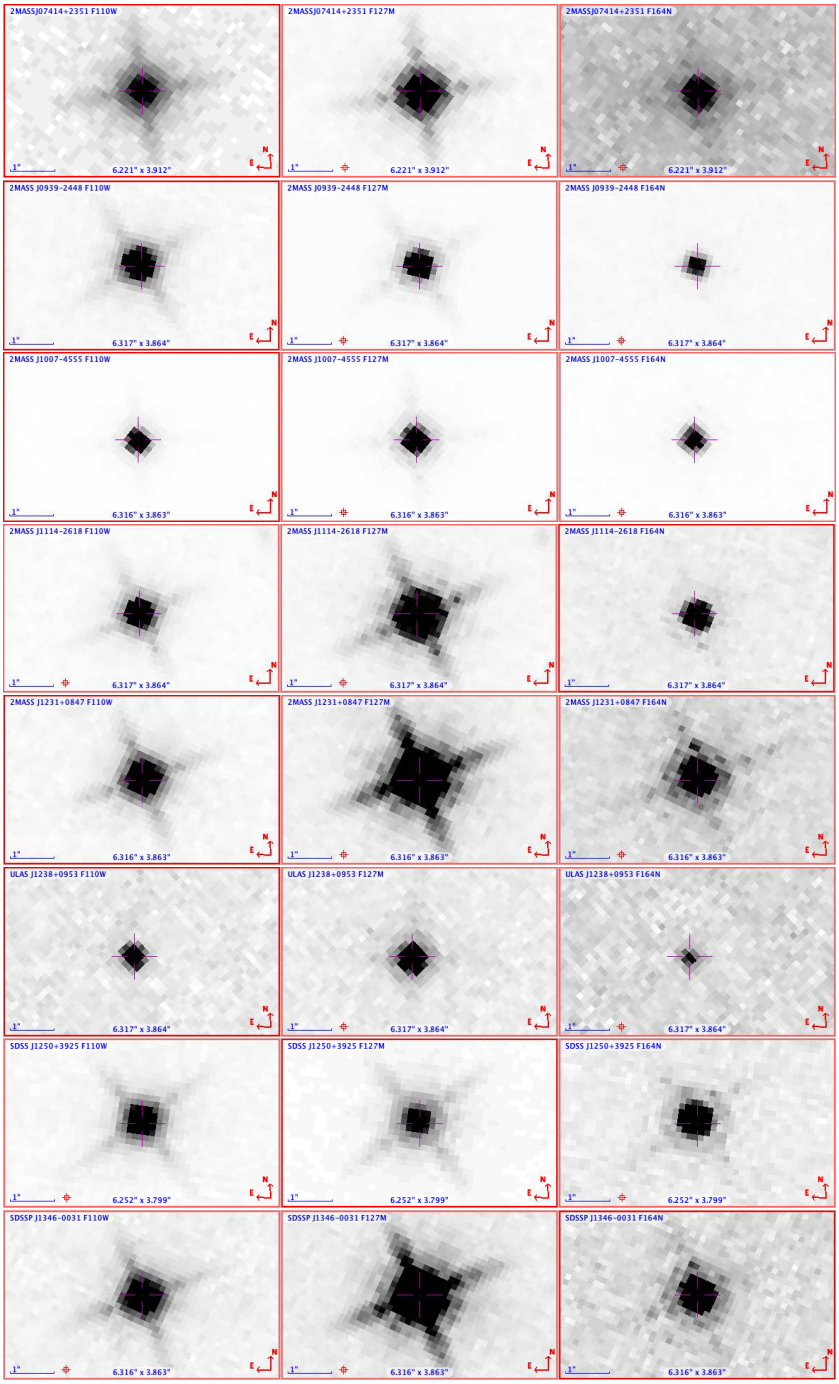

Figure 6.10: Targets of 11666 program (continued).

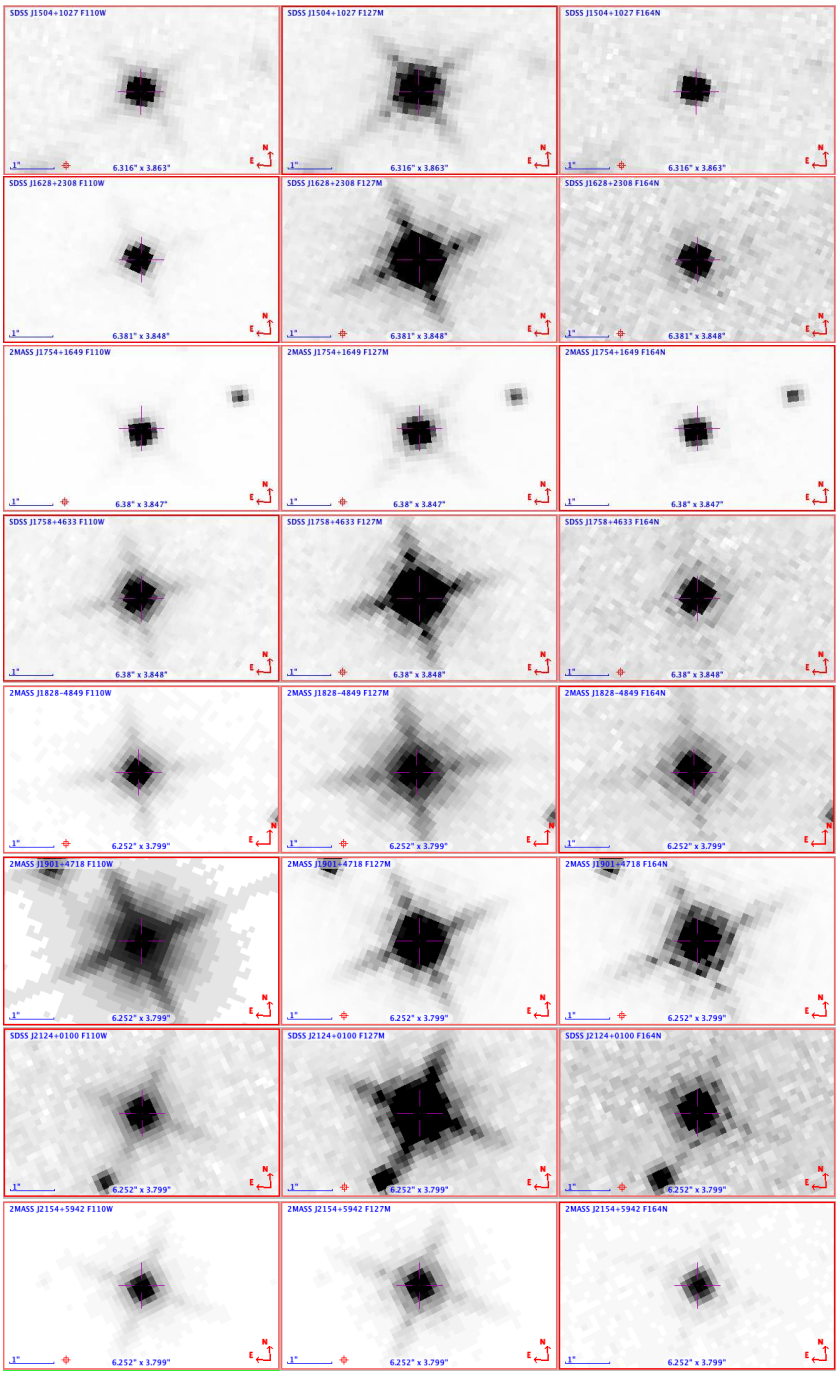

Figure 6.10: Targets of 11666 program (continued).

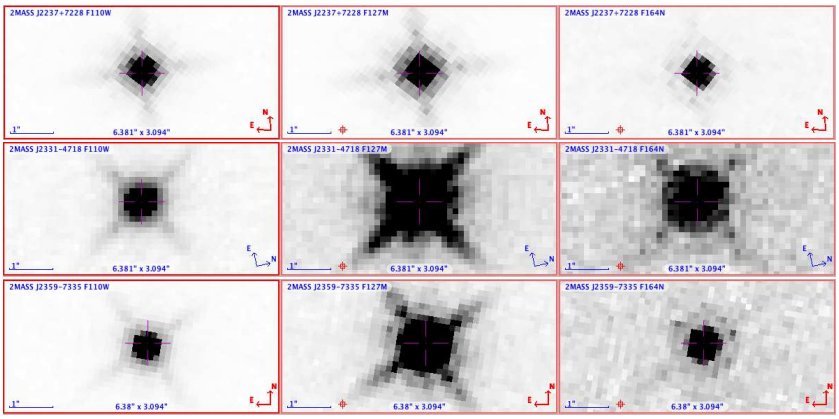

Figure 6.10: Target of 11666 program (continued).

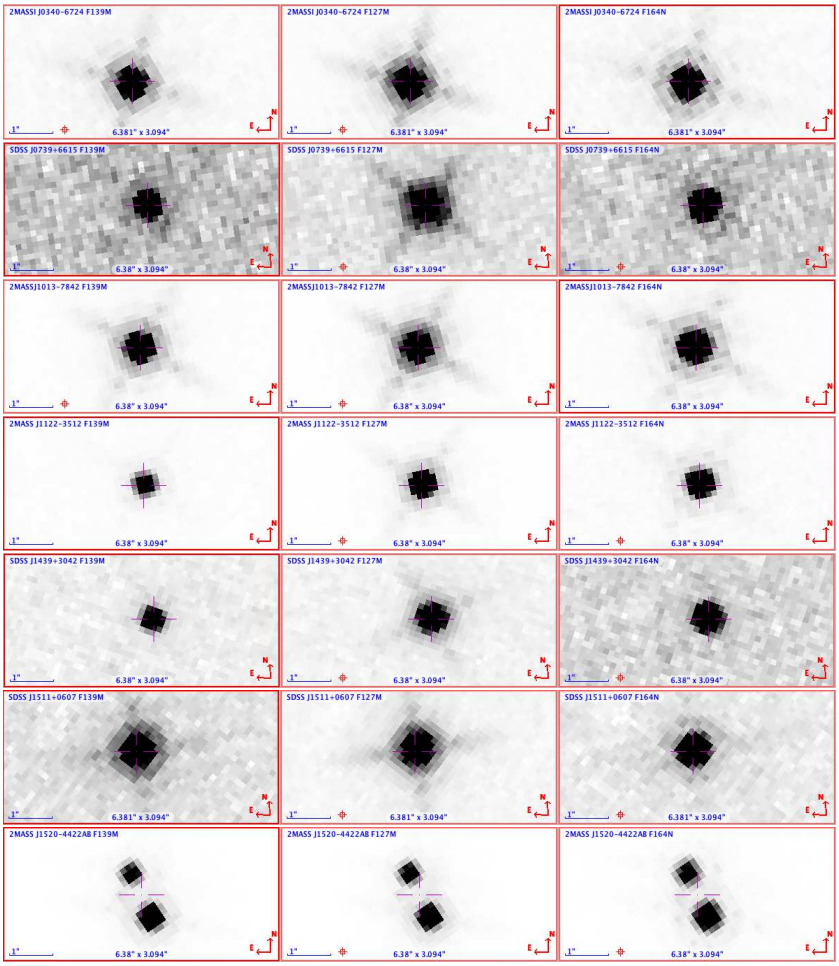

Figure 6.10: WFC3 F139M (left), F127M (center) and F164N (right) images of late L and early T dwarfs observed in 11631 program. All images are centered at the target. Image scale are indicated.

6.8 Appendix A

6.8.1 2MASSJ1520−4422AB

The only well-resolved target in our sample is the previously identified L dwarf binary 2MASS J1520−4422AB, originally reported by Kendall et al. (2007a) and Burgasser et al. (2007a) and found to have an angular separation of 1174±16 mas at position angle **27.°1±0.°7**(east of north; epoch 2006 April 8 UT)[8] and an estimated projected separation of 22±2 AU. Our WFC3 observations yield a separation of 1.20±0.01″ and PA=29.65.°±0.70.°.

The components of this system are classified L1.5 and L4.5 based on NIR spectroscopy, and to date only a combined-light optical spectrum has been reported (Phan-Bao et al., 2008). Because the optical spectra of L dwarfs contain a number of diagnostics of age and mass, including Hα emission at 6563 Å and Li I absorption at 6708 Å, we obtained resolved optical spectroscopy of the system using the Low Dispersion Survey Spectrograph (LDSS-3; Allington-Smith et al. 1994) mounted on the Magellan 6.5m Clay Telescope. Observations were obtained on 2006 May 8 (UT) in clear conditions with moderate seeing (0.″7 at *R*-band). Data acquisition and reduction procedures are identical to those described in Burgasser et al. (2009).

Figure 6.11 displays the reduced red optical spectra of both components, compared to equivalent data for the L1 standard 2MASS J14392836+1929149 (Kirkpatrick et al., 1999) and the L4.5 2MASS J22244381−0158521 (Kirkpatrick et al., 2000). The overall spectral morphologies between the 2MASS J1520−4422AB components and templates are in good agreement, confirming the NIR classifications. Note that the 8521 Å Cs I line in 2MASS J1520-4422B is considerably stronger than the template, which may reflect slight differences in temperature, metallicity or surface gravity.

Importantly, neither component shows evidence of Hα emission or Li I absorption. The latter implies implies individual masses greater than 0.065 $M_\odot$ (Rebolo et al., 1992; Bildsten et al., 1997) and hence a combined system mass greater than 0.13 $M_\odot$. Transforming the measured spectral types into bolometric luminosities using the relation of Burgasser (2007a) and comparing these to the evolutionary models of Burrows et al. (2001), we infer a minimum system age of 0.8–1.1 Gyr for 2MASS J1520−4422AB and a minimum primary mass of 0.07 $M_\odot$ (Figure 6.12). This system appears to be a fairly normal, inactive field binary with component masses around the hydrogen burning mass limit.

[8] In Burgasser et al. (2007a), the position angle of this binary is reported as 152.°1±0.°7, pointing from primary to secondary. However, the authors failed to take into account an image flip in the data, so the actual position angle of the source should have been reported as 27.°1. Our measurement have been also verified in our LDSS3 acquisition images.

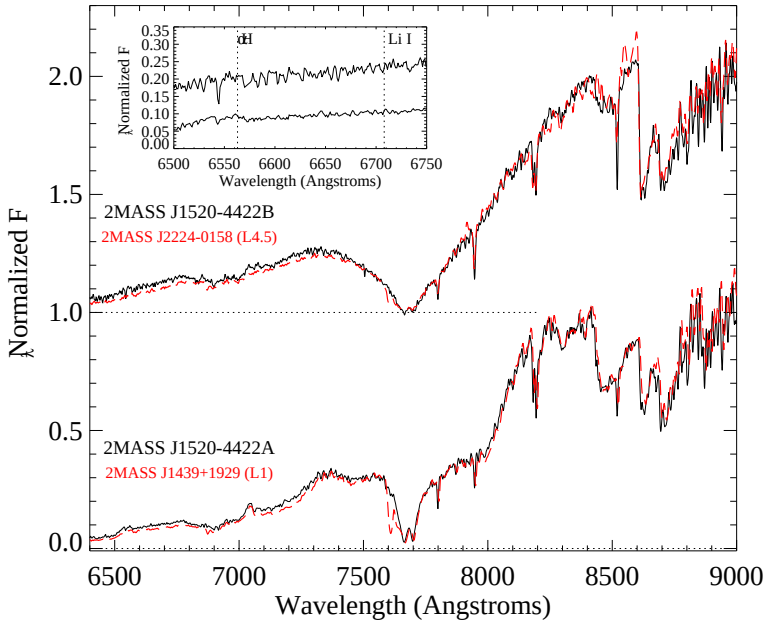

Figure 6.11: Optical spectra of 2MASS J1520−4422AB (solid black lines) compared to the L1 standard 2MASS J14392836+1929149 (Kirkpatrick et al., 1999) and the L4.5 2MASS J22244381−0158521 (Kirkpatrick et al. 2000; red dashed lines). All spectra are gaussian-smoothed to a common resolution of $\lambda/\Delta\lambda$ = 1500 and normalized at 8300 Å, with the L4.5 dwarfs offset by a constant (dotted line). Note that the comparison spectra have not been corrected for telluric absorption (7150–7300 Å; 7600-7650 Å). The inset box highlights the 6500–6750 Å, region revealing no evidence of Hα emission or Li I absorption.

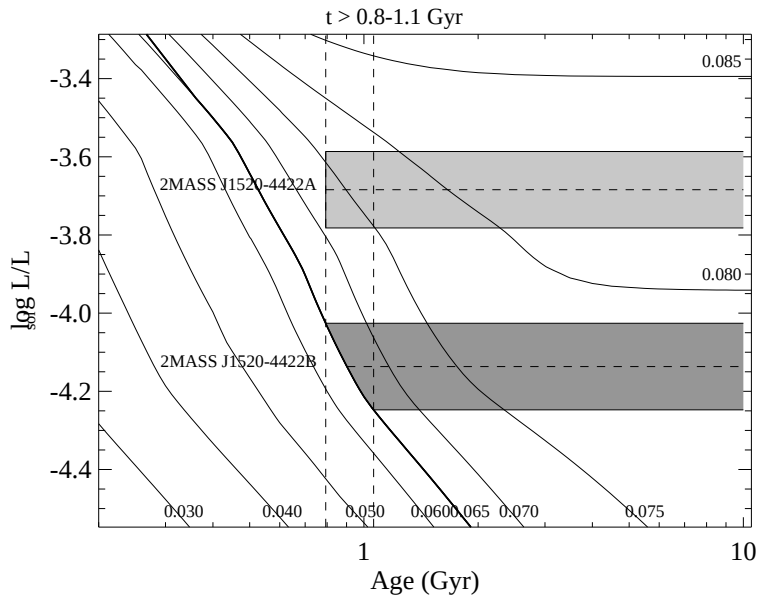

Figure 6.12: Model-dependent age constraints for the 2MASS J1520−4422AB system, based on the absence of Li I absorption in the component spectra. Bolometric luminosities as a function of time are shown for various masses (labeled in units of $M_{\odot}$), based on the models of Burrows et al. (2001). Component luminosities of 2MASS J1520−4422AB (horizontal dashed lines) were estimated from the M_{bol}/SpT relation of Burgasser (2007a) and include uncertainties in that relation and component optical classifications (L1±0.5 and L4.5±0.5; shaded regions). Assuming a minimum mass of 0.065 $M_{\odot}$ for both components (thick mass track), we infer a minimum system age of 0.8–1.1 Gyr.

6.9 Appendix B

6.9.1 DENISJ1013−7842

A new source reported here is DENIS J1013−7842, identified in a search for nearby, young, very low-mass objects in the southern sky with DENIS (Looper et al., in prep.). We obtained an optical spectrum of this source with Magellan/LDSS-3 on 2007 May 8 (UT) in clear conditions with 1.″3 seeing, using the identical configuration as described above but with the slit aligned with the parallactic angle. Two exposures of 1500 s were obtained. The telluric-corrected spectrum is shown in Figure 6.13 and compared to that of the L3 optical standard 2MASSW J1146345+223053 (Kirkpatrick et al., 1999). The spectra are nearly identical from 6300–9000 Å, with the exception of DENIS J1013−7842 having pronounced Hα emission and somewhat weaker TiO absorption at 8500 Å. The Hα emission is particularly strong, with an equivalent width (EW) = 10.3±0.2 Å. Using the χ formalism of Walkowicz et al. (2004) with a χ value computed from Reiners & Basri (2008) assuming T_{eff} = 1950 K (Vrba et al., 2004), we estimate $\log_{10} L_{H\alpha}/L_{bol} = -5.12\pm0.15$ for DENIS J1013−7842, consistent with trends among (rare) active early- and mid-type L dwarfs (Schmidt et al., 2007). The spectrum of this source also shows strong Li I absorption (EW = −5.8±0.2), indicating that it is a brown dwarf with M < 0.065 $M_\odot$ and age $\lesssim$750 Myr (Burrows et al., 2001). There is no evidence of low surface gravity spectral features in this spectrum, however, so this source is likely to be at least 100-300 Myr old (Kirkpatrick et al. 2008; Cruz et al. 2009; Martín et al. 2010).

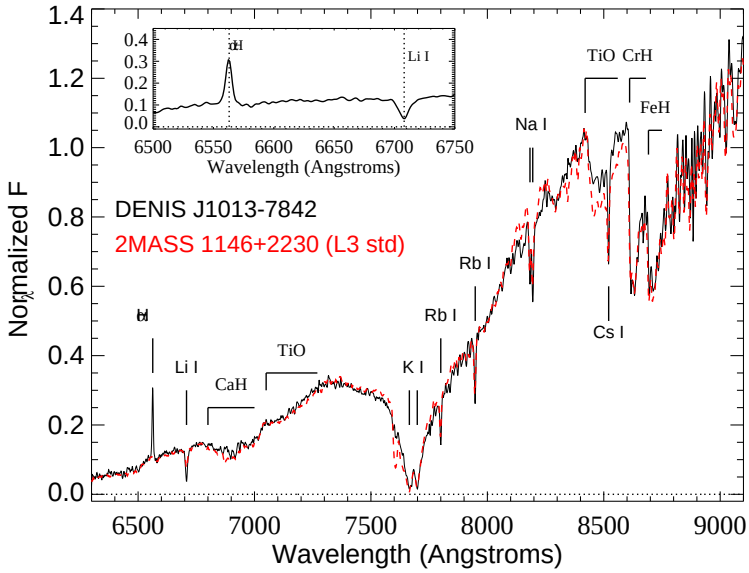

Figure 6.13: Optical spectrum of DENIS J1013−7842 (solid black line) compared to the L3 standard 2MASSW J1146345+223053 (Kirkpatrick et al., 1999). Both spectra are gaussian-smoothed to a common resolution of $\lambda/\Delta\lambda$ = 1500 and normalized at 8400 Å. Note that the comparison spectrum has not been corrected for telluric absorption. The inset box highlights the 6500–6750 Å region showing strong Hα emission and Li I absorption.

6.10 Appendix C

6.10.1 2MASSJ2237+7228

One of our HST targets is the previously unreported T dwarf 2MASS J2237+7228. This source was uncovered by Looper et al. (2007) in a search of the 2MASS survey for mid- and late-type T dwarfs, but at the time of that paper's publication suitable spectral data were unavailable to verify its nature.

Optical spectral data of 2MASS J2237+7228 were obtained with the Subaru 8m Faint Object Camera and Spectrograph (FOCAS) instrument (Kashikawa et al., 2002) on 20 August 2007 (UT) in clear conditions with moderate humidity and light winds. A single 3600 s exposure of the target was obtained with the 0.″5 longslit, 150 line/mm grating blazed at 6500 Å and SO58 order-blocking filter, providing 5860–10270 Å spectroscopy at a resolution $\lambda/\Delta\lambda$ = 400 and dispersion of 1.3 Å/pixel. A standard flux calibrator from Hamuy et al. (1994) was also observed along with flat field and arc lamps. Data were reduced using the FOCAS reduction pipeline in IRAF[9]; no telluric correction was applied to the data. Figure 6.14 displays the reduced spectrum compared to equivalent data for the T6 dwarf SDSSp J162414.37+002915.6 (Strauss et al., 1999; Liebert et al., 2000), which is an excellent match. We therefore nominally assign an optical classification of T6 for this source.

2MASS J2237+7228 is also detected in the WISE survey ($W2$ = 13.62±0.04, $W1-W2$ = 2.06±0.07), and comparison of 2MASS and WISE coordinates separated by over a decade indicates a modest proper motion: $\mu_\alpha \cos\delta = -73\pm2$ mas/yr and $\mu_\delta = -116\pm2$ mas/yr. At the estimated 13±2 pc distance[10] of 2MASSJ2237+7228, this implies a tangential velocity of only 8.3±1.7 km/s, one of the smallest such motions reported for a T dwarf (Faherty et al., 2009).

[9]Image Reduction and Analysis Facility; Tody (1986).

[10]This estimate is based on the 2MASS J-band magnitude of the source (J = 15.76±0.07) and the absolute-magnitude/spectral type relation from Looper et al. (2008), assuming an ±0.5 uncertainty on the subtype.

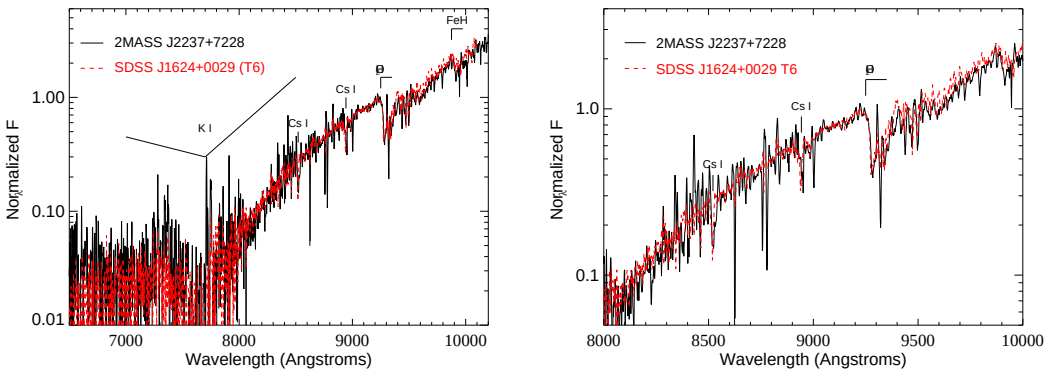

Figure 6.14: Optical spectrum of 2MASS J2237+7228 obtained with Subaru/FOCAS (black line) compared to equivalent data for the T6 spectral standard SDSS J1624+0029 (red line; data from Liebert et al. 2000). Both spectra are normalized at 9500 Å and plotted on a logarithmic vertical scale. Primary absorption features in the red optical spectra of T dwarfs are indicated.

Chapter 7

Conclusions

This chapter summarizes the main findings of this work. As I explain in the Introduction, three VO-projects in the framework of very low-mass stars and brown dwarfs were tackled in this thesis, namely, the search for brown dwarfs using multiwavelenght information from different catalogues (Chapter 4), the search for nearby, bright M dwarfs and their subsequent spectroscopic characterization (Chapter 5), and a study on the binary properties of mid- to late- T dwarfs using HST/WFC3 (Chapter 6).

The main conclusion that can be drawn from these studies is that VO ultimate's goal ("ensure an easy and efficient access and analysis of the information hosted in astronomical archives") has been fully accomplished as the Virtual Observatory has proved to be an excellent research methodology. In particular, it allowed an efficient management of the queries to different catalogues and archives as well as the estimation of physical parameters through VO-tools like VOSA. The main results obtained from this VO analysis are summarized below:

In Aberasturi et al. (2011), we present the identification of 31 BDs (25 known and 6 strong candidates not previously reported in the literature) identified in the sky area in common to the *W*ISE Preliminary Release, the 2MASS Point Source and the SDSS Data Release 7 catalogues. The main conclusions of the Aberasturi et al. (2011) are listed below:

- The number of new candidates is remarkable, considering that 2MASS has been extensively searched for ultracool dwarfs. These results clearly show how new surveys and the use of VO tools can help to mine older surveys: all but one of our BD candidates are very close to the 2MASS limiting magnitude, which puts them beyond the limits of previous, much shallower 2MASS-based BD searches (e.g. J$<$16, Looper et al. 2007).
- Three brown dwarfs were spectroscopically characterized which confirms the robustness of our methodology. WISE J0821+1443 shows strong methane bands, indicating signatures of late-T dwarfs. WISE J0838+1511 was resolved by Radigan et al. (2013) in

three T dwarf components (T3±1, T3±1, and T4.5±1 for the A, B, and C respectively) with high angular resolution images. The system constitutes the first triple T-dwarf system ever reported. Finally, WISE J0920+4538 was confirmed by Mace et al. (2013a), suggesting a L/T dwarf binary system.

- Finally, our work clearly demonstrates the suitability of exploiting *W*ISE data following a VO methodology and increases the expectations of building an accurate census of substellar objects in the solar vicinity. Also remarkable is the fact that the methodology used in this paper is not limited to brown dwarfs but can be easily extrapolated to searches for other rare objects (e.g. high z−quasars)

Aberasturi et al. (2014b) searched for new, bright intermediate M dwarfs in the solar neighborhood using VO tools and the CMC14 and 2MASS catalogues. In this work we combined our VO search with a low-resolution spectroscopic follow-up, an astrometric and photometric study, and an activity analysis (based on our Hα measurements and X-ray emission from public databases) to successfully identify not only potential targets for exoplanet hunting at less than 20 pc, but also to serendipitously discover three young very low-mass stars in the Taurus-Auriga region. The main conclusions and findings of this paper are listed below:

- We showed the potential of the VO for finding new bright nearby M dwarfs, some of which can be targeted by current or forthcoming exoplanet surveys. Actually, 12 of the M dwarfs reported in this paper have been included in the CARMENES input catalogue of M dwarfs (Alonso-Floriano et al. 2015). These objects are: J0012+3028, J0013+2733, J0024+2626, J0058+3919, J0156+3033, J0327+2212, J0507+3730, J0515+2336, J0909+2247, J1547+2241, J2211+4059 y J2248+1819.

- In spite of their relative brightness, (J $<$ 10.2 mag in seven cases and $J < 9.7$ mag in one case), 16 M dwarfs (60 % of our sample of spectroscopically analyzed objects) had escaped previous surveys and are, therefore, discovered and characterized here for the first time. The reason for this is mainly due to the fact that our search is purely photometric, contrary to most searches for M dwarfs based on proper motions. Our work demonstrates that PM surveys might miss nearby dwarfs in the solar neighbourhood (∼20 %).

- Among our 27 M dwarfs, there are two stars at less than 10 pc, for which we recommend measuring their parallaxes: J0122+2209/G 34–53 (M4.0 V, d = 8±2 pc) and J2211+4059/1RXS J221124.3+410000 (M5.5 V, d = 9±2 pc). Besides, there are another five stars at 10–15 pc, four of which are presented here for the first time. The identification of new relatively bright, low-active, single stars much closer to Earth than the median distance to M-dwarf exoplanet-survey targets (>13 pc) is still a matter of interest. In addition, this kind of VO color-based searches may shed light on the complete identification and characterization of all M dwarfs in the 10 pc radius sphere centered on the Sun, until the ESA space mission *G*aia delivers its final catalogue by 2022.

- We reported the discovery of three low proper motion, low surface gravity M dwarfs. One of them, J0422+2439, has a strong Hα (indicative of accretion) and X-ray emission. We assigned membership of J0422+2439 to the Taurus-Auriga star-forming region based not only on low surface gravity and the Hα and X-ray emissions, but also based on coincidence of spatial location, proper motion, and color-magnitude combinations with a large sample of known Taurus-Auriga members. We also assigned membership to this star-forming region of J0435+2523 and J0439+2333, the other two low-gravity stars. The identification of three new intermediate M dwarfs in Taurus-Auriga may help alleviate the reported lack of them, which has made many authors to claim the uniqueness of the initial mass function in Taurus-Auriga.
- We also looked for proper-motion companions to our 27 stars. We recovered a fragile, wide, already known pair and reported and characterized a new pair of an M4.5 V star and an M5.0 V companion separated by 6.5 arcsec ($\sim$110 AU).

Finally, Aberasturi et al. (2014a) attempted to refine the multiplicity properties of T dwarfs studying the largest sample so far (31 objects with spectral types T2-T9) observed with high angular resolution imaging (the previous study was done by Burgasser et al. (2003b) with 23 objects with spectral types T0-T8.5). We undertook two parallel programs using the Wide Field Camara 3 (WFC3) installed on the *H*ubble Space Telescope (*H*ST). The main conclusions from Aberasturi et al. (2014a) are listed below:

- We have analysed data of 34 brown dwarfs obtained in two imaging campaigns with *H*ST/WFC3. The sample comprises 8 L and early-T dwarfs that we have used to study color-color and color-SpT relations, and 26 mid- to late T dwarfs employed in a search for $\geq$T5 dwarf companions. Only one previously identified widely-separated system was recovered: 2MASS J1520-4422AB. PSF-fitting subtraction did not reveal any new close companion to mid-late T sources in our sample. Comparing with previous BD binary surveys made with *H*ST, we can conclude that WFC3 is more sensitive to cool companions than NICMOS and WFPC2 but its lower angular resolution makes it unsuitable to detect tight brown dwarf binary systems.
- Based on Monte Carlo simulations we should have been able to detect faint objects at average separations $\geq$0.325$''$ and with $\Delta m_{F127M} \leq 3.0$. Our failure to detect such companions implies a low binary fraction or a significant population of tight binaries. We determined the fraction of binaries that would have been detected around each source based on assumed separation and mass ratio distributions and all possible orientations of these systems. Since the WFC3 angular resolution separation does not allow us to detect these sources, we infer an upper limit for the binary fraction of $<$16 – $<$25 %, depending of the underlying mass ratio distribution. This binary fraction is consistent with previous works (e.g. Burgasser et al. 2003b; Bate 2012).
- Finally, the paper also includes spectroscopic analyses of the known resolved binary 2MASS J1520$-$4422AB (Burgasser et al. 2007a), and the previously unreported DENIS J1013$-$7842 (L3 dwarf) and 2MASS J2237+7228 (T6 dwarf).

Chapter 8

Future work

In this PhD thesis I have demonstrated the suitability of VO tools to tackle different projects related to low-mass stars and brown dwarfs. The natural follow-up of this work is outlined below:

- **Searching for bright M dwarfs**
  I will continue to search for bright, nearby M dwarfs using VO tools, in particular for potential targets for exoplanet hunting. For that, we will not only plan to conclude the analysis of our CMC14+2MASS data with a new spectroscopic follow-up, but also start a new study with the latest release of the Carlsberg Meridian Catalogue (CMC15[1]), with a larger spatial coverage than CMC14. The multiwavelength correlations (PPMXL, UCAC4, *W*ISE, *G*ALEX, *R*OSAT, VISTA, ...) necessary to properly characterized the new candidates will pave the way for further super-massive correlations when the first *G*aia and EUCLID data releases are available.

- **Searching for brown dwarfs**
  As described in Chapter 3, *W*ISE is an excellent instrument to increase the number of BDs of known types (Kirkpatrick et al. 2011a) and to discover new types (Y dwarfs, Cushing et al. 2011b). In Aberasturi et al. (2014a), we demonstrated the suitability of exploiting *W*ISE data following a VO methodology. It is my aim to follow-up this work using deeper surveys in the infrared (e.g UKIDSS or VISTA)

- **Discovery new tight brown dwarf binary systems**
  In view of the results of Aberasturi et al. (2014a), we concluded that WFC3 is more sensitive to cool companions than NICMOS and WFPC2 but its lower angular resolution makes it poorly suited for typically tight BD binary systems. Our targets cannot be observed with AO techniques because both sub-samples of objects are too faint to serve as a natural guide star and are located in sparse fields without suitable

[1] http://svo2.cab.inta-csic.es/vocats/cmc15/

tip-tilt correction stars. In order to study the sample with higher angular resolution, we will propose to observe again our sample with NICMOS onboard at *HST*.

NASA's next generation successor to the *HST* is The James Webb Space Telescope (*JWST*[2]), which is scheduled to launch in October 2018. The *JWST* will offer unprecedented resolution and sensitivity from long-wavelength visible to the mid-infrared (from 0.6−28.3 μm) in wide fields of view. The telescope will have a 6.5-meter diameter primary mirror and will be located near the L2 point. Due its large collecting area, JWST will reach diffraction limits lower than those provided by HST (Table 8.1) and limiting magnitudes three times higher at 1.6 μm (Figure 8.1). This will allow to discover tighter and fainter BDs binary systems.

Table 8.1: Diffraction limit comparision for *JWST* and *HST*

James Webb 6..5 m		Hubble 2.4 m	
Wavelength λ (nm)	Diffraction limit $''$	Wavelength λ (nm)	Diffraction limit $''$
1.15	0.044	1.10	0.115
1.40	0.054	1.39	0.146
1.62	0.062	1.64	0.172

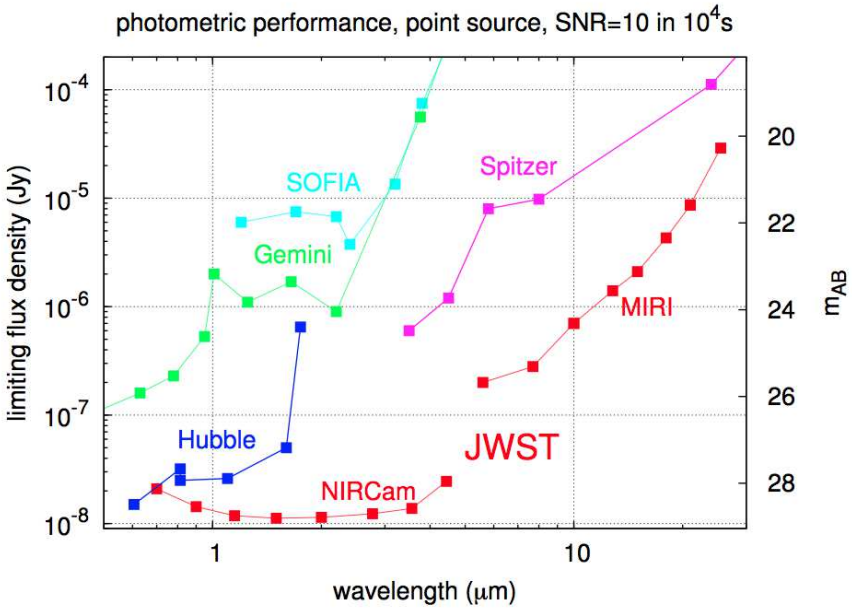

Figure 8.1: *JWST* sensitivity (http://www.stsci.edu/jwst/science/sensitivity)

[2]http://www.stsci.edu/jwst

Chapter 9

Appendix: Collaborations

The experience gained in this thesis on the usage of Virtual Observatory tools for low-mass and brown dwarf studies allowed me to participate as co-author in other similar projects. Among them, I would highlight the following ones:

9.1 Ultracool sudwarfs

Cool subdwarfs are metal-deficient population-II dwarfs that appear less luminous than their solar-metallicity counterparts due to the dearth of metals in their atmospheres (Baraffe et al. 1997). They tend to exhibit halo or thick-disk kinematics, including noticeable proper motion and high heliocentric velocities (Gizis 1997). M-type subdwarfs have typically effective temperatures below $\sim$3500$-$4000 K depending on the metallicity (Baraffe et al. 1997; Woolf et al. 2009; Rajpurohit et al. 2014), and should display high gravity (log$g$ $\sim$ 5.5) although some variations are seen among low-metallicity spectra (Jao et al. 2008). They are classified in three categories: subdwarfs (sdM), extreme subdwarfs (esdM) and ultra-subdwarfs (usdM) with a range of metallicities spanning -0.5 and -1.0, -1.0 and -1.5 and below -1.5, respectively (Gizis 1997; Lépine et al. 2007; Woolf et al. 2009).

Subdwarfs were originally identified from photographic plates at different epochs (e.g. Luyten 1979a; Luyten 1980) but it was not until the advent of the large-scale optical and infrared surveys when the number of these objects significantly increased. Nowadays, we count with $>$ 20 subdwarfs with L spectral type. T subdwarfs have also been discovered showing moderate metallicities ($-$ 0.4 $<$ [M/H] $<$ 0.0; Burgasser 2006) and thin-disc kinematics (e.g Murray et al. 2011; Mace et al. 2013b; Burningham et al. 2014; Pinfield et al. 2014a).

The number of ultracool subdwarfs (subdwarfs with spectral types later than M7) remains, however, very small and is at odds with the numerous L and T dwarfs reported in

the solar neighborhood. Increasing the number of ultracool subdwarfs is essential to study the chemistry in cool atmospheres with low metal content, the role of metallicity in the shape of the IMF (Salpeter 1955; Miller & Scalo 1979; Scalo 1986a), and the impact of chemical composition on the properties of binary stars (Riaz et al. 2008; Jao et al. 2008; Lodieu et al. 2009).

Lodieu et al. (2010)

In this Letter we presented the discovery of the first L subdwarf identified in 234 $\deg^2$ common to the UKIDSS LAS DR2 (Warren et al. 2007a) and the SDSS DR3 (Abazajian et al. 2005). Using different photometric, astrometric and quality flag criteria, we got seven photometric candidates, which only one source, ULAS J135058.86+081506.8 (ULAS1350), showed negative $J - H$ color and optical and near infrared colors similar to the previous known subdwarf, 2MASS J1626 (sdL4; Burgasser 2004a). This source also presented lower proper motion than the other sdLs known until 2010 and also showed fainter J magnitude, suggesting that ULAS1350 lies at larger distance. Also the reduced proper motion was used to help the low-metallicity hypothesis.

ULAS1350 was spectroscopically followed-up with the OSIRIS spectrograph mounted on the Gran Telescopio de Canarias (GTC) telescope. The GTC spectrum confirms the cool and low-luminosity atmosphere of our candidate, for which we determined sdL5$\pm$1 after comparison to the four known bright L subdwarfs. The distance was determined using the absolute magnitude versus spectral type relations given by Cushing et al. (2009) as no L5 subdwarf with known trigonometric parallax exist. A value of 140 pc was adopted. Combining the proper motion and the distance, a tangential velocity of 186 km s^{-1} was derived. This is a value 2$-$4 times larger than the mean values of tangential velocity reported for L dwarfs in the solar neighborhood and quite similar to the tangencial velocities of previously known ultracool subdwarfs indicating that ULAS1350 likely exhibits halo kinematics. A metallicity between [M/H]=$-$0.5 and $-$1.0 was also adopted.

Lodieu et al. (2012b)

In this paper we report the outcome of a photometric and proper motion search of ultracool subdwarfs using large-scale surveys. In particular the UKIDSS Large Area Survey (LAS) Data Release 5 (DR5) and the Sloan Digital Sky Survey (SDSS) Data Release 7 (DR7). This search was complemented by ancillary data from 2MASS, DENIS, and SuperCOSMOS.

Imposing a number of criteria, our search returned a total of 33 ultracool subdwarf candidates. One of them was rejected after visual inspection and only two were recognised as a subdwarf in the literature. Twenty two candidates were followed-up spectroscopically in the optical with the Very Large Telescope and the Nordic Optical Telescope. Spectra from five candidates were extracted from the Sloan spectroscopic database. We confirm nine candidates with spectral types later than M5 as subdwarfs, seven as extreme subdwarfs,

and two ultra-subdwarfs suggesting a fairly quick decrease in the numbers of subdwarfs as a function of metallicity. We also identified two early-L subdwarfs, very likely located within 100 pc, that can be used as templates for future searches.

Spectral types were derived from direct comparison with spectral templates downloaded from the Sloan spectroscopic database. Radial velocities were computed by measuring the shift in wavelength of several resolved lines and by cross-correlating the candidate spectra with a radial velocity standard. Distances were estimated by comparing our candidates with subdwarfs of similar spectral types with known trigonometric parallaxes. Finally, we estimate a lower limit of the surface density of ultracool subdwarfs about 5000−5700 times lower than that of solar-metallicity late-M dwarfs.

9.2 Wide low and very low-mass binary systems.

As I explain in Chapter 3 and Chapter 6, many works have estimated binary fractions and separation distributions for tight (<100 AU) very low-mass star and brown dwarf binary systems (see Table 3.3).

For wide (>100 AU) very low-mass binaries, Burgasser et al. (2009) and Allen (2007) estimated a fraction of VLM wide multiples in the field of no more than 1 %-2 %. These wide binaries, with large separations and low binding energies, have a strong impact on the proposed formation theoretical models. In particular, it challenges the ejection model (Reipurth & Clarke 2001; Bate & Bonnell 2005) since such fragile systems are not expected to survive the ejection process from their birth environments. They also raise some concerns on the disk fragmentation scenario (Padoan & Nordlund 2002) as such wide systems would require the existence of disks of unreasonably mass and size.

Gálvez-Ortiz et al (submitted).

Making use of VO tools, we report the discovery of 47 low-mass (M0−L0), wide (separations between 200 and 92000 AU) candidate binary/multiple systems in the 2MASS Point Source, SDSS DR9, UKIDSS LAS DR10, *W*ISE and GLIMPSE databases.The physical associations are confirmed through common proper motions, distances and low probabilities of chance alignment. This list doubles the previous sampling (∼50) in their mass-separation parameter space. We have also found 52 low-mass objects that we can classify as L0−T2 according to their photometric information. Only one of these objects presents a common proper motion high mass companion. We also found two multiple systems formed only by low and very low-mass components. One with components with M6.0, M7.5 and M8.5 spectral types, and other with components with spectral types M0.5, M7.0 and M8.5.

Chapter 10

Curriculum

Education

Complutense (UCM) and Autónoma University of Madrid (UAM), Spain.

Physics degree, in the Astrophysics branch, September 2000 - June 2007.

Undergraduate final-year research project, January 2007 - June 2007.

- Title: *"Searching for blank regions in the sky for flatfielding."*
- Adviser: Dr. Nicolás Cardiel, UCM.

Master in Astrophysics, September 2007 - June 2008.

Master Thesis Research, October 2008.

- Title: *"Identification and characterization of brown dwarfs using Virtual Observatory tools."*
- Adviser: Dr. Enrique Solano Márquez, head of the Spanish Virtual Observatory.

Professional experience

Grant by the Instituto Nacional de Técnica Aerospacial (INTA) to work in Spanish Virtual Observatory team as scientific collaboration. June 2007- September 2009

Grant by the Spanish Ministry of Science and Innovation (MICINN) to develop a PhD thesis on the identification and characterization of brown dwarfs using Virtual Observatory tools, October 2009 - September 2013.

- Advisers: Dr. Enrique Solano Márquez and Prof. Eduardo Martín.

Grant by MICINN to carry out a stay in UCSD (University of California, San Diego). May 2012 - December 2012

  - Adviser: Dr. Adam Burgasser

Contract by the Instituto Nacional de Técnica Aerospacial (INTA) to work in Spanish Virtual Observatory team as scientific collaboration. March 2014 - December 2014

  - Scientific support to Spanish research groups with interests in the Virtual Observatory field.
  - Implementation of requirements list provided by the Spanish astrophysics community.

Member of the Rosetta Science Ground Segment Centre: Validation & Verification of the Operational Software and Quick Look Data Analysis. European Space Agency Center, ESAC, Madrid . January 2015 - December 2017

Member of the Herschel Community Support Group: Scientific Mission Planning and archival related tasks. European Space Agency Center, ESAC, Madrid. January 2015 - December 2017

Computer Skills

- Astronomical software: Aladin, TOPCAT, STILS, IRAF (long/broad experience in script programming).
- Computer programming: IDL, SExtractor, Phyton, Matlab
- Operating systems: GNU/linux (Ubuntu, Fedora); Microsoft WINDOWS; Macintosh Operating System.
- Office automation: Openoffice (word processing, spreadsheets, presentations), Microsoft Office XP (Word, Excel, PowerPoint).
- Latex language (documentation and presentations).

Astronomy Skills

- Optical spectroscopy.
- Infrared photometry.
- Handling large databases.
- Handling high resolution images.
- PSF modeling and fitting.
- Monte-Carlo simulations.
- Virtual Observatory methodology.
- Statistical Analysis.
- Telescopes observation Logs (operations).

Observing Experience

- Optical spectroscopy at the 2.2m Calar Alto Observatory Telescope (Almería), using CAFOS (Calar Alto Faint Object Spectrograph), November 2009.
- Infrared photometry at the 1.52m Carlos Sánchez Telescopio (Tenerife, Canary Islands), using CAIN III, November 2009.
- Infrared Photometry at the 3.5m Telescopio Nazionale Galileo (La Palma, Canary Islands), using NICS (Near Infrared Camera Spectrometer), October 2011.
- Optical Spectroscopy at the 2.54m Isaac Newton Telescope (La Palma, Canary Islands), using IDS (Intermediate Dispersion Spectrograph), January 2012.
- Hubble Space Telescope Infrared Images. May 2012-Dicember 2013.

Teaching Experience

Teaching Assistant at:

- First Spanish Virtual Observatory (SVO) Workshop, Granada, Spain, October 2009.
- Second Community Feedback Workshop, Strasbourg, France, January 2010
- Second SVO Workshop, La Laguna, Canary Island, Spain, March 2010.
- Third SVO Workshop, Madrid, Spain. June 2010.
- Fourth SVO Workshop, Barcelona, Spain. November 2010.
- RoPACS Madrid, Spain. November 2011.
- Fifth SVO Workshop, Santander, Spain. June 2014.
- Sixth SVO Workshop, Valencia, Spain. July 2014.

Publications

- N. Cardiel and **M. Aberasturi** *"Searching for Good Blank Regions in the Sky for Flatfielding."* 2010, Highlights of Spanish Astrophysics V, 473
- A. Moya; P.J. Amado, D. Barrado; A. García Hernández ; **M. Aberasturi**; B. Montesinos; F. Aceituno *"The planetary system host HR8799: on its λ Bootis nature."* 2010, MNRAS, 406, 566.
- A. Moya; P.J. Amado, D. Barrado; A. García Hernández; **M. Aberasturi**; B. Montesinos; F. Aceituno *"Age determination of the HR8799 planetary system using asteroseismology."* 2010, MNRAS, 405L, 81.
- N. Lodieu; M.R. Zapatero Osorio; E.L. Martín; E. Solano; **M. Aberasturi** *"GTC/OSIRIS Spectroscopic Identification of a Faint L Subdwarf in the UKIRT Infrared Deep Sky Survey."* 2010, ApJ, 708L, 107.

- N. Cardiel; F.M. Jiménez-Esteban; J.M. Alacid; E. Solano; **M. Aberasturi** *"TESELA: a new tool to determine blank fields for astronomical observations."*. 2011, MNRAS, 417, 3061C.
- **M. Aberasturi**; E. Solano and E. Martín *"WISE/2MASS/SDSS Brown Dwarfs candidates using Virtual Observatory tools."*. 2011, A&A, 534L, 7A.
- **M. Aberasturi** and E. Solano, *"The Virtual Observatory in the classroom."* 2011 Highlights of Spanish Astrophysics VI, 797
- **M. Aberasturi**, C. Rodrigo, E. Solano, A. Bayo *"New functionalities of VOSA."* 2011 Highlights of Spanish Astrophysics VI, 523
- N. Lodieu, M. Espinoza, M.R. Zapatero Osorio, E. Solano, **M. Aberasturi** and E.L. Martín *"New ultracool subdwarfs in large-scale surveys: Part I: UKIDSS LAS DR5 vs SDSS DR7."* 2012, A&A, 542, A105
- A. Burgasser, C. Nicholls, and **M. Aberasturi** *"NIR Spectrum of SN 2009ip on 2012 Sep 27.3 Confirms Interpretation as a Type IIn"* The Astronomer's Telegram, 4431, 1
- N. Cardiel, F. Jiménez-Esteban, J. M Alacid, E Solano, E. and **M. Aberasturi**, *"TESELA: A New Virtual Observatory Tool to Determine Blank Fields"* 2012, Astronomical Data Analysis Software and Systems XXI, 461, 173
- G. Olofsson, R. Nilsson, H.-G. Florén, A. Djupvik and **M. Aberasturi** *"Polarimetric coronagraphy of BD + 31° 643 "* 2012, A&A, 544, A43
- **M. Aberasturi**, J.A. Caballero, B. Montesinos, M.C. Gálvez-Ortiz, E. Solano and E.L. Martín.*"Search for bright late-type M dwarfs with Virtual Observatory."* 2013, AJ, 148, 36A
- **M. Aberasturi**, A.J. Burgasser, A. Mora, I.N. Reid, D. Looper, E. Solano and E. Martín. *"Hubble Space Telescope WFC3 Observations of L and T dwarfs."* 2014, AJ, 148, 129A

Papers in Preparation

- M.C. Gálvez-Ortiz, E. Solano, **M. Aberasturi** and N. Lodieu. *"Discovery of wide very low mass binary systems using Virtual Observatory tools."*

Conferences and Schools

- VIII Scientific Meeting of the Spanish Astronomical Society, Santander, Spain, July 2008.
- Virtual Observatory Workshop, Lisbon, Portugal, October 2008.
- Euro-VO Workshop, European Space Astronomy Centre (ESAC), Madrid, Spain, December 2008.
- ASTROCAM School: Young Stellar Objects: From Cool Stars to Exoplanets, El Escorial, Madrid, Spain, July 2009.

- III Robotic Telescopes Meeting, Madrid, Spain, September 2009.
- Recipes for Making Brownies: Theory vs. Observations, European Space Research and Technology Centre (ESTEC), Noordwijk, The Netherlands, September 2009.
- Scientific and technological challenges in the development of astronomical instrumentation: E-ELT & ALMA, Complutense University, Madrid, Spain, September 2009.
- III Consolider-GTC Meeting in Cádiz, Spain, October 2009.
- Gaia: First Scientific Meeting, San Fernando, Cádiz, Spain, June 2010.
- IX Scientific Meeting of the Spanish Astronomical Society, Madrid, Spain, September 2010.
- First VISTA Variables in the Vía Láctea (VVV) Science Meeting, Viña del Mar, Chile, December 2010.
- University of California, San Diego conference *"WISE/2MASS/SDSS Brown Dwarfs candidates using Virtual Observatory tools."* October 2012.

References

ABAZAJIAN, K., ADELMAN-MCCARTHY, J. K., AGÜEROS, M. A., ALLAM, S. S., ANDERSON, K. S. J. ET AL. (2005). The Third Data Release of the Sloan Digital Sky Survey. *AJ*, 129, 1755–1759.

ABAZAJIAN, K. N. ET AL. (2009). The Seventh Data Release of the Sloan Digital Sky Survey. *ApJS*, 182, 543–558.

ABERASTURI, M., BURGASSER, A. J., MORA, A., SOLANO, E., MARTÍN, E. L. ET AL. (2014a). Constraints on the Binary Properties of Mid- to Late T Dwarfs from Hubble Space Telescope WFC3 Observations. *AJ*, 148, 129.

ABERASTURI, M., CABALLERO, J. A., MONTESINOS, B., GÁLVEZ-ORTIZ, M. C., SOLANO, E. ET AL. (2014b). Search for Bright Nearby M Dwarfs with Virtual Observatory Tools. *AJ*, 148, 36.

ABERASTURI, M., SOLANO, E. & MARTÍN, E. L. (2011). WISE/2MASS-SDSS brown dwarfs candidates using Virtual Observatory tools. *A&A*, 534, L7.

ACKERMAN, A. S. & MARLEY, M. S. (2001). Precipitating Condensation Clouds in Substellar Atmospheres. *ApJ*, 556, 872–884.

AHMIC, M., JAYAWARDHANA, R., BRANDEKER, A., SCHOLZ, A., VAN KERKWIJK, M. H. ET AL. (2007). Multiplicity among Young Brown Dwarfs and Very Low Mass Stars. *ApJ*, 671, 2074–2081.

AIHARA, H., ALLENDE PRIETO, C., AN, D., ANDERSON, S. F., AUBOURG, É. ET AL. (2011). The Eighth Data Release of the Sloan Digital Sky Survey: First Data from SDSS-III. *ApJS*, 193, 29.

ALBERT, L., ARTIGAU, É., DELORME, P., REYLÉ, C., FORVEILLE, T. ET AL. (2011). 37 New T-type Brown Dwarfs in the Canada-France Brown Dwarfs Survey. *AJ*, 141, 203.

ALLARD, F. (2014). The BT-Settl Model Atmospheres for Stars, Brown Dwarfs and Planets. In BOOTH, M., MATTHEWS, B. C. & GRAHAM, J. R., eds., IAU Symposium, vol. 299 of *IAU Symposium*. 271–272.

ALLARD, F., HAUSCHILDT, P. H., ALEXANDER, D. R., TAMANAI, A. & SCHWEITZER, A. (2001). The Limiting Effects of Dust in Brown Dwarf Model Atmospheres. *ApJ*, 556, 357–372.

ALLEN, P. R. (2007). Star Formation via the Little Guy: A Bayesian Study of Ultracool Dwarf Imaging Surveys for Companions. *ApJ*, 668, 492–506.

ALLEN, P. R., KOERNER, D. W., REID, I. N. & TRILLING, D. E. (2005). The Substellar Mass Function: A Bayesian Approach. *ApJ*, 625, 385–397.

ALLER, K. M., KRAUS, A. L., LIU, M. C., BURGETT, W. S., CHAMBERS, K. C. ET AL. (2013). A Pan-STARRS + UKIDSS Search for Young, Wide Planetary-mass Companions in Upper Scorpius. *ApJ*, 773, 63.

ALLINGTON-SMITH, J., BREARE, M., ELLIS, R., GELLATLY, D., GLAZEBROOK, K. ET AL. (1994). A low-dispersion survey spectrograph (LDSS-2) for the William Herschel Telescope. *PASP*, 106, 983–991.

ALONSO-FLORIANO, F. J., MORALES, J. C., CABALLERO, J. A., MONTES, D., KLUTSCH, A. ET AL. (2015). CARMENES input catalogue of M dwarfs. I. Low-resolution spectroscopy with CAFOS. *A&A*, 577, A128.

ALVES DE OLIVEIRA, C., MORAUX, E., BOUVIER, J., DUCHÊNE, G., BOUY, H. ET AL. (2013). Spectroscopy of brown dwarf candidates in IC 348 and the determination of its substellar IMF down to planetary masses. *A&A*, 549, A123.

ANGLADA-ESCUDÉ, G., ARRIAGADA, P., VOGT, S. S., RIVERA, E. J., BUTLER, R. P. ET AL. (2012). A Planetary System around the nearby M Dwarf GJ 667C with At Least One Super-Earth in Its Habitable Zone. *ApJ*, 751, L16.

ANGLADA-ESCUDÉ, G. & TUOMI, M. (2012). A planetary system with gas giants and super-Earths around the nearby M dwarf GJ 676A. Optimizing data analysis techniques for the detection of multi-planetary systems. *A&A*, 548, A58.

APPS, K., CLUBB, K. I., FISCHER, D. A., GAIDOS, E., HOWARD, A. ET AL. (2010). M2K: I. A Jupiter-Mass Planet Orbiting the M3V Star HIP 79431. *PASP*, 122, 156–161.

ARTIGAU, É., DONATI, J.-F. & DELFOSSE, X. (2011a). Planet Detection, Magnetic Field of Protostars and Brown Dwarfs Meteorology with SPIRou. In JOHNS-KRULL, C., BROWNING, M. K. & WEST, A. A., eds., 16th Cambridge Workshop on Cool Stars, Stellar Systems, and the Sun, vol. 448 of *Astronomical Society of the Pacific Conference Series*. 771.

ARTIGAU, É., KOUACH, D., DONATI, J.-F., DOYON, R., DELFOSSE, X. ET AL. (2014). SPIRou: the near-infrared spectropolarimeter/high-precision velocimeter for the Canada-France-Hawaii telescope. In Society of Photo-Optical Instrumentation Engineers (SPIE) Conference Series, vol. 9147 of *Society of Photo-Optical Instrumentation Engineers (SPIE) Conference Series*. 15.

ARTIGAU, É., LAFRENIÈRE, D., DOYON, R., ALBERT, L., NADEAU, D. ET AL. (2007). Discovery of the Widest Very Low Mass Binary. *ApJ*, 659, L49–L52.

ARTIGAU, É., LAFRENIÈRE, D., DOYON, R., LIU, M., DUPUY, T. J. ET AL. (2011b). Discovery of Two L and T Binaries with Wide Separations and Peculiar Photometric Properties. *ApJ*, 739, 48.

ATTWOOD, R. E., GOODWIN, S. P., STAMATELLOS, D. & WHITWORTH, A. P. (2009). Simulating star formation in molecular cloud cores. IV. The role of turbulence and thermodynamics. *A&A*, 495, 201–215.

BARAFFE, I., CHABRIER, G., ALLARD, F. & HAUSCHILDT, P. H. (1997). Evolutionary models for metal-poor low-mass stars. Lower main sequence of globular clusters and halo field stars. *A&A*, 327, 1054–1069.

BARAFFE, I., CHABRIER, G., ALLARD, F. & HAUSCHILDT, P. H. (1998). Evolutionary models for solar metallicity low-mass stars: mass-magnitude relationships and color-magnitude diagrams. *A&A*, 337, 403–412.

BARON, F., LAFRENIÈRE, D., ARTIGAU, É., DOYON, R., GAGNÉ, J. ET AL. (2015). Discovery and Characterization of Wide Binary Systems with a Very Low Mass Component. *ApJ*, 802, 37.

BARRADO Y NAVASCUÉS, D., BOUVIER, J., STAUFFER, J. R., LODIEU, N. & MCCAUGHREAN, M. J. (2002). A substellar mass function for Alpha Persei. *A&A*, 395, 813–821.

BARRADO Y NAVASCUÉS, D. & MARTÍN, E. L. (2003). An Empirical Criterion to Classify T Tauri Stars and Substellar Analogs Using Low-Resolution Optical Spectroscopy. *AJ*, 126, 2997–3006.

BARRADO Y NAVASCUÉS, D., STAUFFER, J. R. & JAYAWARDHANA, R. (2004). Spectroscopy of Very Low Mass Stars and Brown Dwarfs in IC 2391: Lithium Depletion and Hα Emission. *ApJ*, 614, 386–397.

BASRI, G. & BROWN, M. E. (2006). Planetesimals to Brown Dwarfs: What is a Planet? *Annual Review of Earth and Planetary Sciences*, 34, 193–216.

BASRI, G., MARCY, G. W. & GRAHAM, J. R. (1996). Lithium in Brown Dwarf Candidates: The Mass and Age of the Faintest Pleiades Stars. *ApJ*, 458, 600–+.

BASRI, G. & MARTÍN, E. L. (1999). PPL 15: The First Brown Dwarf Spectroscopic Binary. *AJ*, 118, 2460–2465.

BASRI, G., MOHANTY, S., ALLARD, F., HAUSCHILDT, P. H., DELFOSSE, X. ET AL. (2000). An Effective Temperature Scale for Late-M and L Dwarfs, from Resonance Absorption Lines of Cs I and Rb I. *ApJ*, 538, 363–385.

BASRI, G. & REINERS, A. (2006). A Survey for Spectroscopic Binaries among Very Low Mass Stars. *AJ*, 132, 663–675.

BASTIAN, N., COVEY, K. R. & MEYER, M. R. (2010). A Universal Stellar Initial Mass Function? A Critical Look at Variations. *ARA&A*, 48, 339–389.

BATALHA, N. M., BORUCKI, W. J., KOCH, D. G., BROWN, T. M., BRYSON, S. T. ET AL. (2010a). Characteristics of the Kepler Target Stars. In American Astronomical Society Meeting Abstracts, vol. 42 of *Bulletin of the American Astronomical Society*. 305.06.

BATALHA, N. M., BORUCKI, W. J., KOCH, D. G., BRYSON, S. T., HAAS, M. R. ET AL. (2010b). Selection, Prioritization, and Characteristics of Kepler Target Stars. *ApJ*, 713, L109–L114.

BATE, M. R. (2009). Stellar, brown dwarf and multiple star properties from hydrodynamical simulations of star cluster formation. *MNRAS*, 392, 590–616.

BATE, M. R. (2012). Stellar, brown dwarf and multiple star properties from a radiation hydrodynamical simulation of star cluster formation. *MNRAS*, 419, 3115–3146.

BATE, M. R. & BONNELL, I. A. (2005). The origin of the initial mass function and its dependence on the mean Jeans mass in molecular clouds. *MNRAS*, 356, 1201–1221.

BATE, M. R., BONNELL, I. A. & BROMM, V. (2002). The formation mechanism of brown dwarfs. *MNRAS*, 332, L65–L68.

BATE, M. R., BONNELL, I. A. & BROMM, V. (2003). The formation of a star cluster: predicting the properties of stars and brown dwarfs. *MNRAS*, 339, 577–599.

BAYO, A., BARRADO, D., STAUFFER, J., MORALES-CALDERÓN, M., MELO, C. ET AL. (2011). Spectroscopy of very low mass stars and brown dwarfs in the Lambda Orionis star forming region. I. Enlarging the census down to the planetary mass domain in Collinder 69. *A&A*, 536, A63.

BAYO, A., RODRIGO, C., BARRADO Y NAVASCUÉS, D., SOLANO, E., GUTIÉRREZ, R. ET AL. (2008). VOSA: virtual observatory SED analyzer. An application to the Collinder 69 open cluster. *A&A*, 492, 277–287.

BEAMÍN, J. C., IVANOV, V. D., BAYO, A., MUŽIĆ, K., BOFFIN, H. M. J. ET AL. (2014). Temperature constraints on the coldest brown dwarf known: WISE 0855-0714. *A&A*, 570, L8.

BEAN, J., SEIFAHRT, A., HARTMAN, H., NILSSON, H., WIEDEMANN, G. ET AL. (2010). The CRIRES Search for Planets at the Bottom of the Main Sequence. *The Messenger*, 140, 41–45.

BECKLIN, E. E. & ZUCKERMAN, B. (1988). A low-temperature companion to a white dwarf star. *Nature*, 336, 656–658.

BEICHMAN, C., GELINO, C. R., KIRKPATRICK, J. D., BARMAN, T. S., MARSH, K. A. ET AL. (2013). The Coldest Brown Dwarf (or Free-floating Planet)?: The Y Dwarf WISE 1828+2650. *ApJ*, 764, 101.

BEICHMAN, C., GELINO, C. R., KIRKPATRICK, J. D., CUSHING, M. C., DODSON-ROBINSON, S. ET AL. (2014). WISE Y Dwarfs as Probes of the Brown Dwarf-Exoplanet Connection. *ApJ*, 783, 68.

BÉJAR, V. J. S., MARTÍN, E. L., ZAPATERO OSORIO, M. R., REBOLO, R., BARRADO Y NAVASCUÉS, D. ET AL. (2001). The Substellar Mass Function in σ Orionis. *ApJ*, 556, 830–836.

BÉJAR, V. J. S., ZAPATERO OSORIO, M. R., PÉREZ-GARRIDO, A., ÁLVAREZ, C., MARTÍN, E. L. ET AL. (2008). Discovery of a Wide Companion near the Deuterium-burning Mass Limit in the Upper Scorpius Association. *ApJ*, 673, L185–L189.

BÉJAR, V. J. S., ZAPATERO OSORIO, M. R. & REBOLO, R. (1999). A Search for Very Low Mass Stars and Brown Dwarfs in the Young sigma Orionis Cluster. *ApJ*, 521, 671–681.

BERGFORS, C., BRANDNER, W., JANSON, M., DAEMGEN, S., GEISSLER, K. ET AL. (2010). Lucky Imaging survey for southern M dwarf binaries. *A&A*, 520, A54.

BERTA, Z. K., IRWIN, J. & CHARBONNEAU, D. (2013). Constraints on Planet Occurrence around Nearby Mid-to-late M Dwarfs from the MEARTH Project. *ApJ*, 775, 91.

BERTA, Z. K., IRWIN, J., CHARBONNEAU, D., BURKE, C. J. & FALCO, E. E. (2012). Transit Detection in the MEarth Survey of Nearby M Dwarfs: Bridging the Clean-first, Search-later Divide. *AJ*, 144, 145.

BERTIN, E. & ARNOUTS, S. (1996). SExtractor: Software for source extraction. *A&AS*, 117, 393–404.

BERTOUT, C. & GENOVA, F. (2006). A kinematic study of the Taurus-Auriga T association. *A&A*, 460, 499–518.

BEST, W. M. J., LIU, M. C., MAGNIER, E. A., ALLER, K. M., DEACON, N. R. ET AL. (2013). A Search for L/T Transition Dwarfs with Pan-STARRS1 and WISE: Discovery of Seven Nearby Objects Including Two Candidate Spectroscopic Variables. *ApJ*, 777, 84.

BIHAIN, G., SCHOLZ, R.-D., STORM, J. & SCHNURR, O. (2013). An overlooked brown dwarf neighbour (T7.5 at d ~ 5 pc) of the Sun and two additional T dwarfs at about 10 pc. *A&A*, 557, A43.

BILDSTEN, L., BROWN, E. F., MATZNER, C. D. & USHOMIRSKY, G. (1997). Lithium Depletion in Fully Convective Pre-Main-Sequence Stars. *ApJ*, 482, 442–+.

BILLER, B., ALLERS, K., LIU, M., CLOSE, L. M. & DUPUY, T. (2011). A Keck LGS AO Search for Brown Dwarf and Planetary Mass Companions to Upper Scorpius Brown Dwarfs. *ApJ*, 730, 39.

BILLER, B. A., KASPER, M., CLOSE, L. M., BRANDNER, W. & KELLNER, S. (2006). Discovery of a Brown Dwarf Very Close to the Sun: A Methane-rich Brown Dwarf Companion to the Low-Mass Star SCR 1845-6357. *ApJ*, 641, L141–L144.

BILLÈRES, M., DELFOSSE, X., BEUZIT, J.-L., FORVEILLE, T., MARCHAL, L. ET AL. (2005). The first wide ultracool binary dwarf in the field: DENIS-J055146.0-443412.2 (M8.5 + L0). *A&A*, 440, L55–L58.

BLAKE, C. H., CHARBONNEAU, D. & WHITE, R. J. (2010). The NIRSPEC Ultracool Dwarf Radial Velocity Survey. *ApJ*, 723, 684–706.

BOCHANSKI, J. J., HAWLEY, S. L., COVEY, K. R., WEST, A. A., REID, I. N. ET AL. (2010). The Luminosity and Mass Functions of Low-mass Stars in the Galactic Disk. II. The Field. *AJ*, 139, 2679.

BOCHANSKI, J. J., HAWLEY, S. L. & WEST, A. A. (2011). The Sloan Digital Sky Survey Data Release 7 Spectroscopic M Dwarf Catalog. II. Statistical Parallax Analysis. *AJ*, 141, 98.

BONFILS, X., DELFOSSE, X., UDRY, S., FORVEILLE, T., MAYOR, M. ET AL. (2013a). The HARPS search for southern extra-solar planets. XXXI. The M-dwarf sample. *A&A*, 549, A109.

BONFILS, X., GILLON, M., FORVEILLE, T., DELFOSSE, X., DEMING, D. ET AL. (2011). A short-period super-Earth orbiting the M2.5 dwarf GJ 3634. Detection with HARPS velocimetry and transit search with Spitzer photometry. *A&A*, 528, A111.

BONFILS, X., LO CURTO, G., CORREIA, A. C. M., LASKAR, J., UDRY, S. ET AL. (2013b). The HARPS search for southern extra-solar planets. XXXIV. A planetary system around the nearby M dwarf <ASTROBJ>GJ 163</ASTROBJ>, with a super-Earth possibly in the habitable zone. *A&A*, 556, A110.

BONNAREL, F., FERNIQUE, P., BIENAYMÉ, O., EGRET, D., GENOVA, F. ET AL. (2000). The ALADIN interactive sky atlas. A reference tool for identification of astronomical sources. *A&AS*, 143, 33–40.

BONNELL, I. A., CLARK, P. & BATE, M. R. (2008). Gravitational fragmentation and the formation of brown dwarfs in stellar clusters. *MNRAS*, 389, 1556–1562.

BORYSOW, A., JORGENSEN, U. G. & ZHENG, C. (1997). Model atmospheres of cool, low-metallicity stars: the importance of collision-induced absorption. *A&A*, 324, 185–195.

BOSS, A. P. (2001). Formation of Planetary-Mass Objects by Protostellar Collapse and Fragmentation. *ApJ*, 551, L167–L170.

BOUVIER, J., STAUFFER, J. R., MARTIN, E. L., BARRADO Y NAVASCUES, D., WALLACE, B. ET AL. (1998). Brown dwarfs and very low-mass stars in the Pleiades cluster: a deep wide-field imaging survey. *A&A*, 336, 490–502.

BOUY, H., BRANDNER, W., MARTÍN, E. L., DELFOSSE, X., ALLARD, F. ET AL. (2003). Multiplicity of Nearby Free-Floating Ultracool Dwarfs: A Hubble Space Telescope WFPC2 Search for Companions. *AJ*, 126, 1526–1554.

BOUY, H., BRANDNER, W., MARTÍN, E. L., DELFOSSE, X., ALLARD, F. ET AL. (2004a). A young binary brown dwarf in the R-CrA star formation region. *A&A*, 424, 213–226.

BOUY, H., DUCHÊNE, G., KÖHLER, R., BRANDNER, W., BOUVIER, J. ET AL. (2004b). First determination of the dynamical mass of a binary L dwarf. *A&A*, 423, 341–352.

BOUY, H., MARTÍN, E. L., BRANDNER, W., ZAPATERO-OSORIO, M. R., BÉJAR, V. J. S. ET AL. (2006a). Multiplicity of very low-mass objects in the Upper Scorpius OB association: a possible wide binary population. *A&A*, 451, 177–186.

BOUY, H., MORAUX, E., BOUVIER, J., BRANDNER, W., MARTÍN, E. L. ET AL. (2006b). A Hubble Space Telescope Advanced Camera for Surveys Search for Brown Dwarf Binaries in the Pleiades Open Cluster. *ApJ*, 637, 1056–1066.

BRICEÑO, C., HARTMANN, L., STAUFFER, J. & MARTÍN, E. (1998). A Search for Very Low Mass Pre-Main-Sequence Stars in Taurus. *AJ*, 115, 2074–2091.

BRICEÑO, C., LUHMAN, K. L., HARTMANN, L., STAUFFER, J. R. & KIRKPATRICK, J. D. (2002). The Initial Mass Function in the Taurus Star-forming Region. *ApJ*, 580, 317–335.

BROWNING, M. K. (2008). Simulations of Dynamo Action in Fully Convective Stars. *ApJ*, 676, 1262–1280.

BROWNING, M. K., BASRI, G., MARCY, G. W., WEST, A. A. & ZHANG, J. (2010). Rotation and Magnetic Activity in a Sample of M-Dwarfs. *AJ*, 139, 504–518.

BURGASSER, A. J. (2004a). Discovery of a Second L Subdwarf in the Two Micron All Sky Survey. *ApJ*, 614, L73–L76.

BURGASSER, A. J. (2004b). T Dwarfs and the Substellar Mass Function. I. Monte Carlo Simulations. *ApJS*, 155, 191–207.

BURGASSER, A. J. (2006). Spitzer Studies of Ultracool Subdwarfs: Metal-poor Late-type M, L and T Dwarfs. In ARMUS, L. & REACH, W. T., eds., Astronomical Society of the Pacific Conference Series, vol. 357 of *Astronomical Society of the Pacific Conference Series*. 62–+.

BURGASSER, A. J. (2007a). Binaries and the L Dwarf/T Dwarf Transition. *ApJ*, 659, 655–674.

BURGASSER, A. J. (2007b). SDSS J080531.84+481233.0: An Unresolved L Dwarf/T Dwarf Binary. *AJ*, 134, 1330–1336.

BURGASSER, A. J., BARDALEZ-GAGLIUFFI, D. C. & GIZIS, J. E. (2011a). Hubble Space Telescope Imaging and Spectral Analysis of Two Brown Dwarf Binaries at the L Dwarf/T Dwarf Transition. *AJ*, 141, 70–+.

BURGASSER, A. J. & BLAKE, C. H. (2009). An Age Constraint for the Very Low Mass Stellar/Brown Dwarf Binary 2MASS J03202839. *AJ*, 137, 4621–4626.

BURGASSER, A. J., CRUZ, K. L., CUSHING, M., GELINO, C. R., LOOPER, D. L. ET AL. (2010). SpeX Spectroscopy of Unresolved Very Low Mass Binaries. I. Identification of 17 Candidate Binaries Straddling the L Dwarf/T Dwarf Transition. *ApJ*, 710, 1142–1169.

BURGASSER, A. J., CUSHING, M. C., KIRKPATRICK, J. D., GELINO, C. R., GRIFFITH, R. L. ET AL. (2011b). Fire Spectroscopy of Five Late-type T Dwarfs Discovered with the Wide-field Infrared Survey Explorer. *ApJ*, 735, 116.

BURGASSER, A. J., DHITAL, S. & WEST, A. A. (2009). Resolved Spectroscopy of M Dwarf/L Dwarf Binaries. III. The "Wide" L3.5/L4 Dwarf Binary 2Mass J15500845+1455180AB. *AJ*, 138, 1563–1569.

BURGASSER, A. J., GEBALLE, T. R., LEGGETT, S. K., KIRKPATRICK, J. D. & GOLIMOWSKI, D. A. (2006a). A Unified Near-Infrared Spectral Classification Scheme for T Dwarfs. *ApJ*, 637, 1067–1093.

BURGASSER, A. J., GELINO, C. R., CUSHING, M. C. & KIRKPATRICK, J. D. (2012). Resolved Spectroscopy of a Brown Dwarf Binary at the T Dwarf/Y Dwarf Transition. *ApJ*, 745, 26.

BURGASSER, A. J., GILLON, M., MELIS, C., BOWLER, B. P., MICHELSEN, E. L. ET AL. (2015). WISE J072003.20-084651.2: an Old and Active M9.5 + T5 Spectral Binary 6 pc from the Sun. *AJ*, 149, 104.

BURGASSER, A. J., KIRKPATRICK, J. D., BROWN, M. E., REID, I. N., BURROWS, A. ET AL. (2002a). The Spectra of T Dwarfs. I. Near-Infrared Data and Spectral Classification. *ApJ*, 564, 421–451.

BURGASSER, A. J., KIRKPATRICK, J. D., CRUZ, K. L., REID, I. N., LEGGETT, S. K. ET AL. (2006b). Hubble Space Telescope NICMOS Observations of T Dwarfs: Brown Dwarf Multiplicity and New Probes of the L/T Transition. *ApJS*, 166, 585–612.

BURGASSER, A. J., KIRKPATRICK, J. D., LIEBERT, J. & BURROWS, A. (2003a). The Spectra of T Dwarfs. II. Red Optical Data. *ApJ*, 594, 510–524.

BURGASSER, A. J., KIRKPATRICK, J. D. & LOWRANCE, P. J. (2005a). Multiplicity among Widely Separated Brown Dwarf Companions to Nearby Stars: Gliese 337CD. *AJ*, 129, 2849–2855.

BURGASSER, A. J., KIRKPATRICK, J. D., REID, I. N., BROWN, M. E., MISKEY, C. L. ET AL. (2003b). Binarity in Brown Dwarfs: T Dwarf Binaries Discovered with the Hubble Space Telescope Wide Field Planetary Camera 2. *ApJ*, 586, 512–526.

BURGASSER, A. J., LOOPER, D. L., KIRKPATRICK, J. D. & LIU, M. C. (2007a). Discovery of a High Proper Motion L Dwarf Binary: 2MASS J15200224-4422419AB. *ApJ*, 658, 557–568.

BURGASSER, A. J., MARLEY, M. S., ACKERMAN, A. S., SAUMON, D., LODDERS, K. ET AL. (2002b). Evidence of Cloud Disruption in the L/T Dwarf Transition. *ApJ*, 571, L151–L154.

BURGASSER, A. J. & MCELWAIN, M. W. (2006). Resolved Spectroscopy of M Dwarf/L Dwarf Binaries. I. DENIS J220002.05-303832.9AB. *AJ*, 131, 1007–1014.

BURGASSER, A. J., MCELWAIN, M. W., KIRKPATRICK, J. D., CRUZ, K. L., TINNEY, C. G. ET AL. (2004). The 2MASS Wide-Field T Dwarf Search. III. Seven New T Dwarfs and Other Cool Dwarf Discoveries. *AJ*, 127, 2856–2870.

BURGASSER, A. J., REID, I. N., LEGGETT, S. K., KIRKPATRICK, J. D., LIEBERT, J. ET AL. (2005b). SDSS J042348.57-041403.5AB: A Brown Dwarf Binary Straddling the L/T Transition. *ApJ*, 634, L177–L180.

BURGASSER, A. J., REID, I. N., SIEGLER, N., CLOSE, L., ALLEN, P. ET AL. (2007b). Not Alone: Tracing the Origins of Very-Low-Mass Stars and Brown Dwarfs Through Multiplicity Studies. *Protostars and Planets V*, 427–441.

BURGASSER, A. J., SHEPPARD, S. S. & LUHMAN, K. L. (2013). Resolved Near-infrared Spectroscopy of WISE J104915.57-531906.1AB: A Flux-reversal Binary at the L dwarf/T Dwarf Transition. *ApJ*, 772, 129.

BURNINGHAM, B., CARDOSO, C. V., SMITH, L., LEGGETT, S. K., SMART, R. L. ET AL. (2013). 76 T dwarfs from the UKIDSS LAS: benchmarks, kinematics and an updated space density. *MNRAS*, 433, 457–497.

BURNINGHAM, B., LEGGETT, S. K., LUCAS, P. W., PINFIELD, D. J., SMART, R. L. ET AL. (2010a). The discovery of a very cool binary system. *MNRAS*, 404, 1952–1961.

BURNINGHAM, B., LUCAS, P. W., LEGGETT, S. K., SMART, R., BAKER, D. ET AL. (2011). The discovery of the T8.5 dwarf UGPS J0521+3640. *MNRAS*, 414, L90–L94.

BURNINGHAM, B., NAYLOR, T., LITTLEFAIR, S. P. & JEFFRIES, R. D. (2005). Contamination and exclusion in the σ Orionis young group. *MNRAS*, 356, 1583–1591.

BURNINGHAM, B., PINFIELD, D. J., LUCAS, P. W., LEGGETT, S. K., DEACON, N. R. ET AL. (2010b). 47 new T dwarfs from the UKIDSS Large Area Survey. *MNRAS*, 406, 1885–1906.

BURNINGHAM, B., SMITH, L., CARDOSO, C. V., LUCAS, P. W., BURGASSER, A. J. ET AL. (2014). The discovery of a T6.5 subdwarf. *MNRAS*, 440, 359–364.

BURNINGHAM, B. ET AL. (2008). Exploring the substellar temperature regime down to ˜550K. *MNRAS*, 391, 320–333.

BURROWS, A., HUBBARD, W. B., LUNINE, J. I. & LIEBERT, J. (2001). The theory of brown dwarfs and extrasolar giant planets. *Reviews of Modern Physics*, 73, 719–765.

BURROWS, A., SUDARSKY, D. & LUNINE, J. I. (2003). Beyond the T Dwarfs: Theoretical Spectra, Colors, and Detectability of the Coolest Brown Dwarfs. *ApJ*, 596, 587–596.

CABALLERO, J. A. (2007a). Southern Very Low Mass Stars and Brown Dwarfs in Wide Binary and Multiple Systems. *ApJ*, 667, 520–526.

CABALLERO, J. A. (2007b). The widest ultracool binary. *A&A*, 462, L61–L64.

CABALLERO, J. A. (2007c). The widest ultracool binary. *A&A*, 462, L61–L64.

CABALLERO, J. A. (2009). From 1000 AU to 1000 pc: high proper-motion stars in the solar neighbourhood radio sources in the sigma Orionis cluster, and new X-ray stars surrounding Alnilam. In BAINES, D. & OSUNA, P., eds., Multi-wavelength Astronomy and Virtual Observatory. 3.

CABALLERO, J. A. (2012). Cool dwarfs in wide multiple systems. Paper 1: Two mid-M dwarfs in a loosely-bound common-proper-motion pair. *The Observatory*, 132, 1–7.

CABALLERO, J. A., ALBACETE-COLOMBO, J. F. & LÓPEZ-SANTIAGO, J. (2010). HRC-I/Chandra X-ray observations towards σ Orionis. *A&A*, 521, A45.

CABALLERO, J. A., BÉJAR, V. J. S., REBOLO, R., EISLÖFFEL, J., ZAPATERO OSORIO, M. R. ET AL. (2007). The substellar mass function in σ Orionis. II. Optical, near-infrared and IRAC/Spitzer photometry of young cluster brown dwarfs and planetary-mass objects. *A&A*, 470, 903–918.

CABALLERO, J. A., BURGASSER, A. J. & KLEMENT, R. (2008). Contamination by field late-M, L, and T dwarfs in deep surveys. *A&A*, 488, 181–190.

CABALLERO, J. A., CORTÉS-CONTRERAS, M., ALONSO-FLORIANO, F. J., LÓPEZ-SANTIAGO, J., KLUTSCH, A. ET AL. (2013). CARMENES at PPVI. CARMENCITA Herbs and Spices to Help you Prepare a Genuine Target Sample. In Protostars and Planets VI, Heidelberg, July 15-20, 2013. Poster #2K020. 20.

CHABRIER, G. (2001). The Galactic Disk Mass Budget. I. Stellar Mass Function and Density. *ApJ*, 554, 1274–1281.

CHABRIER, G. (2002). The Galactic Disk Mass Budget. II. Brown Dwarf Mass Function and Density. *ApJ*, 567, 304–313.

CHABRIER, G. (2003). Galactic Stellar and Substellar Initial Mass Function. *PASP*, 115, 763–795.

CHABRIER, G. & BARAFFE, I. (2000). Theory of Low-Mass Stars and Substellar Objects. *ARA&A*, 38, 337–377.

CHABRIER, G., BARAFFE, I., ALLARD, F. & HAUSCHILDT, P. (2000a). Deuterium Burning in Substellar Objects. *ApJ*, 542, L119–L122.

CHABRIER, G., BARAFFE, I., ALLARD, F. & HAUSCHILDT, P. (2000b). Evolutionary Models for Very Low-Mass Stars and Brown Dwarfs with Dusty Atmospheres. *ApJ*, 542, 464–472.

CHABRIER, G., JOHANSEN, A., JANSON, M. & RAFIKOV, R. (2014). Giant Planet and Brown Dwarf Formation. *Protostars and Planets VI*, 619–642.

CHARBONNEAU, D., BERTA, Z. K., IRWIN, J., BURKE, C. J., NUTZMAN, P. ET AL. (2009). A super-Earth transiting a nearby low-mass star. *Nature*, 462, 891–894.

CHAUVIN, G., LAGRANGE, A.-M., BONAVITA, M., ZUCKERMAN, B., DUMAS, C. ET AL. (2010). Deep imaging survey of young, nearby austral stars . VLT/NACO near-infrared Lyot-coronographic observations. *A&A*, 509, A52.

CHAUVIN, G., LAGRANGE, A.-M., DUMAS, C., ZUCKERMAN, B., MOUILLET, D. ET AL. (2004). A giant planet candidate near a young brown dwarf. Direct VLT/NACO observations using IR wavefront sensing. *A&A*, 425, L29–L32.

CHIU, K., FAN, X., LEGGETT, S. K., GOLIMOWSKI, D. A., ZHENG, W. ET AL. (2006). Seventy-One New L and T Dwarfs from the Sloan Digital Sky Survey. *AJ*, 131, 2722–2736.

CHOI, J.-Y., HAN, C., UDALSKI, A., SUMI, T., GAUDI, B. S. ET AL. (2013). Microlensing Discovery of a Population of Very Tight, Very Low Mass Binary Brown Dwarfs. *ApJ*, 768, 129.

CLOSE, L. M., SIEGLER, N. & FREED, M. (2003a). Detection of Nine M8.0–L0.5 Binaries: The Very Low Mass Binary Population and Its Implications for Brown Dwarf Formation Theories. In MARTÍN, E., ed., Brown Dwarfs, vol. 211 of *IAU Symposium*. 249–+.

CLOSE, L. M., SIEGLER, N., FREED, M. & BILLER, B. (2003b). Detection of Nine M8.0-L0.5 Binaries: The Very Low Mass Binary Population and Its Implications for Brown Dwarf and Very Low Mass Star Formation. *ApJ*, 587, 407–422.

CLOSE, L. M., SIEGLER, N., POTTER, D., BRANDNER, W. & LIEBERT, J. (2002). An Adaptive Optics Survey of M8-M9 Stars: Discovery of Four Very Low Mass Binaries with at Least One System Containing a Brown Dwarf Companion. *ApJ*, 567, L53–L57.

CLOSE, L. M., WILDI, F., LLOYD-HART, M., BRUSA, G., FISHER, D. ET AL. (2003c). High-Resolution Images of Orbital Motion in the Trapezium Cluster: First Scientific Results from the Multiple Mirror Telescope Deformable Secondary Mirror Adaptive Optics System. *ApJ*, 599, 537–547.

COMERÓN, F., PASQUALI, A., RODIGHIERO, G., STANISHEV, V., DE FILIPPIS, E. ET AL. (2002). On the massive star contents of Cygnus OB2. *A&A*, 389, 874–888.

COPENHAGEN UNIVERSITY, O., INSTITUTE, A. O., CAMBRIDGE, UK & REAL INSTITUTO Y OBSERVATORIO DE LA ARMADA, F. E. S. (2006). Carlsberg Meridian Catalog 14 (CMC14) (CMC, 2006). *VizieR Online Data Catalog*, 1304, 0.

COVEY, K. R., HAWLEY, S. L., BOCHANSKI, J. J., WEST, A. A., REID, I. N. ET AL. (2008). The Luminosity and Mass Functions of Low-Mass Stars in the Galactic Disk. I. The Calibration Region. *AJ*, 136, 1778–1798.

COVEY, K. R., IVEZIĆ, Ž., SCHLEGEL, D., FINKBEINER, D., PADMANABHAN, N. ET AL. (2007). Stellar SEDs from 0.3 to 2.5 μm: Tracing the Stellar Locus and Searching for Color Outliers in the SDSS and 2MASS. *AJ*, 134, 2398–2417.

CREPP, J. R., JOHNSON, J. A., FISCHER, D. A., HOWARD, A. W., MARCY, G. W. ET AL. (2012). The Dynamical Mass and Three-dimensional Orbit of HR7672B: A Benchmark Brown Dwarf with High Eccentricity. *ApJ*, 751, 97.

CRUZ, K. L., KIRKPATRICK, J. D. & BURGASSER, A. J. (2009). Young L Dwarfs Identified in the Field: A Preliminary Low-Gravity, Optical Spectral Sequence from L0 to L5. *AJ*, 137, 3345–3357.

CRUZ, K. L. & REID, I. N. (2002). Meeting the Cool Neighbors. III. Spectroscopy of Northern NLTT Stars. *AJ*, 123, 2828–2840.

CRUZ, K. L., REID, I. N., KIRKPATRICK, J. D., BURGASSER, A. J., LIEBERT, J. ET AL. (2007). Meeting the Cool Neighbors. IX. The Luminosity Function of M7-L8 Ultracool Dwarfs in the Field. *AJ*, 133, 439–467.

CRUZ, K. L., REID, I. N., LIEBERT, J., KIRKPATRICK, J. D. & LOWRANCE, P. J. (2003). Meeting the Cool Neighbors. V. A 2MASS-Selected Sample of Ultracool Dwarfs. *AJ*, 126, 2421–2448.

CUSHING, M. C., KIRKPATRICK, J. D., GELINO, C. R., GRIFFITH, R. L., SKRUTSKIE, M. F. ET AL. (2011a). The Discovery of Y Dwarfs Using Data from the Wide-field Infrared Survey Explorer (WISE). *ArXiv e-prints*, ApJ.

CUSHING, M. C., KIRKPATRICK, J. D., GELINO, C. R., GRIFFITH, R. L., SKRUTSKIE, M. F. ET AL. (2011b). The Discovery of Y Dwarfs using Data from the Wide-field Infrared Survey Explorer (WISE). *ApJ*, 743, 50.

CUSHING, M. C., KIRKPATRICK, J. D., GELINO, C. R., MACE, G. N., SKRUTSKIE, M. F. ET AL. (2014a). Three New Cool Brown Dwarfs Discovered with the Wide-field Infrared Survey Explorer (WISE) and an Improved Spectrum of the Y0 Dwarf WISE J041022.71+150248.4. *AJ*, 147, 113.

CUSHING, M. C., KIRKPATRICK, J. D., GELINO, C. R., MACE, G. N., SKRUTSKIE, M. F. ET AL. (2014b). Three New Cool Brown Dwarfs Discovered with the Wide-field Infrared Survey Explorer (WISE) and an Improved Spectrum of the Y0 Dwarf WISE J041022.71+150248.4. *ArXiv e-prints*.

CUSHING, M. C., LOOPER, D., BURGASSER, A. J., KIRKPATRICK, J. D., FAHERTY, J. ET AL. (2009). 2MASS J06164006-6407194: The First Outer Halo L Subdwarf. *ApJ*, 696, 986–993.

CUTRI, R. M. & ET AL. (2012). WISE All-Sky Data Release (Cutri+ 2012). *VizieR Online Data Catalog*, 2311, 0.

DAHN, C. C., HARRIS, H. C., LEVINE, S. E., TILLEMAN, T., MONET, A. K. B. ET AL. (2008). Trigonometric Parallaxes for Two Late-Type Subdwarfs: LSR 1425+71 (sdM8.0) and the Binary LSR 1610-00 (sd?M6pec). *ApJ*, 686, 548–559.

DAHN, C. C., HARRIS, H. C., VRBA, F. J., GUETTER, H. H., CANZIAN, B. ET AL. (2002). Astrometry and Photometry for Cool Dwarfs and Brown Dwarfs. *AJ*, 124, 1170–1189.

DE LEE, N., GE, J., CREPP, J. R., EASTMAN, J., ESPOSITO, M. ET AL. (2013). Very Low Mass Stellar and Substellar Companions to Solar-like Stars from MARVELS. V. A Low Eccentricity Brown Dwarf from the Driest Part of the Desert, MARVELS-6b. *AJ*, 145, 155.

DEACON, N. R., LIU, M. C., MAGNIER, E. A., ALLER, K. M., BEST, W. M. J. ET AL. (2014). Wide Cool and Ultracool Companions to Nearby Stars from Pan-STARRS. *ApJ*, 792, 119.

DEACON, N. R., LIU, M. C., MAGNIER, E. A., BOWLER, B. P., GOLDMAN, B. ET AL. (2011a). Four New T Dwarfs Identified in Pan-STARRS 1 Commissioning Data. *AJ*, 142, 77.

DEACON, N. R., PINFIELD, D. J., LUCAS, P. W., LIU, M. C., BESSELL, M. S. ET AL. (2011b). Ultracool Dwarf Science from Widefield Multi-Epoch Surveys. In JOHNS-KRULL, C., BROWNING, M. K. & WEST, A. A., eds., 16th Cambridge Workshop on Cool Stars, Stellar Systems, and the Sun, vol. 448 of *Astronomical Society of the Pacific Conference Series*. 429.

DELFOSSE, X., BEUZIT, J.-L., MARCHAL, L., BONFILS, X., PERRIER, C. ET AL. (2004). M dwarfs binaries: Results from accurate radial velocities and high angular resolution observations. In R. W. HILDITCH, H. HENSBERGE, & K. PAVLOVSKI, ed., Spectroscopically and Spatially Resolving the Components of the Close Binary Stars, vol. 318 of *Astronomical Society of the Pacific Conference Series*. 166–174.

DELFOSSE, X., FORVEILLE, T., MAYOR, M., PERRIER, C., NAEF, D. ET AL. (1998). The closest extrasolar planet. A giant planet around the M4 dwarf GL 876. *A&A*, 338, L67–L70.

DELFOSSE, X. ET AL. (1997). Field brown dwarfs found by DENIS. *A&A*, 327, L25–L28.

DELORME, P., DELFOSSE, X., ALBERT, L., ARTIGAU, E., FORVEILLE, T. ET AL. (2008a). CFBDS J005910.90-011401.3: reaching the T-Y brown dwarf transition? *A&A*, 482, 961–971.

DELORME, P., WILLOTT, C. J., FORVEILLE, T., DELFOSSE, X., REYLÉ, C. ET AL. (2008b). Finding ultracool brown dwarfs with MegaCam on CFHT: method and first results. *A&A*, 484, 469–478.

DHITAL, S., WEST, A. A., STASSUN, K. G. & BOCHANSKI, J. J. (2010). Sloan Low-mass Wide Pairs of Kinematically Equivalent Stars (SLoWPoKES): A Catalog of Very Wide, Low-mass Pairs. *AJ*, 139, 2566–2586.

DIETERICH, S. B., HENRY, T. J., GOLIMOWSKI, D. A., KRIST, J. E. & TANNER, A. M. (2012). The Solar Neighborhood. XXVIII. The Multiplicity Fraction of Nearby Stars from 5 to 70 AU and the Brown Dwarf Desert around M Dwarfs. *AJ*, 144, 64.

DOBBIE, P. D., LODIEU, N. & SHARP, R. G. (2010). IC 2602: a lithium depletion boundary age and new candidate low-mass stellar members. *MNRAS*, 409, 1002–1012.

DOBLER, W., STIX, M. & BRANDENBURG, A. (2006). Magnetic Field Generation in Fully Convective Rotating Spheres. *ApJ*, 638, 336–347.

DUCHÊNE, G. & KRAUS, A. (2013). Stellar Multiplicity. *ARA&A*, 51, 269–310.

DUPUY, T. J. & LIU, M. C. (2011). On the Distribution of Orbital Eccentricities for Very Low-mass Binaries. *ApJ*, 733, 122–+.

DUPUY, T. J. & LIU, M. C. (2012a). The Hawaii Infrared Parallax Program. I. Ultracool Binaries and the L/T Transition. *ApJS*, 201, 19.

DUPUY, T. J. & LIU, M. C. (2012b). The Hawaii Infrared Parallax Program. I. Ultracool Binaries and the L/T Transition. *ArXiv e-prints*.

DUPUY, T. J., LIU, M. C. & BOWLER, B. P. (2009a). Dynamical Mass of the M8+M8 Binary 2MASS J22062280 - 2047058AB. *ApJ*, 706, 328–342.

DUPUY, T. J., LIU, M. C. & IRELAND, M. J. (2009b). Keck Laser Guide Star Adaptive Optics Monitoring of the M8+L7 Binary LHS 2397aAB: First Dynamical Mass Benchmark at the L/T Transition. *ApJ*, 699, 168–185.

DUPUY, T. J., LIU, M. C. & IRELAND, M. J. (2014). New Evidence for a Substellar Luminosity Problem: Dynamical Mass for the Brown Dwarf Binary Gl 417BC. *ApJ*, 790, 133.

DUPUY, T. J., LIU, M. C. & LEGGETT, S. K. (2015). Discovery of a Low-luminosity, Tight Substellar Binary at the T/Y Transition. *ApJ*, 803, 102.

DUQUENNOY, A. & MAYOR, M. (1991). Multiplicity among solar-type stars in the solar neighbourhood. II - Distribution of the orbital elements in an unbiased sample. *A&A*, 248, 485–524.

DUQUENNOY, A., MAYOR, M. & HALBWACHS, J.-L. (1991). Multiplicity among solar type stars in the solar neighbourhood. I - CORAVEL radial velocity observations of 291 stars. *A&AS*, 88, 281–324.

EISENHARDT, P. R. M., GRIFFITH, R. L., STERN, D., WRIGHT, E. L., ASHBY, M. L. N. ET AL. (2010). Ultracool Field Brown Dwarf Candidates Selected at 4.5 μm. *AJ*, 139, 2455–2464.

ELMEGREEN, B. G. (2011). On the Initial Conditions for Star Formation and the Initial Mass Function. *ApJ*, 731, 61.

EPCHTEIN, N. ET AL. (1997). The deep near-infrared southern sky survey (DENIS). *The Messenger*, 87, 27–34.

EVANS, D. W. (2001). The Carlsberg Meridian Telescope: an astrometric robotic telescope. *Astronomische Nachrichten*, 322, 347–351.

EVANS, D. W., IRWIN, M. J. & HELMER, L. (2002). The Carlsberg Meridian Telescope CCD drift scan survey. *A&A*, 395, 347–356.

EVANS, T. M., IRELAND, M. J., KRAUS, A. L., MARTINACHE, F., STEWART, P. ET AL. (2012). Mapping the Shores of the Brown Dwarf Desert. III. Young Moving Groups. *ApJ*, 744, 120.

FAHERTY, J. K., BELETSKY, Y., BURGASSER, A. J., TINNEY, C., OSIP, D. J. ET AL. (2014). Signatures of Cloud, Temperature, and Gravity from Spectra of the Closest Brown Dwarfs. *ApJ*, 790, 90.

FAHERTY, J. K., BURGASSER, A. J., CRUZ, K. L., SHARA, M. M., WALTER, F. M. ET AL. (2009). The Brown Dwarf Kinematics Project I. Proper Motions and Tangential Velocities for a Large Sample of Late-Type M, L, and T Dwarfs. *AJ*, 137, 1–18.

FAHERTY, J. K., BURGASSER, A. J., WALTER, F. M., VAN DER BLIEK, N., SHARA, M. M. ET AL. (2012). The Brown Dwarf Kinematics Project (BDKP). III. Parallaxes for 70 Ultracool Dwarfs. *ApJ*, 752, 56.

FAHERTY, J. K., BURGASSER, A. J., WEST, A. A., BOCHANSKI, J. J., CRUZ, K. L. ET AL. (2010). The Brown Dwarf Kinematics Project. II. Details on Nine Wide Common Proper Motion Very Low Mass Companions to Nearby Stars. *AJ*, 139, 176–194.

FISCHER, D. A. & MARCY, G. W. (1992). Multiplicity among M dwarfs. *ApJ*, 396, 178–194.

FLEMING, T. A. (1998). A New Sample of Nearby M Dwarfs Discovered by ROSAT. *ApJ*, 504, 461.

FOLKES, S. L., PINFIELD, D. J., KENDALL, T. R. & JONES, H. R. A. (2007). Discovery of a nearby L-T transition object in the Southern Galactic plane. *MNRAS*, 378, 901–909.

FORVEILLE, T., BEUZIT, J.-L., DELORME, P., SÉGRANSAN, D., DELFOSSE, X. ET AL. (2005). LP 349-25: A new tight M8V binary. *A&A*, 435, L5–L8.

FREED, M., CLOSE, L. M. & SIEGLER, N. (2003). Discovery of a Tight Brown Dwarf Companion to theLow-Mass Star LHS 2397a. *ApJ*, 584, 453–458.

FREEDMAN, R. S., MARLEY, M. S. & LODDERS, K. (2008). Line and Mean Opacities for Ultracool Dwarfs and Extrasolar Planets. *ApJS*, 174, 504–513.

FRITH, J., PINFIELD, D. J., JONES, H. R. A., BARNES, J. R., PAVLENKO, Y. ET AL. (2013). A catalogue of bright (K < 9) M dwarfs. *MNRAS*, 435, 2161–2170.

FRUCHTER, A. S. & HOOK, R. N. (2002). Drizzle: A Method for the Linear Reconstruction of Undersampled Images. *PASP*, 114, 144–152.

FUHRMEISTER, B. & SCHMITT, J. H. M. M. (2003). A systematic study of X-ray variability in the ROSAT all-sky survey. *A&A*, 403, 247–260.

GAIDOS, E., HAGHIGHIPOUR, N., AGOL, E., LATHAM, D., RAYMOND, S. ET AL. (2007). New Worlds on the Horizon: Earth-Sized Planets Close to Other Stars. *Science*, 318, 210–.

GAIDOS, E., MANN, A. W., LÉPINE, S., BUCCINO, A., JAMES, D. ET AL. (2014). Trumpeting M dwarfs with CONCH-SHELL: a catalogue of nearby cool host-stars for habitable exoplanets and life. *MNRAS*, 443, 2561–2578.

GARCIA, E. V., DUPUY, T. J., ALLERS, K. N., LIU, M. C. & DEACON, N. R. (2015). On the Binary Frequency of the Lowest Mass Members of the Pleiades with Hubble Space Telescope Wide Field Camera 3. *ApJ*, 804, 65.

GEBALLE, T. R., KNAPP, G. R., LEGGETT, S. K., FAN, X., GOLIMOWSKI, D. A. ET AL. (2002). Toward Spectral Classification of L and T Dwarfs: Infrared and Optical Spectroscopy and Analysis. *ApJ*, 564, 466–481.

GELINO, C. R., KIRKPATRICK, J. D., CUSHING, M. C., EISENHARDT, P. R., GRIFFITH, R. L. ET AL. (2011). WISE Brown Dwarf Binaries: The Discovery of a T5+T5 and a T8.5+T9 System. *AJ*, 142, 57–+.

GERSHBERG, R. E., KATSOVA, M. M., LOVKAYA, M. N., TEREBIZH, A. V. & SHAKHOVSKAYA, N. I. (1999). Catalogue and bibliography of the UV Cet-type flare stars and related objects in the solar vicinity. *A&AS*, 139, 555–558.

GICLAS, H. L., BURNHAM, R. & THOMAS, N. G. (1961). Lowell proper motions III : proper motion survey of the Northern Hemisphere with the 13-inch photographic telescope of the Lowell Observatory. *Lowell Observatory Bulletin*, 5, 61–132.

GICLAS, H. L., BURNHAM, R. & THOMAS, N. G. (1971). Lowell proper motion survey Northern Hemisphere. *Book*.

GICLAS, H. L., BURNHAM, R., JR. & THOMAS, N. G. (1978). Lowell Proper Motion Survey - Southern Hemisphere Catalog 1978. *Lowell Observatory Bulletin*, 8, 89.

GICLAS, H. L., SLAUGHTER, C. D. & BURNHAM, R. (1959). Lowell proper motions II : proper motion survey of the Northern Hemisphere with the 13-inch photographic telescope of the Lowell Observatory. *Lowell Observatory Bulletin*, 4, 136–251.

GIZIS, J. E. (1997). M-Subdwarfs: Spectroscopic Classification and the Metallicity Scale. *AJ*, 113, 806–822.

GIZIS, J. E., MONET, D. G., REID, I. N., KIRKPATRICK, J. D., LIEBERT, J. ET AL. (2000). New Neighbors from 2MASS: Activity and Kinematics at the Bottom of the Main Sequence. *AJ*, 120, 1085–1099.

GIZIS, J. E., REID, I. N., KNAPP, G. R., LIEBERT, J., KIRKPATRICK, J. D. ET AL. (2003). Hubble Space Telescope Observations of Binary Very Low Mass Stars and Brown Dwarfs. *AJ*, 125, 3302–3310.

GLIESE, W. (1969). Catalogue of Nearby Stars. Edition 1969. *Veroeffentlichungen des Astronomischen Rechen-Instituts Heidelberg*, 22, 1.

GLIESE, W. & JAHREISS, H. (1991). The Third Catalogue of Nearby Stars - Errors and uncertainties. *NASA STI/Recon Technical Report A*, 92, 33932.

GOLDMAN, B., MARSAT, S., HENNING, T., CLEMENS, C. & GREINER, J. (2010). A new benchmark T8-9 brown dwarf and a couple of new mid-T dwarfs from the UKIDSS DR5+ LAS. *MNRAS*, 405, 1140–1152.

GOLIMOWSKI, D. A., HENRY, T. J., KRIST, J. E., DIETERICH, S., FORD, H. C. ET AL. (2004a). The Solar Neighborhood. IX. Hubble Space Telescope Detections of Companions to Five M and L Dwarfs within 10 Parsecs of the Sun. *AJ*, 128, 1733–1747.

GOLIMOWSKI, D. A., NAKAJIMA, T., KULKARNI, S. R. & OPPENHEIMER, B. R. (1995). Detection of a very low mass companion to the astrometric binary Gliese 105A. *ApJ*, 444, L101–L104.

GOLIMOWSKI, D. A. ET AL. (2004b). L' and M' Photometry of Ultracool Dwarfs. *AJ*, 127, 3516–3536.

GOODWIN, S. P. & WHITWORTH, A. (2007). Brown dwarf formation by binary disruption. *A&A*, 466, 943–948.

GRETHER, D. & LINEWEAVER, C. H. (2006). How Dry is the Brown Dwarf Desert? Quantifying the Relative Number of Planets, Brown Dwarfs, and Stellar Companions around Nearby Sun-like Stars. *ApJ*, 640, 1051–1062.

GÜDEL, M., BRIGGS, K. R., ARZNER, K., AUDARD, M., BOUVIER, J. ET AL. (2007). The XMM-Newton extended survey of the Taurus molecular cloud (XEST). *A&A*, 468, 353–377.

GUENTHER, E. W. & WUCHTERL, G. (2003). Companions of old brown dwarfs, and very low mass stars. *A&A*, 401, 677–683.

GUIEU, S., DOUGADOS, C., MONIN, J.-L., MAGNIER, E. & MARTÍN, E. L. (2006). Seventeen new very low-mass members in Taurus. The brown dwarf deficit revisited. *A&A*, 446, 485–500.

HAAKONSEN, C. B. & RUTLEDGE, R. E. (2009). XID II: Statistical Cross-Association of ROSAT Bright Source Catalog X-ray Sources with 2MASS Point Source Catalog Near-Infrared Sources. *ApJS*, 184, 138–151.

HAMBLY, N. C., MACGILLIVRAY, H. T., READ, M. A., TRITTON, S. B., THOMSON, E. B. ET AL. (2001). The SuperCOSMOS Sky Survey - I. Introduction and description. *MNRAS*, 326, 1279–1294.

HAMUY, M., SUNTZEFF, N. B., HEATHCOTE, S. R., WALKER, A. R., GIGOUX, P. ET AL. (1994). Southern spectrophotometric standards, 2. *PASP*, 106, 566–589.

HAN, C., JUNG, Y. K., UDALSKI, A., SUMI, T., GAUDI, B. S. ET AL. (2013). Microlensing Discovery of a Tight, Low-mass-ratio Planetary-mass Object around an Old Field Brown Dwarf. *ApJ*, 778, 38.

HARTMAN, J. D., BAKOS, G. Á., NOYES, R. W., SIPŐCZ, B., KOVÁCS, G. ET AL. (2011). A Photometric Variability Survey of Field K and M Dwarf Stars with HATNet. *AJ*, 141, 166.

HAWLEY, S. L., GIZIS, J. E. & REID, I. N. (1996). The Palomar/MSU Nearby Star Spectroscopic Survey.II.The Southern M Dwarfs and Investigation of Magnetic Activity. *AJ*, 112, 2799.

HAWLEY, S. L., GIZIS, J. E. & REID, N. I. (1997). The Palomar/MSU Nearby Star Spectroscopic Survey.II.The Southern M Dwarfs and Investigation of Magnetic Activity. *AJ*, 113, 1458.

HAWLEY, S. L. ET AL. (2002). Characterization of M, L, and T Dwarfs in the Sloan Digital Sky Survey. *AJ*, 123, 3409–3427.

HAYASHI, C. & NAKANO, T. (1963). Evolution of Stars of Small Masses in the Pre-Main-Sequence Stages. *Progress of Theoretical Physics*, 30, 460–474.

HEARTY, F., LEVI, E., NELSON, M., MAHADEVAN, S., BURTON, A. ET AL. (2014). Environmental control system for Habitable-zone Planet Finder (HPF). In Society of

Photo-Optical Instrumentation Engineers (SPIE) Conference Series, vol. 9147 of *Society of Photo-Optical Instrumentation Engineers (SPIE) Conference Series*. 52.

HELLING, C., ACKERMAN, A., ALLARD, F., DEHN, M., HAUSCHILDT, P. ET AL. (2008). A comparison of chemistry and dust cloud formation in ultracool dwarf model atmospheres. *MNRAS*, 391, 1854–1873.

HELOU, G. & WALKER, D. W. (1988). Infrared astronomical satellite (IRAS) catalogs and atlases. Volume 7: The small scale structure catalog. *Proceeding*, 7.

HENNEBELLE, P. & TEYSSIER, R. (2008). Magnetic processes in a collapsing dense core. II. Fragmentation. Is there a fragmentation crisis? *A&A*, 477, 25–34.

HENRY, T. J., JAO, W.-C., SUBASAVAGE, J. P., BEAULIEU, T. D., IANNA, P. A. ET AL. (2006). The Solar Neighborhood. XVII. Parallax Results from the CTIOPI 0.9 m Program: 20 New Members of the RECONS 10 Parsec Sample. *AJ*, 132, 2360–2371.

HESTER, J. J., SCOWEN, P. A., SANKRIT, R., LAUER, T. R., AJHAR, E. A. ET AL. (1996). Hubble Space Telescope WFPC2 Imaging of M16: Photoevaporation and Emerging Young Stellar Objects. *AJ*, 111, 2349.

HILLENBRAND, L. A. (1997). On the Stellar Population and Star-Forming History of the Orion Nebula Cluster. *AJ*, 113, 1733–1768.

HOWARD, A. W., MARCY, G. W., BRYSON, S. T., JENKINS, J. M., ROWE, J. F. ET AL. (2012). Planet Occurrence within 0.25 AU of Solar-type Stars from Kepler. *ApJS*, 201, 15.

HUBENY, I. & BURROWS, A. (2007). A Systematic Study of Departures from Chemical Equilibrium in the Atmospheres of Substellar Mass Objects. *ApJ*, 669, 1248–1261.

HUÉLAMO, N., IVANOV, V. D., KURTEV, R., GIRARD, J. H., BORISSOVA, J. ET AL. (2015). WISE J061213.85-303612.5: a new T-dwarf binary candidate. *A&A*, 578, A1.

IRELAND, M. J., KRAUS, A., MARTINACHE, F., LLOYD, J. P. & TUTHILL, P. G. (2008). Dynamical Mass of GJ 802B: A Brown Dwarf in a Triple System. *ApJ*, 678, 463–471.

IRWIN, J. M., QUINN, S. N., BERTA, Z. K., LATHAM, D. W., TORRES, G. ET AL. (2011). LSPM J1112+7626: Detection of a 41 Day M-dwarf Eclipsing Binary from the MEarth Transit Survey. *ApJ*, 742, 123.

ISAACSON, H. & FISCHER, D. (2010). Chromospheric Activity and Jitter Measurements for 2630 Stars on the California Planet Search. *ApJ*, 725, 875–885.

JAO, W.-C., HENRY, T. J., BEAULIEU, T. D. & SUBASAVAGE, J. P. (2008). Cool Subdwarf Investigations. I. New Thoughts on the Spectral Types of K and M Subdwarfs. *AJ*, 136, 840–880.

JAYAWARDHANA, R., ARDILA, D. R., STELZER, B. & HAISCH, K. E., JR. (2003). A Disk Census for Young Brown Dwarfs. *AJ*, 126, 1515–1521.

JAYAWARDHANA, R., COFFEY, J., SCHOLZ, A., BRANDEKER, A. & VAN KERKWIJK, M. H. (2006). Accretion Disks around Young Stars: Lifetimes, Disk Locking, and Variability. *ApJ*, 648, 1206–1218.

JAYAWARDHANA, R. & IVANOV, V. D. (2006). Discovery of a Young Planetary-Mass Binary. *Science*, 313, 1279–1281.

JEFFRIES, R. D., NAYLOR, T., MAYNE, N. J., BELL, C. P. M. & LITTLEFAIR, S. P. (2013). A lithium depletion boundary age of 22 Myr for NGC 1960. *MNRAS*, 434, 2438–2450.

JIMÉNEZ-ESTEBAN, F. M., CABALLERO, J. A., DORDA, R., MILES-PÁEZ, P. A. & SOLANO, E. (2012). Identification of red high proper-motion objects in Tycho-2 and 2MASS catalogues using Virtual Observatory tools. *A&A*, 539, A86.

JOERGENS, V. (2006a). Improved kinematics for brown dwarfs and very low-mass stars in Chamaeleon I and a discussion of brown dwarf formation. *A&A*, 448, 655–663.

JOERGENS, V. (2006b). Radial velocity survey for planets and brown dwarf companions to very young brown dwarfs and very low-mass stars in Chamaeleon I with UVES at the VLT. *A&A*, 446, 1165–1176.

JOERGENS, V. & GUENTHER, E. (2001). UVES spectra of young brown dwarfs in Cha I: Radial and rotational velocities. *A&A*, 379, L9–L12.

JOHNSON, J. A., APPS, K., GAZAK, J. Z., CREPP, J. R., CROSSFIELD, I. J. ET AL. (2011). LHS 6343 C: A Transiting Field Brown Dwarf Discovered by the Kepler Mission. *ApJ*, 730, 79.

JOHNSON, J. A., HOWARD, A. W., MARCY, G. W., BOWLER, B. P., HENRY, G. W. ET AL. (2010). The California Planet Survey. II. A Saturn-Mass Planet Orbiting the M Dwarf Gl 649. *PASP*, 122, 149–155.

JUMPER, P. H. & FISHER, R. T. (2013). Shaping the Brown Dwarf Desert: Predicting the Primordial Brown Dwarf Binary Distributions from Turbulent Fragmentation. *ApJ*, 769, 9.

KASHIKAWA, N., AOKI, K., ASAI, R., EBIZUKA, N., INATA, M. ET AL. (2002). FOCAS: The Faint Object Camera and Spectrograph for the Subaru Telescope. *PASJ*, 54, 819–832.

KENDALL, T. R., JONES, H. R. A., PINFIELD, D. J., POKORNY, R. S., FOLKES, S. ET AL. (2007a). New nearby, bright southern ultracool dwarfs. *MNRAS*, 374, 445–454.

KENDALL, T. R., TAMURA, M., TINNEY, C. G., MARTÍN, E. L., ISHII, M. ET AL. (2007b). Two T dwarfs from the UKIDSS early data release. *A&A*, 466, 1059–1064.

KENWORTHY, M., HOFMANN, K.-H., CLOSE, L., HINZ, P., MAMAJEK, E. ET AL. (2001). Gliese 569B: A Young Multiple Brown Dwarf System? *ApJ*, 554, L67–L70.

KENYON, M. J., JEFFRIES, R. D., NAYLOR, T., OLIVEIRA, J. M. & MAXTED, P. F. L. (2005). Membership, binarity and accretion among very low-mass stars and brown dwarfs of the σ Orionis cluster. *MNRAS*, 356, 89–106.

KENYON, S. J., GÓMEZ, M. & WHITNEY, B. A. (2008). Low Mass Star Formation in the Taurus-Auriga Clouds. *Book*, 405.

KING, R. R., MCCAUGHREAN, M. J., HOMEIER, D., ALLARD, F., SCHOLZ, R. ET AL. (2010). ϵ Indi Ba, Bb: a detailed study of the nearest known brown dwarfs. *A&A*, 510, A99.

KIRKPATRICK, J. D. (2000). The L and T Dwarf Spectral Sequences: First Steps in Bridging the Gap Between Planets and Stars. In GRIFFITH, C. A. & MARLEY, M. S., eds., From Giant Planets to Cool Stars, vol. 212 of *Astronomical Society of the Pacific Conference Series*. 20.

KIRKPATRICK, J. D. (2005). New Spectral Types L and T. *ARA&A*, 43, 195–245.

KIRKPATRICK, J. D., CUSHING, M. C., GELINO, C. R., BEICHMAN, C. A., TINNEY, C. G. ET AL. (2013). Discovery of the Y1 Dwarf WISE J064723.23-623235.5. *ApJ*, 776, 128.

KIRKPATRICK, J. D., CUSHING, M. C., GELINO, C. R., GRIFFITH, R. L., SKRUTSKIE, M. F. ET AL. (2011a). The First Hundred Brown Dwarfs Discovered by the Wide-field Infrared Survey Explorer (WISE). *ApJS*, 197, 19.

KIRKPATRICK, J. D., CUSHING, M. C., GELINO, C. R., GRIFFITH, R. L., SKRUTSKIE, M. F. ET AL. (2011b). The First Hundred Brown Dwarfs Discovered by the Wide-field Infrared Survey Explorer (WISE). *ApJS*, in press.

KIRKPATRICK, J. D., CUSHING, M. C., GELINO, C. R., GRIFFITH, R. L., SKRUTSKIE, M. F. ET AL. (2012a). First brown dwarfs discovered by WISE (Kirkpatrick+, 2011). *VizieR Online Data Catalog*, 219, 70019.

KIRKPATRICK, J. D., GELINO, C. R., CUSHING, M. C., MACE, G. N., GRIFFITH, R. L. ET AL. (2012b). Further Defining Spectral Type "Y" and Exploring the Low-mass End of the Field Brown Dwarf Mass Function. *ApJ*, 753, 156.

KIRKPATRICK, J. D., HENRY, T. J. & MCCARTHY, D. W., JR. (1991). A standard stellar spectral sequence in the red/near-infrared - Classes K5 to M9. *ApJS*, 77, 417–440.

KIRKPATRICK, J. D., KELLY, D. M., RIEKE, G. H., LIEBERT, J., ALLARD, F. ET AL. (1993). M dwarf spectra from 0.6 to 1.5 micron - A spectral sequence, model atmosphere fitting, and the temperature scale. *ApJ*, 402, 643–654.

KIRKPATRICK, J. D., REID, I. N., LIEBERT, J., CUTRI, R. M., NELSON, B. ET AL. (1999). Dwarfs Cooler than "M": The Definition of Spectral Type "L" Using Discoveries from the 2 Micron All-Sky Survey (2MASS). *ApJ*, 519, 802–833.

KIRKPATRICK, J. D., REID, I. N., LIEBERT, J., GIZIS, J. E., BURGASSER, A. J. ET AL. (2000). 67 Additional L Dwarfs Discovered by the Two Micron All Sky Survey. *AJ*, 120, 447–472.

KIRKPATRICK, J. D. ET AL. (2008). A Sample of Very Young Field L Dwarfs and Implications for the Brown Dwarf "Lithium Test" at Early Ages. *ApJ*, 689, 1295–1326.

KLESSEN, R. S. (2001). The Formation of Stellar Clusters: Mass Spectra from Turbulent Molecular Cloud Fragmentation. *ApJ*, 556, 837–846.

KLESSEN, R. S., HEITSCH, F. & MAC LOW, M.-M. (2000). Gravitational Collapse in Turbulent Molecular Clouds. I. Gasdynamical Turbulence. *ApJ*, 535, 887–906.

KNAPP, G. R., LEGGETT, S. K., FAN, X., MARLEY, M. S., GEBALLE, T. R. ET AL. (2004). Near-Infrared Photometry and Spectroscopy of L and T Dwarfs: The Effects of Temperature, Clouds, and Gravity. *AJ*, 127, 3553–3578.

KOERNER, D. W., KIRKPATRICK, J. D., MCELWAIN, M. W. & BONAVENTURA, N. R. (1999). Keck Imaging of Binary L Dwarfs. *ApJ*, 526, L25–L28.

KONOPACKY, Q. M., GHEZ, A. M., BARMAN, T. S., RICE, E. L., BAILEY, J. I. ET AL. (2010). High-precision Dynamical Masses of Very Low Mass Binaries. *ApJ*, 711, 1087–1122.

KONOPACKY, Q. M., GHEZ, A. M., RICE, E. L. & DUCHÊNE, G. (2007). New Very Low Mass Binaries in the Taurus Star-forming Region. *ApJ*, 663, 394–399.

KOPYTOVA, T. G., CROSSFIELD, I. J. M., DEACON, N. R., BRANDNER, W., BUENZLI, E. ET AL. (2014). Deep z-band Observations of the Coolest Y Dwarf. *ApJ*, 797, 3.

KOUWENHOVEN, M. B. N., GOODWIN, S. P., PARKER, R. J., DAVIES, M. B., MALMBERG, D. ET AL. (2010). The formation of very wide binaries during the star cluster dissolution phase. *MNRAS*, 404, 1835–1848.

KRAUS, A. L. & HILLENBRAND, L. A. (2012). Multiple Star Formation to the Bottom of the Initial Mass Function. *ApJ*, 757, 141.

KRAUS, A. L., WHITE, R. J. & HILLENBRAND, L. A. (2005). Multiplicity at the Stellar/Substellar Boundary in Upper Scorpius. *ApJ*, 633, 452–459.

KRAUS, A. L., WHITE, R. J. & HILLENBRAND, L. A. (2006). Multiplicity and Optical Excess across the Substellar Boundary in Taurus. *ApJ*, 649, 306–318.

KRIST, J. (1995). Simulation of HST PSFs using Tiny Tim. In SHAW, R. A., PAYNE, H. E. & HAYES, J. J. E., eds., Astronomical Data Analysis Software and Systems IV, vol. 77 of *Astronomical Society of the Pacific Conference Series*. 349–+.

KROUPA, P. (2001). On the variation of the initial mass function. *MNRAS*, 322, 231–246.

KROUPA, P. (2002). The Initial Mass Function of Stars: Evidence for Uniformity in Variable Systems. *Science*, 295, 82–91.

KROUPA, P. & BOUVIER, J. (2003). The dynamical evolution of Taurus-Auriga-type aggregates. *MNRAS*, 346, 343–353.

KROUPA, P., TOUT, C. A. & GILMORE, G. (1993). The distribution of low-mass stars in the Galactic disc. *MNRAS*, 262, 545–587.

KUBAS, D., BEAULIEU, J. P., BENNETT, D. P., CASSAN, A., COLE, A. ET AL. (2012). A frozen super-Earth orbiting a star at the bottom of the main sequence. *A&A*, 540, A78.

KUMAR, S. S. (1962). Study of Degeneracy in Very Light Stars. *AJ*, 67, 579–+.

KUMAR, S. S. (1963). The Structure of Stars of Very Low Mass. *ApJ*, 137, 1121–+.

KUROSAWA, R., HARRIES, T. J. & LITTLEFAIR, S. P. (2006). Radial and rotational velocities of young brown dwarfs and very low-mass stars in the Upper Scorpius OB association and the ρ Ophiuchi cloud core. *MNRAS*, 372, 1879–1887.

LADA, C. J., MUENCH, A. A., RATHBORNE, J., ALVES, J. F. & LOMBARDI, M. (2008). The Nature of the Dense Core Population in the Pipe Nebula: Thermal Cores Under Pressure. *ApJ*, 672, 410–422.

LAW, N. M., HODGKIN, S. T. & MACKAY, C. D. (2006). Discovery of five very low mass close binaries, resolved in the visible with lucky imaging. *MNRAS*, 368, 1917–1924.

LAWRENCE, A. ET AL. (2007). The UKIRT Infrared Deep Sky Survey (UKIDSS). *MNRAS*, 379, 1599–1617.

LEGGETT, S. K., ALBERT, L., ARTIGAU, E., BURNINGHAM, B., DELFOSSE, X. ET AL. (2011). Spitzer Mid-Infrared Photometry of 500 - 750 K Brown Dwarfs. In JOHNS-KRULL, C., BROWNING, M. K. & WEST, A. A., eds., 16th Cambridge Workshop on Cool Stars, Stellar Systems, and the Sun, vol. 448 of *Astronomical Society of the Pacific Conference Series*. 913.

LEGGETT, S. K., ALLARD, F., DAHN, C., HAUSCHILDT, P. H., KERR, T. H. ET AL. (2000a). Spectral Energy Distributions for Disk and Halo M Dwarfs. *ApJ*, 535, 965–974.

LEGGETT, S. K., ALLARD, F., GEBALLE, T. R., HAUSCHILDT, P. H. & SCHWEITZER, A. (2001). Infrared Spectra and Spectral Energy Distributions of Late M and L Dwarfs. *ApJ*, 548, 908–918.

LEGGETT, S. K., BURNINGHAM, B., SAUMON, D., MARLEY, M. S., WARREN, S. J. ET AL. (2010). Mid-Infrared Photometry of Cold Brown Dwarfs: Diversity in Age, Mass, and Metallicity. *ApJ*, 710, 1627–1640.

LEGGETT, S. K., CUSHING, M. C., SAUMON, D., MARLEY, M. S., ROELLIG, T. L. ET AL. (2009). The Physical Properties of Four ˜600 K T Dwarfs. *ApJ*, 695, 1517–1526.

LEGGETT, S. K., GEBALLE, T. R., FAN, X., SCHNEIDER, D. P., GUNN, J. E. ET AL. (2000b). The Missing Link: Early Methane ("T") Dwarfs in the Sloan Digital Sky Survey. *ApJ*, 536, L35–L38.

LEGGETT, S. K., MARLEY, M. S., FREEDMAN, R., SAUMON, D., LIU, M. C. ET AL. (2007). Physical and Spectral Characteristics of the T8 and Later Type Dwarfs. *ApJ*, 667, 537–548.

LEGGETT, S. K., SAUMON, D., ALBERT, L., CUSHING, M. C., LIU, M. C. ET AL. (2008). HN Peg B: A Test of Models of the L to T Dwarf Transition. *ApJ*, 682, 1256–1263.

LEGGETT, S. K., SAUMON, D., MARLEY, M. S., LODDERS, K., CANTY, J. ET AL. (2012). The Properties of the 500 K Dwarf UGPS J072227.51-054031.2 and a Study of the Far-red Flux of Cold Brown Dwarfs. *ApJ*, 748, 74.

LEGGETT, S. K. ET AL. (2002). Infrared Photometry of Late-M, L, and T Dwarfs. *ApJ*, 564, 452–465.

LEINERT, C., JAHREISS, H., WOITAS, J., ZUCKER, S., MAZEH, T. ET AL. (2001). Dynamical mass determination for the very low mass stars LHS 1070 B and C. *A&A*, 367, 183–188.

LÉPINE, S. (2011). Cool Stars in Wide Binaries: 23,000 Common Proper Motion Doubles from the SUPERBLINK Proper Motion Survey. In JOHNS-KRULL, C., BROWNING, M. K. & WEST, A. A., eds., 16th Cambridge Workshop on Cool Stars, Stellar Systems, and the Sun, vol. 448 of *Astronomical Society of the Pacific Conference Series*. 1375.

LÉPINE, S. & GAIDOS, E. (2011). An All-sky Catalog of Bright M Dwarfs. *AJ*, 142, 138.

LÉPINE, S., HILTON, E. J., MANN, A. W., WILDE, M., ROJAS-AYALA, B. ET AL. (2013). A Spectroscopic Catalog of the Brightest (J < 9) M Dwarfs in the Northern Sky. *AJ*, 145, 102.

LÉPINE, S., RICH, R. M. & SHARA, M. M. (2003a). Spectroscopy of New High Proper Motion Stars in the Northern Sky. I. New Nearby Stars, New High-Velocity Stars, and an Enhanced Classification Scheme for M Dwarfs. *AJ*, 125, 1598–1622.

LÉPINE, S., RICH, R. M. & SHARA, M. M. (2007). Revised Metallicity Classes for Low-Mass Stars: Dwarfs (dM), Subdwarfs (sdM), Extreme Subdwarfs (esdM), and Ultrasubdwarfs (usdM). *ApJ*, 669, 1235–1247.

LÉPINE, S. & SHARA, M. M. (2005). A Catalog of Northern Stars with Annual Proper Motions Larger than 0.15" (LSPM-NORTH Catalog). *AJ*, 129, 1483–1522.

LÉPINE, S., SHARA, M. M. & RICH, R. M. (2003b). New High Proper Motion Stars from the Digitized Sky Survey. II. Northern Stars with 0.5 arcsec at High Galactic Latitudes. *AJ*, 126, 921–934.

LIEBERT, J., REID, I. N., BURROWS, A., BURGASSER, A. J., KIRKPATRICK, J. D. ET AL. (2000). An Improved Red Spectrum of the Methane or T Dwarf SDSS 1624+0029: The Role of the Alkali Metals. *ApJ*, 533, L155–L158.

LIU, M. C., DELORME, P., DUPUY, T. J., BOWLER, B. P., ALBERT, L. ET AL. (2011). CFBDSIR J1458+1013B: A Very Cold (>T10) Brown Dwarf in a Binary System. *ApJ*, 740, 108.

LIU, M. C., DUPUY, T. J., BOWLER, B. P., LEGGETT, S. K. & BEST, W. M. J. (2012). Two Extraordinary Substellar Binaries at the T/Y Transition and the Y-band Fluxes of the Coolest Brown Dwarfs. *ApJ*, 758, 57.

LIU, M. C., DUPUY, T. J. & IRELAND, M. J. (2008). Keck Laser Guide Star Adaptive Optics Monitoring of 2MASS J15344984-2952274AB: First Dynamical Mass Determination of a Binary T Dwarf. *ApJ*, 689, 436–460.

LIU, M. C. & LEGGETT, S. K. (2005). Kelu-1 Is a Binary L Dwarf: First Brown Dwarf Science from Laser Guide Star Adaptive Optics. *ApJ*, 634, 616–624.

LIU, M. C., LEGGETT, S. K., GOLIMOWSKI, D. A., CHIU, K., FAN, X. ET AL. (2006). SDSS J1534+1615AB: A Novel T Dwarf Binary Found with Keck Laser Guide Star Adaptive Optics and the Potential Role of Binarity in the L/T Transition. *ApJ*, 647, 1393–1404.

LIU, Y., HERCZEG, G. J., GONG, M., ALLERS, K. N., BROWN, J. M. ET AL. (2015). Herschel/PACS view of disks around low-mass stars and brown dwarfs in the TW Hydrae association. *A&A*, 573, A63.

LODIEU, N., BÉJAR, V. J. S. & REBOLO, R. (2013a). GTC OSIRIS z-band imaging of Y dwarfs. *A&A*, 550, L2.

LODIEU, N., DEACON, N. R. & HAMBLY, N. C. (2012a). Astrometric and photometric initial mass functions from the UKIDSS Galactic Clusters Survey - I. The Pleiades. *MNRAS*, 422, 1495–1511.

LODIEU, N., DOBBIE, P. D., CROSS, N. J. G., HAMBLY, N. C., READ, M. A. ET AL. (2013b). Probing the Upper Scorpius mass function in the planetary-mass regime. *MNRAS*, 435, 2474–2482.

LODIEU, N., DOBBIE, P. D. & HAMBLY, N. C. (2011). Multi-fibre optical spectroscopy of low-mass stars and brown dwarfs in Upper Scorpius. *A&A*, 527, A24.

LODIEU, N., ESPINOZA CONTRERAS, M., ZAPATERO OSORIO, M. R., SOLANO, E., ABERASTURI, M. ET AL. (2012b). New ultracool subdwarfs identified in large-scale surveys using Virtual Observatory tools. I. UKIDSS LAS DR5 vs. SDSS DR7. *A&A*, 542, A105.

LODIEU, N., HAMBLY, N. C., JAMESON, R. F. & HODGKIN, S. T. (2008). Near-infrared cross-dispersed spectroscopy of brown dwarf candidates in the UpperSco association. *MNRAS*, 383, 1385–1396.

LODIEU, N., HAMBLY, N. C., JAMESON, R. F., HODGKIN, S. T., CARRARO, G. ET AL. (2007a). New brown dwarfs in Upper Sco using UKIDSS Galactic Cluster Survey science verification data. *MNRAS*, 374, 372–384.

LODIEU, N., PINFIELD, D. J., LEGGETT, S. K., JAMESON, R. F., MORTLOCK, D. J. ET AL. (2007b). Eight new T4.5-T7.5 dwarfs discovered in the UKIDSS Large Area Survey Data Release 1. *MNRAS*, 379, 1423–1430.

LODIEU, N., ZAPATERO OSORIO, M. R. & MARTÍN, E. L. (2009). Lucky Imaging of M subdwarfs. *A&A*, 499, 729–736.

LODIEU, N., ZAPATERO OSORIO, M. R., MARTÍN, E. L., SOLANO, E. & ABERASTURI, M. (2010). GTC/OSIRIS Spectroscopic Identification of a Faint L Subdwarf in the UKIRT Infrared Deep Sky Survey. *ApJ*, 708, L107–L111.

LOOPER, D. L., GELINO, C. R., BURGASSER, A. J. & KIRKPATRICK, J. D. (2008). Discovery of a T Dwarf Binary with the Largest Known J-Band Flux Reversal. *ApJ*, 685, 1183–1192.

LOOPER, D. L., KIRKPATRICK, J. D. & BURGASSER, A. J. (2007). Discovery of 11 New T Dwarfs in the Two Micron All Sky Survey, Including a Possible L/T Transition Binary. *AJ*, 134, 1162–1182.

LÓPEZ, C., CALANDRA, F., CHALELA, M., LÓPEZ, C., PEREYRA, L. ET AL. (2012). Common Proper Motion Pairs in the LSPM-North Catalog. *Journal of Double Star Observations*, 8, 73–80.

LÓPEZ MARTÍN, B., JIMÉNEZ-ESTEBAN, F., BAYO, A., BARRADO, D., SOLANO, E. ET AL. (2013). Proper motions of young stars in Chamaeleon. II. New kinematical candidate members of Chamaeleon I and II. *A&A*, 556, A144.

LOW, C. & LYNDEN-BELL, D. (1976). The minimum Jeans mass or when fragmentation must stop. *MNRAS*, 176, 367–390.

LUCAS, P. W., ROCHE, P. F., ALLARD, F. & HAUSCHILDT, P. H. (2001). Infrared spectroscopy of substellar objects in Orion. *MNRAS*, 326, 695–721.

LUHMAN, K. L. (2004a). New Brown Dwarfs and an Updated Initial Mass Function in Taurus. *ApJ*, 617, 1216–1232.

LUHMAN, K. L. (2004b). The First Discovery of a Wide Binary Brown Dwarf. *ApJ*, 614, 398–403.

LUHMAN, K. L. (2005). Discovery of a Wide, Low-Mass Binary System in Upper Scorpius. *ApJ*, 633, L41–L44.

LUHMAN, K. L. (2006). The Spatial Distribution of Brown Dwarfs in Taurus. *ApJ*, 645, 676–687.

LUHMAN, K. L. (2007). The Stellar Population of the Chamaeleon I Star-forming Region. *ApJS*, 173, 104–136.

LUHMAN, K. L. (2012). The Formation and Early Evolution of Low-Mass Stars and Brown Dwarfs. *ARA&A*, 50, 65–106.

LUHMAN, K. L. (2013). Discovery of a Binary Brown Dwarf at 2 pc from the Sun. *ApJ*, 767, L1.

LUHMAN, K. L. (2014). Discovery of a ˜250 K Brown Dwarf at 2 pc from the Sun. *ApJ*, 786, L18.

LUHMAN, K. L., BRICEÑO, C., STAUFFER, J. R., HARTMANN, L., BARRADO Y NAVASCUÉS, D. ET AL. (2003). New Low-Mass Members of the Taurus Star-forming Region. *ApJ*, 590, 348–356.

LUHMAN, K. L., BURGASSER, A. J. & BOCHANSKI, J. J. (2011a). Discovery of a Candidate for the Coolest Known Brown Dwarf. *ApJ*, 730, L9.

LUHMAN, K. L., BURGASSER, A. J., LABBÉ, I., MARLEY, M. S., SAUMON, D. ET AL. (2011b). CONFIRMATION OF THE COOLEST KNOWN BROWN DWARF. *ApJ*, submitted.

LUHMAN, K. L., BURGASSER, A. J., LABBÉ, I., SAUMON, D., MARLEY, M. S. ET AL. (2012a). Confirmation of One of the Coldest Known Brown Dwarfs. *ApJ*, 744, 135.

LUHMAN, K. L., LOUTREL, N. P., MCCURDY, N. S., MACE, G. N., MELSO, N. D. ET AL. (2012b). New M, L, and T Dwarf Companions to Nearby Stars from the Wide-field Infrared Survey Explorer. *ApJ*, 760, 152.

LUHMAN, K. L., MAMAJEK, E. E., ALLEN, P. R. & CRUZ, K. L. (2009a). An Infrared/X-Ray Survey for New Members of the Taurus Star-Forming Region. *ApJ*, 703, 399–419.

LUHMAN, K. L., MAMAJEK, E. E., ALLEN, P. R., MUENCH, A. A. & FINKBEINER, D. P. (2009b). Discovery of a Wide Binary Brown Dwarf Born in Isolation. *ApJ*, 691, 1265–1275.

LUHMAN, K. L., PATTEN, B. M., MARENGO, M., SCHUSTER, M. T., HORA, J. L. ET AL. (2007). Discovery of Two T Dwarf Companions with the Spitzer Space Telescope. *ApJ*, 654, 570–579.

LUHMAN, K. L., WHITNEY, B. A., MEADE, M. R., BABLER, B. L., INDEBETOUW, R. ET AL. (2006). A Survey for New Members of Taurus with the Spitzer Space Telescope. *ApJ*, 647, 1180–1191.

LUYTEN, W. J. (1979a). LHS catalogue. A catalogue of stars with proper motions exceeding 0″5 annually. *Book*.

LUYTEN, W. J. (1979b). New Luyten catalogue of stars with proper motions larger than two tenths of an arcsecond; and first supplement; NLTT. (Minneapolis (1979)); Label 12 = short description; Label 13 = documentation by Warren; Label 14 = catalogue. *Book*.

LUYTEN, W. J. (1980). NLTT Catalogue. Volume_III. 0__to -30_. University of Minnesota.

MACE, G. N., KIRKPATRICK, J. D., CUSHING, M. C., GELINO, C. R., GRIFFITH, R. L. ET AL. (2013a). A Study of the Diverse T Dwarf Population Revealed by WISE. *ApJS*, 205, 6.

MACE, G. N., KIRKPATRICK, J. D., CUSHING, M. C., GELINO, C. R., MCLEAN, I. S. ET AL. (2013b). The Exemplar T8 Subdwarf Companion of Wolf 1130. *ApJ*, 777, 36.

MAGAZZU, A., MARTIN, E. L. & REBOLO, R. (1993). A spectroscopic test for substellar objects. *ApJ*, 404, L17–L20.

MAGAZZU, A., REBOLO, R. & PAVLENKO, I. V. (1992). Lithium abundances in classical and weak T Tauri stars. *ApJ*, 392, 159–171.

MAHADEVAN, S., RAMSEY, L., BENDER, C., TERRIEN, R., WRIGHT, J. T. ET AL. (2012). The habitable-zone planet finder: a stabilized fiber-fed NIR spectrograph for the Hobby-Eberly Telescope. In Society of Photo-Optical Instrumentation Engineers (SPIE) Conference Series, vol. 8446 of *Society of Photo-Optical Instrumentation Engineers (SPIE) Conference Series*.

MAINZER, A., CUSHING, M. C., SKRUTSKIE, M., GELINO, C. R., KIRKPATRICK, J. D. ET AL. (2011). The First Ultra-cool Brown Dwarf Discovered by the Wide-field Infrared Survey Explorer. *ApJ*, 726, 30–+.

MALO, L., DOYON, R., LAFRENIÈRE, D., ARTIGAU, É., GAGNÉ, J. ET AL. (2013). Bayesian Analysis to Identify New Star Candidates in Nearby Young Stellar Kinematic Groups. *ApJ*, 762, 88.

MANJAVACAS, E., BONNEFOY, M., SCHLIEDER, J. E., ALLARD, F., ROJO, P. ET AL. (2014). New constraints on the formation and settling of dust in the atmospheres of young M and L dwarfs. *A&A*, 564, A55.

MANZI, S., RANDICH, S., DE WIT, W. J. & PALLA, F. (2008). Detection of the lithium depletion boundary in the young open cluster IC 4665. *A&A*, 479, 141–148.

MARLEY, M. S., SAUMON, D. & GOLDBLATT, C. (2010). A Patchy Cloud Model for the L to T Dwarf Transition. *ApJ*, 723, L117–L121.

MARSH, K. A., WRIGHT, E. L., KIRKPATRICK, J. D., GELINO, C. R., CUSHING, M. C. ET AL. (2013). Parallaxes and Proper Motions of Ultracool Brown Dwarfs of Spectral Types Y and Late T. *ApJ*, 762, 119.

MARTÍN, E. L., BARRADO Y NAVASCUÉS, D., BARAFFE, I., BOUY, H. & DAHM, S. (2003). A Hubble Space Telescope Wide Field Planetary Camera 2 Survey for Brown Dwarf Binaries in the α Persei and Pleiades Open Clusters. *ApJ*, 594, 525–532.

MARTÍN, E. L., BASRI, G., DELFOSSE, X. & FORVEILLE, T. (1997). Keck HIRES spectra of the brown dwarf DENIS-P J1228.2-1547. *A&A*, 327, L29–L32.

MARTIN, E. L., BRANDNER, W. & BASRI, G. (1999). A Search for Companions to Nearby Brown Dwarfs: The Binary DENIS-P J1228.2-1547. *Science*, 283, 1718–+.

MARTÍN, E. L., BRANDNER, W., BOUY, H., BASRI, G., DAVIS, J. ET AL. (2006). Resolved Hubble space spectroscopy of ultracool binary systems. *A&A*, 456, 253–259.

MARTÍN, E. L., CABRERA, J., MARTIOLI, E., SOLANO, E. & TATA, R. (2013). Kepler observations of very low-mass stars. *A&A*, 555, A108.

MARTÍN, E. L., DELFOSSE, X., BASRI, G., GOLDMAN, B., FORVEILLE, T. ET AL. (1999). Spectroscopic Classification of Late-M and L Field Dwarfs. *AJ*, 118, 2466–2482.

MARTÍN, E. L., DOUGADOS, C., MAGNIER, E., MÉNARD, F., MAGAZZÙ, A. ET AL. (2001). Four Brown Dwarfs in the Taurus Star-Forming Region. *ApJ*, 561, L195–L198.

MARTÍN, E. L., PHAN-BAO, N., BESSELL, M., DELFOSSE, X., FORVEILLE, T. ET AL. (2010). Spectroscopic characterization of 78 DENIS ultracool dwarf candidates in the solar neighborhood and the Upper Scorpii OB association. *A&A*, 517, A53.

MARTÍN, E. L., REBOLO, R. & ZAPATERO-OSORIO, M. R. (1996). Spectroscopy of New Substellar Candidates in the Pleiades: Toward a Spectral Sequence for Young Brown Dwarfs. *ApJ*, 469, 706–+.

MASON, B. D., WYCOFF, G. L., HARTKOPF, W. I., DOUGLASS, G. G. & WORLEY, C. E. (2001). The 2001 US Naval Observatory Double Star CD-ROM. I. The Washington Double Star Catalog. *AJ*, 122, 3466–3471.

MASTERS, D., MCCARTHY, P., BURGASSER, A. J., HATHI, N. P., MALKAN, M. ET AL. (2012). Discovery of Three Distant, Cold Brown Dwarfs in the WFC3 Infrared Spectroscopic Parallels Survey. *ApJ*, 752, L14.

MAXTED, P. F. L. & JEFFRIES, R. D. (2005). On the frequency of close binary systems among very low-mass stars and brown dwarfs. *MNRAS*, 362, L45–L49.

MCCARTHY, M. F. & TREANOR, P. J. (1964). M stars in the region of the Pleiades. *Ricerche Astronomiche*, 6, 535.

MCCAUGHREAN, M. J., CLOSE, L. M., SCHOLZ, R.-D., LENZEN, R., BILLER, B. ET AL. (2004a). ϵ Indi Ba,Bb: The nearest binary brown dwarf. *A&A*, 413, 1029–1036.

MCCAUGHREAN, M. J., CLOSE, L. M., SCHOLZ, R.-D., LENZEN, R., BILLER, B. ET AL. (2004b). ϵ Indi Ba,Bb: The nearest binary brown dwarf. *A&A*, 413, 1029–1036.

MCGOVERN, M. R., KIRKPATRICK, J. D., MCLEAN, I. S., BURGASSER, A. J., PRATO, L. ET AL. (2004). Identifying Young Brown Dwarfs Using Gravity-Sensitive Spectral Features. *ApJ*, 600, 1020–1024.

MCKEE, C. F. & OSTRIKER, E. C. (2007). Theory of Star Formation. *ARA&A*, 45, 565–687.

MEEUS, G. & MCCAUGHREAN, M. J. (2005). Using near-IR spectroscopy to classify substellar candidates in the Trapezium Cluster. *Astronomische Nachrichten*, 326, 977–980.

METCHEV, S. A., KIRKPATRICK, J. D., BERRIMAN, G. B. & LOOPER, D. (2008). A Cross-Match of 2MASS and SDSS: Newly Found L and T Dwarfs and an Estimate of the Space Density of T Dwarfs. *ApJ*, 676, 1281–1306.

MILLER, G. E. & SCALO, J. M. (1979). The initial mass function and stellar birthrate in the solar neighborhood. *ApJS*, 41, 513–547.

MILLER-RICCI, E. & FORTNEY, J. J. (2010). The Nature of the Atmosphere of the Transiting Super-Earth GJ 1214b. *ApJ*, 716, L74–L79.

MOCHNACKI, S. W., GLADDERS, M. D., THOMSON, J. R., LU, W., EHLERS, P. ET AL. (2002). A Spectroscopic Survey of a Sample of Active M Dwarfs. *AJ*, 124, 2868–2882.

MOHANTY, S., GREAVES, J., MORTLOCK, D., PASCUCCI, I., SCHOLZ, A. ET AL. (2013). Protoplanetary Disk Masses from Stars to Brown Dwarfs. *ApJ*, 773, 168.

MONTAGNIER, G., SÉGRANSAN, D., BEUZIT, J.-L., FORVEILLE, T., DELORME, P. ET AL. (2006). Five new very low mass binaries. *A&A*, 460, L19–L22.

MOOLEY, K., HILLENBRAND, L., REBULL, L., PADGETT, D. & KNAPP, G. (2013). B- and A-type Stars in the Taurus-Auriga Star-forming Region. *ApJ*, 771, 110.

MORAUX, E., KROUPA, P. & BOUVIER, J. (2004). The Pleiades mass function: Models versus observations. *A&A*, 426, 75–80.

MORIN, J., DONATI, J.-F., PETIT, P., DELFOSSE, X., FORVEILLE, T. ET AL. (2010). Large-scale magnetic topologies of late M dwarfs. *MNRAS*, 407, 2269–2286.

MORLEY, C. V., FORTNEY, J. J., MARLEY, M. S., VISSCHER, C., SAUMON, D. ET AL. (2012). Neglected Clouds in T and Y Dwarf Atmospheres. *ApJ*, 756, 172.

MUENCH, A. A., LADA, E. A., LADA, C. J. & ALVES, J. (2002). The Luminosity and Mass Function of the Trapezium Cluster: From B Stars to the Deuterium-burning Limit. *ApJ*, 573, 366–393.

MUGRAUER, M., SEIFAHRT, A. & NEUHÄUSER, R. (2007). The multiplicity of planet host stars - new low-mass companions to planet host stars. *MNRAS*, 378, 1328–1334.

MUGRAUER, M., SEIFAHRT, A., NEUHÄUSER, R. & MAZEH, T. (2006). HD3651B: the first directly imaged brown dwarf companion of an exoplanet host star. *MNRAS*, 373, L31–L35.

MUIRHEAD, P. S., HAMREN, K., SCHLAWIN, E., ROJAS-AYALA, B., COVEY, K. R. ET AL. (2012). Characterizing the Cool Kepler Objects of Interests. New Effective Temperatures, Metallicities, Masses, and Radii of Low-mass Kepler Planet-candidate Host Stars. *ApJ*, 750, L37.

MUNDT, R., ALONSO-FLORIANO, F. J., CABALLERO, J. A., KLUTSCH, A., MONTES, D. ET AL. (2013). CARMENES at PPVI. Low-Resolution Spectroscopy of M Dwarfs with CAFOS at Calar Alto. In Protostars and Planets VI, Heidelberg, July 15-20, 2013. Poster #2K055. 55.

MURRAY, D. N., BURNINGHAM, B., JONES, H. R. A., PINFIELD, D. J., LUCAS, P. W. ET AL. (2011). Blue not brown: UKIRT Infrared Deep Sky Survey T dwarfs with suppressed K-band flux. *MNRAS*, 414, 575–586.

MUŽIĆ, K., RADIGAN, J., JAYAWARDHANA, R., IVANOV, V. D., FAHERTY, J. K. ET AL. (2012). Discovery of Two Very Wide Binaries with Ultracool Companions and a New Brown Dwarf at the L/T Transition. *AJ*, 144, 180.

MUŽIĆ, K., SCHOLZ, A., GEERS, V. C., JAYAWARDHANA, R. & LÓPEZ MARTÍ, B. (2014). Substellar Objects in Nearby Young Clusters (SONYC). VIII. Substellar Population in Lupus 3. *ApJ*, 785, 159.

MUZEROLLE, J., HILLENBRAND, L., CALVET, N., BRICEÑO, C. & HARTMANN, L. (2003). Accretion in Young Stellar/Substellar Objects. *ApJ*, 592, 266–281.

MUZEROLLE, J., LUHMAN, K. L., BRICEÑO, C., HARTMANN, L. & CALVET, N. (2005). Measuring Accretion in Young Substellar Objects: Approaching the Planetary Mass Regime. *ApJ*, 625, 906–912.

NAKAJIMA, T., OPPENHEIMER, B. R., KULKARNI, S. R., GOLIMOWSKI, D. A., MATTHEWS, K. ET AL. (1995). Discovery of a Cool Brown Dwarf. *Nature*, 378, 463–+.

NATTA, A., TESTI, L., COMERÓN, F., OLIVA, E., D'ANTONA, F. ET AL. (2002). Exploring brown dwarf disks in rho Ophiuchi. *A&A*, 393, 597–609.

OFFNER, S. S. R., HANSEN, C. E. & KRUMHOLZ, M. R. (2009). Stellar Kinematics of Young Clusters in Turbulent Hydrodynamic Simulations. *ApJ*, 704, L124–L128.

OFFNER, S. S. R., KLEIN, R. I. & MCKEE, C. F. (2008). Driven and Decaying Turbulence Simulations of Low-Mass Star Formation: From Clumps to Cores to Protostars. *ApJ*, 686, 1174–1194.

OLIVEIRA, J. M., JEFFRIES, R. D., DEVEY, C. R., BARRADO Y NAVASCUÉS, D., NAYLOR, T. ET AL. (2003). The lithium depletion boundary and the age of NGC 2547. *MNRAS*, 342, 651–663.

OLIVEIRA, J. M., JEFFRIES, R. D., KENYON, M. J., THOMPSON, S. A. & NAYLOR, T. (2002). No disks around low-mass stars and brown dwarfs in the young sigma Orionis cluster? *A&A*, 382, L22–L25.

OPPENHEIMER, B. R., KULKARNI, S. R., MATTHEWS, K. & NAKAJIMA, T. (1995). Infrared Spectrum of the Cool Brown Dwarf GL:229B. *Science*, 270, 1478–+.

PADOAN, P. & NORDLUND, Å. (2002). The Stellar Initial Mass Function from Turbulent Fragmentation. *ApJ*, 576, 870–879.

PADOAN, P. & NORDLUND, Å. (2004). The "Mysterious" Origin of Brown Dwarfs. *ApJ*, 617, 559–564.

PARKER, R. J., BOUVIER, J., GOODWIN, S. P., MORAUX, E., ALLISON, R. J. ET AL. (2011). On the mass segregation of stars and brown dwarfs in Taurus. *MNRAS*, 412, 2489–2497.

PATTEN, B. M., STAUFFER, J. R., BURROWS, A., MARENGO, M., HORA, J. L. ET AL. (2006). Spitzer IRAC Photometry of M, L, and T Dwarfs. *ApJ*, 651, 502–516.

PEÑA RAMÍREZ, K., BÉJAR, V. J. S., ZAPATERO OSORIO, M. R., PETR-GOTZENS, M. G. & MARTÍN, E. L. (2012). New Isolated Planetary-mass Objects and the Stellar and Substellar Mass Function of the σ Orionis Cluster. *ApJ*, 754, 30.

PEÑA RAMÍREZ, K., ZAPATERO OSORIO, M. R. & BÉJAR, V. J. S. (2015). Characterization of the known T-type dwarfs towards the σ Orionis cluster. *A&A*, 574, A118.

PERGER, M., LODIEU, N., MARTÍN, E. L. & BARRADO, D. (2013). New low-mass member candidates of Taurus. *Mem. Soc. Astron. Italiana*, 84, 948.

PHAN-BAO, N., BESSELL, M. S., MARTÍN, E. L., SIMON, G., BORSENBERGER, J. ET AL. (2008). Discovery of new nearby L and late-M dwarfs at low Galactic latitude from the DENIS data base. *MNRAS*, 383, 831–844.

PINFIELD, D. J., GOMES, J., DAY-JONES, A. C., LEGGETT, S. K., GROMADZKI, M. ET AL. (2014a). A deep WISE search for very late type objects and the discovery of two halo/thick-disc T dwarfs: WISE 0013+0634 and WISE 0833+0052. *MNRAS*, 437, 1009–1026.

PINFIELD, D. J., GROMADZKI, M., LEGGETT, S. K., GOMES, J., LODIEU, N. ET AL. (2014b). Discovery of a new Y dwarf: WISE J030449.03-270508.3. *ArXiv e-prints*.

PINFIELD, D. J., GROMADZKI, M., LEGGETT, S. K., GOMES, J., LODIEU, N. ET AL. (2014c). Discovery of a new Y dwarf: WISE J030449.03-270508.3. *MNRAS*, 444, 1931–1939.

PINFIELD, D. J. ET AL. (2008). Fifteen new T dwarfs discovered in the UKIDSS Large Area Survey. *MNRAS*, 390, 304–322.

POPE, B., MARTINACHE, F. & TUTHILL, P. (2013). Dancing in the Dark: New Brown Dwarf Binaries from Kernel Phase Interferometry. *ApJ*, 767, 110.

POTTER, D., MARTÍN, E. L., CUSHING, M. C., BAUDOZ, P., BRANDNER, W. ET AL. (2002). Hokupa'a-Gemini Discovery of Two Ultracool Companions to the Young Star HD 130948. *ApJ*, 567, L133–L136.

QUIRRENBACH, A., AMADO, P. J., MANDEL, H., CABALLERO, J. A., RIBAS, I. ET AL. (2010). CARMENES: Calar Alto High-Resolution Search for M Dwarfs with Exo-earths with a Near-infrared Echelle Spectrograph. In COUDÉ DU FORESTO, V., GELINO, D. M. & RIBAS, I., eds., Pathways Towards Habitable Planets, vol. 430 of *Astronomical Society of the Pacific Conference Series*. 521.

QUIRRENBACH, A., AMADO, P. J., SEIFERT, W., SÁNCHEZ CARRASCO, M. A., MANDEL, H. ET AL. (2012). CARMENES. I: instrument and survey overview. In Society of Photo-Optical Instrumentation Engineers (SPIE) Conference Series, vol. 8446 of *Society of Photo-Optical Instrumentation Engineers (SPIE) Conference Series*.

RADIGAN, J., JAYAWARDHANA, R., LAFRENIÈRE, D., DUPUY, T. J., LIU, M. C. ET AL. (2013). Discovery of a Visual T-dwarf Triple System and Binarity at the L/T Transition. *ApJ*, 778, 36.

RADIGAN, J., LAFRENIÈRE, D., JAYAWARDHANA, R. & DOYON, R. (2008). Discovery of a Wide Substellar Companion to a Nearby Low-Mass Star. *ApJ*, 689, 471–477.

RADIGAN, J., LAFRENIÈRE, D., JAYAWARDHANA, R. & DOYON, R. (2009). Discovery of the Widest Very Low Mass Field Binary. *ApJ*, 698, 405–409.

RAJPUROHIT, A. S., REYLÉ, C., ALLARD, F., HOMEIER, D., SCHULTHEIS, M. ET AL. (2013). The effective temperature scale of M dwarfs. *A&A*, 556, A15.

RAJPUROHIT, A. S., REYLÉ, C., ALLARD, F., SCHOLZ, R.-D., HOMEIER, D. ET AL. (2014). High-resolution spectroscopic atlas of M subdwarfs. Effective temperature and metallicity. *A&A*, 564, A90.

RANC, C., CASSAN, A., ALBROW, M. D., KUBAS, D., BOND, I. A. ET AL. (2015). MOA-2007-BLG-197: Exploring the brown dwarf desert. *A&A*, 580, A125.

REBOLO, R., MARTIN, E. L., BASRI, G., MARCY, G. W. & ZAPATERO-OSORIO, M. R. (1996). Brown Dwarfs in the Pleiades Cluster Confirmed by the Lithium Test. *ApJ*, 469, L53+.

REBOLO, R., MARTIN, E. L. & MAGAZZU, A. (1992). Spectroscopy of a brown dwarf candidate in the Alpha Persei open cluster. *ApJ*, 389, L83–L86.

REBOLO, R., ZAPATERO-OSORIO, M. R. & MARTIN, E. L. (1995). Discovery of a Brown Dwarf in the Pleiades Star Cluster. *Nature*, 377, 129–+.

REID, I. N. & CRUZ, K. L. (2002). Meeting the Cool Neighbors. I. Nearby Stars in the NLTT Catalogue: Defining the Sample. *AJ*, 123, 2806–2821.

REID, I. N., CRUZ, K. L., ALLEN, P., MUNGALL, F., KILKENNY, D. ET AL. (2003). Meeting the Cool Neighbors. VII. Spectroscopy of Faint Red NLTT Dwarfs. *AJ*, 126, 3007–3016.

REID, I. N., CRUZ, K. L., BURGASSER, A. J. & LIU, M. C. (2008). L-Dwarf Binaries in the 20-PARSEC Sample. *AJ*, 135, 580–587.

REID, I. N. & GIZIS, J. E. (1997a). Low-Mass Binaries and the Stellar Luminosity Function. *AJ*, 113, 2246.

REID, I. N. & GIZIS, J. E. (1997b). Low-Mass Binaries in the Hyades: A Scarcity of Brown Dwarfs. *AJ*, 114, 1992–+.

REID, I. N., GIZIS, J. E., KIRKPATRICK, J. D. & KOERNER, D. W. (2001). A Search for L Dwarf Binary Systems. *AJ*, 121, 489–502.

REID, I. N., HAWLEY, S. L. & GIZIS, J. E. (1995). The Palomar/MSU Nearby-Star Spectroscopic Survey. I. The Northern M Dwarfs -Bandstrengths and Kinematics. *AJ*, 110, 1838.

REID, I. N., KIRKPATRICK, J. D., LIEBERT, J., BURROWS, A., GIZIS, J. E. ET AL. (1999). L Dwarfs and the Substellar Mass Function. *ApJ*, 521, 613–629.

REID, I. N., KIRKPATRICK, J. D., LIEBERT, J., GIZIS, J. E., DAHN, C. C. ET AL. (2002). High-Resolution Spectroscopy of Ultracool M Dwarfs. *AJ*, 124, 519–540.

REID, I. N., LEWITUS, E., ALLEN, P. R., CRUZ, K. L. & BURGASSER, A. J. (2006a). A Search for Binary Systems among the Nearest L Dwarfs. *AJ*, 132, 891–901.

REID, I. N., LEWITUS, E., BURGASSER, A. J. & CRUZ, K. L. (2006b). 2MASS J22521073-1730134: A Resolved L/T Binary at 14 Parsecs. *ApJ*, 639, 1114–1119.

REINERS, A. & BASRI, G. (2008). Chromospheric Activity, Rotation, and Rotational Braking in M and L Dwarfs. *ApJ*, 684, 1390–1403.

REINERS, A., BEAN, J. L., HUBER, K. F., DREIZLER, S., SEIFAHRT, A. ET AL. (2010). Detecting Planets Around Very Low Mass Stars with the Radial Velocity Method. *ApJ*, 710, 432–443.

REIPURTH, B. & CLARKE, C. (2001). The Formation of Brown Dwarfs as Ejected Stellar Embryos. *AJ*, 122, 432–439.

REYLÉ, C., DELORME, P., ARTIGAU, E., DELFOSSE, X., ALBERT, L. ET AL. (2014). CFBDS J111807-064016: A new L/T transition brown dwarf in a binary system. *A&A*, 561, A66.

REYLÉ, C., DELORME, P., WILLOTT, C. J., ALBERT, L., DELFOSSE, X. ET AL. (2010). The ultracool field dwarf luminosity function and space density from the Canada-France Brown Dwarf Survey. *A&A*, 522, A112+.

RIAZ, B., GIZIS, J. E. & SAMADDAR, D. (2008). Hubble Space Telescope Search for M Subdwarf Binaries. *ApJ*, 672, 1153–1158.

RICA (2012). Common Proper Motion Pairs in the LSPM-North Catalog. *Journal of Double Star Observations*, 8, 73–80.

RICE, W. K. M., ARMITAGE, P. J., BONNELL, I. A., BATE, M. R., JEFFERS, S. V. ET AL. (2003). Substellar companions and isolated planetary-mass objects from protostellar disc fragmentation. *MNRAS*, 346, L36–L40.

RICKER, G. R., LATHAM, D. W., VANDERSPEK, R. K., ENNICO, K. A., BAKOS, G. ET AL. (2010). Transiting Exoplanet Survey Satellite (TESS). In American Astronomical Society Meeting Abstracts, vol. 42 of *Bulletin of the American Astronomical Society*. 450.06.

RICKER, G. R., WINN, J. N., VANDERSPEK, R., LATHAM, D. W., BAKOS, G. Á. ET AL. (2015). Transiting Exoplanet Survey Satellite (TESS). *Journal of Astronomical Telescopes, Instruments, and Systems*, 1, 014003.

RODLER, F., DEL BURGO, C., WITTE, S., HELLING, C., HAUSCHILDT, P. H. ET AL. (2011). Detecting planets around very cool dwarfs at near infrared wavelengths with the radial velocity technique. *A&A*, 532, A31.

ROESER, S., DEMLEITNER, M. & SCHILBACH, E. (2010). The PPMXL Catalog of Positions and Proper Motions on the ICRS. Combining USNO-B1.0 and the Two Micron All Sky Survey (2MASS). *AJ*, 139, 2440–2447.

ROJAS-AYALA, B., COVEY, K. R., MUIRHEAD, P. S. & LLOYD, J. P. (2010). Metal-rich M-Dwarf Planet Hosts: Metallicities with K-band Spectra. *ApJ*, 720, L113–L118.

ROJAS-AYALA, B., COVEY, K. R., MUIRHEAD, P. S. & LLOYD, J. P. (2012). Metallicity and Temperature Indicators in M Dwarf K-band Spectra: Testing New and Updated Calibrations with Observations of 133 Solar Neighborhood M Dwarfs. *ApJ*, 748, 93.

ROSS, F. E. (1939). New proper motion stars (11th list). *AJ*, 48, 163–166.

RUIZ, M. T., LEGGETT, S. K. & ALLARD, F. (1997). Kelu-1: A Free-floating Brown Dwarf in the Solar Neighborhood. *ApJ*, 491, L107+.

SAHLMANN, J., BURGASSER, A. J., MARTÍN, E. L., LAZORENKO, P. F., BARDALEZ GAGLIUFFI, D. C. ET AL. (2015a). DE0823-49 is a juvenile binary brown dwarf at 20.7 pc. *A&A*, 579, A61.

SAHLMANN, J., LAZORENKO, P. F., SÉGRANSAN, D., MARTÍN, E. L., MAYOR, M. ET AL. (2015b). Astrometric planet search around southern ultracool dwarfs. III. Discovery of a brown dwarf in a 3-year orbit around DE0630-18. *A&A*, 577, A15.

SAHLMANN, J., LAZORENKO, P. F., SÉGRANSAN, D., MARTÍN, E. L., QUELOZ, D. ET AL. (2013). Astrometric orbit of a low-mass companion to an ultracool dwarf. *A&A*, 556, A133.

SALPETER, E. E. (1955). The Luminosity Function and Stellar Evolution. *ApJ*, 121, 161.

SAUMON, D., BERGERON, P., LUNINE, J. I., HUBBARD, W. B. & BURROWS, A. (1994). Cool zero-metallicity stellar atmospheres. *ApJ*, 424, 333–344.

SAUMON, D., HUBBARD, W. B., BURROWS, A., GUILLOT, T., LUNINE, J. I. ET AL. (1996). A Theory of Extrasolar Giant Planets. *ApJ*, 460, 993.

SAUMON, D., MARLEY, M. S., CUSHING, M. C., LEGGETT, S. K., ROELLIG, T. L. ET AL. (2006). Ammonia as a Tracer of Chemical Equilibrium in the T7.5 Dwarf Gliese 570D. *ApJ*, 647, 552–557.

SAUMON, D., MARLEY, M. S., LEGGETT, S. K., GEBALLE, T. R., STEPHENS, D. ET AL. (2007). Physical Parameters of Two Very Cool T Dwarfs. *ApJ*, 656, 1136–1149.

SAVCHEVA, A. S., WEST, A. A. & BOCHANSKI, J. J. (2014). A New Sample of Cool Subdwarfs from SDSS: Properties and Kinematics. *ApJ*, 794, 145.

SCALO, J. M. (1986a). The initial mass function of massive stars in galaxies Empirical evidence. In DE LOORE, C. W. H., WILLIS, A. J. & LASKARIDES, P., eds., Luminous Stars and Associations in Galaxies, vol. 116 of *IAU Symposium*. 451–466.

SCALO, J. M. (1986b). The stellar initial mass function. *Fund. Cosmic Phys.*, 11, 1–278.

SCELSI, L., MAGGIO, A., MICELA, G., PILLITTERI, I., STELZER, B. ET AL. (2007). New pre-main sequence candidates in the Taurus-Auriga star forming region. *A&A*, 468, 405–412.

SCHLAUFMAN, K. C. & LAUGHLIN, G. (2010). A physically-motivated photometric calibration of M dwarf metallicity. *A&A*, 519, A105.

SCHLIEDER, J. E., LÉPINE, S., RICE, E., SIMON, M., FIELDING, D. ET AL. (2012). The Na 8200 Å Doublet as an Age Indicator in Low-mass Stars. *AJ*, 143, 114.

SCHMIDT, S. J., CRUZ, K. L., BONGIORNO, B. J., LIEBERT, J. & REID, I. N. (2007). Activity and Kinematics of Ultracool Dwarfs, Including an Amazing Flare Observation. *AJ*, 133, 2258–2273.

SCHMITT, J. H. M. M., FLEMING, T. A. & GIAMPAPA, M. S. (1995). The X-Ray View of the Low-Mass Stars in the Solar Neighborhood. *ApJ*, 450, 392.

SCHOLZ, A., FROEBRICH, D., DAVIS, C. J. & MEUSINGER, H. (2010). A near-infrared variability study in the cloud IC1396W: low star-forming efficiency and two new eclipsing binaries. *MNRAS*, 406, 505–516.

SCHOLZ, R.-D., BIHAIN, G., SCHNURR, O. & STORM, J. (2011). Two very nearby (d ~ 5 pc) ultracool brown dwarfs detected by their large proper motions from WISE, 2MASS, and SDSS data. *A&A*, 532, L5.

SCHOLZ, R.-D., BIHAIN, G., SCHNURR, O. & STORM, J. (2012). UKIDSS detections of cool brown dwarfs. Proper motions of 14 known >T5 dwarfs and discovery of three new T5.5-T6 dwarfs. *A&A*, 541, A163.

SCHOLZ, R.-D., LODIEU, N., IBATA, R., BIENAYMÉ, O., IRWIN, M. ET AL. (2004). An active M8.5 dwarf wide companion to the M4/DA binary LHS 4039/LHS 4040. *MNRAS*, 347, 685–690.

SEELIGER, M., NEUHÄUSER, R. & EISENBEISS, T. (2011). Spectral classification of Pleiades brown dwarf candidates. *Astronomische Nachrichten*, 332, 821.

SHIN, I.-G., HAN, C., GOULD, A., UDALSKI, A., SUMI, T. ET AL. (2012). Microlensing Binaries with Candidate Brown Dwarf Companions. *ApJ*, 760, 116.

SHKOLNIK, E. L., LIU, M. C., REID, I. N., DUPUY, T. & WEINBERGER, A. J. (2011). Searching for Young M Dwarfs with GALEX. *ApJ*, 727, 6.

SHOWMAN, A. P. & KASPI, Y. (2013). Atmospheric Dynamics of Brown Dwarfs and Directly Imaged Giant Planets. *ApJ*, 776, 85.

SIEGLER, N., CLOSE, L. M., BURGASSER, A. J., CRUZ, K. L., MAROIS, C. ET AL. (2007). Discovery of a 66 mas Ultracool Binary with Laser Guide Star Adaptive Optics. *AJ*, 133, 2320–2326.

SIEGLER, N., CLOSE, L. M., CRUZ, K. L., MARTÍN, E. L. & REID, I. N. (2005). Discovery of Two Very Low Mass Binaries: Final Results of an Adaptive Optics Survey of Nearby M6.0-M7.5 Stars. *ApJ*, 621, 1023–1032.

SIEGLER, N., CLOSE, L. M., MAMAJEK, E. E. & FREED, M. (2003). An Adaptive Optics Survey of M6.0-M7.5 Stars: Discovery of Three Very Low Mass Binary Systems Including Two Probable Hyades Members. *ApJ*, 598, 1265–1276.

SKRUTSKIE, M. F. ET AL. (2006). The Two Micron All Sky Survey (2MASS). *AJ*, 131, 1163–1183.

SKRZYPEK, N., WARREN, S. J., FAHERTY, J. K., MORTLOCK, D. J., BURGASSER, A. J. ET AL. (2015). Photometric brown-dwarf classification. I. A method to identify and accurately classify large samples of brown dwarfs without spectroscopy. *A&A*, 574, A78.

SLESNICK, C. L., CARPENTER, J. M. & HILLENBRAND, L. A. (2006a). A Large-Area Search for Low-Mass Objects in Upper Scorpius. I. The Photometric Campaign and New Brown Dwarfs. *AJ*, 131, 3016–3027.

SLESNICK, C. L., CARPENTER, J. M., HILLENBRAND, L. A. & MAMAJEK, E. E. (2006b). A Distributed Population of Low-Mass Pre-Main-Sequence Stars near the Taurus Molecular Clouds. *AJ*, 132, 2665–2674.

SLESNICK, C. L., HILLENBRAND, L. A. & CARPENTER, J. M. (2008). A Large-Area Search for Low-Mass Objects in Upper Scorpius. II. Age and Mass Distributions. *ApJ*, 688, 377–397.

SODERBLOM, D. R., HILLENBRAND, L. A., JEFFRIES, R. D., MAMAJEK, E. E. & NAYLOR, T. (2013). Ages of young stars. *ArXiv e-prints*.

STAMATELLOS, D., HUBBER, D. A. & WHITWORTH, A. P. (2007). Brown dwarf formation by gravitational fragmentation of massive, extended protostellar discs. *MNRAS*, 382, L30–L34.

STAMATELLOS, D. & WHITWORTH, A. P. (2009). The properties of brown dwarfs and low-mass hydrogen-burning stars formed by disc fragmentation. *MNRAS*, 392, 413–427.

STASSUN, K. G., MATHIEU, R. D. & VALENTI, J. A. (2006). Discovery of two young brown dwarfs in an eclipsing binary system. *Nature*, 440, 311–314.

STASSUN, K. G., MATHIEU, R. D., VAZ, L. P. R., STROUD, N. & VRBA, F. J. (2004). Dynamical Mass Constraints on Low-Mass Pre-Main-Sequence Stellar Evolutionary Tracks: An Eclipsing Binary in Orion with a 1.0 M_{solar} Primary and a 0.7 M_{solar} Secondary. *ApJS*, 151, 357–385.

STAUFFER, J. R., HAMILTON, D. & PROBST, R. G. (1994). A CCD-based search for very low mass members of the Pleiades cluster. *AJ*, 108, 155–159.

STAUFFER, J. R., SCHULTZ, G. & KIRKPATRICK, J. D. (1998). Keck Spectra of Pleiades Brown Dwarf Candidates and a Precise Determination of the Lithium Depletion Edge in the Pleiades. *ApJ*, 499, L199+.

STEELE, I. A. & JAMESON, R. F. (1995). Optical spectroscopy of low-mass stars and brown dwarfs in the Pleiades. *MNRAS*, 272, 630–646.

STELZER, B., MARINO, A., MICELA, G., LÓPEZ-SANTIAGO, J. & LIEFKE, C. (2013). The UV and X-ray activity of the M dwarfs within 10 pc of the Sun. *MNRAS*, 431, 2063–2079.

STEPHENS, D. C., LEGGETT, S. K., CUSHING, M. C., MARLEY, M. S., SAUMON, D. ET AL. (2009). The 0.8-14.5 μm Spectra of Mid-L to Mid-T Dwarfs: Diagnostics of Effective Temperature, Grain Sedimentation, Gas Transport, and Surface Gravity. *ApJ*, 702, 154–170.

STRAUSS, M. A. ET AL. (1999). The Discovery of a Field Methane Dwarf from Sloan Digital Sky Survey Commissioning Data. *ApJ*, 522, L61–L64.

STUMPF, M. B., GEISSLER, K., BOUY, H., BRANDNER, W., GOLDMAN, B. ET AL. (2011). Resolving the L/T transition binary SDSS J2052-1609 AB. *A&A*, 525, A123.

TARTER, J. C., BACKUS, P. R., MANCINELLI, R. L., AURNOU, J. M., BACKMAN, D. E. ET AL. (2007). A Reappraisal of The Habitability of Planets around M Dwarf Stars. *Astrobiology*, 7, 30–65.

TAYLOR, M. B. (2006). STILTS - A Package for Command-Line Processing of Tabular Data. In GABRIEL, C., ARVISET, C., PONZ, D. & ENRIQUE, S., eds., Astronomical Data Analysis Software and Systems XV, vol. 351 of *Astronomical Society of the Pacific Conference Series*. 666.

THIES, I. & KROUPA, P. (2007). A Discontinuity in the Low-Mass Initial Mass Function. *ApJ*, 671, 767–780.

THOMPSON, M. A., KIRKPATRICK, J. D., MACE, G. N., CUSHING, M. C., GELINO, C. R. ET AL. (2013). Nearby M, L, and T Dwarfs Discovered by the Wide-field Infrared Survey Explorer (WISE). *PASP*, 125, 809–837.

TINETTI, G., BEAULIEU, J. P., HENNING, T., MEYER, M., MICELA, G. ET AL. (2012). EChO. Exoplanet characterisation observatory. *Experimental Astronomy*, 34, 311–353.

TINNEY, C. G., BURGASSER, A. J. & KIRKPATRICK, J. D. (2003). Infrared Parallaxes for Methane T Dwarfs. *AJ*, 126, 975–992.

TINNEY, C. G., BURGASSER, A. J., KIRKPATRICK, J. D. & MCELWAIN, M. W. (2005). The 2MASS Wide-Field T Dwarf Search. IV. Hunting Out T Dwarfs with Methane Imaging. *AJ*, 130, 2326–2346.

TINNEY, C. G., FAHERTY, J. K., KIRKPATRICK, J. D., WRIGHT, E. L., GELINO, C. R. ET AL. (2012). WISE J163940.83-684738.6: A Y Dwarf Identified by Methane Imaging. *ApJ*, 759, 60.

TODOROV, K., LUHMAN, K. L. & MCLEOD, K. K. (2010). Discovery of a Planetary-mass Companion to a Brown Dwarf in Taurus. *ApJ*, 714, L84–L88.

TODOROV, K. O., LUHMAN, K. L., KONOPACKY, Q. M., MCLEOD, K. K., APAI, D. ET AL. (2014). A Search for Companions to Brown Dwarfs in the Taurus and Chamaeleon Star-Forming Regions. *ApJ*, 788, 40.

TODY, D. (1986). The IRAF Data Reduction and Analysis System. In CRAWFORD, D. L., ed., Society of Photo-Optical Instrumentation Engineers (SPIE) Conference Series, vol. 627 of *Society of Photo-Optical Instrumentation Engineers (SPIE) Conference Series*. 733–+.

TSUJI, T. (2005). Dust in the Photospheric Environment. III. A Fundamental Element in the Characterization of Ultracool Dwarfs. *ApJ*, 621, 1033–1048.

TSUJI, T. & NAKAJIMA, T. (2003). Transition from L to T Dwarfs on the Color-Magnitude Diagram. *ApJ*, 585, L151–L154.

TSVETANOV, Z. I. ET AL. (2000). The Discovery of a Second Field Methane Brown Dwarf from Sloan Digital Sky Survey Commissioning Data. *ApJ*, 531, L61–L65.

UMBREIT, S., BURKERT, A., HENNING, T., MIKKOLA, S. & SPURZEM, R. (2005). The Decay of Accreting Triple Systems as Brown Dwarf Formation Scenario. *ApJ*, 623, 940–951.

VALDIVIELSO, L., MARTÍN, E. L., BOUY, H., SOLANO, E., DREW, J. E. ET AL. (2009). An IPHAS-based search for accreting very low-mass objects using VO tools. *A&A*, 497, 973–981.

VAN MAANEN, A. (1915). List of Stars with Proper Motion Exceeding 0″.50 Annually. *ApJ*, 41, 187.

VOGES, W., ASCHENBACH, B., BOLLER, T., BRÄUNINGER, H., BRIEL, U. ET AL. (1999). The ROSAT all-sky survey bright source catalogue. *A&A*, 349, 389–405.

VRBA, F. J., HENDEN, A. A., LUGINBUHL, C. B., GUETTER, H. H., MUNN, J. A. ET AL. (2004). Preliminary Parallaxes of 40 L and T Dwarfs from the US Naval Observatory Infrared Astrometry Program. *AJ*, 127, 2948–2968.

WALKOWICZ, L. M., HAWLEY, S. L. & WEST, A. A. (2004). The χ Factor: Determining the Strength of Activity in Low-Mass Dwarfs. *PASP*, 116, 1105–1110.

WARREN, S. J., CROSS, N. J. G., DYE, S., HAMBLY, N. C., ALMAINI, O. ET AL. (2007a). The UKIRT Infrared Deep Sky Survey Second Data Release. *ArXiv Astrophysics e-prints*.

WARREN, S. J. ET AL. (2007b). A very cool brown dwarf in UKIDSS DR1. *MNRAS*, 381, 1400–1412.

WEST, A. A., HAWLEY, S. L., BOCHANSKI, J. J., COVEY, K. R., REID, I. N. ET AL. (2008). Constraining the Age-Activity Relation for Cool Stars: The Sloan Digital Sky Survey Data Release 5 Low-Mass Star Spectroscopic Sample. *AJ*, 135, 785–795.

WEST, A. A., HAWLEY, S. L., WALKOWICZ, L. M., COVEY, K. R., SILVESTRI, N. M. ET AL. (2004). Spectroscopic Properties of Cool Stars in the Sloan Digital Sky Survey: An Analysis of Magnetic Activity and a Search for Subdwarfs. *AJ*, 128, 426–436.

WEST, A. A., MORGAN, D. P., BOCHANSKI, J. J., ANDERSEN, J. M., BELL, K. J. ET AL. (2011). The Sloan Digital Sky Survey Data Release 7 Spectroscopic M Dwarf Catalog. I. Data. *AJ*, 141, 97–+.

WEST, A. A., WALKOWICZ, L. M. & HAWLEY, S. L. (2005). Updated Colors for Cool Stars in the SDSS. *ArXiv Astrophysics e-prints*.

WHITE, R. J. & BASRI, G. (2003). Very Low Mass Stars and Brown Dwarfs in Taurus-Auriga. *ApJ*, 582, 1109–1122.

WHITWORTH, A. P. & STAMATELLOS, D. (2006). The minimum mass for star formation, and the origin of binary brown dwarfs. *A&A*, 458, 817–829.

WHITWORTH, A. P. & ZINNECKER, H. (2004). The formation of free-floating brown dwarves and planetary-mass objects by photo-erosion of prestellar cores. *A&A*, 427, 299–306.

WOLF, M. (1919). Katalog von 1053 staerker bewegten Fixsternen. *Veroeffentlichungen der Badischen Sternwarte zu Heidelberg*, 7, 195.

WOOLF, V. M., LÉPINE, S. & WALLERSTEIN, G. (2009). Calibrating M-Dwarf Metallicities Using Molecular Indices: Extension to Low-metallicity Stars. *PASP*, 121, 117–124.

WRIGHT, E. L., EISENHARDT, P. R. M., MAINZER, A. K., RESSLER, M. E., CUTRI, R. M. ET AL. (2010). The Wide-field Infrared Survey Explorer (WISE): Mission Description and Initial On-orbit Performance. *AJ*, 140, 1868–1881.

YORK, D. G. ET AL. (2000). The Sloan Digital Sky Survey: Technical Summary. *AJ*, 120, 1579–1587.

YURCHENKO, S. N. & TENNYSON, J. (2014). ExoMol line lists - IV. The rotation-vibration spectrum of methane up to 1500 K. *MNRAS*, 440, 1649–1661.

ZACHARIAS, N., FINCH, C. T., GIRARD, T. M., HENDEN, A., BARTLETT, J. L. ET AL. (2012). UCAC4 Catalogue (Zacharias+, 2012). *VizieR Online Data Catalog*, 1322, 0.

ZAPATERO OSORIO, M. R., BÉJAR, V. J. S., MARTÍN, E. L., GÁLVEZ ORTIZ, M. C., REBOLO, R. ET AL. (2014a). Spectroscopic follow-up of L- and T-type proper-motion member candidates in the Pleiades. *A&A*, 572, A67.

ZAPATERO OSORIO, M. R., BÉJAR, V. J. S., MARTÍN, E. L., REBOLO, R., BARRADO Y NAVASCUÉS, D. ET AL. (2000). Discovery of Young, Isolated Planetary Mass Objects in the σ Orionis Star Cluster. *Science*, 290, 103–107.

ZAPATERO OSORIO, M. R., GÁLVEZ ORTIZ, M. C., BIHAIN, G., BAILER-JONES, C. A. L., REBOLO, R. ET AL. (2014b). Search for free-floating planetary-mass objects in the Pleiades. *A&A*, 568, A77.

ZAPATERO OSORIO, M. R., LANE, B. F., PAVLENKO, Y., MARTÍN, E. L., BRITTON, M. ET AL. (2004). Dynamical Masses of the Binary Brown Dwarf GJ 569 Bab. *ApJ*, 615, 958–971.

ZASOWSKI, G., JOHNSON, J. A., FRINCHABOY, P. M., MAJEWSKI, S. R., NIDEVER, D. L. ET AL. (2013). Target Selection for the Apache Point Observatory Galactic Evolution Experiment (APOGEE). *AJ*, 146, 81.

ZICKGRAF, F.-J., ENGELS, D., HAGEN, H.-J., REIMERS, D. & VOGES, W. (2003). The Hamburg/RASS Catalogue of optical identifications. Northern high-galactic latitude ROSAT Bright Source Catalogue X-ray sources. *A&A*, 406, 535–553.

ZUCKERMAN, B. & SONG, I. (2009). The minimum Jeans mass, brown dwarf companion IMF, and predictions for detection of Y-type dwarfs. *A&A*, 493, 1149–1154.